Journal of Double Star Observations

VOLUME 14 NUMBER 4 October 1, 2018

Inside this issue:

Inside this issue:

Double Star Measurements with an AltAz Telescope: Report for 2016

Lucian Curelaru
Brasov, Romania
lucian.curelaru@gmail.com

Abstract: This article presents a set of double star measurements using a small AltAz computerised telescope and a DSLR camera during the year 2016.

The Telescope and the Camera:

I used a Celestron CPC 800 computerised AltAz mounted telescope and a Canon 1100D camera in order to obtain measurements for some double stars, part of them neglected, in many observing sessions during the entire year of 2016. This equipment is positioned in a fixed location, connected and remotely controlled thru a computer. This small fixed observatory is also used to do asteroid astrometry and is enrolled at the Minor Planet Center having the MPC code L13. The physical position is in Brasov, a medium city located in the center of Romania. The telescope is a SCT having a mirror with diameter of 200 mm and a focal of 2000 mm. The Canon camera is mounted in prime focus having a CMOS of 4272 × 2848 pixels. Through this setup, I can image fields having about 36 × 24 arcminutes with a resolution of 0.512 arcsecond per pixel. The current magnitude limit of the setup is up to 16 mag. A better magnitude limit could be obtained by increasing the exposure time, but because of the field rotation effect which occurs in AltAz mounted telescopes at medium and long exposures, I prefered to limit the exposures mostly to 30 seconds and very rarely to go up to 45 seconds. I also used a bahtinov mask to get sharp focusing.

The Method

Using the described setup I imaged fields centered on some neglected doubles selected from the WDS using a web-tool built by myself some years ago. This tool named WDSFilter [4] helped me to select double stars from the WDS [1] which meets different criteria. Using this tool, I isolated some neglected double stars visible to my fixed observatory because I have some limitations caused by local buildings near my home position. I also selected my targets requiring them to have a separation bigger than 5 arcseconds and magnitudes brighter than 16. The 5 arcseconds limit was used because I previously performed some precision tests around 5 arcseconds separation which showed that 5 arcseconds or higher separated doubles can produce results with a good enough precision for double star astrometry. The precision results will be presented in the next paragraph.

Because my camera field is pretty big next to the targeted neglected doubles I also measured some other doubles that were occasionally in my imaged fields or in fields imaged for other purposes like the asteroid work that I also do.

In order to obtain the measurements, I imaged fields centered on the coordinates of each targeted object. Each picture was saved as raw image at first on the observatory computer and then it was converted to grayscale PNG and after that converted to FITS using the Astrometry.net webtool [7]. The resulted FITS was reduced using Astrometrica [2] software measuring there the precise position (RA and DEC) of each targeted object components. The obtained coordinates I've inserted in a google spreadsheet taken from an older double star project presented in a JDSO article in the past [5]. This spreadsheet computes the separation and position angle from the coordinates. In Astrometrica I used the UCAC4 catalogue [6] for field matching.

Measurements Precision

Some basic computations based on the equipment

Double Star Measurements with an AltAz Telescope: Report for 2016

Table 1. Measurements comparison between my determinations and WDS values.

Name	RA+Dec	Measured PA	Measured Sep	WDS PA	WDS Sep	PA O-C	Sep O-C
DAM 942	17103+2856	281.8514050	4.869160858	281.6	4.96	0.251405041	-0.09083914
UC 3340	17264+1352	89.3172991	6.714171699	90.6	6.7	-1.282700865	0.01417170
STF3086	14323+1718	270.6470147	5.313356728	271.2	5.72	-0.552985314	-0.40664327
BAL1899	14286+0144	235.5691116	6.198730270	236.8	6.02	-1.230888395	0.17873027
J 1611	14121-0846	338.1479712	6.187944533	337.5	6.47	0.647971162	-0.28205547

characteristics suggested to me that I shall be able to get good enough accuracy for double stars down to a few arcseconds, but I wanted to confirm this by test measurements. I first decided to test the accuracy around 5 - 6 arcseconds and I selected 5 low speed doubles with recent measurements and separation close to my target separation limit. Initially I planned to use some calibration doubles for this process, but unfortunately I was unable to find appropriate objects to meet both separation and visibility constraints for my observatory in the desired timeframe. I present the list of these measurements in Table 1. For a better overview of the results, I also built two graphs presenting the PA differences (Figure 1) and separation differences (Figure 2).

As can be seen in the presented data and graphs, the average errors are 0.79 degrees in PA and 0.19 arcseconds in separation. Maximal errors obtained on the test sample are 1.28 degrees in PA and 0.41 arcseconds in separation. The obtained error values seem to be good enough to consider that measuring doubles down to 5 arcseconds with this equipment provides enough precision of the data.

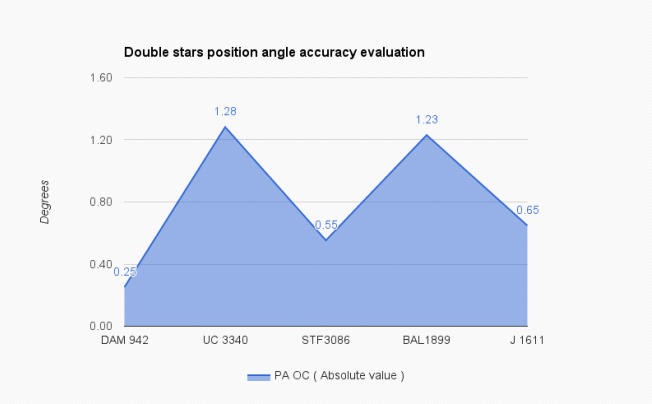

Figure 1. Position Angle differences for five selected comparison objects

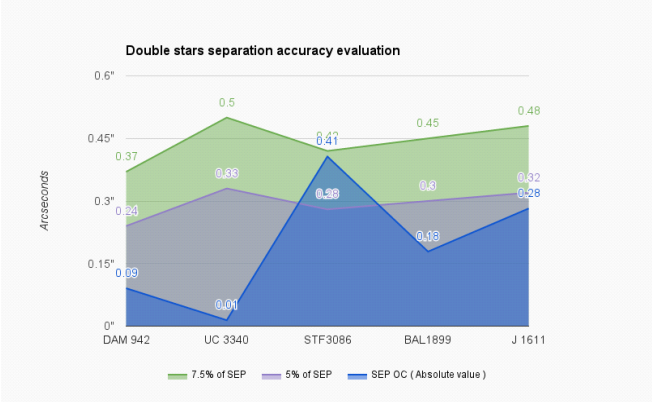

Figure 2. Separation differences for five selected comparision objects

The Measurements

In the next tables, I present the obtained measurements. Please note that all the magnitudes presented are taken from WDS and not measured on images.

Neglected Measurements

In Table 2 I present a list of neglected double stars measured with the described methods.

Missing and erroneous objects:

As in almost any neglected doubles hunt, I found pretty much objects with different issues which can not be measured for various reasons. I will list them here with my notes:

- Objects where the main star is on precise position but no secondary candidate can be identified: **BAR44 , LDS 9104, POU 5843, LDS 6054, SCA 122, BU 1124 AB,POU 310**
- Objects where even the main star can not be identified in the precise position neither in neighborhood: **LDS 6123, LDS 5336, LDS 2959, SCA 145, HDO 158**
- The secondary not found on my images, but close to expected position there is a very faint star barely visible in survey images with Aladin software[3]. Clearly the secondary is much weaker than catalog and also weaker than my magnitude limit (16) : **POU 635 , LDS1174 AC, HL 24, SLE349 AC**
- There is no object on the position. But there is an object that is matching closely by separation and PA in the neighborhood. Still the secondary star is much more fainter than the catalog value and it drops under the magnitude limit of my image (16) . The pair was identified with Aladin but I'm unable to precisely measure it on my image due to the presented reasons. The correct position of the main star is 23 52 26.998 +24 17 26.59 I presume having last measurements for more than 100 years is plausible that the precise position has a little shift: **POU 5868**
- Main star found . A secondary found at 77 arcsec instead of 18. Having the last observations older than one century some typo is not impossible if we consider 77/78 arcseconds are 1 minute and 17/18 arcseconds or even more simply 7 could be mistaken with 1. The difference on PA is 10 degrees which is not completely not plausible **BAL 2539** with my determinations at JD 2457570.5 being : PA=91.89718 and SEP=77.02532

Other Double Stars Measurements

In Table 3 I present a list of double stars measured with the described methods. These stars were not intentionally targeted. They were on the same FITS with at least one of the targeted objects, so it could be measured with minimal effort.

Acknowledgements

This research has made use of the Washington Double Star catalogs maintained at the U.S. Naval Observatory.

Data reduction was carried out using the Astrometrica software developed and maintained by Herbert Raab.

This research made use of the Aladin Sky Atlas developed at CDS, Strasbourg Observatory, France.

Table 2. Measured Neglected Double Stars

Name	RA+Dec	Mags	PA	Sep	Date	N	Notes
JSP 423	10430-5951	9.9; 10.7	270.5	2.24	2015.084	1	1
J 1200	18052+0645	12.4; 16.4	207.7	5.23	2016.499	1	
SLE 156	18209+0930	10.9; 11.3	340.7	87.49	2016.499	1	2
J 104AB	18435-0817	10.1; 13.8	98.2	14.61	2016.499	1	
KUI 87AD	18435-0817	10.1; 15.1	308.6	16.05	2016.499	1	
HO 115AB	19549+1715	11.7; 13.6	351.8	5.92	2016.499	1	
BEW 5	16561+0125	10.4; 13.7	187.4	9.69	2016.499	1	3
BU 1371AB	02193-0259	10.2; 13.7	69.0	73.56	2016.750	1	
BAL2922	18146+0422	12.0; 14.3	75.7	60.82	2016.499	1	
RST4268	05096-0356	11.1; 15.2	228.8	6.83	2016.846	1	

NOTES

1. This double is under my accuracy test limits so I can not guarantee for high accuracy in the measured values but since I had it in a field and I could identify it I decided to measure it because the object is neglected and not measured from 1964.
2. This is a strange object. There is no 10 arcsec double in the field. But there is one 1 minute separated double which have close magnitudes with the targeted one and a perfectly matching PA. More strangely the precise coordinates seems to point to the secondary from this pair. I presume the separation from catalog is wrong (all other stuff seems to match). In my determination the correct precise coordinates seems to be 18 20 57.477+09 28 32.89.
3. Main star precise coordinates seems a little wrong. In my determination the coordinates are 16 56 05.600 01 25 13.68

Double Star Measurements with an AltAz Telescope: Report for 2016

Table 3. Other Double Stars Found in Analyzed Images

Name	RA+Dec	Mags	PA	Sep	Date	N	Notes
H6 2AC	18006+0256	9.4; 11.2	142.2	55.07	2016.499	1	
BU 634CD	18006+0256	11.2; 13.9	120.0	6.24	2016.499	1	
BU 634AE	18006+0256	9.4; 13.7	179.7	45.12	2016.499	1	
SLE 349AB	18310+0648	12.4; 13.4	355.2	20.81	2016.499	1	
J 1372	18318+0641	13.8; 12.8	118.3	5.19	2016.499	1	
J 104AC	18435-0817	10.1; 13.7	195.4	39.30	2016.499	1	
SLE 237AF	18435-0817	10.1; 11.8	142.6	78.93	2016.499	1	
SLE 238	18441-0817	12.1; 11.5	67.7	11.68	2016.499	1	
SLE 236	18434-0814	12.1; 12.4	294.8	10.60	2016.499	1	
BRT 483	18425-0807	14.3; 13.2	48.8	4.08	2016.499	1	
HO 115AC	19549+1715	11.7; 12.4	84.5	49.15	2016.499	1	
BAL1560	20281+0140	11.7; 14.7	3.3	6.56	2016.499	1	
POU5840	23397+2359	10.5; 12.7	175.4	19.82	2016.698	1	
HJ 291	22050+1128	12.9; 12.1	264.4	8.67	2016.698	1	1
HJ 290A		13.4; 13.8	281.4	12.15	2016.698	1	2
SCA 149	23151+0348	10.4; 10.9	19.7	65.86	2016.698	1	
BAL 948	00531+0100	13.0; 13.5	53.3	8.02	2016.750	1	
H6 1AC	02193-0259	10.2; 10.3	68.3	123.80	2016.750	1	
STG 1AD	02193-0259	10.2; 13.1	324.2	165.57	2016.750	1	
H6 1BC	02193-0259	13.7; 10.3	67.2	50.26	2016.750	1	
HL 32AC	03497+2343	8.6; 12.7	201.7	117.07	2016.846	1	
HL 27AB	03489+2351	8.7; 14.8	241.9	78.68	2016.846	1	
POU 649	05182+2411	16.1; 14.6	90.7	10.18	2016.846	1	3
POU 659	05194+2433	11.8; 14.1	124.4	16.47	2016.846	1	
POU 387	04056+2330	11.7; 13.0	215.8	8.78	2016.898	1	
POU 385	04053+2337	11.1; 14.0	7.8	16.68	2016.898	1	

Table Notes:

1. The main component as indicated by the coordinates seems to be the fainter star from the combination. Still the other measurements indicated as the brightest. The difference is not big. I presume there was a mistake in deciding the primary or the magnitudes has changed in time (maybe one of the stars from the pair is variable)
2. This object is missing in the last WDS catalogue. Still it is present in the old versions at the precise position but with brighter magnitudes (I have magnitudes of 13.4 / 13.8 instead of 10/10.8 in the catalogue) and also the PA seems shifted with 180 (probably a quadrant computation error in the original observation)
3. Primary star weaker than secondary and weaker than catalog value. Secondary magnitude close to catatog magnitude

References

[1] Mason, D.B., Wycoff G.L., Hartkopf, W.I. Washington Double Star Catalog, USNO, 2015, http://www.usno.navy.mil/USNO/astrometry/optical-IR-prod/wds/WDS.

[2] Herbert Raab, Astrometrica software, http://www.astrometrica.at/.

[3] Aladin Sky Atlas software, http://aladin.u-strasbg.fr/.

[4] WDS Filter webtool, http://brasov.astroclubul.org/wdsfilter/.

[5] Lucian Curelaru, Ovidiu Tercu, Alexandru Dumitriu, Valentin Gavrila, Felician Ursache, Catalin Vladu, "Neglected Double Star Measurements at the Astronomical Observatory of the Natural Science Museum Galati", *Journal of Double Star Observations*, **8** (3), 201-209, 2012.

[6] UCAC Catalogue, http://www.usno.navy.mil/USNO/astrometry/optical-IR-prod/ucac.

[7] Astrometry.net, http://www.astrometry.net.

Jonckheere Double Star Photometry – Part XII: Mon I

Wilfried R.A. Knapp
Vienna, Austria
wilfried.knapp@gmail.com

John Nanson
Star Splitters Double Star Blog
Manzanita, Oregon
jnanson@nehalemtel.net

Abstract: If any double star discoverer is in urgent need of photometry then it is Jonckheere. There are over 3000 Jonckheere objects listed in the WDS catalog and a good part of them with magnitudes obviously far too bright. This report covers about half of the Jonckheere objects in the constellation Monoceros. At least one image per object was taken with V-filter to allow for visual magnitude measurement by differential photometry. All objects were additionally checked for common proper motion and about 10 qualify indeed as potential physical pairs.

Introduction

As follow up to the reports on J-objects photometry beginning with Knapp/Nanson 2016 we selected this time the J-objects in Monoceros. The number of J-objects in Mon is quite large and weather conditions did not allow for taking images for all objects so we decided to split this constellation into two separate reports with about 170 doubles covered in this paper including a few additional non Jonckheere objects by chance included in the images taken. Some objects were too close to be resolved with the equipment available to us but we kept these objects in the lists as we thought also the combined magnitude of interest.

Results of photometry and catalog checking

With a few exceptions for all selected J-objects one single image was taken with iTelescope iT27 with V-filter and 3s exposure time – iT27 was the telescope of choice because the constellation Mon is rather low in the northern sky and iT27 is located in Australia. The technical specifications of iT27 are even better than those of iT24 (our working horse telescope) but the image quality is overall not up to the expectations and plate solving was due to unexpected changes in image rotation and orientation from image to image a bit difficult so in hindsight this decision was despite the higher altitude of our targets not the best. While for these reasons the astrometry results have to be taken with caution beyond the given error range the effects seem less significant for the with V-filter measured magnitudes as a magnitude error of ~0.1 or even a bit larger seems negligible in comparison with those for the Jonckheere objects, which often have given magnitude errors in the range of up to 2 or more magnitudes. With the availability of precise GAIA positions for most of the listed components the value of astrometry results from processing of CCD images taken with traditional earth-bound telescopes seems anyway a bit questionable.

Several objects were too faint to be resolved with a 3s exposure time – additional images with longer exposure time were taken for these and stacked with AAVSO VPhot. The images were then plate solved with Astrometrica using the URAT1 catalog with reference stars in the Vmag range of 8.5 to 14.5 giving not only RA/Dec coordinates but also photometry results for all reference stars used including an average dVmag error. The J-objects were then located in the center of the image and astrometry/photometry was then done by the rather comfortable Astrometrica procedure with point and click at the components delivering RA/Dec coordinates and Vmag measurements based on all ref-

erence stars used for plate solving.

The measurement results are given in table 1 below with the following structure:

- First row gives the WDS data:
  - Name gives number and components of the J-object
  - RA/Dec gives the position in the HH:MM:SS/ DD:MM:SS format for the primary
  - Sep, PA, M1, M1, pmRA and pmDec give the WDS catalog data for this object
  - Date gives the year of the last observation
  - Source/Notes gives additional references to the WDS catalog
- Data rows give data from other checked catalogs like especially GAIA DR1:
  - RA/Dec gives the position in degrees for the primary
  - Sep gives the calculated separation in arcseconds if coordinates for both components are available
  - PA gives the calculated position angle in degrees if coordinates for both components are available
  - M1 and M2 if visual magnitudes are given in the used catalog or estimated visual magnitudes according to Knapp and Nanson 2018
  - Proper motion data if available in the used catalogs or in some cases calculated from position comparison between catalog positions
  - Ap and Me give aperture and used observation method
  - CPM Rat gives the common proper motion rating based on the available PM data according to the description in Appendix A
  - CPM % gives an estimated probability for being a physical pair (see Appendix A)
  - Source/Notes refers to the used catalogs with additional comments if necessary
- Measurement row gives the results from processing of own images:
  - RA/Dec gives the position in degrees for the primary
  - Sep gives the calculated separation in arcseconds for resolved pairs
  - PA gives the calculated position angle in degrees for resolved pairs
  - M1 and M1 give Vmags for both components measured by differential photometry
  - Date gives the Julian observation epoch
  - Notes indicate the telescope used, number of images with exposure time and additional comments if considered necessary.

Summary

A good part of the listed J-objects in Mon show the expected significant magnitude difference compared with the WDS catalog data. Further about 10 of these objects qualify as solid or at least good CPM candidates based on a rating scheme using UCAC5 proper motion data if for both components available with the caveat of rather small proper motion values for some of them. For objects with G/J/H/K-magnitude values available we calculated also estimated visual magnitudes according to Knapp and Nanson 2018 to compare these estimated values with the results of the differential photometry as kind of proof of concept for this formula and found a very consistent pattern confirming the high quality of the calculated estimated Vmags.

Acknowledgements

The following tools and resources have been used for this research:

2MASS catalog
2MASS images
AAVSO VPhot
Aladin Sky Atlas v9.0
Astrometrica v4.10.0.427
AstroPlanner v2.2
iTelescope

iT24: 610mm CDK with 3962mm focal length. Resolution 0.625 arcsec/pixel. V-filter. No transformation coefficients available. Located in Auberry, California. Elevation 1405m

iT27: 700mm CDK with 4531mm focal length. CCD: FLI PL09000. Resolution 0.53 arcsec/pixel. V-filter. Siding Spring, Australia. Elevation 1122m

GAIA DR1 catalog
MaxIm DL6 v6.08
POSS images
SIMBAD
UCAC4 catalog
UCAC5 catalog
URAT1 catalog
VizieR
Washington Double Star Catalog

References

Knapp, Wilfried R. A.; Nanson, John, 2016, "Jonckheere Double Star Photometry – Part I: Cyg", *Journal of Double Star Observations*, **12** (2), 68-179.

(Text continues on page 640)

Table 1. Measurement Results for J objects in Monoceros

Name	RA	Dec	Sep	PA	M1	M2	pmRA1	pmDec1	e_pm1	pmRA2	pmDec2	e_pm2	Ap	Me	Date	CPM Rat	CPM %	Source/Notes
J 21 AB	07 02 18.811	+10 30 47.9	3.2	277	10.59	11.20	73	-13							2016			WDS 07023+1030, WDS data as of August 2017.
	105.578377	10.513308	3.242	274.905	10.64	11.09	1.10	-3.30	1.56	-4.00	-2.80	3.11	0.96	Hg	2015.000	CCCB	**6**	GAIA DR1. M1 and M2 are visual estimate from G-J-K-H mags. PM data from UCAC5 catalog
	105.578372	10.513321	3.170	274.887									0.20	Eu	2000.888			UCAC5.
	105.578271	10.513347	3.237	276.741	10.68	11.08							0.70	C	2016.022			iT27 1x3s
J 40 AB	06 41 49.391	-00 15 59.1	3.1	102	11.27	11.90	-47	9							2000			WDS 06418-0016, WDS data as of August 2017.
	100.455764	-0.266428	3.154	102.377	10.97	11.82	-0.50	-0.90	1.56	-0.30	-1.00	1.70	0.96	Hg	2015.000	CACC	**15**	GAIA DR1. M1 is visual estimate from G-J-K-H mags, M2 is GAIA DR1 Gmag (secondary not identified in 2MASS and URAT1). PM data from UCAC5 catalog
	100.455766	-0.266424	3.151	102.369									0.20	Eu	200.100			UCAC5.
	100.455825	-0.266406	2.909	108.435	11.08	11.73							0.70	C	2016.096			iT27 1x3s. Touching star disks
J 55 AB	06 49 36.610	+01 59 54.2	2.2	166	10.85	11.16	-5	-1							1995			WDS 06496+0200, WDS data as of August 2017.
	102.402499	1.998374			11.14		-9.56	-0.86	1.92				0.96	Hg	2015.000			GAIA DR1. M1 is visual estimate from G-J-K-H mags. PM data from GAIA DR1 catalog. Secondary not identified in GAIA DR1.
	102.402361	1.999066					-8.00	0.30	4.38				0.20	Eu	200.122			UCAC5. PM data from UCAC5 catalog. Secondary not identified in UCAC5.
													0.70	C				iT Vmag Data
	102.402350	1.999014	2.486	167.816	10.71	10.71							0.70	C	2016.090			iT27 1x3s. Touching star disks
J 56 AB	06 52 37.649	+03 14 17.8	1.5	334	9.39	9.72	-3	-2		-3	-2				2015			WDS 06526+0314, WDS data as of August 2017.
	103.156890	3.238159	1.546	332.907	9.67	9.59	16.05	-40.64	5.61				0.96	Hg	2015.000			GAIA DR1. M1 is visual estimate from G-J-K-H mags, M2 is GAIA DR1 Gmag. PM data from position comparison with 2MASS. Secondary not identified in 2MASS or URAT1.
													0.20	Eu				UCAC5. Neither component identified in UCAC5.
	103.156763	3.238394			8.91								0.70	C	2016.022			iT27 1x3s. Overlapping star disks. A and B too bright for resolution
J 60 AB	07 13 14.080	-02 38 35.8	1.3	38	9.44	9.47	-5	4		-5	4				1991			WDS 07132-0239, WDS data as of August 2017.
	108.308469	-2.643527	1.288	34.144	8.93	9.47	-12.42	4.38	6.17				0.96	Hg	2015.000			GAIA DR1. M1 and M2 are GAIA DR1 Gmag. PM data from position comparison with 2MASS. Secondary not identified in 2MASS. URAT1 Gmag is questionable relative to GAIA DR1 Gmag, so didn't use it.
													0.20	Eu				UCAC5. Neither component identified in UCAC5.
	108.308542	-2.643483			8.76								0.70	C	2016.107			iT27 1x3s. Heavily overlapping star disks. Both components too bright for resolution

Table 1 continues on the next page.

Table 1 (continued). Measurement Results for J objects in Monoceros

Name	RA	Dec	Sep	PA	M1	M2	pmRA1	pmDec1	e_pm1	pmRA2	pmDec2	e_pm2	Ap	Me	Date	CPM Rat	CPM %	Source/Notes
J 65 AB	07 44 12.580	-01 15 13.0	2.1	210	9.86	10.72	3	-7		3	-7				1995			WDS 07442-0115, WDS data as of August 2017.
	116.052465	-1.253493	2.069	211.068	10.16	10.61	5.20	7.26	5.26				0.96	Hg	2015.000			GAIA DR1. M1 is visual estimate from G-J-K-H mags, M2 is GAIA DR1 Gmag. PM data from position comparison with 2MASS. Secondary not identified in 2MASS or URAT1.
	116.052436	-1.253520					7.00	6.50	1.84				0.20	Eu	2000.118			UCAC5. PM data from UCAC5 catalog. Secondary not identified in UCAC5.
	116.052458	-1.253531			9.77								0.70	C	2016.022			iT27 1x3s. Heavily overlapping star disks. Both components too bright for clear resolution
J 66 AB	07 47 40.890	-00 54 23.3	3.9	196	10.54	11.58	0	5		-2	-1				2000			WDS 07477-0056, WDS data as of August 2017.
	116.920319	-0.906510	3.872	196.226	10.30	11.54	-5.00	-0.80	1.56	-4.90	-1.40	3.25	0.96	Hg	2015.000	CACB	**16**	GAIA DR1. M1 and M2 are visual estimates from G-J-K-H mags. PM data from UCAC5 catalog
	116.920340	-0.906507	3.864	196.285									0.20	Eu	2000.128			UCAC5.
	116.920338	-0.906517	3.856	195.801	10.44	11.55							0.70	C	2016.022			iT27 1x3s
																		GAIA DR1 lists a parallax of 1.5 (2174.421 LY) for the primary and 1.45 (2249.401 LY) for the secondary, which would indicate the two stars are too far apart for any physical relation to exist. (Parallax errors are listed as 0.62 and 0.33, respectively).
J 187 AB	06 06 38.740	-04 11 37.8	29.5	145	5.38	11.60	-8	-5		6	-21				2010			WDS 06066-0412, WDS data as of August 2017.
	91.661375	-4.193836	29.507	145.305	5.52	11.49	-9.28	-3.69	5.58	1.37	-14.37	5.58	0.20	Eu	2014.035	CCCC	**6**	URAT1. M1 and M2 are visual estimates from URAT1 J- and K-Bands. PM data from position comparison with 2MASS.
						11.60							0.96	Hg	2015.000			GAIA DR1. M2 is visual estimate from G-J-K-H mags. Primary not identified by GAIA DR1.
										3.50	-16.80	1.41	0.20	Eu	2000.036			UCAC5. Primary not identified by UCAC5, PM data for secondary from UCAC5 catalog.
	91.661296	-4.193733	29.908	145.339		11.64							0.70	C	2016.164			iT27 1x3s. Primary star disc saturated
J 189 AB	07 45 34.360	-05 58 30.0	1.5	240	10.15	10.20	4	12							1983			WDS 07456-0559, WDS data as of August 2017.
	116.393177	-5.974959			10.38								0.96	Hg	2015.000			GAIA DR1. M1 is visual estimate from G-J-K-H mags. Secondary not identified in GAIA DR1.
	116.393143	-5.975019					8.20	14.40	1.70				0.20	Eu	2000.087			UCAC5. PM data from UCAC5 catalog. Secondary not identified in UCAC5.
	116.393092	-5.975000			10.18								0.70	C	2016.096			iT27 1x3s. No resolution of B
																		Note: Secondary not identified in URAT1 or 2MASS.
J 265 AB	06 35 46.310	+05 07 23.3	4.2	242	11.18	11.70	61	32							2010			WDS 06358+0508, WDS data as of August 2017.
	98.943006	5.123096	4.077	243.343	11.25	11.93	1.30	-2.90	1.70	-4.30	8.30	1.70	0.96	Hg	2015.000	BCCB	**25**	GAIA DR1. M1 and M2 are visual estimates from G-J-K-H mags. PM data from UCAC5 catalog.
	98.943000	5.123108	4.081	240.736									0.20	Eu	2000.155			UCAC5.
	98.943008	5.123078	4.089	244.971	11.23	11.96							0.70	C	2016.022			iT27 1x3s

Table 1 continues on the next page.

Table 1 (continued). Measurement Results for J objects in Monoceros

Name	RA	Dec	Sep	PA	M1	M2	pmRA1	pmDec1	e_pm1	pmRA2	pmDec2	e_pm2	Ap	Me	Date	CPM Rat	CPM %	Source/Notes
J 266 AB	06 36 41.070	+03 18 56.8	4.5	176	9.65	12.00	1	9		1	-8				2000			WDS 06367+0319, WDS data as of August 2017.
	99.171143	3.315769			9.71		1.03	-4.46	1.92				0.96	Hg	2015.000			GAIA DR1. M1 is visual estimate from G-J-K-H mags. PM data from GAIA DR1 catalog. Secondary not identified in GAIA DR1.
	99.171138	3.315788					1.20	-4.60	1.70				0.20	Eu	2000.138			UCAC5. PM data from UCAC5 catalog. Secondary not identified in UCAC5.
	99.171125	3.315758	4.438	174.773	9.57	11.30							0.70	C	2016.022			iT27 1x3s
																		Note: Secondary not identified in URAT1; both components are identified in 2MASS.
J 314 AB	06 47 07.320	-03 51 30.4	3.7	48	11.40	13.40	1	-1							2000			WDS 06472-0351, WDS data as of August 2017.
	101.780506	-3.858482	3.743	47.988	11.32	13.45	0.20	-1.70	1.63	0.30	-0.60	2.05	0.96	Hg	2015.000	CCCC	**6**	GAIA DR1. M1 and M2 are visual estimates from G-J-K-H mags. PM data from UCAC5 catalog.
	101.780506	-3.858475	3.730	48.163									0.20	Eu	2000.079			UCAC5.
	101.780500	-3.858492	3.584	47.307	11.45	13.35							0.70	C	2016.164			iT27 1x3s
J 348 AB	06 29 49.170	+11 07 49.8	3.7	144	12.67	12.89	-6	13		6	-14				2003			WDS 06299+1110, WDS data as of August 2017.
	97.454715	11.130877	3.849	141.644	12.59	12.80	-7.10	10.20	1.70	-6.90	10.20	1.70	0.96	Hg	2015.000	AACB	**78**	GAIA DR1. M1 and M2 are visual estimates from G-J-K-H mags. PM data from UCAC5 catalog
	97.454744	11.130837	3.846	141.689									0.20	Eu	2000.890			UCAC5.
	97.454750	11.130867	3.617	141.491	12.53	12.74							0.70	C	2016.022			iT27 1x3s
																		Good CPM candidate with qualifier that UCAC5 error rates are somewhat high given the minimal proper motion of the components.
J 349 AB	06 32 59.371	+04 56 22.4	5.5	100	9.63	11.60	-4	4		5	1				2014			WDS 06330+0457, WDS data as of August 2017.
	98.247395	4.939586	5.461	100.317	9.60	12.07	-2.10	1.40	1.98	-3.80	-2.30	4.17	0.96	Hg	2015.000	ACCC	**30**	GAIA DR1. M1 and M2 are visual estimates from G-J-K-H mags. PM data from UCAC5 catalog. Error rates high relative to minimal motion.
	98.247404	4.939580	5.476	99.704									0.20	Eu	2000.147			UCAC5.
	98.247408	4.939594	5.463	100.868	9.60	12.17							0.70	C	2016.022			iT27 1x3s
J 350 AB	06 35 41.829	+00 29 31.1	3.7	103	9.50	9.50	-21	11							2002			WDS 06357+0029, WDS data as of August 2017.
	98.923851	0.492130	3.681	105.656	12.42	12.62	0.90	5.50	1.41	1.40	3.90	1.41	0.96	Hg	2015.000	CCCB	**6**	GAIA DR1. M1 and M2 are visual estimate from G-J-K-H mags. PM data from UCAC5 catalog.
	98.923847	0.492108	3.666	105.339									0.20	Eu	2000.100			UCAC5.
	98.923913	0.492203	3.395	108.195	12.38	12.59							0.70	C	2016.096			iT27 1x3s
J 351 AB	06 37 58.389	+11 33 19.1	3.6	208	10.81	12.70	-4	-4							2000			WDS 06380+1135, WDS data as of August 2017.
	99.493287	11.555327	3.587	208.326	10.60	12.96	-5.80	-7.30	1.70	-5.90	-4.80	4.68	0.96	Hg	2015.000	CCCB	**6**	GAIA DR1. M1 and M2 are visual estimates from G-J-K-H mags. PM data from UCAC5 catalog.
	99.493310	11.555355	3.618	208.035									0.20	Eu	2000.911			UCAC5.
	99.493313	11.555333	3.681	209.936	10.67	12.79							0.70	C	2016.022			iT27 1x3s
J 352 AB	06 38 39.990	-08 15 37.8	4.7	93	10.22	12.70	-7	-2							2010			WDS 06386-0815, WDS data as of August 2017.
	99.666653	-8.260511	4.588	94.360	10.08	12.46	-3.10	1.00	1.56	-4.30	1.50	2.05	0.96	Hg	2015.000	ACCC	**30**	GAIA DR1. M1 and M2 are visual estimates from G-J-K-H mags. PM data from UCAC5 catalog. Error rates high relative to minimal motion.
	99.666666	-8.260515	4.607	94.446									0.20	Eu	2000.017			UCAC5.
	99.666675	-8.260533	4.459	92.828	10.35	12.56							0.70	C	2016.172			iT27 1x3s

Table 1 continues on the next page.

Table 1 (continued). Measurement Results for J objects in Monoceros

Name	RA	Dec	Sep	PA	M1	M2	pmRA1	pmDec1	e_pm1	pmRA2	pmDec2	e_pm2	Ap	Me	Date	CPM Rat	CPM %	Source/Notes
J 354 AB	06 53 51.779	+01 43 28.2	6.0	264	9.50	10.50	-2	-2		-44	-13				2014			WDS 06539+0144, WDS data as of August 2017.
	103.465759	1.724496	5.924	262.875	11.65	13.09	-3.80	-4.40	1.41	0.60	-1.20	1.56	0.96	Hg	2015.000	CCCC	**6**	GAIA DR1. M1 and M2 are visual estimate from G-J-K-H mags. PM data from UCAC5 catalog
	103.465774	1.724514	5.995	262.505									0.20	Eu	2000.125			UCAC5.
	103.465788	1.724461	5.944	263.625	11.73	13.15							0.70	C	2016.090			iT27 1x3s
J 360 AB	07 05 11.330	+00 54 01.5	3.8	30	11.78	12.73	-5	-10		-7	50				2000			WDS 07052+0054, WDS data as of August 2017.
	106.297071	0.900133	3.845	29.714	12.05	12.47	-2.50	-0.80	1.70	-3.10	0.10	1.70	0.96	Hg	2015.000	CCCC	**6**	GAIA DR1. M1 and M2 are visual estimate from G-J-K-H mags. PM data from UCAC5 catalog
	106.297081	0.900136	3.836	29.925									0.20	Eu	2000.117			UCAC5.
	106.297063	0.900192	3.670	29.635	12.22	12.55							0.70	C	2016.090			iT27 1x3s
J 363 AB	07 16 02.840	-06 36 52.1	2.8	292	10.60	12.80	3	1							2000			WDS 07161-0637, WDS data as of August 2017.
	109.011837	-6.614480			10.61		-2.30	0.74	1.92				0.96	Hg	2015.000			GAIA DR1. M1 is visual estimate from G-J-K-H mags. PM data from GAIA DR1 catalog. Secondary not identified in GAIA DR1.
	109.011840	-6.614484					-0.80	1.00	1.70				0.20	Eu	2000.067			UCAC5. PM data from UCAC5 catalog. Secondary not identified in UCAC5.
	109.011833	-6.614486			10.65								0.70	C	2016.164			iT27 1x3s. Hint of elongation but no resolution of B
																		Note: Secondary not identified by URAT1 or 2MASS.
J 364 AB	07 16 09.540	-06 34 38.8	5.3	340	9.40	13.00	3	-18		-22	25				2000			WDS 07162-0634, WDS data as of August 2017.
	109.039701	-6.577413	5.272	339.779	11.19	13.67	-4.50	0.30	1.84	-5.50	-0.50	3.96	0.96	Hg	2015.000	ACCC	**30**	GAIA DR1. M1 and M2 are visual estimate from G-J-K-H mags. PM data from UCAC5 catalog. Error rates high relative to minimal motion.
	109.039719	-6.577414	5.278	339.989									0.20	Eu	2000.069			UCAC5.
	109.039708	-6.577444	5.156	339.529	11.08	13.62							0.70	C	2016.164			iT27 1x3s
J 365 AB	07 17 17.130	-06 35 27.0	3.2	262	12.57	14.80	27	5							2000			WDS 07173-0635, WDS data as of August 2017.
	109.321354	-6.590867	3.053	264.716	12.84	14.33	-8.40	-6.90	1.77	2.40	2.20	9.14	0.96	Hg	2015.000	BCCB	**25**	GAIA DR1. M1 is visual estimate from UCAC5 G-J-K-H mags, M2 is GAIA DR1 Gmag (secondary not identified in 2MASS and URAT1). PM data from UCAC5 catalog. Error rate of secondary unusually high.
	109.321389	-6.590838	3.228	262.573									0.20	Eu	2000.069			UCAC5. No J-K-H mags in UCAC5 for the secondary.
	109.321358	-6.590919	2.072	271.106	12.84	14.93							0.70	C	2016.164			iT27 1x3s. Touching star disks, B barely resolved. SNR B<10
J 417 AB	07 40 11.870	-08 56 18.8	1.9	356	11.01	13.00	-4	-5							1911			WDS 07402-0857, WDS data as of August 2017. Only one observation (1911) in WDS, but not coded X.
	115.049468	-8.938581			10.79								0.96	Hg	2015.000			GAIA DR1. M1 is visual estimate from G-J-K-H mags. Secondary not identified in GAIA DR1.
	115.049478	-8.938564					-2.30	-4.20	1.56				0.20	Eu	2000.063			UCAC5. PM data from UCAC5 catalog. Secondary not identified in UCAC5.
	115.049458	-8.938561			10.88								0.70	C	2016.164			iT27 1x3s. Slightest hint of elongtion but no resolution of B

Table 1 continues on the next page.

Table 1 (continued). Measurement Results for J objects in Monoceros

Name	RA	Dec	Sep	PA	M1	M2	pmRA1	pmDec1	e_pm1	pmRA2	pmDec2	e_pm2	Ap	Me	Date	CPM Rat	CPM %	Source/Notes
J 595 AB	06 26 24.319	+11 27 47.5	4.8	42	10.81	10.80	-3	12		0	16				2016			WDS 06264+1128, WDS data as of August 2017.
	96.601338	11.463268	4.807	42.206	10.72	10.95	-5.10	9.00	1.41	-4.10	8.00	2.55	0.96	Hg	2015.000	ACCB	**31**	GAIA DR1. M1 and M2 are visual estimates from G-J-K-H mags. PM data from UCAC5 catalog
	96.601358	11.463233	4.808	41.972									0.20	Eu	2000.890			UCAC5.
	96.601329	11.463242	4.879	41.750	10.76	10.97							0.70	C	2016.022			iT27 1x3s
																		Note: GAIA DR1 shows a parallax of 4.04 (807.334 LY) for the primary; no parallax for the secondary, B, is shown.
J 595 AC	06 26 24.319	+11 27 47.5	43.7	245	10.81	10.96	-3	12		2	-1				2016			WDS 06264+1128, WDS data as of August 2017.
	96.601338	11.463268	43.970	244.721	10.70	10.76	-5.10	9.00	1.41	3.30	-5.60	1.41	0.96	Hg	2015.000	ACCC	**30**	GAIA DR1. M1 and M2 are visual estimate from G-J-K-H mags. PM data from UCAC5 catalog
	96.601358	11.463233	43.990	245.031									0.20	Eu	2000.890			UCAC5.
	96.601329	11.463242	43.783	244.673	10.76	10.88							0.70	C	2016.022			iT27 1x3s
																		Note: GAIA DR1 shows a parallax of 4.04 (807.334 LY) for the primary and a parallax of 0.34 (9593 LY) for the secondary, C, which indicates the absence of any physical relation between the two stars (parallax errors are 0.25 and 0.84, respectively).
J 596 AB	06 41 03.801	+02 14 21.4	5.0	48	10.60	11.00	6	-2		40	26				2010			WDS 06410+0215, WDS data as of August 2017.
	100.265846	2.239279	4.898	47.053	10.68	11.14	-2.20	-2.50	1.56	1.30	-1.80	3.25	0.96	Hg	2015.000	BCCC	**24**	GAIA DR1. M1 and M2 are visual estimates from G-J-K-H mags. PM data from UCAC5 catalog.
	100.265855	2.239289	4.853	46.721									0.20	Eu	2000.118			UCAC5.
	100.265871	2.239272	4.804	46.116	10.79	11.18							0.70	C	2016.090			iT27 1x3s
J 597 AB	06 41 21.619	+02 06 05.8	5.3	52	10.27	10.90	0	1		1	-6				2010			WDS 06414+0206, WDS data as of August 2017.
	100.340116	2.101614	5.167	52.582	10.25	10.87	-0.50	1.70	1.56	-0.80	-4.60	3.25	0.96	Hg	2015.000	CCCC	**6**	GAIA DR1. M1 and M2 are visual estimates from G-J-K-H mags. PM data from UCAC5 catalog.
	100.340118	2.101607	5.229	51.811									0.20	Eu	2000.118			UCAC5.
	100.340142	2.101589	5.062	53.089	10.42	10.93							0.70	C	2016.090			iT27 1x3s
J 659 AB	06 28 40.529	+04 52 47.3	1.9	240	10.51	12.30	4	-3							1992			WDS06287+0452, WDS data as of August 2017.
	97.168910	4.879846			10.53		-4.06	-3.72	1.92				0.96	Hg	2015.000			GAIA DR1. GAIA DR1. M1 is visual estimate from G-J-K-H mags. PM data from UCAC5 catalog. PM data from GAIA DR1 catalog. Secondary not identified in GAIA DR1.
	97.168924	4.879850					-3.30	-0.90	1.56				0.20	Eu	2000.138			UCAC5. PM data from UCAC5 catalog. Secondary not identified in UCAC5.
	97.168929	4.879828	1.882	243.828	10.49	11.15							0.70	C	2016.022			iT27 1x3s. Touching/overlapping star disks
																		Note: Secondary not identified by URAT1 or 2MASS.
J 660 AB	06 28 40.801	+04 50 11.9	2.5	99	10.29	10.40	-19	-15		0	-17				2008			WDS 06287+0448, WDS data as of August 2017.
	97.169701	4.836627	2.633	97.351	10.07	10.25	0.20	-12.80	1.70	2.70	-12.50	2.26	0.96	Hg	2015.000	CACB	**16**	GAIA DR1. M1 and M2 are GAIA DR1 Gmags (primary not identified in 2MASS and URAT1, URAT1 Gmag for secondary different from GAIA DR1). PM data from UCAC5 catalog
	97.169700	4.836680	2.597	97.542									0.20	Eu	2000.136			UCAC5. No J-K-H mags in UCAC5 for the primary.
	97.169700	4.836681	2.589	99.113	10.19	10.27							0.70	C	2016.022			iT27 1x3s. Touching star disks

Table 1 continues on the next page.

Table 1 (continued). Measurement Results for J objects in Monoceros

Name	RA	Dec	Sep	PA	M1	M2	pmRA1	pmDec1	e_pm1	pmRA2	pmDec2	e_pm2	Ap	Me	Date	CPM Rat	CPM %	Source/Notes
J 690 AB	06 30 47.051	+10 03 46.6	1.7	359	9.38	10.82	-6	-16		-6	-16				2015			WDS06308+1004, WDS data as of August 2017.
	97.696055	10.062879			9.32		-2.49	-5.03	1.92				0.96	Hg	2015.000			GAIA DR1. GAIA DR1. M1 is visual estimate from G-J-K-H mags. PM data from UCAC5 catalog. PM data from GAIA DR1 catalog. Secondary not identified in GAIA DR1.
	97.696055	10.062943					0.10	-16.50	2.26				0.20	Eu	2000.879			UCAC5. PM data from UCAC5 catalog. Secondary not identified in UCAC5.
	97.696117	10.062922			9.27								0.70	C	2016.022			iT27 1x3s. Hint of elongation but no resolution of B
																		Note: Secondary not identified by URAT1 or 2MASS.
J 691 AB	06 30 52.431	+04 38 59.7	1.3	205	9.40	10.37	-1	-5		-1	-5				2008			WDS 06309+0439, WDS data as of August 2017.
	97.718477	4.649950			9.46								0.96	Hg	2015.000			GAIA DR1. GAIA DR1. M1 is visual estimate from G-J-K-H mags. PM data from UCAC5 catalog. Secondary not identified in GAIA DR1.
	97.718469	4.649894					1.80	13.60	2.69				0.20	Eu	2000.144			UCAC5. PM data from UCAC5 catalog. Secondary not identified in UCAC5.
	97.718425	4.649944			9.25								0.70	C	2016.022			iT27 1x3s. Hint of elongation but no resolution of B
																		Note: Secondary not identified by URAT1 or 2MASS.
J 697 AB	06 43 33.811	+11 09 04.6	2.0	182	9.15	10.53	-2	1		-2	1				2015			WDS 06436+1109, WDS data as of August 2017.
	100.890860	11.151347			9.21								0.96	Hg	2015.000			GAIA DR1. GAIA DR1. M1 is visual estimate from G-J-K-H mags. PM data from UCAC5 catalog. Secondary not identified in GAIA DR1.
	100.890869	11.151312					-2.30	9.00	2.83				0.20	Eu	2000.895			UCAC5. PM data from UCAC5 catalog. Secondary not identified in UCAC5.
	100.890825	11.151358	2.001	181.686	9.04	9.96							0.70	C	2016.022			iT27 1x3s. Touching star disks
																		Note: Secondary not identified by URAT1 or 2MASS.
J 700 AB	06 54 44.440	+10 14 47.4	1.7	103	9.50	9.50				18	-3				2011			WDS 06547+1014, WDS data as of August 2017.
	103.685103	10.246579	3.031	106.884	12.00	12.06	-4.60	5.00	1.56	-4.40	3.20	1.63	0.96	Hg	2015.000	CCCB	**6**	GAIA DR1. M1 is visual estimate from G-J-K-H mags, M2 is GAIA DR1 Gmag (secondary not identified in 2MASS and URAT1). PM data from UCAC5 catalog. Error rate of secondary unusually high.
	103.685122	10.246559	3.020	106.444									0.20	Eu	2000.883			UCAC5.
	103.685096	10.246558	2.841	104.890	11.89	12.21							0.70	C	2016.022			iT27 1x3s. Touching star disks

Table 1 continues on the next page.

Table 1 (continued). Measurement Results for J objects in Monoceros

Name	RA	Dec	Sep	PA	M1	M2	pmRA1	pmDec1	e_pm1	pmRA2	pmDec2	e_pm2	Ap	Me	Date	CPM Rat	CPM %	Source/Notes
J 723 AB	06 45 03.419	+09 58 31.0	2.3	74	11.20	13.00	-3	-6							2000			WDS 06450+0958, WDS data as of August 2017.
	101.264239	9.975243	2.331	73.604	11.98	12.18	2.20	-6.80	1.84	10.30	-6.50	3.11	0.96	Hg	2015.000	CCCB	**6**	GAIA DR1. M1 is visual estimate from G-J-K-H mags, M2 is GAIA DR1 Gmag (secondary not identified in 2MASS and URAT1). PM data from UCAC5 catalog
	101.264230	9.975270	2.221	72.897									0.20	Eu	2000.880			UCAC5. No J-K-H mags in UCAC5 for the secondary.
	101.264196	9.975294	2.192	76.010	11.64	11.96							0.70	C	2016.022			iT27 1x3s. Touching star disks
J 726 AB	06 46 51.920	+10 10 00.2	2.3	128	9.50	9.50	-2	-14							2008			WDS 06468+1008, WDS data as of August 2017.
	101.716349	10.166654			12.26		-10.26	-6.71	1.92				0.96	Hg	2015.000			GAIA DR1. M1 is visual estimate from G-J-K-H mags. PM data from GAIA DR1 catalog. Secondary not identified in GAIA DR1.
	101.716388	10.166685					-9.80	-8.10	1.70				0.20	Eu	2000.882			UCAC5. PM data from UCAC5 catalog. Secondary not identified in UCAC5.
	101.715800	10.167081	2.641	131.494	12.22	11.93							0.70	C	2016.022			iT27 1x3s. Touching star disks
																		Note: Secondary not identified by URAT1 or 2MASS.
J 730 AB	07 18 20.250	-02 35 28.6	2.9	144	9.50	9.80	-16	-21							2000			WDS 07183-0236, WDS data as of August 2017.
	109.584505	-2.591624	3.080	147.406	11.58	11.87	10.30	-56.80	1.70	10.20	-59.30	1.70	0.96	Hg	2015.000	ABAA	**80**	GAIA DR1. M1 is visual estimate from G-J-K-H mags, M2 is GAIA DR1 Gmag (secondary not identified in 2MASS and URAT1). PM data from UCAC5 catalog
	109.584463	-2.591389	3.049	147.010									0.20	Eu	2000.099			UCAC5. No J-K-H mags in UCAC5 for the secondary.
	109.584571	-2.591597	2.751	154.855	11.27	11.83							0.70	C	2016.096			iT27 1x3s. Touching star disks
																		Note: Good CPM candidate. GAIA DR1 shows a parallax of 5.7 (572.216 LY) for the primary, but none listed for the secondary.
J 733 AB	08 05 33.421	-03 46 10.1	2.7	147	11.10	11.30	9	-12							2005			WDS 08055-0346, WDS data as of August 2017.
	121.389360	-3.769616			11.01		16.13	-24.08	1.92				0.96	Hg	2015.000			GAIA DR1. M1 is visual estimate from G-J-K-H mags. PM data from GAIA DR1 catalog. Secondary not identified in GAIA DR1.
	121.389312	-3.769530					11.50	-20.70	1.84				0.20	Eu	2000.110			UCAC5. PM data from UCAC5 catalog. Secondary not identified in UCAC5.
	121.389329	-3.769639	2.115	149.369	10.81	11.78							0.70	C	2016.022			iT27 1x3s. Touching/overlapping star disks. SNR B <20
																		Note: Secondary not identified by URAT1 or 2MASS.
J 741 AB	06 22 52.531	-08 12 34.2	3.6	91	10.90	12.60	-15	-1							2000			WDS 06228-0809, WDS data as of August 2017.
	95.718834	-8.209484	3.511	91.257	10.95	13.69	-1.60	0.50	1.56	-1.10	-0.70	2.05	0.96	Hg	2015.000	CCCC	**6**	GAIA DR1. M1 and M2 are visual estimates from G-J-K-H mags. PM data from UCAC5 catalog.
	95.718841	-8.209486	3.504	90.960									0.20	Eu	1999.998			UCAC5.
	95.718879	-8.209503	3.355	90.512	10.95	12.77							0.70	C	2016.172			iT27 1x3s. Touching star disks

Table 1 continues on the next page.

Table 1 (continued). Measurement Results for J objects in Monoceros

Name	RA	Dec	Sep	PA	M1	M2	pmRA1	pmDec1	e_pm1	pmRA2	pmDec2	e_pm2	Ap	Me	Date	CPM Rat	CPM %	Source/Notes
J 802 AB	06 46 43.570	-04 13 36.5	4.3	132	10.85	12.40	-2	23							2010			WDS 06468-0414, WDS data as of August 2017.
	101.681569	-4.226796	4.119	132.637	10.90	11.90							1.30	E2	1998.757			2MASS. M1 and M2 are visual estimates from 2MASS J- and K-bands.
	101.681592	-4.226736	4.247	135.630	11.11	11.47	5.32	14.00	5.54	1.39	-2.05	5.55	0.20	Eu	2014.068	CCCB	**6**	URAT1. M1 and M2 are visual estimates from URAT1 G-J-K-H mags. Note the URAT1 Vmags for the two components are identical, 10.431. PM data from comparison with 2MASS positions.
	101.681583	-4.226736	4.326	135.967	10.89	11.98							0.70	C	2016.164			iT27 1x3s
																		Note: Neither of the two components are identified in GAIA DR1 and UCAC5.
J 979 AB	06 30 34.200	+11 40 00.8	2.9	263	11.50	12.00	18	-7							2000			WDS 06306+1139, WDS data as of August 2017.
	97.642538	11.666820	2.984	262.603	11.24	12.26	9.20	-11.50	1.70	5.30	-12.70	1.84	0.96	Hg	2015.000	CBCB	**12**	GAIA DR1. M1 is visual estimate from G-J-K-H mags, M2 is GAIA DR1 Gmag (secondary not identified in 2MASS and URAT1). PM data from UCAC5 catalog
	97.642501	11.666865	2.928	262.816									0.20	Eu	2000.896			UCAC5.
	97.642442	11.666833	2.639	265.217	11.23	12.15							0.70	C	2016.022			iT27 1x3s. Touching star disks
J 982 AB	06 32 22.470	+03 29 08.1	3.1	216	10.10	10.60	23	9		9	-12				2015			WDS 06324+0329, WDS data as of August 2017.
	98.093662	3.485544			10.33								0.96	Hg	2015.000			GAIA DR1. M1 is visual estimate from G-J-K-H mags. Secondary not identified in GAIA DR1.
	98.093656	3.485586					1.60	-10.30	1.56				0.20	Eu	2000.137			UCAC5. PM data from UCAC5 catalog. Secondary not identified in UCAC5.
	98.093654	3.485544	3.345	215.587	10.07	10.75							0.70	C	2016.022			iT27 1x3s. Touching star disks
																		Note: Secondary not identified by URAT1 or 2MASS.
J 984 AB	06 36 31.330	+05 19 53.8	4.8	305	11.82	11.82	-5	-9		-18	0				2010			WDS 06365+0521, WDS data as of August 2017.
	99.130413	5.331365	4.941	306.226	11.30	11.52	-1.80	-4.40	1.70	-1.60	-4.10	1.70	0.96	Hg	2015.000	ABCC	**61**	GAIA DR1. M1 and M2 are visual estimates from G-J-K-H mags. PM data from UCAC5 catalog
	99.130420	5.331383	4.940	306.159									0.20	Eu	2000.155			UCAC5.
	99.130408	5.331331	5.080	307.462	11.40	11.62							0.70	C	2016.022			iT27 1x3s
																		Note: Possible CPM candidate. However motion is minimal and error rates relative to motion are high. No parallax data for either component in GAIA DR1.
J 993 AB	06 48 18.791	+11 37 31.7	4.8	146	9.80	11.50	-1	-3							2000			WDS 06482+1143, WDS data as of August 2017.
	102.078301	11.625483	4.849	146.516	12.97	15.25	-0.20	-2.20	1.70	-0.40	-4.50	4.53	0.96	Hg	2015.000	ACCC	**30**	GAIA DR1. M1 and M2 are visual estimates from G-J-K-H mags. PM data from UCAC5 catalog
	102.078302	11.625491	4.823	146.267									0.20	Eu	2000.896			UCAC5.
	102.078354	11.625494			12.98								0.70	C	2016.022			iT27 1x3s. No resolution of B. Has to be fainter than 14.5mag. Estimation from G/J/H/K-mags: 15.25Vmag
																		Note: High error rate relative to minimal motion. No parallax data available in GAIA DR1 for either component.

Table 1 continues on the next page.

Table 1 (continued). Measurement Results for J objects in Monoceros

Name	RA	Dec	Sep	PA	M1	M2	pmRA1	pmDec1	e_pm1	pmRA2	pmDec2	e_pm2	Ap	Me	Date	CPM Rat	CPM %	Source/Notes
J 996 AB	07 00 05.461	+09 18 26.9	5.0	138	11.24	12.60	-1	-5		2	-12				2000			WDS 07001+0918, WDS data as of August 2017.
	105.022760	9.307442	5.002	137.463	11.34	12.93	-0.50	-3.50	1.41	-0.30	-1.70	1.70	0.96	Hg	2015.000	ACCC	**30**	GAIA DR1. M1 and M2 are visual estimate from G-J-K_H mags. PM data from UCAC5 catalog
	105.022762	9.307456	5.019	137.690									0.20	Eu	2000.874			UCAC5.
	105.022771	9.307444	5.058	138.365	11.14	12.97							0.70	C	2016.022			iT27 1x3s
																		Note: High error rate relative to minimal motion. GAIA DR1 lists a parallax of 0.87 (3749 LY) for the primary, none for the secondary.
J 1005 AB	06 34 00.420	-04 44 09.5	2.7	282	9.60	10.80	7	-9							2000			WDS 06340-0445, WDS data as of August 2017.
	98.501830	-4.736034	2.858	284.553	11.91	13.04	2.90	-10.20	1.70	-2.90	-0.70	2.76	0.96	Hg	2015.000	CCCB	**6**	GAIA DR1. M1 is visual estimate from G-J-K-H mags, M2 is GAIA DR1 Gmag (secondary not identified in 2MASS and URAT1). PM data from UCAC5 catalog
	98.501818	-4.735992	2.742	282.127									0.20	Eu	2000.062			UCAC5.
	98.501900	-4.736111	2.873	286.791	11.80	12.83							0.70	C	2016.164			iT27 1x3s. Touching star disks
J 1006 AB	06 34 18.270	-04 43 40.4	3.4	291	9.30	9.70	7	-2							2002			WDS 06343-0444, WDS data as of August 2017.
	98.576142	-4.727899	3.382	291.856	11.33	11.97	-2.10	1.40	1.63	-2.70	2.10	1.77	0.96	Hg	2015.000	BCCC	**24**	GAIA DR1. M1 is visual estimate from G-J-K-H mags, M2 is GAIA DR1 Gmag (secondary not identified in 2MASS and URAT1). PM data from UCAC5 catalog. Error rate of secondary unusually high.
	98.576150	-4.727904	3.369	291.743									0.20	Eu	2000.061			UCAC5.
	98.576167	-4.727917	2.879	287.172	11.28	11.89							0.70	C	2016.164			iT27 1x3s. Touching star disks
J 1057 AB	06 53 11.849	-00 12 35.9	3.0	35	11.56	13.30	-5	-6							2014			WDS 06532-0013, WDS data as of August 2017.
	103.299380	-0.209935	3.000	35.134	11.88	12.85	-1.10	-0.20	1.84	1.00	1.20	2.26	0.96	Hg	2015.000	CCCC	**6**	GAIA DR1. M1 is visual estimate from G-J-K-H mags, M2 is GAIA DR1 Gmag (secondary not identified in 2MASS and URAT1). PM data from UCAC5 catalog
	103.299384	-0.209934	2.964	34.860									0.20	Eu	2000.111			UCAC5.
	103.299392	-0.209894	2.258	36.717	12.00	12.24							0.70	C	2016.096			iT27 1x3s. Touching star disks
J 1057 AC	06 53 11.849	-00 12 35.9	11.4	84	11.56	11.34	-5	-6		1	0				2014			WDS 06532-0013, WDS data as of August 2017.
	103.299380	-0.209935	11.339	83.940	11.88	11.26	-1.10	-0.20	1.84	-1.30	0.90	1.63	0.96	Hg	2015.000	CCCC	**6**	GAIA DR1. M1 and M2 are visual estimates from G-J-K-H mags. PM data from UCAC5 catalog
	103.299384	-0.209934	11.341	84.022									0.20	Eu	2000.110			UCAC5.
	103.299392	-0.209894	11.318	86.353	12.00	11.32							0.70	C	2016.096			iT27 1x3s
BAL 732 AD	06 53 11.849	-00 12 35.9	23.4	53	11.56	13.4	-5	-6		1	-2				2014			WDS 06532-0013, WDS data as of August 2017. This is the AD pairing of J 1057.
	103.299380	-0.209935	23.173	52.723	11.88	13.36	-1.10	-0.20	1.84	-2.20	0.60	1.77	0.96	Hg	2015.000	BCCC	**24**	GAIA DR1. M1 and M2 are visual estimates from G-J-K-H mags. PM data from UCAC5 catalog
	103.299384	-0.209934	23.178	52.770									0.20	Eu	2000.110			UCAC5.
	103.299392	-0.209894	22.764	52.810	12.00	13.40							0.70	C	2016.096			iT27 1x3s. SNR D<20
BAL 732 CE	06 53 11.849	-00 12 35.9	27.9	44	11.34	12.82	1	0		2	-1				2014			WDS 06532-0013, WDS data as of August 2017. This includes the E component of the J 1057 cluster.
	103.302512	-0.209603	27.559	43.610	11.71	12.57	-1.30	0.90	1.63	-1.20	0.20	1.70	0.96	Hg	2015.000	CCCC	**6**	GAIA DR1. M1 and M2 are visual estimates from G-J-K-H mags. PM data from UCAC5 catalog
	103.302518	-0.209606	27.565	43.593									0.20	Eu	2000.110			UCAC5.
	103.302529	-0.209694	27.483	42.847	11.32	12.62							0.70	C	2016.096			iT27 1x3s

Table 1 continues on the next page.

Table 1 (continued). Measurement Results for J objects in Monoceros

Name	RA	Dec	Sep	PA	M1	M2	pmRA1	pmDec1	e_pm1	pmRA2	pmDec2	e_pm2	Ap	Me	Date	CPM Rat	CPM %	Source/Notes
J 1065 AB	07 31 08.170	-03 43 06.0	2.7	334	11.67	9.60	25	-84		-36	31				2005			WDS 07312-0343, WDS data as of August 2017.
	112.783906	-3.718409	2.691	334.883	11.76	11.47	-12.90	-22.10	1.56	-14.60	-20.10	1.56	0.96	Hg	2015.000	CABB	**18**	GAIA DR1. M1 is visual estimate from G-J-K-H mags, M2 is GAIA DR1 Gmag (secondary not identified in 2MASS and URAT1). PM data from UCAC5 catalog
	112.783959	-3.718317	2.654	335.094									0.20	Eu	2000.096			UCAC5.
	112.783917	-3.718419	2.727	332.545	11.43	11.60							0.70	C	2016.096			iT27 1x3s. Touching star disks
																		Note: Possible CPM candidate. However GAIA DR1 doesn't list a parallax for either component.
J 1065 AC	07 31 08.170	-03 43 06.0	8.0	155	11.67	15.00	25	-84							2000			WDS 07312-0343, WDS data as of August 2017.
	112.783906	-3.718409	5.098	150.932	11.76	12.41	-12.90	-22.10	1.56	-4.80	2.60	5.59	0.96	Hg	2015.000	CCCB	**6**	GAIA DR1. M1 and M2 are visual estimates from G-J-K-H mags. PM data from UCAC5 catalog
	112.783959	-3.718317	5.369	153.967									0.20	Eu	2000.097			UCAC5.
	112.783746	-3.718283			11.36								0.70	C	2016.096			iT27 1x3s. No resolution of C. Has to be fainter than 14.5mag
J 1106 AB	06 44 28.581	+10 05 37.0	1.4	249	10.50	10.95	-13	-16		-13	-16				1991			WDS 06444+1005, WDS data as of August 2017.
	101.119131	10.093629	1.464	249.066	10.27	10.42	23.36	4.48	5.59				0.96	Hg	2015.000			GAIA DR1. M1 and M2 are GAIA DR1 Gmags. PM data from position comparison with 2MASS. Secondary not identified in 2MASS (or URAT1).
	101.119036	10.093617					23.80	3.00	1.84				0.20	Eu	2000.885			UCAC5. PM data from UCAC5 catalog. Secondary not identified in UCAC5.
	101.118967	10.093556			9.99								0.70	C	2016.022			iT27 1x3s. No resolution of B. Not even a hint of an elongation
																		Note: GAIA DR1 shows a Gmag for the primary of 10.273, URAT1 shows a Gmag of 10.531. The G-J-K-H formula results in a visual estimate of 10.702 using the GAIA DR1 Gmag value, and 11.090 using the URAT1 Gmag value.
J 1467 AB	07 38 32.090	-10 03 01.8	119.0	101	8.78	11.31	1	-1		-8	6				2000			WDS 07385-1003, WDS data as of August 2017.
	114.633724	-10.050530	118.838	100.918	8.67	11.87	-1.60	-0.20	2.69	-9.30	7.70	1.70	0.96	Hg	2015.000	CCCC	**6**	GAIA DR1. M1 and M2 are visual estimates from G-J-K-H mags. PM data from UCAC5 catalog
	114.633730	-10.050529	118.975	100.963									0.20	Eu	2000.056			UCAC5.
	114.633704	-10.050542	119.009	100.908	8.78	11.63							0.70	C	2016.164			iT27 1x3s
J 1467 BC	07 38 40.000	-10 03 24.5	7.6	35	11.20	11.20	-8	6		16	2				2000			WDS07385-1003, WDS data as of August 2017.
	114.666642	-10.056782	7.564	36.693	11.87	12.64	-9.30	7.70	1.70	-3.40	-2.30	1.70	0.96	Hg	2015.000	BCCB	**25**	GAIA DR1. M1 and M2 are visual estimates from G-J-K-H mags. PM data from UCAC5 catalog
	114.666681	-10.056814	7.632	35.491									0.20	Eu	2000.057			UCAC5.
	114.666671	-10.056797	7.444	36.811	11.63	12.46							0.70	C	2016.164			iT27 1x3s

Table 1 continues on the next page.

Table 1 (continued). Measurement Results for J objects in Monoceros

Name	RA	Dec	Sep	PA	M1	M2	pmRA1	pmDec1	e_pm1	pmRA2	pmDec2	e_pm2	Ap	Me	Date	CPM Rat	CPM %	Source/Notes
J 1472 AB	06 24 15.931	-07 34 30.1	8.2	327	9.88	12.90	4	-7							2000			WDS 06250-0724, WDS data as of August 2017.
	96.066338	-7.575029	8.274	326.431	11.81	15.01	-0.70	-2.80	1.56	-2.20	-1.00	2.83	0.96	Hg	2015.000	CCCC	**6**	GAIA DR1. M1 and M2 are visual estimates from G-J-K-H mags. PM data from UCAC5 catalog
	96.066341	-7.575017	8.238	326.458									0.20	Eu	2000.009			UCAC5.
	96.066325	-7.575103	8.508	327.432	11.69	15.13							0.61	C	2018.088			iT24 5x3s
J 1474 AB	06 33 35.681	-08 10 28.8	6.8	330	8.89	11.10	-1	3							2014			WDS 06336-0810, WDS data as of August 2017.
	98.398699	-8.174681	6.742	330.036	9.08	10.64	0.38	-2.25	5.64	-0.33	0.20	5.64	0.20	Eu	2014.075	CCCC	**6**	URAT1. M1 is URAT1 Vmag, M2 is visual estimate from URAT1 j- and K-bands (no Gmag for the secondary in URAT1). PM data from comparison with 2MASS positions.
	98.398682	-8.174679			8.84		-3.79	1.26	1.92				0.96	Hg	2015.000			GAIA DR1. M1 is visual estimate from G-J-K-H mags. PM data from GAIA DR1 catalog. Secondary not identified in GAIA DR1.
	98.398689	-8.174679					-1.90	0.10	2.69				0.20	Eu	2000.009			UCAC5. PM data from UCAC5 catalog. Secondary not identified in UCAC5.
	98.398696	-8.174683	6.795	330.263	8.93	10.84							0.70	C	2016.172			iT27 1x3s
J 1475 AB	06 42 55.841	-08 50 18.5	9.3	224	9.20	10.40	0	-2		-8	-5				2014			WDS 06429-0850, WDS data as of August 2017.
	100.732638	-8.838477	9.290	223.617	11.19	12.52	-3.30	-0.30	1.56	-3.70	1.70	1.63	0.96	Hg	2015.000	CCCC	**6**	GAIA DR1. M1 and M2 are visual estimates from G-J-K-H mags. PM data from UCAC5 catalog
	100.732652	-8.838475	9.308	223.465									0.20	Eu	2000.011			UCAC5.
	100.732613	-8.838486	9.489	223.172	11.03	12.60							0.70	C	2016.172			iT27 1x3s
J 1479 AB	06 49 16.660	-04 55 41.4	6.9	317	11.30	12.10	5	-5		-8	6				2000			WDS 06491-0453, WDS data as of August 2017.
	102.319413	-4.928158	6.898	317.204	11.23	12.08	-2.10	-0.30	1.70	-1.40	0.50	1.70	0.96	Hg	2015.000	CCCC	**6**	GAIA DR1. M1 and M2 are visual estimates from G-J-K-H mags. PM data from UCAC5 catalog
	102.319421	-4.928157	6.898	317.076									0.20	Eu	2000.073			UCAC5.
	102.319404	-4.928150	7.006	316.953	11.57	12.36							0.70	C	2016.164			iT27 1x3s
J 1481 AB	06 53 44.870	-05 34 29.3	5.2	59	10.00	11.80	-11	-30		5	-7				2000			WDS 06539-0536, WDS data as of August 2017.
	103.436934	-5.574868	5.209	58.560	10.37	12.37	2.80	-13.30	2.69	0.50	-12.50	3.82	0.96	Hg	2015.000	CBCB	**12**	GAIA DR1. M1 and M2 are visual estimates from G-J-K-H mags. PM data from UCAC5 catalog
	103.436922	-5.574813	5.232	58.869									0.20	Eu	2000.066			UCAC5.
	103.436933	-5.574864	5.179	59.864	10.17	11.90							0.70	C	2016.164			iT27 1x3s
HJ 2353 AC	06 53 44.870	-05 34 29.3	15.9	150	10.00	11.10	-11	-30		10	-4				2000			WDS 06539-0536, WDS data as of August 2017. This is the C component of J 1481.
	103.436934	-5.574868	15.827	149.946	10.37	11.70	2.80	-13.30	2.69	5.30	-6.50	1.70	0.96	Hg	2015.000	CCCC	**6**	GAIA DR1. M1 and M2 are visual estimates from G-J-K-H mags. PM data from UCAC5 catalog
	103.436922	-5.574813	15.896	150.248									0.20	Eu	2000.066			UCAC5.
	103.436933	-5.574864	16.027	149.862	10.17	11.52							0.70	C	2016.164			iT27 1x3s
J 1482 AB	06 53 31.970	-09 58 48.8	8.4	351	10.59	10.73	9	-19		2	-5				2010			WDS 06536-0957, WDS data as of August 2017.
	103.383206	-9.980253	8.394	350.756	10.98	11.24	-1.20	-6.50	1.56	-1.40	-5.30	1.56	0.96	Hg	2015.000	BCCC	**24**	GAIA DR1. M1 and M2 are visual estimates from G-J-K-H mags. PM data from UCAC5 catalog
	103.383211	-9.980226	8.376	350.753									0.20	Eu	2000.006			UCAC5.
	103.383213	-9.980281	8.347	351.245	10.97	11.16							0.70	C	2016.172			iT27 1x3s
																		Note: Error rates high relative to minimal motion of components. No parallax for either component available in GAIA DR1.

Table 1 continues on the next page.

Table 1 (continued). Measurement Results for J objects in Monoceros

Name	RA	Dec	Sep	PA	M1	M2	pmRA1	pmDec1	e_pm1	pmRA2	pmDec2	e_pm2	Ap	Me	Date	CPM Rat	CPM %	Source/Notes
J 1483 AB	06 59 46.650	-08 42 39.0	4.0	330	10.59	11.60	0	-13							1941			WDS 06598-0841, WDS data as of August 2017. Only 1 Obs recorded in WDS, not coded X in WDS.
	104.944402	-8.710901			10.56		1.34	-11.45	1.92				0.96	Hg	2015.000			GAIA DR1. M1 is visual estimate from G-J-K-H mags. Secondary not identified in GAIA DR1.
	104.944401	-8.710852					0.40	-11.70	1.98				0.20	Eu	2000.031			UCAC5. PM data from UCAC5 catalog. Secondary not identified in UCAC5.
	104.944433	-8.710964			10.52								0.61	C	2018.088			iT24 5x10s. No resolution. B would have to be fainter than 15.5mag to get not resolved - bogus assumed
																		Note: Secondary not identified by URAT1 or 2MASS. No hint of elongation in the Aladin image.
J 1484 AB	07 01 25.010	-10 35 44.7	4.0	61	11.00	12.50	-1	-8		31	7				2000			WDS 07014-1036, WDS data as of August 2017.
	105.354215	-10.595768	4.045	60.789	12.04	13.28	0.80	-4.90	1.56	0.50	-4.90	1.91	0.96	Hg	2015.000	BACB	**62**	GAIA DR1. M1 and M2 are visual estimates from G-J-K-H mags. PM data from UCAC5 catalog
	105.354211	-10.595748	4.050	60.832									0.20	Eu	2000.006			UCAC5.
	105.354254	-10.595800	3.952	59.936	12.10	13.41							0.70	C	2016.172			iT27 1x3s
DAM 1197 AC	07 01 25.010	-10 35 44.7	9.0	39	11.00	14.30	-1	-8							2000			WDS 07014-1036, WDS data as of August 2017. This is the C component of J 1484.
	105.354215	-10.595768	9.129	37.658	12.04	14.86	0.80	-4.90	1.56	-2.60	7.60	2.91	0.96	Hg	2015.000	CCCC	**6**	GAIA DR1. M1 and M2 are visual estimates from G-J-K-H mags. PM data from UCAC5 catalog
	105.354211	-10.595748	9.013	38.650									0.20	Eu	2000.007			UCAC5.
	105.354254	-10.595800	9.017	38.057	12.10	14.63							0.70	C	2016.172			iT27 1x3s
DAM 1197 AD	07 01 25.010	-10 35 44.7	10.6	89	11.00	14.40	-1	-8							2000			WDS 07014-1036, WDS data as of August 2017. This is the D component of J 1484.
	105.354215	-10.595768	10.575	87.760	12.04	14.96	0.80	-4.90	1.56	-6.50	10.10	2.48	0.96	Hg	2015.000	CCCC	**6**	GAIA DR1. M1 and M2 are visual estimates from G-J-K-H mags. PM data from UCAC5 catalog
	105.354211	-10.595748	10.679	88.992									0.20	Eu	2000.008			UCAC5.
	105.354254	-10.595800	10.690	89.357	12.10	14.90							0.70	C	2016.172			iT27 1x3s. SNR D<20
J 1485 AB	07 03 22.299	-08 44 28.3	6.7	8	10.81	11.20	2	-6		1	-4				2013			WDS 07033-0843, WDS data as of August 2017.
	105.842981	-8.741213	6.632	8.407	10.91	11.18	-0.40	-1.00	1.56	-0.20	0.30	1.98	0.96	Hg	2015.000	CCCC	**6**	GAIA DR1. M1 and M2 are visual estimates from G-J-K-H mags. PM data from UCAC5 catalog
	105.842982	-8.741209	6.612	8.416									0.20	Eu	2000.037			UCAC5.
	105.842967	-8.741242	6.667	8.698	11.02	11.32							0.70	C	2016.172			iT27 1x3s
J 1487 AB	07 12 03.690	-05 26 42.5	4.2	154	10.84	12.80	1	35		2	1				2000			WDS 07120-0526, WDS data as of August 2017.
	108.015637	-5.445333	3.544	159.340	11.58	13.02	34.60	-30.50	1.27	-4.70	2.90	2.12	0.96	Hg	2015.000	CCCB	**6**	GAIA DR1. M1 is visual estimate from G-J-K-H mags, M2 is GAIA DR1 Gmag (secondary not identified in 2MASS and URAT1). PM data from UCAC5 catalog
	108.015493	-5.445206	4.233	154.292									0.20	Eu	2000.079			UCAC5.
	108.015683	-5.445381	3.499	161.075	11.50	13.08							0.70	C	2016.164			iT27 1x3s
																		Note: Significant difference in separation and PA between UCAC5 and GAIA DR1. The PM numbers listed in GAIA DR1 for the primary (38.769 RA, -31.287 Dec) are very close to the UCAC5 numbers shown here; no PM data in GAIA DR1 for the secondary.

Table 1 continues on the next page.

Table 1 (continued). Measurement Results for J objects in Monoceros

Name	RA	Dec	Sep	PA	M1	M2	pmRA1	pmDec1	e_pm1	pmRA2	pmDec2	e_pm2	Ap	Me	Date	CPM Rat	CPM %	Source/Notes
J 1488 AB	07 12 04.880	-05 26 03.6	8.2	262	9.90	12.00	-1	1		-1	9				2010			WDS 07121-0525, WDS data as of August 2017.
	108.020358	-5.434381	8.619	260.370	12.61	13.99	-1.00	-1.40	1.27	-2.20	0.60	1.41	0.96	Hg	2015.000	CCCC	**6**	GAIA DR1. M1 and M2 are visual estimates from G-J-K-H mags. PM data from UCAC5 catalog
	108.020362	-5.434376	8.606	260.159									0.20	Eu	2000.080			UCAC5.
	108.020383	-5.434375	8.631	260.463	12.77	13.90							0.70	C	2016.164			iT27 1x3s
J 1496 AB	07 33 57.830	-01 41 39.9	11.2	10	11.00	11.00	10	-17		-1	0				2016			WDS 07340-0142, WDS data as of August 2017.
	113.490986	-1.694493	11.260	10.532	11.36	11.80	7.20	-17.20	1.70	-4.90	-1.10	1.70	0.96	Hg	2015.000	CCCB	**6**	GAIA DR1. M1 and M2 are visual estimates from G-J-K-H mags. PM data from UCAC5 catalog
	113.490956	-1.694422	11.061	11.675									0.20	Eu	2000.114			UCAC5.
	113.490988	-1.694525	11.274	11.430	11.18	11.80							0.70	C	2016.090			iT27 1x3s
J 1498 AB	07 34 44.021	-10 50 39.6	7.2	178	10.95	11.40	-2	-5		2	-15				2010			WDS 07347-1050, WDS data as of August 2017.
	113.683448	-10.844551	7.343	176.627	10.84	11.36	2.30	-5.90	1.56	1.60	-13.00	1.98	0.96	Hg	2015.000	CCCB	**6**	GAIA DR1. M1 and M2 are visual estimates from G-J-K-H mags. PM data from UCAC5 catalog
	113.683438	-10.844526	7.249	176.491									0.20	Eu	2000.034			UCAC5.
	113.683454	-10.844553	7.353	176.554	10.66	11.26							0.70	C	2016.167			iT27 1x3s
J 1500 AB	07 39 15.560	-08 39 45.0	6.8	180	12.30	13.90	-1	-14							2016			WDS 07392-0838, WDS data as of August 2017.
	114.814829	-8.662582	6.521	183.721	12.29	13.93	-7.20	-12.20	1.70	-3.60	-2.30	2.26	0.96	Hg	2015.000	CCCB	**6**	GAIA DR1. M1 and M2 are visual estimates from G-J-K-H mags. PM data from UCAC5 catalog
	114.814859	-8.662531	6.671	184.096									0.20	Eu	2000.064			UCAC5.
	114.814863	-8.662639	6.431	184.629	12.35	13.94							0.70	C	2016.164			iT27 1x3s
J 1504 AB	07 52 51.710	-07 58 17.1	9.1	251	9.44	11.56	-3	-1		9	-2				2016			WDS 07529-0758, WDS data as of August 2017.
	118.215446	-7.971403	9.350	251.312	9.27	11.61	-6.90	-1.90	2.26	-5.10	2.00	1.70	0.96	Hg	2015.000	cccc	**6**	GAIA DR1. M1 and M2 are visual estimates from G-J-K-H mags. PM data from UCAC5 catalog
	118.215475	-7.971395	9.395	251.028									0.20	Eu	2000.078			UCAC5.
	118.215458	-7.971428	9.320	251.805	9.46	11.45							0.70	C	2016.107			iT27 1x3s
J 1828 AB	07 04 04.990	-09 13 23.2	5.6	172	10.47	11.00	-10	11		1	-12				2011			WDS 07040-0913, WDS data as of August 2017.
	106.020767	-9.223127	5.585	171.401	10.34	11.66	-3.20	0.10	1.56	-3.30	0.10	1.56	0.96	Hg	2015.000	AACC	**76**	GAIA DR1. M1 and M2 is visual estimate from G-J-K-H mags. PM data from UCAC5 catalog
	106.020781	-9.223128	5.581	171.387									0.20	Eu	2000.029			UCAC5.
	106.020863	-9.223175	5.596	169.943	10.62	11.90							0.70	C	2016.172			iT27 1x3s
																		Good CPM candidate, although motion is very minimal and UCAC5 error rates are high relative to the motion. GAIA DR1 shows a parallax of 1.52 (2145.810 LY) for the primary, but none is shown for the secondary.
J 1923 AB	06 10 31.530	-04 22 36.6	5.2	37	9.80	9.80	-29	-19		24	26				2016			WDS 06106-0421, WDS data as of August 2017.
	92.631429	-4.376785	5.315	36.513	11.73	12.05	-1.00	2.10	1.41	-1.40	-2.40	1.41	0.96	Hg	2015.000	BCCC	**24**	GAIA DR1. M1 and M2 are visual estimates from G-J-K-H mags. PM data from UCAC5 catalog
	92.631433	-4.376776	5.323	36.536									0.20	Eu	2000.045			UCAC5.
	92.631425	-4.376808	5.339	35.440	11.74	12.06							0.70	C	2016.164			iT27 1x3s

Table 1 continues on the next page.

Table 1 (continued). Measurement Results for J objects in Monoceros

Name	RA	Dec	Sep	PA	M1	M2	pmRA1	pmDec1	e_pm1	pmRA2	pmDec2	e_pm2	Ap	Me	Date	CPM Rat	CPM %	Source/Notes
J 1944 AB	06 23 54.620	+02 00 09.1	8.1	31	11.60	12.30	-11	-21		67	120				2016			WDS 06240+0158, WDS data as of August 2017.
	95.977554	2.002462	8.224	29.365	12.16	12.96	-8.40	-19.60	1.27	-0.60	1.10	1.35	0.96	Hg	2015.000	BCCB	**25**	GAIA DR1. M1 and M2 are visual estimates from G-J-K-H mags. PM data from UCAC5 catalog
	95.977589	2.002543	7.898	29.726									0.20	Eu	2000.103			UCAC5.
	95.977550	2.002461	8.051	29.320	12.09	13.46							0.70	C	2016.090			iT27 1x3s
J 1945 AB	06 27 12.931	+11 17 55.2	7.6	93	11.90	12.30	-9	-1		8	-3				2016			WDS 06272+1118, WDS data as of August 2017.
	96.803858	11.298661	7.641	93.246	12.58	12.54	1.50	-4.20	1.56	1.70	-7.10	1.41	0.96	Hg	2015.000	CCCC	**6**	GAIA DR1. M1 and M2 are visual estimates from G-J-K-H mags. PM data from UCAC5 catalog
	96.803852	11.298677	7.637	92.942									0.20	Eu	2000.891			UCAC5.
	96.803875	11.298653	7.594	91.887	12.34	12.43							0.70	C	2016.022			iT27 1x3s
J 1949 AB	06 28 22.580	-04 27 43.7	50.4	246	9.23	10.67	1	1		12	-12				2007			WDS 06284-0428, WDS data as of August 2017.
	97.094095	-4.462146	50.395	245.422	9.14	11.01	0.30	-0.30	2.69	6.70	-17.40	1.70	0.96	Hg	2015.000	CCCC	**6**	GAIA DR1. M1 and M2 are visual estimates from G-J-K-H mags. PM data from UCAC5 catalog
	97.094094	-4.462145	50.376	245.732									0.20	Eu	2000.048			UCAC5.
	97.094146	-4.462206	50.482	245.593	9.26	10.84							0.70	C	2016.164			iT27 1x3s
J 1949 BC	06 28 19.520	-04 28 04.4	7.4	224	10.67	11.10	12	-12		2	-12				2006			WDS 06284-0428, WDS data as of August 2017.
	97.081326	-4.467969	7.472	221.928	11.01	11.54	6.70	-17.40	1.70	6.70	-17.70	1.70	0.96	Hg	2015.000	AABB	**92**	GAIA DR1. M1 and M2 are visual estimates from G-J-K-H mags. PM data from UCAC5 catalog
	97.081299	-4.467896	7.469	221.960									0.20	Eu	2000.049			UCAC5.
	97.081338	-4.468000	7.475	222.856	10.84	11.37							0.70	C	2016.164			iT27 1x3s
																		Note: Very good CPM candidate with one reservation. GAIA DR1 shows a parallax of 1.49 for B (2189 LY), but unfortunately none for the secondary, C, which would really be helpful given the distance involved.
J 1963 AB	06 37 21.740	-03 42 10.0	8.7	237	9.20	9.70	11	-33		5	-40				2015			WDS 06375-0336, WDS data as of August 2017.
	99.340637	-3.702955	8.780	237.273	10.95	11.56	9.30	-38.50	1.70	10.10	-39.10	1.70	0.96	Hg	2015.000	AAAB	**97**	GAIA DR1. M1 and M2 are visual estimates from G-J-K-H mags. PM data from UCAC5 catalog
	99.340599	-3.702795	8.785	237.364									0.20	Eu	2000.070			UCAC5.
	99.340604	-3.702939	8.796	237.392	10.94	11.55							0.70	C	2016.164			iT27 1x3s
																		Note: Excellent CPM candidate. No parallax listed for either component in GAIA DR1.
J 1966 AB	06 40 17.950	+02 16 54.0	11.4	349	11.81	13.10	0	-6		-6	3				2010			WDS 06404+0218, WDS data as of August 2017.
	100.074778	2.281665	11.440	349.033	11.88	13.67	-1.50	-1.70	1.70	-3.60	0.40	1.84	0.96	Hg	2015.000	CCCC	**6**	GAIA DR1. M1 and M2 are visual estimates from G-J-K-H mags. PM data from UCAC5 catalog
	100.074784	2.281672	11.404	349.164									0.20	Eu	2000.117			UCAC5.
	100.074792	2.281631	11.517	349.123	11.86	13.48							0.70	C	2016.090			iT27 1x3s

Table 1 continues on the next page.

Table 1 (continued). Measurement Results for J objects in Monoceros

Name	RA	Dec	Sep	PA	M1	M2	pmRA1	pmDec1	e_pm1	pmRA2	pmDec2	e_pm2	Ap	Me	Date	CPM Rat	CPM %	Source/Notes
J 1967 AB	06 40 35.090	+02 17 25.8	6.7	75	11.99	12.00	1	-1							2000			WDS 06406+0217, WDS data as of August 2017.
	100.146175	02.290613	6.615	75.340	11.40	12.10							1.30	E2	2000.007			2MASS. M1 and M2 are visual estimates from 2MASS J- and K-bands. Note differences in separation and PA from URAT1 data.
	100.146178	2.290590	7.535	84.747	11.36	12.13	0.79	-5.79	6.53	79.00	-75.55	6.53	0.20	Eu	2014.123	CCCC	**6**	URAT1. M1 and M2 are URAT1 visual estimates from URAT1 J- and K-bands. PM data from comparison with 2MASS positions.
	100.146175	2.290600			12.05								0.96	Hg	2015.000			GAIA DR1. M1 is visual estimate from G-J-K-H mags. Secondary not identified in GAIA DR1. No G mag for secondary available in URAT1.
	100.146185	2.290595					-2.40	1.20	1.70				0.20	Eu	2000.117			UCAC5. PM data from UCAC5 catalog. Secondary not identified in UCAC5.
	100.146204	2.290575	7.737	84.661	11.86	12.58							0.70	C	2016.090			iT27 1x3s
																		Note: Difference between 2MASS/WDS sep-PA data and URAT1 data raised initial concerns about accuracy of the proper motion data for the secondary. However, a comparison of POSSI and POSSII images confirms the secondary's motion.
J 1972 AB	06 44 07.640	+00 07 00.4	5.4	221	11.76	12.40	3	4		0	-2				2000			WDS 06441+0007, WDS data as of August 2017
	101.031831	0.116813	5.382	221.442	11.91	12.73	-1.50	1.70	1.70	-2.10	1.80	1.70	0.96	Hg	2015.000	CCCC	**6**	GAIA DR1. M1 and M2 are visual estimates from G-J-K-H mags. PM data from UCAC5 catalog
	101.031838	0.116806	5.378	221.363									0.20	Eu	2000.106			UCAC5.
	101.031904	0.116856	5.410	223.877	12.06	12.85							0.70	C	2016.096			iT27 1x3s
J 1977 AB	06 56 35.879	+04 12 58.6	9.9	168	10.29	14.00	-6	-1		9	-14				2010			WDS 06566+0413, WDS data as of August 2017.
	104.149486	4.216306	9.834	166.189	10.43	13.14	-8.50	-3.80	1.41	0.90	-3.20	1.56	0.96	Hg	2015.000	CCCC	**6**	GAIA DR1. M1 and M2 are visual estimates from G-J-K-H mags. PM data from UCAC5 catalog
	104.149519	4.216321	9.813	166.943									0.20	Eu	2000.492			UCAC5.
	104.149450	4.216331	9.947	165.276	10.22	13.00							0.70	C	2016.022			iT27 1x3s
J 1978 AB	06 56 38.030	+03 18 08.7	5.8	268	9.40	11.00	3	-11		9	-8				2010			WDS 06567+0315, WDS data as of August 2017.
	104.158500	3.302158	5.738	266.241	9.14	10.20	0.10	-9.00	1.84	-0.90	-7.60	3.39	0.96	Hg	2015.000	CCCB	**6**	GAIA DR1. M1 and M2 are visual estimates from G-J-K-H mags. PM data from UCAC5 catalog
	104.158500	3.302195	5.723	266.022									0.20	Eu	2000.141			UCAC5.
	104.158504	3.302156	5.650	265.228	9.28	11.10							0.70	C	2016.022			iT27 1x3s
J 1987 AB	07 02 36.911	+02 50 16.6	6.0	265	10.20	10.70	-1	-5		1	-5				2015			WDS 07026+0250, WDS data as of August 2017.
	105.653800	2.837955	5.990	265.364	10.49	11.56	-1.20	-3.20	1.41	-2.50	-3.90	1.56	0.96	Hg	2015.000	CCCC	**6**	GAIA DR1. M1 and M2 are visual estimates from G-J-K-H mags. PM data from UCAC5 catalog
	105.653805	2.837969	5.971	265.445									0.20	Eu	2000.142			UCAC5.
	105.653775	2.837975	5.999	265.219	10.54	11.69							0.70	C	2016.022			iT27 1x3s

Table 1 continues on the next page.

Table 1 (continued). Measurement Results for J objects in Monoceros

Name	RA	Dec	Sep	PA	M1	M2	pmRA1	pmDec1	e_pm1	pmRA2	pmDec2	e_pm2	Ap	Me	Date	CPM Rat	CPM %	Source/Notes
J 1988 AB	07 02 41.320	+02 50 25.3	8.3	236	11.88	12.58	-6	1		-3	-6				2015			WDS 07028+0250, WDS data as of August 2017.
	105.672015	2.840357	8.330	236.431	11.13	11.84	-5.50	-0.80	1.27	4.10	-4.00	1.27	0.96	Hg	2015.000	CACC	**15**	GAIA DR1. M1 and M2 are visual estimates from G-J-K-H mags. PM data from UCAC5 catalog
	105.672038	2.840360	8.320	236.783									0.20	Eu	2000.142			UCAC5.
	105.671996	2.840397	8.361	234.795	10.99	11.58							0.70	C	2016.022			iT27 1x3s
J 1995 AB	06 27 37.730	+00 37 12.0	9.5	128	12.14	13.43	3	2		17	-24				2015			WDS 06276+0035, WDS data as of August 2017.
	96.907200	0.619991	9.490	128.092	12.39	13.83	1.10	-2.70	1.70	-4.10	0.80	1.84	0.96	Hg	2015.000	CCCC	**6**	GAIA DR1. M1 and M2 are visual estimates from G-J-K-H mags. PM data from UCAC5 catalog
	96.907196	0.620002	9.583	128.055									0.20	Eu	2000.094			UCAC5.
	96.907267	0.620078	9.853	127.808	12.42	13.91							0.70	C	2016.096			iT27 1x3s
J 2006 AB	06 40 35.791	-00 39 35.9	6.7	125	10.80	11.60	-2	-2							2010			WDS 06408-0040, WDS data as of August 2017.
	100.149112	-0.659964	7.010	124.665	10.58	11.73	-3.70	0.90	1.56	-4.50	1.50	1.70	0.96	Hg	2015.000	BCCC	**24**	GAIA DR1. M1 and M2 are visual estimates from G-J-K-H mags. PM data from UCAC5 catalog
	100.149127	-0.659968	7.025	124.669									0.20	Eu	2000.094			UCAC5.
	100.149129	-0.659947	6.808	124.742	10.75	11.76							0.70	C	2016.096			iT27 1x3s
J 2010 AB	07 02 47.349	-04 34 31.7	6.4	77	10.34	10.70	-3	-1		-2	-3				2010			WDS 07028-0435, WDS data as of August 2017.
	105.697327	-4.575483	6.344	76.526	10.18	10.97	-1.60	-1.30	1.56	-1.40	-1.60	3.25	0.96	Hg	2015.000	CACC	**15**	GAIA DR1. M1 and M2 are visual estimates from G-J-K-H mags. PM data from UCAC5 catalog
	105.697333	-4.575477	6.343	76.496									0.20	Eu	2000.077			UCAC5.
	105.697367	-4.575550	6.249	75.165	10.42	11.19							0.70	C	2016.164			iT27 1x3s
J 2024 AB	06 42 13.749	-00 47 49.2	2.3	50	11.12	12.12	-1	-3		1	-4				1991			WDS 06423-0048, WDS data as of August 2017.
	100.557219	-0.797093			11.04								0.96	Hg	2015.000			GAIA DR1. M1 is visual estimates from G-J-K-H mags. Secondary not identified in GAIA DR1.
	100.557254	-0.797049					-8.30	10.50	1.91				0.20	Eu	2000.096			UCAC5. PM data from UCAC5 catalog. Secondary not identified in UCAC5.
	100.557308	-0.797158	2.197	40.938	10.94	11.66							0.70	C	2016.096			iT27 1x3s. Touching star disks
																		Secondary also not identified in 2MASS and URAT1.
BAL 709 AC	06 42 13.749	-00 47 49.2	8.6	30	11.12	12.00	-1	-3		3	-7				2015			WDS 06423-0048, WDS data as of August 2017. This is the C component of J 2024.
	100.557254	-0.797049	8.590	30.676	11.04	12.08	-8.30	-10.50	1.91	1.10	-2.20	2.97	0.96	Hg	2015.000	CCCC	**6**	GAIA DR1. M1 and M2 are visual estimates from G-J-K-H mags. PM data from UCAC5 catalog
	100.557308	-0.797158	8.411	30.282									0.20	Eu	2000.096			UCAC5.
													0.70	C				iT Vmag Data
J 2025 AB	06 44 02.749	-00 57 06.9	4.4	207	11.40	11.60	1	2		-33	-8				2010			WDS 06441-0056, WDS data as of August 2017.
	101.011459	-0.951929	4.466	206.560	12.31	13.27	-2.70	0.30	1.70	-1.90	0.00	1.20	0.96	Hg	2015.000	CCCC	**6**	GAIA DR1. M1 and M2 are visual estimates from G-J-K-H mags. PM data from UCAC5 catalog
	101.011470	-0.951930	4.468	206.706									0.20	Eu	2000.970			UCAC5.
	101.011408	-0.951964	4.240	206.018	12.28	13.19							0.70	C	2018.088			iT24 5x3s
J 2027 AB	06 47 19.420	+10 06 01.3	4.7	267	12.20	12.90	4	-5		-20	-13				2007			WDS 06473+1008, WDS data as of August 2017.
	101.830938	10.100424	4.703	267.196	12.17	12.95	-0.30	-1.80	1.56	0.60	-6.10	1.70	0.96	Hg	2015.000	BCCC	**24**	GAIA DR1. M1 and M2 are visual estimates from G-J-K-H mags. PM data from UCAC5 catalog
	101.830939	10.100431	4.713	267.942									0.20	Eu	2000.882			UCAC5.
	101.830996	10.100425	4.844	265.501	12.14	12.98							0.70	C	2016.022			iT27 1x3s

Table 1 continues on the next page.

Table 1 (continued). Measurement Results for J objects in Monoceros

Name	RA	Dec	Sep	PA	M1	M2	pmRA1	pmDec1	e_pm1	pmRA2	pmDec2	e_pm2	Ap	Me	Date	CPM Rat	CPM %	Source/Notes
J 2427 AB	06 24 48.320	+00 04 30.0	3.7	331	11.60	12.40	3	-26		-12	-11				2015			WDS 06248+0005, WDS data as of August 2017.
	96.201352	0.074955	3.702	331.227	11.85	12.75	-3.30	-12.70	1.70	-5.30	-13.40	1.70	0.96	Hg	2015.000	CBCB	**12**	GAIA DR1. M1 and M2 are visual estimates from G-J-K-H mags. PM data from UCAC5 catalog
	96.201366	0.075007	3.698	331.716									0.20	Eu	2000.088			UCAC5.
	96.201321	0.074992	3.329	330.586	11.91	12.78							0.70	C	2016.096			iT27 1x3s
J 2432 AB	06 41 51.250	+00 06 52.4	3.3	5	11.51	11.57	-2	-1		3	16				2015			WDS 06419+0006, WDS data as of August 2017.
	100.463525	0.114505	3.254	4.670	11.71	11.31	-1.60	-1.70	1.70	-1.90	-1.50	1.70	0.96	Hg	2015.000	CACC	**15**	GAIA DR1. M1 and M2 are visual estimates from G-J-K-H mags. PM data from UCAC5 catalog
	100.463532	0.114512	3.251	4.745									0.20	Eu	2000.103			UCAC5.
	100.463704	0.115336	2.958	7.870	11.77	11.48							0.70	C	2016.096			iT27 1x3s
J 2434 AB	06 45 32.621	+04 23 38.2	6.6	298	9.02	10.70	2	-9		-7	0				2010			WDS 06455+0424, WDS data as of August 2017.
	101.385929	4.393954	6.593	297.637	8.88	11.36	-3.00	-3.30	2.69	-13.00	-4.10	3.82	0.96	Hg	2015.000	CCCB	**6**	GAIA DR1. M1 and M2 are visual estimates from G-J-K-H mags. PM data from UCAC5 catalog
	101.385941	4.393968	6.468	298.346									0.20	Eu	2000.152			UCAC5.
	101.385929	4.393942	6.560	297.511	9.08	11.42							0.70	C	2016.022			iT27 1x3s
J 2446 AB	06 53 46.970	+10 06 56.3	2.5	109	10.00	11.00	-30	-13		12	-3				2000			WDS 06538+1007, WDS data as of August 2017.
	103.445696	10.115671	2.564	109.265	11.44	12.10	-4.80	1.10	2.40	3.20	-2.90	4.46	0.96	Hg	2015.000	CCCB	**6**	GAIA DR1. M1 and M2 are GAIA DR1 Gmags – no J-H-K mags available for the secondary, which is not recognized by 2MASS and URAT1. The G-J-H-K magnitude for the primary is 12.135, but didn't include here for sake of consistency. PM data from UCAC5 catalog
	103.445715	10.115666	2.439	108.904									0.20	Eu	2000.882			UCAC5.
	103.445775	10.115728	2.500	110.117	11.79	12.18							0.70	C	2016.022			iT27 1x3s
J 2447 AB	06 53 45.171	-10 52 01.5	2.8	270	10.32	10.80	28	-17		-8	8				2015			WDS 06537-1051, WDS data as of August 2017.
	103.438265	-10.867159	2.753	270.210	10.54	11.62	5.40	-16.10	1.56	5.70	-16.10	3.25	0.96	Hg	2015.000	AACB	**78**	GAIA DR1. M1 and M2 are visual estimates from G-J-K-H mags. PM data from UCAC5 catalog
	103.438242	-10.867091	2.758	270.209									0.20	Eu	1999.990			UCAC5.
	103.438258	-10.867100	3.756	270.005	10.26	11.29							0.70	C	2016.172			iT27 1x3s
																		2MASS position for secondary doesn't match the WDS position, so can't be positive about the J-H-K values (GAIA Gmag for primary is 10.107, for secondary 10.878). Looks like a good PM candidate, although motion is somewhat minimal in relation to errors. GAIA DR1 shows a parallax of 5.72 (570.215 LY) for the primary, none listed for the secondary.

Table 1 continues on the next page.

Table 1 (continued). Measurement Results for J objects in Monoceros

Name	RA	Dec	Sep	PA	M1	M2	pmRA1	pmDec1	e_pm1	pmRA2	pmDec2	e_pm2	Ap	Me	Date	CPM Rat	CPM %	Source/Notes
J 2450 AB	07 03 03.410	-00 28 21.4	3.9	111	11.03	14.20	-31	14							2000			WDS 07031-0029, WDS data as of August 2017.
	105.764250	-0.472653	3.919	111.321	10.99	12.73	-0.60	-1.40	1.41	-3.00	0.20	1.70	0.96	Hg	2015.000	CCCC	**6**	GAIA DR1. M1 and M2 are visual estimates from G-J-K-H mags. PM data from UCAC5 catalog
	105.764253	-0.472647	3.961	111.457									0.20	Eu	2000.114			UCAC5.
	105.764238	-0.472614	3.484	113.512	11.04	12.64							0.70	C	2016.096			iT27 1x3s. Touching star disks. SNR B<20
J 2453 AB	07 07 53.629	+00 48 48.4	4.9	156	10.50	10.90	-17	21		11	-19				2010			WDS 07078+0050, WDS data as of August 2017.
	106.973455	0.813457	4.730	154.763	12.88	13.24	2.50	-1.30	1.70	-0.50	0.10	1.77	0.96	Hg	2015.000	CCCC	**6**	GAIA DR1. M1 and M2 are visual estimates from G-J-K-H mags. PM data from UCAC5 catalog
	106.973445	0.813463	4.767	154.393									0.20	Eu	2000.118			UCAC5.
	106.973479	0.813397	4.642	153.934	12.94	13.31							0.70	C	2016.090			iT27 1x3s
J 2454 AB	07 09 49.130	+00 28 58.1	4.8	342	11.30	11.30	-5	-5		-4	-1				2016			WDS 07097+0029, WDS data as of August 2017.
	107.454299	0.484056	4.890	160.828	12.35	12.36	-4.70	-1.60	1.70	-3.80	-2.10	1.70	0.96	Hg	2015.000	CCCC	**6**	GAIA DR1. M1 and M2 are visual estimates from G-J-K-H mags. PM data from UCAC5 catalog
	107.454319	0.484063	4.879	160.945									0.20	Eu	2000.118			UCAC5.
	107.454750	0.482756	4.914	161.861	12.39	12.36							0.70	C	2016.090			iT27 1x3s
J 2458 AB	07 14 55.540	-01 13 07.0	4.7	202	10.20	12.20	9	7							2010			WDS 07150-0112, WDS data as of August 2017.
	108.731469	-1.218613	4.512	204.548	11.86	12.74	4.10	-1.00	1.63	-4.20	-10.10	1.70	0.96	Hg	2015.000	CCCB	**6**	GAIA DR1. M1 and M2 are visual estimates from G-J-K-H mags. PM data from UCAC5 catalog
	108.731452	-1.218609	4.337	203.820									0.20	Eu	2000.107			UCAC5.
	108.731513	-1.218633	4.258	203.671	11.86	12.75							0.70	C	2016.096			iT27 2x3s
J 2459 AB	07 15 24.760	-11 05 48.5	6.0	105	10.77	10.90	-15	5		-1	1				2010			WDS 07155-1106, WDS data as of August 2017.
	108.853184	-11.096795	6.015	105.641	11.60	11.64	-10.20	3.60	1.56	-11.50	3.40	1.56	0.96	Hg	2015.000	BCCB	**25**	GAIA DR1. M1 and M2 are visual estimates from G-J-K-H mags. PM data from UCAC5 catalog
	108.853228	-11.096810	6.033	105.577									0.20	Eu	2000.011			UCAC5.
	108.853129	-11.096789	6.076	105.367	11.47	11.56							0.70	C	2016.172			iT27 1x3s
J 2461 AB	07 17 02.360	-10 34 56.5	6.0	343	10.65	12.60	-2	1		-3	3				2010			WDS 07171-1036, WDS data as of August 2017.
	109.259856	-10.582370	6.130	342.068	10.32	11.89	-2.40	1.30	1.56	-3.40	3.90	1.63	0.96	Hg	2015.000	CCCC	**6**	GAIA DR1. M1 and M2 are visual estimates from G-J-K-H mags. PM data from UCAC5 catalog
	109.259866	-10.582376	6.087	342.092									0.20	Eu	2000.018			UCAC5.
	109.259879	-10.582381	6.146	341.248	10.51	11.98							0.70	C	2016.172			iT27 1x3s
J 2462 AB	07 17 06.240	-10 32 23.1	8.8	4	11.87	12.85	-11	-3		-7	1				2000			WDS 07172-1034, WDS data as of August 2017.
	109.275730	-10.539751	8.754	3.335	11.68	12.75	-7.80	-1.60	1.56	-8.90	-0.20	1.56	0.96	Hg	2015.000	CCCC	**6**	GAIA DR1. M1 and M2 are visual estimates from G-J-K-H mags. PM data from UCAC5 catalog
	109.275763	-10.539744	8.734	3.450									0.20	Eu	2000.018			UCAC5.
	109.275729	-10.539786	8.645	1.857	11.68	12.81							0.70	C	2016.172			iT27 1x3s

Table 1 continues on the next page.

Table 1 (continued). Measurement Results for J objects in Monoceros

Name	RA	Dec	Sep	PA	M1	M2	pmRA1	pmDec1	e_pm1	pmRA2	pmDec2	e_pm2	Ap	Me	Date	CPM Rat	CPM %	Source/Notes
J 2464 AB	07 18 11.741	-10 31 32.1	5.4	60	10.70	10.70	-2	0		6	7				2000			WDS 07185-1032, WDS data as of August 2017.
	109.548952	-10.525599	5.371	59.648	12.55	13.07	3.20	1.00	1.56	-2.90	1.90	1.77	0.96	Hg	2015.000	CACC	**15**	GAIA DR1. M1 and M2 are visual estimates from G-J-K-H mags. PM data from UCAC5 catalog
	109.548939	-10.525603	5.445	60.259									0.20	Eu	2000.020			UCAC5.
	109.549008	-10.525692	5.418	57.260	12.57	13.30							0.70	C	2016.172			iT27 1x3s
J 2477 AB	07 28 04.740	-03 31 04.6	3.0	71	11.22	10.80	-68	-19							2005			WDS 07281-0330, WDS data as of August 2017.
	112.019721	-3.517950			11.11								0.96	Hg	2015.000			GAIA DR1. M1 is visual estimates from G-J-K-H mags. Secondary not identified in GAIA DR1.
	112.019748	-3.517929					-6.30	-5.10	1.56				0.20	Eu	2000.093			UCAC5. PM data from UCAC5 catalog. Secondary not identified in UCAC5.
	112.019688	-3.518103	2.797	61.377	11.06	11.71							0.70	C	2016.096			iT27 1x3s
																		Secondary also not identified in 2MASS and URAT1.
J 2482 AB	07 34 14.121	-01 35 04.3	4.4	204	12.60	12.30	10	8		-2	-17				2016			WDS 07343-0135, WDS data as of August 2017.
	113.558833	-1.584529	4.429	202.466	12.79	12.65	4.10	-3.10	1.70	3.70	-3.70	1.70	0.96	Hg	2015.000	CACB	**16**	GAIA DR1. M1 and M2 are visual estimates from G-J-K-H mags. PM data from UCAC5 catalog
	113.558816	-1.584516	4.419	202.432									0.20	Eu	2000.113			UCAC5.
	113.558392	-1.585731	4.377	201.928	12.80	12.50							0.70	C	2016.090			iT27 1x3s
J 2485 AB	07 41 36.561	-10 43 28.3	6.3	126	11.00	13.00	-10	2		19	-19				2010			WDS 07417-1043, WDS data as of August 2017.
	115.402356	-10.724531	6.544	127.460	12.66	13.70	-2.30	1.10	1.70	2.90	-12.90	1.91	0.96	Hg	2015.000	CCCB	**6**	GAIA DR1. M1 and M2 are visual estimates from G-J-K-H mags. PM data from UCAC5 catalog
	115.402366	-10.724535	6.357	126.338									0.20	Eu	2000.043			UCAC5.
	115.402413	-10.724639	6.230	127.356	12.99	13.84							0.70	C	2016.164			iT27 1x3s
J 2487 AB	07 46 13.950	-06 02 29.5	6.7	131	9.50	11.00	-40	3		18	-45				2010			WDS 07461-0603, WDS data as of August 2017.
	116.558116	-6.041629	6.706	131.198	11.63	12.57	-5.80	-19.10	1.41	-6.80	-19.30	1.41	0.96	Hg	2015.000	AABB	**92**	GAIA DR1. M1 and M2 are visual estimates from G-J-K-H mags. PM data from UCAC5 catalog
	116.558140	-6.041549	6.716	131.091									0.20	Eu	2000.084			UCAC5.
	116.558138	-6.041594	6.820	133.797	11.47	12.61							0.70	C	2016.096			iT27 1x3s
																		Good PM candidate. No parallax data for either component in GAIA DR1.
J 2491 AB	07 57 20.130	-03 46 09.9	4.0	10	12.00	13.00	-5	-35							2004			WDS 07574-0345, WDS data as of August 2017.
	119.333894	-3.769418	3.921	7.798	12.59	13.08	-3.20	1.30	1.70	-2.70	2.30	1.70	0.96	Hg	2015.000	CACC	**15**	GAIA DR1. M1 and M2 are visual estimates from G-J-K-H mags. PM data from UCAC5 catalog
	119.333907	-3.769424	3.906	7.710									0.20	Eu	2000.107			UCAC5.
	119.333875	-3.769408	3.864	8.688	12.57	13.09							0.70	C	2016.022			iT27 1x3s
J 2493 AB	08 10 12.749	-11 09 40.6	7.3	314	9.50	12.50	-2	-2		-16	11				2000			WDS 08101-1110, WDS data as of August 2017.
	122.553123	-11.161264	7.266	314.171	11.52	13.18	-2.40	2.50	1.70	-1.40	3.10	1.84	0.96	Hg	2015.000	CACC	**15**	GAIA DR1. M1 and M2 are visual estimates from G-J-K-H mags. PM data from UCAC5 catalog
	122.553133	-11.161274	7.270	314.045									0.20	Eu	2000.041			UCAC5.
	122.553117	-11.161269	7.339	316.230	11.43	13.37							0.70	C	2016.096			iT27 1x3s
J 2611 AB	06 48 07.840	+09 44 12.1	4.5	125	11.92	14.10	-2	2		34	-30				2000			WDS 06482+0944, WDS data as of August 2017.
	102.032654	9.736666	4.507	124.971	11.96	12.93	2.50	-4.70	1.41	1.20	-5.40	1.56	0.96	Hg	2015.000	CACB	**16**	GAIA DR1. M1 and M2 are visual estimates from G-J-K-H mags. PM data from UCAC5 catalog
	102.032644	9.736684	4.516	124.734									0.20	Eu	2000.878			UCAC5.
	102.032675	9.736689	4.312	128.261	11.94	12.92							0.70	C	2016.022			iT27 1x3s

Table 1 continues on the next page.

Table 1 (continued). Measurement Results for J objects in Monoceros

Name	RA	Dec	Sep	PA	M1	M2	pmRA1	pmDec1	e_pm1	pmRA2	pmDec2	e_pm2	Ap	Me	Date	CPM Rat	CPM %	Source/Notes
J 2611 AC	06 48 07.840	+09 44 12.1	17.2	349	11.92	15.60	-2	2		5	8				2000			WDS 06482+0944, WDS data as of August 2017.
	102.032654	9.736666	17.371	348.649	11.96	14.08	2.50	-4.70	1.41	-9.60	2.80	1.70	0.96	Hg	2015.000	CCCC	**6**	GAIA DR1. M1 and M2 are visual estimates from G-J-K-H mags. PM data from UCAC5 catalog
	102.032644	9.736684	17.234	349.136									0.20	Eu	2000.878			UCAC5.
	102.032675	9.736689	17.358	347.856	11.94	14.06							0.70	C	2016.022			iT27 1x3s
J 2616 AB	06 54 24.510	-00 09 09.2	5.1	3	12.80	12.60	-2	-12		-8	1				2016			WDS 06544-0008, WDS data as of August 2017.
	103.602137	-0.152557	5.130	1.218	12.86	12.77	-0.40	-3.90	1.70	3.00	-10.10	1.70	0.96	Hg	2015.000	CCCB	**6**	GAIA DR1. M1 and M2 are visual estimates from G-J-K-H mags. PM data from UCAC5 catalog
	103.602139	-0.152541	5.223	1.635									0.20	Eu	2000.110			UCAC5.
	103.602183	-0.152564	5.121	359.161	13.09	12.88							0.70	C	2016.096			iT27 1x3s
J 2616 AC	06 54 24.510	-00 09 09.2	21.5	20	12.80	14.50	-2	-12		103	-111				2015			WDS 06544-0008, WDS data as of August 2017.
	103.602137	-0.152557	21.455	19.549	12.86	14.50	-0.40	-3.90	1.70	-2.20	-4.70	2.19	0.96	Hg	2015.000	CCCC	**6**	GAIA DR1. M1 and M2 are visual estimates from G-J-K-H mags. PM data from UCAC5 catalog
	103.602139	-0.152541	21.475	19.609									0.20	Eu	2000.110			UCAC5.
	103.602183	-0.152564	21.427	17.982	13.09	14.68							0.70	C	2016.096			iT27 1x3s. SNR B<20
J 2623 AB	07 09 11.890	-05 16 54.5	5.5	115	10.80	11.80	-25	2		23	-12				2010			WDS 07091-0518, WDS data as of August 2017.
	107.299555	-5.281813	5.513	115.805	12.28	12.80	-3.20	-0.30	1.27	-0.90	5.30	1.27	0.96	Hg	2015.000	CCCC	**6**	GAIA DR1. M1 and M2 are visual estimates from G-J-K-H mags. PM data from UCAC5 catalog
	107.299568	-5.281812	5.518	116.748									0.20	Eu	2000.078			UCAC5.
	107.299563	-5.281833	5.451	116.005	12.15	12.69							0.70	C	2016.164			iT27 1x3s
J 2636 AB	08 02 20.021	-06 26 02.4	4.8	62	10.39	12.00	-18	-23		24	-1				2012			WDS 08026-0628, WDS data as of August 2017.
	120.583403	-6.434084	4.596	61.730	10.33	12.50	-11.50	-22.50	1.41	-13.90	-21.70	2.34	0.96	Hg	2015.000	BABB	**74**	GAIA DR1. M1 and M2 are visual estimates from G-J-K-H mags. PM data from UCAC5 catalog
	120.583451	-6.433991	4.623	62.076									0.20	Eu	2000.095			UCAC5.
	120.583425	-6.434136	4.363	59.416	10.22	12.41							0.70	C	2016.090			iT27 1x3s
																		Good CPM candidate. GAIA DR1 shows a parallax for the primary of 3.54 (921.365 LY), but none listed for the secondary.
J 2637 AB	08 02 26.280	-06 25 53.4	7.3	240	11.53	14.00	5	-9		15	9				2000			WDS 08027-0628, WDS data as of August 2017.
	120.609577	-6.431590	7.353	241.709	11.95	13.95	0.00	-9.60	1.41	-10.80	-1.40	1.70	0.96	Hg	2015.000	CCCB	**6**	GAIA DR1. M1 and M2 are visual estimates from G-J-K-H mags. PM data from UCAC5 catalog
	120.609577	-6.431550	7.272	240.263									0.20	Eu	2000.098			UCAC5.
	120.609550	-6.431636	7.008	241.446	11.92	13.86							0.70	C	2016.090			iT27 1x3s
J 2758 AB	06 51 23.450	-03 54 46.3	3.2	126	12.30	13.50	-21	7							2000			WDS 06514-0354, WDS data as of August 2017.
	102.847739	-3.912861	3.215	125.802	12.29	12.83	-2.50	1.70	1.41	-2.40	1.10	1.56	0.96	Hg	2015.000	CCCC	**6**	GAIA DR1. M1 and M2 are GAIA DR1 Gmags. PM data from UCAC5 catalog. Secondary not recognized in 2MASS and URAT1. G-J-H-K magnitude for M1 is 12.233.
	102.847749	-3.912868	3.209	125.683									0.20	Eu	2000.082			UCAC5.
	102.847846	-3.912950	3.062	125.308	12.37	12.81							0.70	C	2016.164			iT27 1x3s
J 2766 AB	06 57 44.310	-04 36 55.8	5.4	38	12.40	12.50	-13	-3		-3	2				2015			WDS 06577-0435, WDS data as of August 2017.
	104.434654	-4.615499	5.446	37.832	12.29	12.35	-1.90	1.30	1.70	-0.80	1.60	1.70	0.96	Hg	2015.000	CCCC	**6**	GAIA DR1. M1 and M2 are visual estimates from G-J-K-H mags. PM data from UCAC5 catalog
	104.434662	-4.615504	5.432	37.717									0.20	Eu	2000.074			UCAC5.
	104.434633	-4.615478	5.376	39.973	12.50	12.56							0.70	C	2016.164			iT27 1x3s

Table 1 continues on the next page.

Table 1 (continued). Measurement Results for J objects in Monoceros

Name	RA	Dec	Sep	PA	M1	M2	pmRA1	pmDec1	e_pm1	pmRA2	pmDec2	e_pm2	Ap	Me	Date	CPM Rat	CPM %	Source/Notes
J 2768 AB	06 58 38.911	-09 09 47.5	5.8	53	11.50	12.00	-14	-5		52	37				2015			WDS 06587-0911, WDS data as of August 2017.
	104.662158	-9.163151	5.830	52.502	12.53	12.62	3.80	17.10	1.56	2.80	16.70	1.56	0.96	Hg	2015.000	BABB	**74**	GAIA DR1. M1 and M2 are visual estimates from G-J-K-H mags. PM data from UCAC5 catalog
	104.662142	-9.163222	5.845	52.539									0.20	Eu	2000.024			UCAC5.
	104.662158	-9.163150	5.868	54.351	12.67	12.76							0.70	C	2016.172			iT27 1x3s
																		Good CPM candidate. No parallax data available in GAIA DR1 for either component.
J 2769 AB	06 59 39.050	+02 19 33.2	5.1	69	12.00	12.60	-22	3		11	6				2010			WDS 06597+0219, WDS data as of August 2017.
	104.912732	2.325935	5.596	67.120	12.24	12.94	-2.50	-0.60	1.70	-3.40	2.70	1.70	0.96	Hg	2015.000	CCCC	**6**	GAIA DR1. M1 and M2 are visual estimates from G-J-K-H mags. PM data from UCAC5 catalog
	104.912742	2.325938	5.589	67.633									0.20	Eu	2000.137			UCAC5.
	104.912742	2.325947	5.548	68.317	12.60	12.35							0.70	C	2016.022			iT27 1x3s
J 2770 AB	06 59 58.210	-05 06 26.0	8.3	176	11.44	12.40	-2	-1		4	-3				2015			WDS 06599-0507, WDS data as of August 2017.
	104.992587	-5.107276	8.307	175.645	11.46	13.38	-1.40	-3.80	1.70	-2.80	-3.40	1.84	0.96	Hg	2015.000	CBCC	**12**	GAIA DR1. M1 and M2 are visual estimates from G-J-K-H mags. PM data from UCAC5 catalog
	104.992593	-5.107260	8.315	175.508									0.20	Eu	2000.072			UCAC5.
	104.992600	-5.107306	8.357	175.386	11.37	13.30							0.70	C	2016.164			iT27 1x3s
J 2772 AB	07 03 06.931	-04 24 29.4	6.9	132	10.50	11.40	-11	1		16	-3				2010			WDS 07030-0424, WDS data as of August 2017.
	105.778890	-4.408173	6.880	130.735	12.10	12.67	1.30	-1.80	1.77	-0.10	-0.30	1.70	0.96	Hg	2015.000	CCCC	**6**	GAIA DR1. M1 and M2 are visual estimates from G-J-K-H mags. PM data from UCAC5 catalog
	105.778885	-4.408165	6.912	130.763									0.20	Eu	2000.082			UCAC5.
	105.778871	-4.408219	6.820	130.840	12.20	12.87							0.70	C	2016.164			iT27 1x3s
J 2774 AB	07 04 21.950	+09 15 56.4	4.1	85	12.57	12.74	3	-21		-3	1				2010			WDS 07044+0917, WDS data as of August 2017.
	106.091520	9.265563	4.061	82.973	12.29	12.84	9.10	-25.30	1.27	-2.30	-1.90	1.27	0.96	Hg	2015.000	CCCB	**6**	GAIA DR1. M1 and M2 are visual estimates from G-J-K-H mags. PM data from UCAC5 catalog
	106.091484	9.265662	4.196	87.743									0.20	Eu	2000.877			UCAC5.
	106.091517	9.265481	3.932	77.216	12.39	12.90							0.70	C	2016.022			iT27 1x3s
																		Unusual disparities in PA for this pair.

Table 1 continues on the next page.

Table 1 (continued). Measurement Results for J objects in Monoceros

Name	RA	Dec	Sep	PA	M1	M2	pmRA1	pmDec1	e_pm1	pmRA2	pmDec2	e_pm2	Ap	Me	Date	CPM Rat	CPM %	Source/Notes
J 2776 AB	07 05 05.391	+00 58 41.1	6.3	216	9.90	13.50	0	1							2010			WDS 07051+0059, WDS data as of August 2017.
	106.272449	0.978109	6.495	216.259	11.88	13.83	-2.00	-2.00	1.70	-4.70	-5.30	1.84	0.96	Hg	2015.000	BCCC	**24**	GAIA DR1. M1 and M2 are visual estimates from G-J-K-H mags. PM data from UCAC5 catalog
	106.272457	0.978118	6.432	216.239									0.20	Eu	2000.117			UCAC5.
	106.272458	0.978078	6.497	216.390	12.00	13.74							0.70	C	2016.090			iT27 1x3s
J 2781 AB	07 08 11.099	-01 51 59.4	25.1	6	10.94	11.63	-1	-1		-3	1				2015			WDS 07082-0151, WDS data as of August 2017.
	107.046266	-1.866534	25.518	9.379	11.15	11.82	-1.40	1.20	1.56	-2.20	0.90	1.70	0.96	Hg	2015.000	CCCC	**6**	GAIA DR1. M1 and M2 are visual estimates from G-J-K-H mags. PM data from UCAC5 catalog
	107.046271	-1.866538	25.523	9.403									0.20	Eu	2000.103			UCAC5.
	107.046204	-1.866458	25.569	9.483	10.93	12.01							0.70	C	2016.096			iT27 1x3s
BAL 409 BC	07 08 11.099	-01 51 59.4	5.0	267	11.80	12.90	-3	1		1.00	-1.00				2008			WDS 07082-0151, WDS data as of August 2017. This is the B component of J 2781 AB.
	107.047421	-1.859540	5.168	266.482	11.82	12.85	-2.20	0.90	1.70	-3.70	1.40	1.84	0.96	Hg	2015.000	ACCC	**30**	GAIA DR1. M1 and M2 are visual estimates from G-J-K-H mags. PM data from UCAC5 catalog
	107.047430	-1.859544	5.145	266.402									0.20	Eu	2000.104			UCAC5.
	107.047375	-1.859453	4.964	268.615	12.01	13.09							0.70	C	2016.096			iT27 1x3s
J 2782 AB	07 08 07.711	-10 36 17.2	3.5	283	10.49	11.10	5	-1							2000			WDS 07081-1036, WDS data as of August 2017.
	107.032169	-10.604815	3.512	282.732	10.46	11.78	0.90	0.60	1.56	-0.60	0.20	3.39	0.96	Hg	2015.000	CCCC	**6**	GAIA DR1. M1 and M2 are visual estimates from G-J-K-H mags. PM data from UCAC5 catalog
	107.032165	-10.604817	3.492	282.885									0.20	Eu	2000.017			UCAC5.
	107.032192	-10.604814	3.547	281.216	10.61	11.21							0.70	C	2016.172			iT27 1x3s
J 2784 AB	07 08 28.480	+00 57 40.2	6.4	159	12.60	12.60	-7	13		0	3				2000			WDS 07086+0059, WDS data as of August 2017.
	107.118682	0.961179	6.371	158.714	13.10	13.14	-1.30	-1.40	1.70	-2.50	-2.80	1.70	0.96	Hg	2015.000	ACCC	**30**	GAIA DR1. M1 and M2 are visual estimates from G-J-K-H mags. PM data from UCAC5 catalog
	107.118687	0.961185	6.358	158.503									0.20	Eu	2000.118			UCAC5.
	107.118688	0.961247	6.506	159.910	12.85	13.17							0.70	C	2016.090			iT27 1x3s

Table 1 continues on the next page.

Table 1 (continued). Measurement Results for J objects in Monoceros

Name	RA	Dec	Sep	PA	M1	M2	pmRA1	pmDec1	e_pm1	pmRA2	pmDec2	e_pm2	Ap	Me	Date	CPM Rat	CPM %	Source/Notes
J 2788 AB	07 10 33.470	-10 11 41.8	5.3	123	12.50	13.50	-172	105		8	2				2000			WDS 07107-1012, WDS data as of August 2017.
	107.640748	-10.195746	5.287	302.116	12.94	13.66	-0.80	-2.20	1.41	2.50	-0.20	1.41	0.96	Hg	2015.000	CBCC	**12**	GAIA DR1. M1 and M2 are visual estimates from G-J-K -H mags. PM data from UCAC5 catalog
	107.640738	-10.195745	5.262	302.668									0.20	Eu	2000.023			UCAC5.
	107.640788	-10.195764	5.215	302.475	12.94	13.66							0.70	C	2016.172			iT27 1x3s. **Note 180 degree difference in PA from WDS data --last WDS PA measurement appears to be in error.**
J 2789 AB	07 11 34.389	-07 48 48.7	6.8	86	11.40	12.10	-14	-5		5	-7				2010			WDS 07115-0750, WDS data as of August 2017.
	107.893289	-7.813533	6.520	84.153	11.89	12.61	-3.70	-0.10	1.70	-5.80	1.10	1.70	0.96	Hg	2015.000	CCCC	**6**	GAIA DR1. M1 and M2 are visual estimates from G-J-K -H mags. PM data from UCAC5 catalog
	107.893304	-7.813533	6.551	84.339									0.20	Eu	2000.061			UCAC5.
	107.893321	-7.813547	6.498	84.170	11.80	12.51							0.70	C	2016.167			iT27 1x3s
J 2792 AB	07 14 40.190	-02 11 43.3	3.6	182	11.81	12.10	-2	19		-7	-20				2000			WDS 07146-0212, WDS data as of August 2017.
	108.667474	-2.195398	3.569	182.357	11.93	12.17	-1.80	-2.60	1.41	-1.60	-3.60	1.41	0.96	Hg	2015.000	CCCC	**6**	GAIA DR1. M1 and M2 are visual estimates from G-J-K -H mags. PM data from UCAC5 catalog
	108.667481	-2.195387	3.554	182.419									0.20	Eu	2000.100			UCAC5.
	108.667433	-2.195444	3.201	181.342	11.76	11.89							0.70	C	2016.096			iT27 1x3s
J 2793 AB	07 14 14.661	-10 06 19.0	3.1	106	11.77	12.68	-6	-2		27	-7				2000			WDS 07144-1007, WDS data as of August 2017.
	108.561222	-10.105362	2.913	105.110	11.02	11.90	6.50	-3.80	1.56	-6.20	0.00	3.25	0.96	Hg	2015.000	CCCB	**6**	GAIA DR1. M1 and M2 are visual estimates from G-J-K -H mags. PM data from UCAC5 catalog
	108.561194	-10.105346	3.111	105.209									0.20	Eu	2000.025			UCAC5.
	108.561263	-10.105372	2.455	104.390	10.92	11.24							0.70	C	2016.172			iT27 1x3s
J 2796 AB	07 15 00.450	-06 52 51.5	5.9	346	12.00	12.00	3	-6		-17	3				2010			WDS 07151-0653, WDS data as of August 2017.
	108.751893	-6.881012	6.023	345.902	12.89	14.04	-2.90	1.00	1.70	-1.20	-0.10	2.13	0.96	Hg	2015.000	CCCC	**6**	GAIA DR1. M1 and M2 are visual estimates from G-J-K -H mags. PM data from UCAC5 catalog
	108.751906	-6.881016	6.045	345.703									0.20	Eu	2000.067			UCAC5.
	108.751842	-6.881133	6.609	349.090	13.36	14.27							0.70	C	2016.164			iT27 1x3s. SNR B<20

Table 1 continues on the next page.

Table 1 (continued). Measurement Results for J objects in Monoceros

Name	RA	Dec	Sep	PA	M1	M2	pmRA1	pmDec1	e_pm1	pmRA2	pmDec2	e_pm2	Ap	Me	Date	CPM Rat	CPM %	Source/Notes
J 2798 AB	07 15 43.781	-10 40 15.5	4.0	143	10.92	11.13	13	7		2	-1				2010			WDS 07157-1040, WDS data as of August 2017.
	108.932399	-10.670942	3.989	141.786	10.90	11.30	-2.80	1.90	1.56	-2.00	4.50	3.25	0.96	Hg	2015.000	CCCB	6	GAIA DR1. M1 and M2 are visual estimates from G-J-K-H mags. PM data from UCAC5 catalog
	108.932411	-10.670950	4.012	142.276									0.20	Eu	2000.018			UCAC5.
	108.932371	-10.670958	4.071	140.685	10.92	11.29							0.70	C	2016.172			iT27 1x3s
J 2802 AB	07 16 06.419	-01 37 34.9	4.1	268	11.35	12.61	0	-3		-41	14				2010			WDS 07161-0138, WDS data as of August 2017.
	109.026739	-1.626434	4.085	270.212	11.11	11.78	-1.20	1.30	1.63	-2.60	0.70	1.70	0.96	Hg	2015.000	CCCC	**6**	GAIA DR1. M1 and M2 are visual estimates from G-J-K-H mags. PM data from UCAC5 catalog
	109.026744	-1.626439	4.065	270.340									0.20	Eu	2000.104			UCAC5.
	109.026800	-1.626428	4.184	269.452	11.17	11.84							0.70	C	2016.096			iT27 1x3s
J 2804 AB	07 16 37.310	-10 05 37.9	5.4	321	12.83	11.52	20	-32		-3	-3				2010			WDS 07167-1007, WDS data as of August 2017.
	109.155359	-10.093899	5.413	321.877	11.42	11.71	-1.90	-3.00	1.56	-1.10	-3.10	1.56	0.96	Hg	2015.000	CBCC	**12**	GAIA DR1. M1 and M2 are visual estimates from G-J-K-H mags. PM data from UCAC5 catalog
	109.155366	-10.093886	5.421	321.800									0.20	Eu	2000.024			UCAC5.
	109.155346	-10.093936	5.341	322.730	11.56	11.90							0.70	C	2016.172			iT27 1x3s
J 2809 AB	07 18 39.419	-06 56 24.5	5.2	213	13.00	13.00	14	21							2000			WDS 07187-0657, WDS data as of August 2017.
	109.664283	-6.940170	5.325	213.019	13.02	14.05	-3.60	-0.30	1.41	-6.20	-6.40	1.98	0.96	Hg	2015.000	CCCB	**6**	GAIA DR1. M1 and M2 are visual estimates from G-J-K-H mags. PM data from UCAC5 catalog
	109.664298	-6.940169	5.229	213.202									0.20	Eu	2000.069			UCAC5.
	109.664313	-6.940167	5.355	213.023	12.90	14.17							0.70	C	2016.164			iT27 1x3s
J 2810 AB	07 19 30.250	-03 03 55.9	5.6	165	11.50	12.00	-3	14		15	6				2016			WDS 07196-0303, WDS data as of August 2017.
	109.876051	-3.065576	5.636	164.292	12.19	13.31	-0.10	0.50	1.56	-5.30	-2.70	1.84	0.96	Hg	2015.000	CCCC	**6**	GAIA DR1. M1 and M2 are visual estimates from G-J-K-H mags. PM data from UCAC5 catalog
	109.876052	-3.065578	5.612	163.409									0.20	Eu	2000.096			UCAC5.
	109.876038	-3.065544	5.769	164.178	12.03	13.37							0.70	C	2016.096			iT27 1x3s
J 2816 AB	07 25 32.440	-03 26 01.4	5.5	316	13.10	13.70	5	2		-15	0				2010			WDS 07255-0326, WDS data as of August 2017.
	111.385159	-3.433748	5.590	315.852	13.21	13.84	-2.60	1.70	1.70	1.00	-3.10	1.84	0.96	Hg	2015.000	CACC	**15**	GAIA DR1. M1 and M2 are visual estimates from G-J-K-H mags. PM data from UCAC5 catalog
	111.385170	-3.433755	5.679	315.973									0.20	Eu	2000.096			UCAC5.
	111.385138	-3.433739	5.685	311.810	13.27	13.98							0.70	C	2016.096			iT27 1x3s. SNR B<20
J 2817 AB	07 26 31.249	-02 33 52.4	4.7	332	10.20	10.40	22	11		-8	22				2012			WDS 07263-0233, WDS data as of August 2017.
	111.630305	-2.564577	4.874	331.799	11.90	12.11	12.10	-3.10	1.70	11.80	-3.40	1.70	0.96	Hg	2015.000	AACB	**78**	GAIA DR1. M1 and M2 are visual estimates from G-J-K-H mags. PM data from UCAC5 catalog
	111.630255	-2.564564	4.878	331.853									0.20	Eu	2000.099			UCAC5.
	111.630317	-2.564456	4.635	327.981	11.83	12.08							0.70	C	2016.096			iT27 1x3s
																		Good CPM candidate, although motion is minimal and UCAC5 error rates are high relative to the motion of the secondary. No parallax for either of the components is listed in GAIA DR1.

Table 1 continues on the next page.

Table 1 (continued). Measurement Results for J objects in Monoceros

Name	RA	Dec	Sep	PA	M1	M2	pmRA1	pmDec1	e_pm1	pmRA2	pmDec2	e_pm2	Ap	Me	Date	CPM Rat	CPM %	Source/Notes
J 2822 AB	07 27 15.869	-03 48 35.9	5.7	285	12.00	13.00	-10	-2							2010			WDS 07274-0348, WDS data as of August 2017.
	111.816153	-3.809994	5.640	285.521	12.42	13.44	-4.40	0.60	1.70	-3.50	4.10	1.84	0.96	Hg	2015.000	CCCC	**6**	GAIA DR1. M1 and M2 are visual estimates from G-J-K-H mags. PM data from UCAC5 catalog
	111.816171	-3.809997	5.640	284.993									0.20	Eu	2000.094			UCAC5.
	111.816238	-3.810067	6.113	285.271	12.55	13.59							0.70	C	2016.096			iT27 1x3s
J 2823 AB	07 27 35.360	-07 01 22.0	5.0	96	13.00	14.00	-5	-18		18	-7				2010			WDS 07277-0701, WDS data as of August 2017.
	111.897376	-7.022819	4.814	93.550	13.04	13.87	5.90	-12.20	1.70	-3.30	2.10	2.12	0.96	Hg	2015.000	CCCB	**6**	GAIA DR1. M1 and M2 are visual estimates from G-J-K-H mags. PM data from UCAC5 catalog
	111.897352	-7.022768	4.967	95.903									0.20	Eu	2000.070			UCAC5.
	111.897483	-7.022744	4.565	95.910	13.27	14.16							0.70	C	2016.164			iT27 1x3s
J 2825 AB	07 28 02.160	-07 44 18.5	6.5	27	12.70	12.80	-13	-24		17	-1				2010			WDS 07279-0745, WDS data as of August 2017.
	112.009028	-7.738526	6.545	25.845	12.66	12.50	-1.40	-1.90	1.70	-4.20	2.40	1.70	0.96	Hg	2015.000	CCCC	**6**	GAIA DR1. M1 and M2 are visual estimates from G-J-K-H mags. PM data from UCAC5 catalog
	112.009034	-7.738519	6.506	26.428									0.20	Eu	2000.069			UCAC5.
	112.009042	-7.738561	6.529	25.772	12.80	12.84							0.70	C	2016.164			iT27 1x3s
J 2831 AB	07 32 23.409	-04 31 02.8	4.4	139	12.68	13.10	-73	66							2000			WDS 07323-0431, WDS data as of August 2017.
	113.097593	-4.517491	4.399	139.221	12.04	13.05	-9.60	-10.60	1.70	-11.50	-11.80	1.70	0.96	Hg	2015.000	ACCB	**31**	GAIA DR1. M1 and M2 are visual estimates from G-J-K-H mags. PM data from UCAC5 catalog
	113.097633	-4.517447	4.406	138.781									0.20	Eu	2000.088			UCAC5.
	113.097579	-4.517500	4.312	140.350	12.07	13.04							0.70	C	2016.096			iT27 1x3s
J 2833 AB	07 33 05.229	-04 29 55.9	7.3	84	12.57	12.57	-15	-5		2	-4				2005			WDS 07330-0430, WDS data as of August 2017.
	113.271805	-4.498822	7.357	83.178	11.86	12.76	-5.36	4.97	5.28	3.21	3.79	5.28	0.96	Hg	2015.000	CCCC	**6**	GAIA DR1. M1 and M2 are visual estimates from G-J-K-H mags. PM data from comparison with 2MASS positions.
	113.271808	-4.498836					-0.80	3.40	1.41				0.20	Eu	2000.089			UCAC5. PM data from UCAC5 catalog. Secondary not identified in UCAC5.
	113.271808	-4.498917	7.603	82.442	11.63	12.73							0.70	C	2016.096			iT27 1x3s
J 2834 AB	07 33 48.260	-04 31 29.1	5.3	204	11.80	11.80	-10	3		-9	5				2000			WDS 07337-0431, WDS data as of August 2017.
	113.451050	-4.524794	5.163	203.971	12.62	12.94	-7.50	-3.50	1.70	-3.50	2.80	1.70	0.96	Hg	2015.000	CCCB	**6**	GAIA DR1. M1 and M2 are visual estimates from G-J-K-H mags. PM data from UCAC5 catalog
	113.451082	-4.524779	5.275	204.156									0.20	Eu	2000.089			UCAC5.
	113.451029	-4.524839	5.036	205.123	12.74	12.90							0.70	C	2016.096			iT27 1x3s
J 2836 AB	07 34 00.750	-09 34 51.6	6.1	53	11.89	12.83	-14	-11		2	3				2010			WDS 07341-0934, WDS data as of August 2017.
	113.502873	-9.581243	6.313	51.360	11.67	12.77	-4.40	-1.50	1.70	-4.90	4.80	1.70	0.96	Hg	2015.000	CCCC	**6**	GAIA DR1. M1 and M2 are visual estimates from G-J-K-H mags. PM data from UCAC5 catalog
	113.502891	-9.581236	6.260	52.072									0.20	Eu	2000.058			UCAC5.
	113.502892	-9.581250	6.192	52.025	11.92	13.16							0.70	C	2016.164			iT27 1x3s
J 2837 AB	07 34 59.230	-04 58 50.3	8.9	186	11.00	12.50	-1	8		0	19				2000			WDS 07350-0457, WDS data as of August 2017.
	113.746776	-4.980662	8.990	185.871	12.06	13.46	-1.30	5.40	1.41	1.00	-0.40	1.41	0.96	Hg	2015.000	CCCC	**6**	GAIA DR1. M1 and M2 are visual estimates from G-J-K-H mags. PM data from UCAC5 catalog
	113.746781	-4.980684	8.909	186.149									0.20	Eu	2000.092			UCAC5.
	113.746771	-4.980661	9.245	185.658	12.13	13.38							0.70	C	2016.107			iT27 1x3s

Table 1 continues on the next page.

Table 1 (continued). Measurement Results for J objects in Monoceros

Name	RA	Dec	Sep	PA	M1	M2	pmRA1	pmDec1	e_pm1	pmRA2	pmDec2	e_pm2	Ap	Me	Date	CPM Rat	CPM %	Source/Notes
J 2839 AB	07 36 25.890	-03 34 42.3	8.6	271	11.80	13.00	4	2		-18	15				2010			WDS 07365-0334, WDS data as of August 2017.
	114.107918	-3.578466	8.653	270.582	12.29	13.33	2.30	-0.50	1.41	-4.40	-1.30	1.41	0.96	Hg	2015.000	BCCC	**24**	GAIA DR1. M1 and M2 are visual estimates from G-J-K-H mags. PM data from UCAC5 catalog
	114.107908	-3.578464	8.554	270.678									0.20	Eu	2000.098			UCAC5.
	114.107854	-3.578506	8.459	270.203	12.08	13.26							0.70	C	2016.096			iT27 1x3s
J 2842 AB	07 37 52.429	-05 21 10.0	9.2	342	11.28	11.82	-6	2		-4	-2				2014			WDS 07379-0522, WDS data as of August 2017.
	114.468562	-5.352872	9.508	339.886	12.04	12.09	19.70	-17.50	1.98	-7.60	-2.80	1.84	0.96	Hg	2015.000	CCCB	**6**	GAIA DR1. M1 and M2 are visual estimates from G-J-K-H mags. PM data from UCAC5 catalog
	114.468480	-5.352800	9.166	341.808									0.20	Eu	2000.088			UCAC5.
	114.468458	-5.352794	9.269	341.494	11.63	12.08							0.70	C	2016.107			iT27 1x3s
J 2845 AB	07 39 33.370	-10 13 57.4	0.6	75	11.68	11.97	1	-2		1	-2				1991			WDS 07396-1013, WDS data as of August 2017.
	114.889058	-10.232627			11.23								0.96	Hg	2015.000			GAIA DR1. M1 is visual estimate from G-J-K-H mags. Secondary not identified in GAIA DR1.
	114.889077	-10.232617					-4.40	-2.40	1.70				0.20	Eu	2000.055			UCAC5. PM data from UCAC5 catalog. Secondary not identified in UCAC5.
	114.907938	-10.208878	4.854	45.868	12.75	12.92							0.70	C	2016.164			iT27 1x3s. Image quality a bit questionable - yet it seems clear that the last "precise" WDS measurement was for a wrong object nearby. Obs1 in the WDS shows a component at 3" and 45 degrees. Secondary not identified in UCAC5, 2MASS, URAT1, and GAIA DR1 at either the WDS Obs1 or Obs2 positions, or at the Astrometrica position.
J 2846 AB	07 39 50.800	-09 26 38.8	6.8	158	12.70	12.82	-23	10	-2	2					2010			WDS 07399-0926, WDS data as of August 2017.
	114.961078	-9.443865	7.005	155.693	12.51	12.80	-17.00	9.30	1.70	-2.10	2.70	1.70	0.96	Hg	2015.000	CCCB	**6**	GAIA DR1. M1 and M2 are visual estimates from G-J-K-H mags. PM data from UCAC5 catalog
	114.961150	-9.443903	6.826	157.059									0.20	Eu	2000.061			UCAC5.
	114.961079	-9.443889	6.949	154.658	12.48	12.92							0.70	C	2016.164			iT27 1x3s
J 2850 AB	07 43 36.229	-02 28 16.3	6.7	239	11.80	12.30	14	4		-13	2				2016			WDS 07438-0227, WDS data as of August 2017.
	115.900974	-2.471199	6.862	238.819	12.50	13.83	-2.60	1.10	1.70	-7.60	3.50	1.98	0.96	Hg	2015.000	ACCC	**30**	GAIA DR1. M1 and M2 are visual estimates from G-J-K-H mags. PM data from UCAC5 catalog
	115.900985	-2.471204	6.818	238.235									0.20	Eu	2000.113			UCAC5.
	115.900983	-2.471192	6.869	237.604	12.66	13.92							0.70	C	2016.090			iT27 1x3s
J 2854 AB	07 50 29.629	-02 06 54.4	6.9	70	11.00	11.20	-13	-12		10	-10				2016			WDS 07506-0205, WDS data as of August 2017.
	117.623436	-2.115156	6.908	69.590	12.65	12.88	-6.30	-8.50	1.70	-7.10	-8.80	1.70	0.96	Hg	2015.000	ABCB	**62**	GAIA DR1. M1 and M2 are visual estimates from G-J-K-H mags. PM data from UCAC5 catalog
	117.623462	-2.115121	6.920	69.593									0.20	Eu	2000.115			UCAC5.
	117.623438	-2.115183	6.956	68.583	12.65	12.81							0.70	C	2016.022			iT27 1x3s
																		Possible CPM candidate. Motion is relatively minimal in comparison to error rate. No parallax for either component in GAIA DR1.
J 2858 AB	07 55 25.900	-07 19 10.1	7.7	18	10.00	11.70	-19	-41		-8	2				2012			WDS 07555-0720, WDS data as of August 2017.
	118.857912	-7.319481	7.621	18.358	12.17	13.51	-6.30	-0.50	1.70	-7.90	-1.70	1.84	0.96	Hg	2015.000	CCCC	**6**	GAIA DR1. M1 and M2 are visual estimates from G-J-K-H mags. PM data from UCAC5 catalog
	118.857939	-7.319479	7.645	18.488									0.20	Eu	2000.081			UCAC5.
	118.857829	-7.319489	7.578	20.455	12.23	13.39							0.70	C	2016.096			iT27 1x3s. SNR B<20

Table 1 continues on the next page.

Table 1 (continued). Measurement Results for J objects in Monoceros

Name	RA	Dec	Sep	PA	M1	M2	pmRA1	pmDec1	e_pm1	pmRA2	pmDec2	e_pm2	Ap	Me	Date	CPM Rat	CPM %	Source/Notes
J 2859	07 57 51.060	-03 42 30.2	2.8	133	10.10	10.10	-23	-23		5	7				2016			WDS 07578-0342, WDS data as of August 2017.
	119.462623	-3.708507	2.974	132.467	11.73	11.60	−32.50	-26.90	1.70	-7.20	3.70	1.70	0.96	Hg	2015.000	CCCB	**6**	GAIA DR1. M1 and M2 are GAIA DR1 Gmags. 2MASS and URAT1 don't identify the the primary, so there are no J-K-H mags. The G-J-H-K magnitude value for the secondary is 12.197. PM data from UCAC5 catalog
	119.462758	-3.708395	3.060	143.596									0.20	Eu	2000.107			UCAC5.
	119.462654	-3.708578	2.797	130.061	11.83	11.83							0.70	C	2016.022			iT27 1x3s
J 2860	07 57 47.450	-04 56 25.0	5.6	253	13.50	14.20	-9	2		21	6				2010			WDS 07579-0455, WDS data as of August 2017.
	119.447719	-4.940294	5.599	254.121	13.49	13.82	-4.50	3.60	1.77	-5.50	0.70	1.98	0.96	Hg	2015.000	CACB	**16**	GAIA DR1. M1 and M2 are visual estimates from G-J-K-H mags. PM data from UCAC5 catalog
	119.447738	-4.940309	5.572	254.500									0.20	Eu	2000.099			UCAC5.
	119.447675	-4.940319	5.599	252.860	13.52	13.91							0.70	C	2016.090			iT27 1x3s
J 2864 AB	08 04 31.609	-09 06 55.8	4.9	56	12.30	12.40	-24	-10		14	11				2010			WDS 08045-0905, WDS data as of August 2017.
	121.131723	-9.115503	5.014	56.206	13.33	13.09	3.80	-3.50	1.70	-0.30	2.40	1.70	0.96	Hg	2015.000	CCCC	**6**	GAIA DR1. M1 and M2 are visual estimates from G-J-K-H mags. PM data from UCAC5 catalog
	121.131707	-9.115489	5.017	57.428									0.20	Eu	2000.063			UCAC5.
	121.132663	-9.114842	4.830	61.290	13.54	13.38							0.70	C	2016.096			iT27 1x3s. Image quality a bit questionable
J 2865 AB	08 04 33.031	-09 09 11.7	4.6	223	11.40	11.70	11.4	11.7							2017			WDS 08045-0909, WDS data as of August 2017.
	121.137642	-9.153286	4.569	223.577	11.39	12.22	-2.90	-3.80	1.70	-2.40	-0.70	1.70	0.96	Hg	2015.000	CCCC	**6**	GAIA DR1. M1 and M2 are visual estimates from G-J-K-H mags. PM data from UCAC5 catalog
	121.137654	-9.153271	4.608	223.262									0.20	Eu	2000.064			UCAC5.
	121.137579	-9.153350	4.607	223.715	11.41	12.13							0.70	C	2016.096			iT27 1x3s
J 2866 AB	08 05 38.932	-04 21 57.6	9.5	281	11.70	11.90	2	2		-3	-3				2012			WDS 08058-0420, WDS data as of August 2017.
	121.4147550	-04.3665058	9.367	280.201	12.45	13.26	-0.73	0.54	5.74	-1.05	-11.07	5.80	0.2	Eu	2013.597	CCCC	**6**	URAT1. PM data from position comparison with 2MASS. M1 and M2 are visual estimates from J and K magnitudes.
	121.414747	-4.366499			12.79								0.96	Hg	2015.000			GAIA DR1. M1 is visual estimate from G-J-K-H mags. Secondary not identified in GAIA DR1.
	121.414756	-4.366501					-2.20	0.40	1.70				0.20	Eu	2000.106			UCAC5. PM data from UCAC5 catalog. Secondary not identified in UCAC5.
	121.414763	-4.366514	9.296	280.037	12.83	13.21							0.70	C	2016.022			iT27 1x3s
J 2866 BC	08 05 38.932	-04 21 57.6	4.9	145	11.90	11.40	-3	-3		9	-6				2012			WDS 08058-0420, WDS data as of August 2017.
	121.4121867	-04.3660450	4.594	143.993	13.26	13.88	-1.05	-11.07	5.80	-0.25	0.71	5.96	0.2	Eu	2013.320	CCCB	**6**	URAT1. PM data from position comparison with 2MASS. M1 and M2 are visual estimates from J and K magnitudes.
						13.93							0.96	Hg	2015.000			GAIA DR1. M2 is visual estimate from G-J-K-H mags. Primary not identified in GAIA DR1.
										-3.40	1.20	3.70	0.20	Eu	2000.106			UCAC5. PM data from UCAC5 catalog. Primary not identified in UCAC5.
	121.412213	-4.366064	4.765	144.722	13.21	13.99							0.70	C	2016.022			iT27 1x3s

Table 1 continues on the next page.

Table 1 (continued). Measurement Results for J objects in Monoceros

Name	RA	Dec	Sep	PA	M1	M2	pmRA1	pmDec1	e_pm1	pmRA2	pmDec2	e_pm2	Ap	Me	Date	CPM Rat	CPM %	Source/Notes
J 2867 AB	08 05 52.761	-06 14 42.4	8.7	304	12.50	12.60	9	-2		10	-5				2000			WDS 08059-0614, WDS data as of August 2017.
	121.469848	-6.245145	8.714	303.344	13.42	13.55	2.70	-3.10	2.70	3.50	-9.20	1.70	0.96	Hg	2015.000	CCCC	**6**	GAIA DR1. M1 and M2 are visual estimates from J and K magnitudes. GAIA DR1 erroneously shows the primary with a Gmag of 19.193. The G-J-H-K magnitude for the secondary is 13.498. PM data from UCAC5 catalog
	121.469836	-6.245132	8.775	303.800									0.20	Eu	2000.096			UCAC5.
	121.469817	-6.245214	9.336	307.009	13.52	13.54							0.70	C	2016.090			iT27 1x3s
J 2868 AB	08 05 56.681	-06 14 52.1	6.5	7	12.30	13.30	-9	-4		-5	15				2016			WDS 08060-0614, WDS data as of August 2017.
	121.486156	-6.247811	6.535	6.983	12.35	13.38	-6.20	2.10	1.70	-2.70	4.60	1.84	0.96	Hg	2015.000	CCCC	**6**	GAIA DR1. M1 and M2 are visual estimates from G-J-K-H mags. PM data from UCAC5 catalog
	121.486182	-6.247820	6.491	6.569									0.20	Eu	2000.096			UCAC5.
	121.486183	-6.247858	6.784	6.562	12.31	13.35							0.70	C	2016.090			iT27 1x3s
J 2869 AB	08 08 33.570	-09 57 44.1	7.5	210	10.19	11.00	5	-13							2011			WDS 08086-0958, WDS data as of August 2017.
	122.139932	-9.962303	7.445	210.267	10.28	11.46	7.10	-14.50	2.69	5.80	-14.10	1.70	0.96	Hg	2015.000	BBCB	**50**	GAIA DR1. M1 and M2 are visual estimates from G-J-K-H mags. PM data from UCAC5 catalog
	122.139903	-9.962243	7.440	210.125									0.20	Eu	2000.062			UCAC5.
	122.139917	-9.962331	7.260	211.806	9.98	11.42							0.70	C	2016.096			iT27 1x3s
																		Possible CPM candidate. Motion is somewhat minimal in comparison to error rate. GAIA DR1 shows a parallax of 2.88 (1332.511 LY) for the primary, none listed for the secondary.
J 2870 AB	08 08 18.178	-09 16 30.4	6.6	132	12.60	14.10	-14	5		1	12				2010			WDS 08088-0917, WDS data as of August 2017.
	122.075761	-9.275099	6.531	131.320	12.70	14.30	-4.10	3.40	1.70	-4.70	3.70	1.98	0.96	Hg	2015.000	ACCC	**30**	GAIA DR1. M1 and M2 are visual estimates from G-J-K-H mags. PM data from UCAC5 catalog
	122.075778	-9.275114	6.541	131.289									0.20	Eu	2000.063			UCAC5.
	122.075725	-9.275053	6.567	130.560	12.71	14.29							0.70	C	2016.096			iT27 1x3s
J 2871 AB	08 09 28.779	-10 47 09.7	4.9	199	12.60	12.67	-7	4		-8	-11				2010			WDS 08096-1047, WDS data as of August 2017.
	122.369611	-10.786007	5.100	197.729	12.01	12.66	-8.10	0.50	1.70	-10.30	-0.30	1.70	0.96	Hg	2015.000	ACCB	**31**	GAIA DR1. M1 and M2 are visual estimates from G-J-K-H mags. PM data from UCAC5 catalog
	122.369646	-10.786009	5.079	197.422									0.20	Eu	2000.048			UCAC5.
	122.369617	-10.786044	5.076	197.920	12.11	12.75							0.70	C	2016.096			iT27 1x3s

Table 1 concludes on the next page.

Table 1 (conclusion). Measurement Results for J objects in Monoceros

Name	RA	Dec	Sep	PA	M1	M2	pmRA1	pmDec1	e_pm1	pmRA2	pmDec2	e_pm2	Ap	Me	Date	CPM Rat	CPM %	Source/Notes
J 3230 AB	07 03 58.899	-07 09 56.9	5.5	82	10.18	12.40	-8	-3							2000			WDS 07040-0710, WDS data as of August 2017.
	105.995498	-7.165836	5.508	82.152	10.25	12.13	1.60	-1.50	1.84	0.40	-0.70	3.96	0.96	Hg	2015.000	CCCC	**6**	GAIA DR1. M1 and M2 are visual estimates from G-J-K-H mags. PM data from UCAC5 catalog
	105.995491	-7.165830	5.525	82.293									0.20	Eu	2000.061			UCAC5.
	105.995504	-7.165842	5.480	82.450	10.11	11.74							0.70	C	2016.167			iT27 1x3s
J 3286 AB	08 05 50.100	-06 14 19.6	2.8	129	12.10	13.00	-74	76		-18	10				2000			WDS 08058-0614, WDS data as of August 2017.
	121.458678	-6.238755	2.782	131.614	13.22	13.69	0.10	-1.10	2.12	-6.00	-2.70	2.62	0.96	Hg	2015.000	CCCB	**6**	GAIA DR1. M1 and M2 are GAIA DR1 Gmags. 2MASS doesn't identify the secondary, so no G-J-H-K magnitudes are available for it. The G-J-H-K magnitude of the primary is 13.592. PM data from UCAC5 catalog
	121.458678	-6.238751	2.835	130.034									0.20	Eu	2000.095			UCAC5.
	121.458746	-6.238750	2.661	130.839	13.38	13.86							0.70	C	2016.090			iT27 1x3s. Touching star disks
J 3309 AB	07 03 32.361	-08 40 29.6	4.0	52	12.00	13.50	-57	-45		19	12				2000			WDS 07035-0838, WDS data as of August 2017.
	105.884871	-8.674934	3.949	51.040	12.75	13.69	2.80	-2.00	1.56	-4.20	-2.10	1.98	0.96	Hg	2015.000	CCCB	**6**	GAIA DR1. M1 and M2 are visual estimates from G-J-K-H mags. PM data from UCAC5 catalog
	105.884860	-8.674926	4.031	51.960									0.20	Eu	2000.035			UCAC5.
	105.884904	-8.674958	3.662	50.289	12.72	13.89							0.70	C	2016.172			iT27 1x3s

Explanations regarding the content of the Notes column:

- "Touching star disks" indicates that the rims of the star disks are touching and that the measurement results might be a bit less precise than with clearly separated star disks
- "Touching/Overlapping star disks" indicates that the star disks overlap to the degree of an elongation and that the measurement results is probably less precise than with clearly separated star disks
- "SNR <20" indicates that the measurement result might be a bit less precise than desired due to a low SNR value but this is already included in the calculation of the magnitude error range estimation
- "SNR <10" indicates that the measurement result is probably a bit less precise than desired due to a very low SNR value but this is already included in the calculation of the magnitude error range estimation
- "Image quality questionable" or similar indicates rather large average errors for the reference stars used for plate solving for different reasons (mostly atmospheric influences). But this is at least to some degree already included in the calculation of the error range estimation

(Continued from page 610)

Knapp, Wilfried R. A.; Nanson, John, 2017, "A New Concept for Counter-Checking of Assumed CPM Pairs, *JDSO*, **13** (1), 31-51.

Knapp, Wilfried R. A., 2018, "A New Concept for Counter-Checking of Assumed Binaries", *JDSO*, **14** (3), 487-491.

Knapp, Wilfried R. A.; Nanson, John, 2018, Estimating Visual Magnitudes for Wide Double Stars, *JDSO*, **14** (3), 496-502.

Appendix A

CPM rating scheme according to Knapp/Nanson 2017 with extensions

Four rating factors are used: Proper motion vector direction, proper motion vector length, size of position error in relation to proper motion vector length and relationship of proper motion speed to angular separation:

- Proper motion vector direction ratings: "A" for within the error range of identical direction, "B" for similar direction within the double error range, "C" for direction within the triple error range and "D" for outside.
- Proper motion vector length ratings: "A" for within the error range of identical length, "B" for similar length within the double error range, "C" for length within the triple error range and "D" for outside.
- Error size ratings: "A" for error size of less than 5% of the proper motion vector length, "B" for less than 10%, "C" for less than 15% and "D" for a larger error size.
- Relationship PM speed to angular separation: "A" for less than 100 years, "B" for less than 1,000 years, "C" for less than 10,000 and "D" for above.

To compensate for excessively large position errors resulting in an "A" rating despite rather high deviations an absolute upper limit is applied regardless of calculated error size:

- Proper motion vector direction: Max. 2.86° difference for an "A".
- Proper motion vector length: Max. 5% difference for an "A".

The letter based rating result is then transformed into an estimated probability for being physical given in the column CPM % (Knapp 2018).

Jonckheere Double Star Photometry – Part XII: Mon I

Appendix B

Table 2 with positions for both components, astrometry measurement errors, signal to noise ratio and photometry measurement errors

Table 2.

Obj	C	RA	Dec	dRA	dDec	Err Sep	Err PA	Err Mag	SNR	Date	Notes
21	A	07 02 18.785	10 30 48.05	0.06	0.05	0.078	1.382	0.101	75.600	2016.022	iT27 1x3s
	B	07 02 18.567	10 30 48.43					0.102	57.870		
40	A	06 41 49.398	-00 15 59.06	0.08	0.08	0.113	2.227	0.082	55.980	2016.096	iT27 1x3s. Touching star disks
	B	06 41 49.582	-00 15 59.98					0.088	28.320		
55	A	06 49 36.564	01 59 56.45	0.07	0.08	0.106	2.448	0.081	90.540	2016.090	iT27 1x3s. Touching star disks
	B	06 49 36.599	01 59 54.02					0.081	106.160		
56	A	06 52 37.623	03 14 18.22	0.07	0.07	0.099	-	0.070	299.910	2016.022	iT27 1x3s. Overlapping star disks. A and B too bright for resolution
	B							-			
60	A	07 13 14.050	-02 38 36.54	0.08	0.09	0.120	-	0.070	176.960	2016.107	iT27 1x3s. Heavily overlapping star disks. Both components too bright for resolution
	B							-			
65	A	07 44 12.590	-01 15 12.71	0.06	0.05	0.078	-	0.070	283.480	2016.022	iT27 1x3s. Heavily overlapping star disks. Both components too bright for clear resolution
	B							-			
66	A	07 47 40.881	-00 54 23.46	0.07	0.08	0.106	1.579	0.060	192.680	2016.022	iT27 1x3s
	B	07 47 40.811	-00 54 27.17					0.061	101.430		
187	A	06 06 38.711	-04 11 37.44	0.10	0.10	0.141	0.271	-		2016.164	iT27 1x3s. Primary star disc saturated
	B	06 06 39.848	-04 12 02.04					0.081	106.670		
189	A	07 45 34.342	-05 58 30.00	0.09	0.12	0.150	-	0.081	86.400	2016.096	iT27 1x3s. No resolution of B
	B							-			
265	A	06 35 46.322	05 07 23.08	0.07	0.07	0.099	1.387	0.070	138.600	2016.022	iT27 1x3s
	B	06 35 46.074	05 07 21.35					0.071	86.630		
266	A	06 36 41.070	03 18 56.73	0.07	0.07	0.099	1.278	0.070	191.440	2016.022	iT27 1x3s
	B	06 36 41.097	03 18 52.31					0.072	63.690		
314	A	06 47 07.320	-03 51 30.57	0.09	0.09	0.127	2.034	0.071	103.490	2016.164	iT27 1x3s
	B	06 47 07.496	-03 51 28.14					0.079	28.830		
348	A	06 29 49.140	11 07 51.12	0.11	0.10	0.149	2.354	0.083	52.150	2016.022	iT27 1x3s
	B	06 29 49.293	11 07 48.29					0.084	42.130		
349	A	06 32 59.378	04 56 22.54	0.10	0.10	0.141	1.483	0.080	207.150	2016.022	iT27 1x3s
	B	06 32 59.737	04 56 21.51					0.082	67.980		
350	A	06 35 41.739	00 29 31.93	0.06	0.05	0.078	1.318	0.096	32.960	2016.096	iT27 1x3s
	B	06 35 41.954	00 29 30.87					0.100	24.720		
351	A	06 37 58.395	11 33 19.20	0.06	0.06	0.085	1.320	0.081	90.180	2016.022	iT27 1x3s
	B	06 37 58.270	11 33 16.01					0.090	25.960		
352	A	06 38 40.002	-08 15 37.92	0.08	0.08	0.113	1.454	0.070	165.090	2016.172	iT27 1x3s
	B	06 38 40.302	-08 15 38.14					0.073	54.810		
354	A	06 53 51.789	01 43 28.06	0.08	0.07	0.106	1.025	0.071	106.070	2016.090	iT27 1x3s
	B	06 53 51.395	01 43 27.40					0.073	53.740		
360	A	07 05 11.295	00 54 00.69	0.07	0.09	0.114	1.779	0.072	62.870	2016.090	iT27 1x3s
	B	07 05 11.416	00 54 03.88					0.073	49.590		
363	A	07 16 02.840	-06 36 52.15	0.08	0.09	0.120	-	0.090	142.170	2016.164	iT27 1x3s. Hint of elongation but no resolution of B
	B							-			
364	A	07 16 09.530	-06 34 38.80	0.08	0.09	0.120	1.338	0.090	148.520	2016.164	iT27 1x3s
	B	07 16 09.409	-06 34 33.97					0.095	36.040		
365	A	07 17 17.126	-06 35 27.31	0.10	0.11	0.149	4.105	0.083	53.040	2016.164	iT27 1x3s. Touching star disks. B barely resolved. SNR B<10
	B	07 17 16.987	-06 35 27.27					0.152	7.880		
417	A	07 40 11.870	-08 56 18.82	0.11	0.12	0.163	-	0.110	110.850	2016.164	iT27 1x3s. Slightest hint of elongtion but no resolution of B
	B							-			
595	A	06 26 24.319	11 27 47.67	0.10	0.11	0.149	1.745	0.130	101.610	2016.022	iT27 1x3s
	B	06 26 24.540	11 27 51.31					0.131	88.080		
595	A	06 26 24.319	11 27 47.67	0.10	0.11	0.149	0.195	0.130	101.610	2016.022	iT27 1x3s
	C	06 26 21.627	11 27 28.94					0.130	111.280		

Table 2 continues on the next page.

Jonckheere Double Star Photometry – Part XII: Mon I

Table 2 (continued).

Obj	C	RA	Dec	dRA	dDec	Err Sep	Err PA	Err Mag	SNR	Date	Notes
596	A	06 41 03.809	02 14 21.38	0.08	0.08	0.113	1.349	0.071	107.520	2016.090	iT27 1x3s
	B	06 41 04.040	02 14 24.71					0.071	104.830		
597	A	06 41 21.634	02 06 05.72	0.08	0.10	0.128	1.449	0.080	159.900	2016.090	iT27 1x3s
	B	06 41 21.904	02 06 08.76					0.081	119.730		
659	A	06 28 40.543	04 52 47.38	0.08	0.07	0.106	3.233	0.061	101.810	2016.022	iT27 1x3s. Touching/ overlapping star disks
	B	06 28 40.430	04 52 46.55					0.063	61.070		
660	A	06 28 40.728	04 50 12.05	0.08	0.07	0.106	2.352	0.061	103.810	2016.022	iT27 1x3s. Touching star disks
	B	06 28 40.899	04 50 11.64					0.061	90.120		
690	A	06 30 47.068	10 03 46.52	0.12	0.10	0.156	-	0.090	137.100	2016.022	iT27 1x3s. Hint of elongation but no resolution of B
	B							-			
691	A	06 30 52.422	04 38 59.80	0.08	0.09	0.120	-	0.070	190.660	2016.022	iT27 1x3s. Hint of elongation but no resolution of B
	B							-			
697	A	06 43 33.798	11 09 04.89	0.14	0.11	0.178	5.085	0.132	45.420	2016.022	iT27 1x3s. Touching star disks
	B	06 43 33.794	11 09 02.89					0.140	20.360		
700	A	06 54 44.423	10 14 47.61	0.08	0.08	0.113	2.281	0.062	68.680	2016.022	iT27 1x3s. Touching star disks
	B	06 54 44.609	10 14 46.88					0.063	59.790		
723	A	06 45 03.407	09 58 31.06	0.07	0.05	0.086	2.247	0.082	57.540	2016.022	iT27 1x3s. Touching star disks
	B	06 45 03.551	09 58 31.59					0.084	43.960		
726	A	06 46 51.792	10 10 01.49	0.09	0.07	0.114	2.472	0.073	50.860	2016.022	iT27 1x3s. Touching star disks
	B	06 46 51.926	10 09 59.74					0.072	65.120		
730	A	07 18 20.297	-02 35 29.75	0.08	0.10	0.128	2.666	0.073	52.000	2016.096	iT27 1x3s. Touching star disks
	B	07 18 20.375	-02 35 32.24					0.078	30.610		
733	A	08 05 33.439	-03 46 10.70	0.08	0.07	0.106	2.877	0.105	34.520	2016.022	iT27 1x3s. Touching/ overlapping star disks. SNR B <20
	B	08 05 33.511	-03 46 12.52					0.120	16.010		
741	A	06 22 52.531	-08 12 34.21	0.08	0.08	0.113	1.931	0.061	133.170	2016.172	iT27 1x3s. Touching star disks
	B	06 22 52.757	-08 12 34.24					0.065	44.270		
802	A	06 46 43.580	-04 13 36.25	0.08	0.08	0.113	1.498	0.081	115.930	2016.164	iT27 1x3s
	B	06 46 43.781	-04 13 39.36					0.081	71.810		
979	A	06 30 34.186	11 40 00.60	0.08	0.06	0.100	2.170	0.101	84.130	2016.022	iT27 1x3s. Touching star disks
	B	06 30 34.007	11 40 00.38					0.103	41.860		
982	A	06 32 22.477	03 29 07.96	0.07	0.07	0.099	1.695	0.061	97.930	2016.022	iT27 1x3s. Touching star disks
	B	06 32 22.347	03 29 05.24					0.061	86.390		
984	A	06 36 31.298	05 19 52.79	0.08	0.08	0.113	1.276	0.061	93.620	2016.022	iT27 1x3s
	B	06 36 31.028	05 19 55.88					0.061	94.420		
993	A	06 48 18.805	11 37 31.78	0.07	0.07	0.099	-	0.095	36.310	2016.022	iT27 1x3s. No resolution of B. Has to be fainter than 14.5mag. Estimation from G/J/H/K -mags: 15.25Vmag
	B							-			
996	A	07 00 05.465	09 18 26.80	0.08	0.08	0.113	1.281	0.071	118.870	2016.022	iT27 1x3s
	B	07 00 05.692	09 18 23.02					0.074	47.600		
1005	A	06 34 00.456	-04 44 10.00	0.08	0.09	0.120	2.400	0.100	24.530	2016.164	iT27 1x3s. Touching star disks
	B	06 34 00.272	-04 44 09.17					0.120	13.160		
1006	A	06 34 18.280	-04 43 40.50	0.09	0.07	0.114	2.268	0.073	53.800	2016.164	iT27 1x3s. Touching star disks
	B	06 34 18.096	-04 43 39.65					0.079	29.470		
1057	A	06 53 11.854	-00 12 35.62	0.08	0.08	0.113	2.868	0.095	36.830	2016.096	iT27 1x3s. Touching star disks
	B	06 53 11.944	-00 12 33.81					0.097	30.010		
1057	A	06 53 11.854	-00 12 35.62	0.08	0.08	0.113	0.573	0.095	36.830	2016.096	iT27 1x3s
	C	06 53 12.607	-00 12 34.90					0.092	57.570		
BAL 732	A	06 53 11.854	-00 12 35.62	0.08	0.08	0.113	0.285	0.095	36.830	2016.096	iT27 1x3s. SNR D<20
	D	06 53 13.063	-00 12 21.86					0.111	16.050		
BAL 732	C	06 53 12.607	-00 12 34.90	0.08	0.08	0.113	0.236	0.092	57.570	2016.096	iT27 1x3s
	E	06 53 13.853	-00 12 14.75					0.096	31.360		
1065	A	07 31 08.140	-03 43 06.31	0.07	0.08	0.106	2.232	0.075	40.600	2016.096	iT27 1x3s. Touching star disks
	B	07 31 08.056	-03 43 03.89					0.073	53.970		
1065	A	07 31 08.099	-03 43 05.82	0.07	0.08	0.106	-	0.074	44.360	2016.096	iT27 1x3s. No resolution of C. Has to be fainter than 14.5mag
	C							-			

Table 2 continues on the next page.

Jonckheere Double Star Photometry – Part XII: Mon I

Table 2 (continued).

Obj	C	RA	Dec	dRA	dDec	Err Sep	Err PA	Err Mag	SNR	Date	Notes
1065	A	07 31 08.140	-03 43 06.31	0.07	0.08	0.106	2.232	0.075	40.600	2016.096	iT27 1x3s. Touching star disks
	B	07 31 08.056	-03 43 03.89					0.073	53.970		
1065	A	07 31 08.099	-03 43 05.82	0.07	0.08	0.106	-	0.074	44.360	2016.096	iT27 1x3s. No resolution of C. Has to be fainter than 14.5mag
	C							-			
1106	A	06 44 28.552	10 05 36.80	0.08	0.07	0.106	-	0.071	95.840	2016.022	iT27 1x3s. No resolution of B. Not even a hint of an elongation
	B							-			
1467	A	07 38 32.089	-10 03 01.95	0.08	0.07	0.106	0.051	0.071	123.190	2016.164	iT27 1x3s
	B	07 38 40.001	-10 03 24.47					0.072	71.760		
1467	A	07 38 40.001	-10 03 24.47	0.08	0.07	0.106	0.818	0.072	71.760	2016.164	iT27 1x3s
	C	07 38 40.303	-10 03 18.51					0.073	48.700		
1472	A	06 24 15.918	-07 34 30.37	0.11	0.11	0.156	1.048	0.091	84.500	2018.088	iT24 5x3s
	B	06 24 15.610	-07 34 23.20					0.100	24.680		
1474	A	06 33 35.687	-08 10 28.86	0.08	0.09	0.120	1.015	0.070	255.000	2016.172	iT27 1x3s
	B	06 33 35.460	-08 10 22.96					0.071	126.060		
1475	A	06 42 55.827	-08 50 18.55	0.08	0.08	0.113	0.683	0.071	111.940	2016.172	iT27 1x3s
	B	06 42 55.389	-08 50 25.47					0.072	64.200		
1479	A	06 49 16.657	-04 55 41.34	0.08	0.08	0.113	0.925	0.091	82.370	2016.164	iT27 1x3s
	B	06 49 16.337	-04 55 36.22					0.092	52.560		
1481	A	06 53 44.864	-05 34 29.51	0.08	0.08	0.113	1.252	0.071	123.700	2016.164	iT27 1x3s
	B	06 53 45.164	-05 34 26.91					0.074	47.760		
HJ 2353	A	06 53 44.864	-05 34 29.51	0.08	0.08	0.113	0.404	0.071	123.700	2016.164	iT27 1x3s
	C	06 53 45.403	-05 34 43.37					0.071	90.570		
1482	A	06 53 31.971	-09 58 49.01	0.08	0.09	0.120	0.826	0.070	144.280	2016.172	iT27 1x3s
	B	06 53 31.885	-09 58 40.76					0.070	132.120		
1483	A	06 59 46.664	-08 42 39.47	0.10	0.11	0.149	-	0.071	121.230	2018.088	iT24 5x10s. No resolution. B would have to be fainter than 15.5mag to get not resolved - bogus assumed
	B							-			
1484	A	07 01 25.021	-10 35 44.88	0.07	0.07	0.099	1.435	0.071	78.770	2016.172	iT27 1x3s
	B	07 01 25.253	-10 35 42.90					0.074	42.140		
DAM 1197	A	07 01 25.021	-10 35 44.88	0.07	0.07	0.099	0.629	0.071	78.770	2016.172	iT27 1x3s
	C	07 01 25.398	-10 35 37.78					0.088	19.650		
DAM 1197	A	07 01 25.021	-10 35 44.88	0.07	0.07	0.099	0.531	0.071	78.770	2016.172	iT27 1x3s. SNR D<20
	D	07 01 25.746	-10 35 44.76					0.092	17.600		
1485	A	07 03 22.312	-08 44 28.47	0.08	0.08	0.113	0.972	0.081	113.930	2016.172	iT27 1x3s
	B	07 03 22.380	-08 44 21.88					0.081	106.280		
1487	A	07 12 03.764	-05 26 43.37	0.07	0.07	0.099	1.621	0.071	111.630	2016.164	iT27 1x3s
	B	07 12 03.840	-05 26 46.68					0.074	44.570		
1488	A	07 12 04.892	-05 26 03.75	0.07	0.08	0.106	0.706	0.072	62.510	2016.164	iT27 1x3s
	B	07 12 04.322	-05 26 05.18					0.076	35.670		
1496	A	07 33 57.837	-01 41 40.29	0.08	0.09	0.120	0.612	0.080	135.840	2016.090	iT27 1x3s
	B	07 33 57.986	-01 41 29.24					0.081	97.260		
1498	A	07 34 44.029	-10 50 40.39	0.06	0.07	0.092	0.718	0.070	173.160	2016.167	iT27 1x3s
	B	07 34 44.059	-10 50 47.73					0.070	131.790		
1500	A	07 39 15.567	-08 39 45.50	0.08	0.08	0.113	1.008	0.062	76.570	2016.164	iT27 1x3s
	B	07 39 15.532	-08 39 51.91					0.069	30.930		
1504	A	07 52 51.710	-07 58 17.14	0.07	0.09	0.114	0.701	0.070	213.840	2016.107	iT27 1x3s
	B	07 52 51.114	-07 58 20.05					0.071	125.040		
1828	A	07 04 05.007	-09 13 23.43	0.08	0.08	0.113	1.158	0.081	105.370	2016.172	iT27 1x3s
	B	07 04 05.073	-09 13 28.94					0.083	48.700		
1923	A	06 10 31.542	-04 22 36.51	0.08	0.07	0.106	1.141	0.071	89.880	2016.164	iT27 1x3s
	B	06 10 31.749	-04 22 32.16					0.072	72.790		
1944	A	06 23 54.612	02 00 08.86	0.08	0.08	0.113	0.805	0.071	90.950	2016.090	iT27 1x3s
	B	06 23 54.875	02 00 15.88					0.074	45.140		
1945	A	06 27 12.930	11 17 55.15	0.07	0.07	0.099	0.747	0.092	53.080	2016.022	iT27 1x3s
	B	06 27 13.446	11 17 54.90					0.093	50.320		
1949	A	06 28 22.595	-04 27 43.94	0.07	0.08	0.106	0.121	0.080	130.010	2016.164	iT27 1x3s
	B	06 28 19.521	-04 28 04.80					0.081	114.810		
1949	B	06 28 19.521	-04 28 04.80	0.07	0.08	0.106	0.815	0.081	114.810	2016.164	iT27 1x3s
	C	06 28 19.181	-04 28 10.28					0.081	103.780		
1963	A	06 37 21.745	-03 42 10.58	0.07	0.08	0.106	0.692	0.060	145.940	2016.164	iT27 1x3s
	B	06 37 21.250	-03 42 15.32					0.061	113.130		

Table 2 continues on the next page.

Jonckheere Double Star Photometry – Part XII: Mon I

Table 2 (continued).

Obj	C	RA	Dec	dRA	dDec	Err Sep	Err PA	Err Mag	SNR	Date	Notes
1966	A	06 40 17.950	02 16 53.87	0.09	0.07	0.114	0.567	0.071	88.930	2016.090	iT27 1x3s
	B	06 40 17.805	02 17 05.18					0.076	37.610		
1967	A	06 40 35.089	02 17 26.07	0.07	0.08	0.106	0.787	0.061	90.950	2016.090	iT27 1x3s
	B	06 40 35.603	02 17 26.79					0.062	71.730		
1972	A	06 44 07.657	00 07 00.68	0.09	0.08	0.120	1.275	0.075	38.780	2016.096	iT27 1x3s
	B	06 44 07.407	00 06 56.78					0.080	27.400		
1977	A	06 56 35.868	04 12 58.79	0.07	0.08	0.106	0.612	0.070	178.500	2016.022	iT27 1x3s
	B	06 56 36.037	04 12 49.17					0.073	55.770		
1978	A	06 56 38.041	03 18 07.76	0.07	0.07	0.099	1.004	0.070	218.250	2016.022	iT27 1x3s
	B	06 56 37.665	03 18 07.29					0.071	88.930		
1987	A	07 02 36.906	02 50 16.71	0.08	0.09	0.120	1.150	0.070	138.600	2016.022	iT27 1x3s
	B	07 02 36.507	02 50 16.21					0.071	77.360		
1988	A	07 02 41.279	02 50 25.43	0.08	0.09	0.120	0.825	0.071	120.860	2016.022	iT27 1x3s
	B	07 02 40.823	02 50 20.61					0.071	89.360		
1995	A	06 27 37.744	00 37 12.28	0.06	0.06	0.085	0.493	0.074	46.900	2016.096	iT27 1x3s
	B	06 27 38.263	00 37 06.24					0.085	22.150		
2006	A	06 40 35.791	-00 39 35.81	0.08	0.09	0.120	1.013	0.071	106.150	2016.096	iT27 1x3s
	B	06 40 36.164	-00 39 39.69					0.071	75.050		
2010	A	07 02 47.368	-04 34 31.98	0.08	0.09	0.120	1.104	0.070	163.440	2016.164	iT27 1x3s
	B	07 02 47.772	-04 34 30.38					0.071	116.670		
2024	A	06 42 13.754	-00 47 49.77	0.08	0.08	0.113	2.947	0.082	57.940	2016.096	iT27 1x3s. Touching star disks
	B	06 42 13.850	-00 47 48.11					0.082	54.660		
2025	A	06 44 02.738	-00 57 07.07	0.13	0.12	0.177	2.390	0.113	42.860	2018.088	iT24 5x3s
	B	06 44 02.614	-00 57 10.88					0.119	24.120		
2027	A	06 47 19.439	10 06 01.53	0.08	0.08	0.113	1.338	0.081	75.460	2016.022	iT27 1x3s
	B	06 47 19.112	10 06 01.15					0.085	37.170		
2427	A	06 24 48.317	00 04 29.97	0.07	0.07	0.099	1.703	0.064	45.480	2016.096	iT27 1x3s
	B	06 24 48.208	00 04 32.87					0.070	28.900		
2432	A	06 41 51.289	00 06 55.21	0.07	0.07	0.099	1.917	0.083	48.880	2016.096	iT27 1x3s
	B	06 41 51.262	00 06 52.28					0.086	34.350		
2434	A	06 45 32.623	04 23 38.19	0.08	0.06	0.100	0.873	0.060	236.390	2016.022	iT27 1x3s
	B	06 45 32.234	04 23 41.22					0.061	96.870		
2446	A	06 53 46.986	10 06 56.62	0.08	0.08	0.113	2.591	0.072	62.280	2016.022	iT27 1x3s
	B	06 53 47.145	10 06 55.76					0.074	45.370		
2447	A	06 53 45.182	-10 52 01.56	0.08	0.07	0.106	1.621	0.061	112.770	2016.172	iT27 1x3s
	B	06 53 44.927	-10 52 01.56					0.062	68.850		
2450	A	07 03 03.417	-00 28 21.41	0.09	0.08	0.120	1.979	0.072	65.100	2016.096	iT27 1x3s. Touching star disks. SNR B<20
	B	07 03 03.630	-00 28 22.80					0.092	17.530		
2453	A	07 07 53.635	00 48 48.23	0.08	0.08	0.113	1.396	0.073	49.430	2016.090	iT27 1x3s
	B	07 07 53.771	00 48 44.06					0.074	43.000		
2454	A	07 09 49.140	00 28 57.92	0.07	0.08	0.106	1.239	0.071	77.650	2016.090	iT27 1x3s
	B	07 09 49.038	00 29 02.59					0.072	73.100		
2458	A	07 14 55.563	-01 13 07.08	0.08	0.08	0.113	1.522	0.083	50.320	2016.096	iT27 2x3s
	B	07 14 55.449	-01 13 10.98					0.088	29.980		
2459	A	07 15 24.751	-11 05 48.44	0.08	0.09	0.120	1.135	0.071	124.990	2016.172	iT27 1x3s
	B	07 15 25.149	-11 05 50.05					0.071	116.570		
2461	A	07 17 02.371	-10 34 56.57	0.08	0.08	0.113	1.055	0.091	98.590	2016.172	iT27 1x3s
	B	07 17 02.237	-10 34 50.75					0.092	60.100		
2462	A	07 17 06.175	-10 32 23.23	0.08	0.08	0.113	0.750	0.081	85.230	2016.172	iT27 1x3s
	B	07 17 06.194	-10 32 14.59					0.083	52.960		
2464	A	07 18 11.762	-10 31 32.49	0.08	0.08	0.113	1.196	0.092	52.630	2016.172	iT27 1x3s
	B	07 18 12.071	-10 31 29.56					0.093	42.970		
2477	A	07 28 04.725	-03 31 05.17	0.07	0.08	0.106	2.176	0.082	55.360	2016.096	iT27 1x3s
	B	07 28 04.889	-03 31 03.83					0.087	32.280		
2482	A	07 34 14.014	-01 35 08.63	0.07	0.09	0.114	1.492	0.070	7094.000	2016.090	iT27 1x3s
	B	07 34 14.123	-01 35 04.57					0.073	50.700		
2485	A	07 41 36.579	-10 43 28.70	0.09	0.09	0.127	1.170	0.074	43.810	2016.164	iT27 1x3s
	B	07 41 36.915	-10 43 32.48					0.081	26.370		
2487	A	07 46 13.953	-06 02 29.74	0.07	0.08	0.106	0.893	0.081	69.820	2016.096	iT27 1x3s
	B	07 46 14.283	-06 02 34.46					0.085	37.140		

Table 2 continues on the next page.

Jonckheere Double Star Photometry – Part XII: Mon I

Table 2 (continued).

Obj	C	RA	Dec	dRA	dDec	Err Sep	Err PA	Err Mag	SNR	Date	Notes
2491	A	07 57 20.130	-03 46 09.87	0.04	0.05	0.064	0.949	0.114	36.740	2016.022	iT27 1x3s
	B	07 57 20.169	-03 46 06.05					0.118	25.370		
2493	A	08 10 12.748	-11 09 40.57	0.09	0.08	0.120	0.940	0.071	81.360	2016.096	iT27 1x3s
	B	08 10 12.403	-11 09 35.27					0.076	37.310		
2611	A	06 48 07.842	09 44 12.08	0.08	0.06	0.100	1.329	0.092	52.220	2016.022	iT27 1x3s
	B	06 48 08.071	09 44 09.41					0.098	27.520		
2611	A	06 48 07.842	09 44 12.08	0.08	0.06	0.100	0.330	0.092	52.220	2016.022	iT27 1x3s
	C	06 48 07.595	09 44 29.05					0.102	22.070		
2616	A	06 54 24.524	-00 09 09.23	0.08	0.08	0.113	1.266	0.075	37.990	2016.096	iT27 1x3s
	B	06 54 24.519	-00 09 04.11					0.075	38.190		
2616	A	06 54 24.524	-00 09 09.23	0.08	0.08	0.113	0.303	0.075	37.990	2016.096	iT27 1x3s. SNR B<20
	C	06 54 24.965	-00 08 48.85					0.101	14.490		
2623	A	07 09 11.895	-05 16 54.60	0.07	0.07	0.099	1.040	0.071	86.730	2016.164	iT27 1x3s
	B	07 09 12.223	-05 16 56.99					0.072	67.480		
2636	A	08 02 20.022	-06 26 02.89	0.08	0.08	0.113	1.485	0.071	88.870	2016.090	iT27 1x3s
	B	08 02 20.274	-06 26 00.67					0.081	26.380		
2637	A	08 02 26.292	-06 25 53.89	0.08	0.08	0.113	0.925	0.071	78.360	2016.090	iT27 1x3s
	B	08 02 25.879	-06 25 57.24					0.079	28.980		
2758	A	06 51 23.483	-03 54 46.62	0.08	0.08	0.113	2.116	0.074	46.660	2016.164	iT27 1x3s
	B	06 51 23.650	-03 54 48.39					0.076	37.850		
2766	A	06 57 44.312	-04 36 55.72	0.07	0.07	0.099	1.055	0.072	65.150	2016.164	iT27 1x3s
	B	06 57 44.543	-04 36 51.60					0.072	59.330		
2768	A	06 58 38.918	-09 09 47.34	0.08	0.08	0.113	1.105	0.082	62.490	2016.172	iT27 1x3s
	B	06 58 39.240	-09 09 43.92					0.082	56.750		
2769	A	06 59 39.058	02 19 33.41	0.07	0.06	0.092	0.952	0.073	56.800	2016.022	iT27 1x3s
	B	06 59 39.402	02 19 35.46					0.072	59.800		
2770	A	06 59 58.224	-05 06 26.30	0.07	0.07	0.099	0.679	0.071	127.040	2016.164	iT27 1x3s
	B	06 59 58.269	-05 06 34.63					0.073	51.020		
2772	A	07 03 06.929	-04 24 29.59	0.08	0.08	0.113	0.950	0.062	68.520	2016.164	iT27 1x3s
	B	07 03 07.274	-04 24 34.05					0.064	49.630		
2774	A	07 04 21.964	09 15 55.73	0.08	0.08	0.113	1.648	0.073	54.600	2016.022	iT27 1x3s
	B	07 04 22.223	09 15 56.60					0.076	37.290		
2776	A	07 05 05.390	00 58 41.08	0.07	0.08	0.106	0.937	0.081	94.790	2016.090	iT27 1x3s
	B	07 05 05.133	00 58 35.85					0.084	40.010		
2781	A	07 08 11.370	-01 51 34.03	0.09	0.08	0.120	1.390	0.082	61.760	2016.096	iT27 1x3s
	B	07 08 11.039	-01 51 34.15					0.088	29.070		
BAL 409	A	07 08 11.089	-01 51 59.25	0.09	0.08	0.120	0.270	0.081	81.030	2016.096	iT27 1x3s
	B	07 08 11.370	-01 51 34.03					0.082	61.760		
2782	A	07 08 07.726	-10 36 17.33	0.07	0.08	0.106	1.716	0.071	110.910	2016.172	iT27 1x3s
	B	07 08 07.490	-10 36 16.64					0.071	77.510		
2784	A	07 08 28.485	00 57 40.49	0.08	0.08	0.113	0.996	0.083	50.080	2016.090	iT27 1x3s
	B	07 08 28.634	00 57 34.38					0.083	45.960		
2788	A	07 10 33.789	-10 11 44.75	0.09	0.09	0.127	1.398	0.073	48.270	2016.172	iT27 1x3s. PA in last WDS measurement in error
	B	07 10 33.491	-10 11 41.95					0.076	35.550		
2789	A	07 11 34.397	-07 48 48.77	0.08	0.07	0.106	0.937	0.071	94.690	2016.167	iT27 1x3s
	B	07 11 34.832	-07 48 48.11					0.072	68.070		
2792	A	07 14 40.184	-02 11 43.60	0.08	0.07	0.106	1.902	0.076	34.740	2016.096	iT27 1x3s
	B	07 14 40.179	-02 11 46.80					0.077	34.440		
2793	A	07 14 14.703	-10 06 19.34	0.07	0.08	0.106	2.480	0.072	62.290	2016.172	iT27 1x3s
	B	07 14 14.864	-10 06 19.95					0.073	48.640		
2796	A	07 15 00.442	-06 52 52.08	0.08	0.10	0.128	1.110	0.088	29.100	2016.164	iT27 1x3s. SNR B<20
	B	07 15 00.358	-06 52 45.59					0.126	10.610		

Table 2 continues on the next page.

Jonckheere Double Star Photometry – Part XII: Mon I

Table 2 (continued).

Obj	C	RA	Dec	dRA	dDec	Err Sep	Err PA	Err Mag	SNR	Date	Notes
2798	A	07 15 43.769	-10 40 15.45	0.08	0.09	0.120	1.694	0.081	72.120	2016.172	iT27 1x3s
	B	07 15 43.944	-10 40 18.60					0.083	53.160		
2802	A	07 16 06.432	-01 37 35.14	0.09	0.07	0.114	1.561	0.082	57.580	2016.096	iT27 1x3s
	B	07 16 06.153	-01 37 35.18					0.084	40.160		
2804	A	07 16 37.283	-10 05 38.17	0.08	0.08	0.113	1.214	0.081	86.820	2016.172	iT27 1x3s
	B	07 16 37.064	-10 05 33.92					0.081	72.250		
2809	A	07 18 39.435	-06 56 24.60	0.07	0.07	0.099	1.059	0.083	51.850	2016.164	iT27 1x3s
	B	07 18 39.239	-06 56 29.09					0.091	24.030		
2810	A	07 19 30.249	-03 03 55.96	0.08	0.08	0.113	1.124	0.072	61.710	2016.096	iT27 1x3s
	B	07 19 30.354	-03 04 01.51					0.085	21.950		
2816	A	07 25 32.433	-03 26 01.46	0.07	0.07	0.099	0.998	0.098	27.640	2016.096	iT27 1x3s. SNR B<20
	B	07 25 32.150	-03 25 57.67					0.118	13.760		
2817	A	07 26 31.276	-02 33 52.04	0.08	0.08	0.113	1.398	0.072	61.610	2016.096	iT27 1x3s
	B	07 26 31.112	-02 33 48.11					0.073	48.750		
2822	A	07 27 15.897	-03 48 36.24	0.07	0.10	0.122	1.144	0.093	43.290	2016.096	iT27 1x3s
	B	07 27 15.503	-03 48 34.63					0.100	24.430		
2823	A	07 27 35.396	-07 01 21.88	0.07	0.09	0.114	1.431	0.075	39.900	2016.164	iT27 1x3s
	B	07 27 35.701	-07 01 22.35					0.084	23.040		
2825	A	07 28 02.170	-07 44 18.82	0.06	0.07	0.092	0.809	0.072	66.170	2016.164	iT27 1x3s
	B	07 28 02.361	-07 44 12.94					0.072	66.140		
2831	A	07 32 23.419	-04 31 03.00	0.08	0.08	0.113	1.503	0.062	73.010	2016.096	iT27 1x3s
	B	07 32 23.603	-04 31 06.32					0.064	49.630		
2833	A	07 33 05.234	-04 29 56.10	0.07	0.08	0.106	0.801	0.072	69.800	2016.096	iT27 1x3s
	B	07 33 05.738	-04 29 55.10					0.074	47.320		
2834	A	07 33 48.247	-04 31 29.42	0.07	0.08	0.106	1.209	0.073	49.530	2016.096	iT27 1x3s
	B	07 33 48.104	-04 31 33.98					0.074	44.110		
2836	A	07 34 00.694	-09 34 52.50	0.08	0.08	0.113	1.047	0.082	66.850	2016.164	iT27 1x3s
	B	07 34 01.024	-09 34 48.69					0.086	33.280		
2837	A	07 34 59.225	-04 58 50.38	0.08	0.08	0.113	0.701	0.061	86.480	2016.107	iT27 1x3s
	B	07 34 59.164	-04 58 59.58					0.064	47.290		
2839	A	07 36 25.885	-03 34 42.62	0.07	0.09	0.114	0.772	0.072	59.270	2016.096	iT27 1x3s
	B	07 36 25.320	-03 34 42.59					0.076	36.140		
2842	A	07 37 52.430	-05 21 10.06	0.08	0.09	0.120	0.744	0.061	100.900	2016.107	iT27 1x3s
	B	07 37 52.233	-05 21 01.27					0.061	96.910		
2845	A	07 39 37.905	-10 12 31.96	0.08	0.22	0.234	2.761	0.109	24.790	2016.164	iT27 1x3s. Image quality a bit questionable - yet it seems clear that the last "precise" measurement was for a wrong object nearby
	B	07 39 38.141	-10 12 28.58					0.108	25.510		
2846	A	07 39 50.659	-09 26 38.00	0.07	0.08	0.106	0.876	0.071	81.640	2016.164	iT27 1x3s
	B	07 39 50.860	-09 26 44.28					0.072	62.240		
2850	A	07 43 36.236	-02 28 16.29	0.07	0.08	0.106	0.887	0.082	57.720	2016.090	iT27 1x3s
	B	07 43 35.849	-02 28 19.97					0.089	26.670		
2854	A	07 50 29.625	-02 06 54.66	0.07	0.08	0.106	0.876	0.072	65.980	2016.022	iT27 1x3s
	B	07 50 30.057	-02 06 52.12					0.072	59.310		
2858	A	07 55 25.879	-07 19 10.16	0.08	0.06	0.100	0.756	0.074	45.290	2016.096	iT27 1x3s. SNR B<20
	B	07 55 26.057	-07 19 03.06					0.092	17.490		
2859	A	07 57 51.037	-03 42 30.88	0.06	0.07	0.092	1.888	0.083	52.720	2016.022	iT27 1x3s
	B	07 57 51.180	-03 42 32.68					0.083	48.260		
2860	A	07 57 47.442	-04 56 25.15	0.07	0.08	0.106	1.088	0.085	38.730	2016.090	iT27 1x3s
	B	07 57 47.084	-04 56 26.80					0.088	29.490		
2864	A	08 04 31.839	-09 06 53.43	0.07	0.08	0.106	1.261	0.077	21.970	2016.096	iT27 1x3s. Image quality a bit questionable
	B	08 04 31.553	-09 06 55.75					0.081	19.280		
2865	A	08 04 33.019	-09 09 12.06	0.06	0.07	0.092	1.146	0.072	70.420	2016.096	iT27 1x3s
	B	08 04 32.804	-09 09 15.39					0.073	51.960		
2866	A	08 05 39.543	-04 21 59.45	0.08	0.07	0.106	0.655	0.072	69.640	2016.022	iT27 1x3s
	B	08 05 38.931	-04 21 57.83					0.073	49.980		
2866	B	08 05 38.931	-04 21 57.83	0.08	0.07	0.106	1.278	0.073	49.980	2016.022	iT27 1x3s
	C	08 05 39.115	-04 22 01.72					0.077	33.370		

Table 2 concludes on the next page.

Jonckheere Double Star Photometry – Part XII: Mon I

Table 2 (conclusion).

Obj	C	RA	Dec	dRA	dDec	Err Sep	Err PA	Err Mag	SNR	Date	Notes
2867	A	08 05 52.756	-06 14 42.77	0.08	0.09	0.120	0.739	0.095	33.940	2016.090	iT27 1x3s
	B	08 05 52.256	-06 14 37.15					0.094	40.290		
2868	A	08 05 56.684	-06 14 52.29	0.07	0.08	0.106	0.898	0.091	68.890	2016.090	iT27 1x3s
	B	08 05 56.736	-06 14 45.55					0.094	40.670		
2869	A	08 08 33.580	-09 57 44.39	0.07	0.06	0.092	0.728	0.081	94.860	2016.096	iT27 1x3s
	B	08 08 33.321	-09 57 50.56					0.083	52.340		
2870	A	08 08 18.174	-09 16 30.19	0.07	0.08	0.106	0.927	0.072	58.890	2016.096	iT27 1x3s
	B	08 08 18.511	-09 16 34.46					0.084	23.020		
2871	A	08 09 28.708	-10 47 09.76	0.08	0.08	0.113	1.277	0.073	52.200	2016.096	iT27 1x3s
	B	08 09 28.602	-10 47 14.59					0.074	44.750		
3230	A	07 03 58.921	-07 09 57.03	0.06	0.07	0.092	0.964	0.060	234.160	2016.167	iT27 1x3s
	B	07 03 59.286	-07 09 56.31					0.061	103.190		
3286	A	08 05 50.099	-06 14 19.50	0.07	0.08	0.106	2.288	0.094	42.340	2016.090	iT27 1x3s. Touching star disks
	B	08 05 50.234	-06 14 21.24					0.097	30.210		
3309	A	07 03 32.377	-08 40 29.85	0.08	0.08	0.113	1.769	0.073	56.170	2016.172	iT27 1x3s
	B	07 03 32.567	-08 40 27.51					0.086	21.230		

- Obj = either J number or discoverer code if no J object
- C = components
- dRA and dDec = average RA and Dec plate solving errors in arcseconds
- Err_Sep = separation error estimation in arcseconds calculated as

$$Err\_Sep = \sqrt{dRA^2 + dDec^2}$$

- Err_PA = position angle error estimation in degrees calculated as

$$Err\_PA = \arctan\left(\frac{Err\_Sep}{Sep}\right)$$

- assuming the worst case that Err_Sep points perpendicular to the separation vector
- dmag = average mag plate solving error (Vmag for images with made V-filter and Imag for images made with I-filter)
- Err_Mag = magnitude error estimation calculated as

$$Err\_Mag = \sqrt{dV_{mag}{}^2 + \left[2.5\log\left(1+\frac{1}{SNR}\right)\right]^2}$$

- SNR = signal to noise ratio for the given object
- Date = Julian observation epoch

Astrometric Measurements of WDS 00198+7518 (HJ 1950) and WDS 01373+6344 (MLB 383AD)

Leilani Trautman, Donald Sheahan, Justin Perng, John Gooding, Robert Zarick, Sébastien Cormier, and Philip Blanco
Grossmont College, El Cajon, California

Abstract: CCD astrometric measurements of the double star systems WDS 00198+7518 HJ 1950 and WDS 01373+6344 MLB 383AD are reported. In conjunction with historical observations the new data suggest that both systems are optical doubles.

Introduction

The systems were selected based on these constraints: right ascension between 00 and 08 hours, declination of greater than +40 degrees, less than six magnitude difference between primary and secondary stars, and a minimum separation of 5.5 arcseconds. To satisfy these criteria the authors chose WDS 00198+7518 (also known as HJ 1950) and WDS 01373+6344 (also known as MLB 383AD).

The renowned double star astronomer J. F. W. Herschel, son of William Herschel, discovered HJ 1950 in Cepheus in 1831. Since then there have been ten observations made with the most recent in 2010. From 1831 to 2010 the position angle (Theta) was measured to change from 71 degrees to 67 degrees while the separation (Rho) varied from 12 to 22.3 arcseconds. The magnitudes of the primary and secondary star are 10.2 and 12.6, respectively. The spectral type of the primary star is K2, a yellow-orange color star. According to Stelle Doppie the relative proper motion (rPM) of HJ 1950 is 1.03 (Stelle Doppie). Relative proper motion is a calculation that roughly indicates whether a system is optical or physical. An rPM greater than 0.8 is predicted to be optical therefore the rPM of 1.03 for HJ 1950 means that the system is predicted to be an optical double (Stelle Doppie).

MLB 383AD is a component of a quadruple system in Cassiopeia. The AD components were the focus of the measurements because the separation between the A and B components was too minimal to be properly imaged by the available equipment. In addition, the authors decided it would be best to focus analysis on AD components rather than the AC components because the AC components had only 4 observations which was deemed insufficient to draw any meaningful conclusions. MLB 383 was first discovered by T. E. Espin and W. Milburn in 1898, and the AD component was first observed in 1898 (Urban, Corbin, Wycoff, et al 1998). Since then there have been nine observations made of the AD components with the most recent in 2015. From 1898 to 2015 Theta was measured to change from 169 degrees to 175 degrees while Rho varied from 30.7 to 31.8 arcseconds. The magnitudes of the primary and secondary star are 10.47 and 11.35, respectively. The spectral type of the primary star is B8, a blue-white color star. According to past measurements it is possibly an optical double as its rPM was found to be 1.09 (Stelle Doppie).

Materials and Methods

Images of HJ 1950 were taken on December 9, 2016 by iTelescope's New Mexico T21 Planewave 17" CDK telescope which uses a FLI-PL6303E CCD camera with a pixel scale of 0.96 arcseconds. The images of MLB 383AD were taken on November 30, 2016 and were provided by iTelescope's New Mexico T11 Planewave 20" CDK telescope which uses a FLI Pro-Line PL11002M CCD camera with a pixel scale of 0.81 arcseconds. MAXIM DL6 was used to provide WCS coordinates for the FITS images and MIRA Pro x64 was used to measure the separations and position angles.

Results

For HJ 1950 Table 1 shows the new calculated position angle and separation, and Table 2 shows a historical comparison to the most recent prior observation and the first observation. These new measurements are consistent with those made by Cutri et al (2010) with a difference of 1 degree in position angle and 0.47 arcseconds in separation. The results are plotted together with historical observations in Figure 1.

For MLB 383AD, Table 3 shows the new calculated position angle and separation, and Table 4 shows a historical comparison to the most recent prior observation and the first observation. The position angle and separation are slightly greater but consistent with the previous values reported by Harshaw (2016) by +0.55 degrees and +0.11 arcseconds, respectively. The results are plotted together with historical observations in Figure 2.

Table 1. Astrometry results for WDS 00198+7518 HJ 1950

WDS 00198+7518 (HJ 1950) Astrometry for Epoch 2016.9390			
Measurement	**Theta (degrees)**	**Rho (arcseconds)**	**Telescope: (number of images used in each filter)**
Mean	65.5	22.78	iTelescope T21 (1 luminance, 2 Hydrogen-alpha)
Standard Deviation	0.48	0.04	
Standard Error of Mean	0.28	0.02	

Table 2. Historical comparisons for WDS 00198+7518 HJ 1950

WDS 00198+7518 (HJ 1950) Historical Comparison		
Epoch	**Theta (degrees)**	**Rho (arcseconds)**
1831.84 (Discovery)	71.3	12.
2010.5589 (Last one previous to this investigation)	66.5	22.31
2016.9390 (The authors' measurement)	65.5	22.78

Table 3. Astrometry results for WDS 01373+6344 MLB 383AD

WDS 01373+6344 (MLB 383AD) Astrometry for Epoch 2016.9090			
Measurement	**Position Angle (degrees)**	**Separation (arcseconds)**	**Telescope: (number of images used in each filter)**
Mean	165.2	31.90	iTelescope T11 (2 luminance, 1 hydrogen-alpha)
Standard Deviation	0.18	0.05	
Standard Error of Mean	0.10	0.03	

Table 4. Historical comparisons for WDS 01373+6344 MLB 383AD

WDS 01373+6344 (MLB 383AD) Historical Comparison		
Epoch	**Theta (degrees)**	**Rho (arcseconds)**
1898.97 (Discovery)	169.4	30.695
2015.877 (Last one previous to this investigation)	164.819	31.752
2016.9090 (The authors' measurement)	165.2	31.90

(Text continues on page 651)

Astrometric Measurements of WDS 00198+7518 (HJ 1950) and WDS 01373+6344 (MLB 383AD)

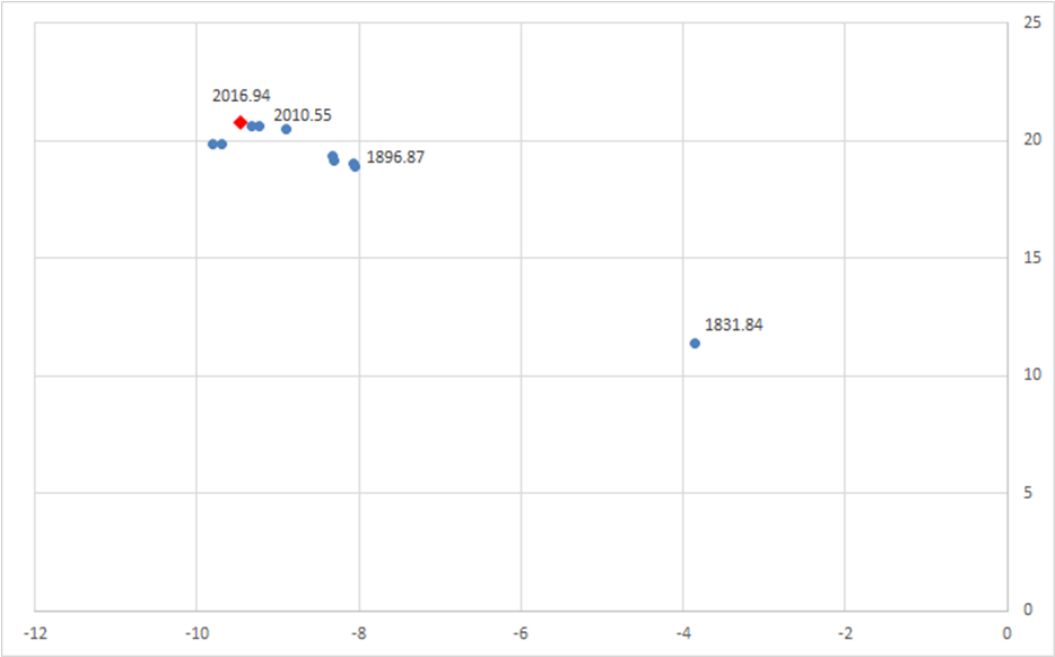

Figure 1. Historical observations of WDS 00198+7518 HJ 1950 with B component plotted with respect to the A component at (0, 0).

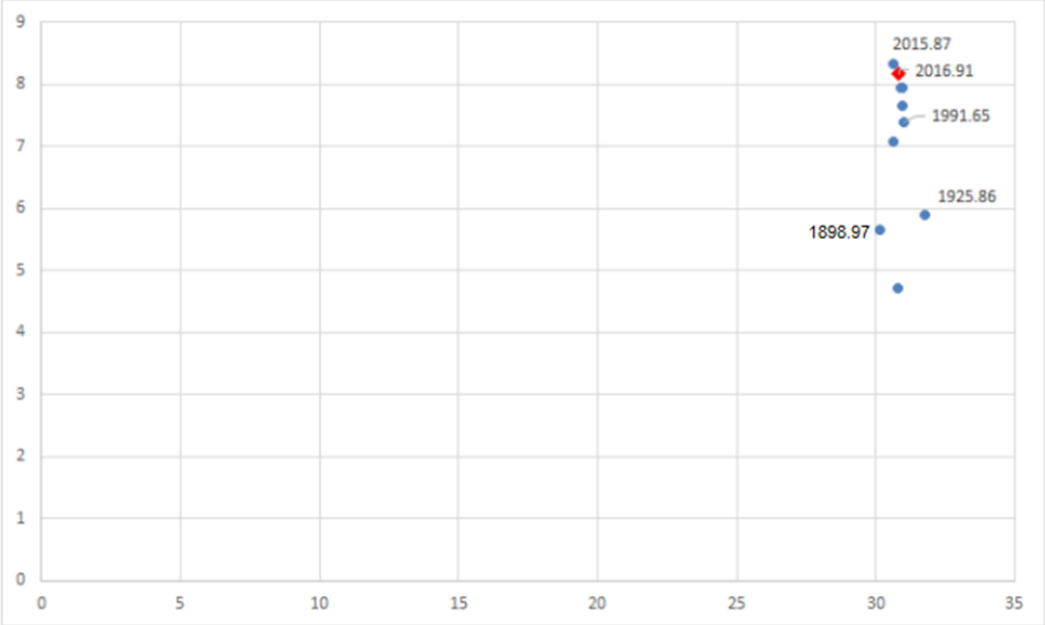

Figure 2. Historical observations of WDS 01373+6344 MLB 383AD with B component plotted with respect to the A component at (0, 0).

Discussion

The graph of WDS 00198+7518 HJ 1950 indicates that the secondary component remains in the same general area as the other measurements if the first measurement in 1831 is considered an outlier. The graph of WDS 01373+6344 MLB 383AD suggests the continuation of a linear trend in motion.

When considered in combination with previous measurements, these results indicate that neither of the two systems currently exhibit the change in position over time characteristic of orbital motion that may indicate a physical double system. These measurements, suggesting the systems are likely continuing their historic linear trends, are important because they contribute to the collection of data in the WDS catalog that can be used to eliminate or confirm physical doubles. Either set of data may or may not represent a small snapshot of a very large orbital path that would require many centuries of measurements to understand accurately. It is possible that either or both of the systems could be long-period physical doubles. An accurate measurement of distance between the components of each system as could be provided by an astrometric satellite would help determine whether or not the stars are close enough to be physical binaries.

Conclusion

A current area of astronomical research is the analysis of double star candidates, such as those identified in the WDS catalog, with the goal of evaluating their status as physical or optical doubles. Specifically, the most recent measurements agree with predictions of a linear trend in motion. Future measurements will help establish the true nature of this system.

Acknowledgements

The authors would like to thank the Boyce Research Initiatives and Education Foundation (BRIEF) for their generous support in the form of iTelescope and remote server services. The authors also thank the U.S. Naval Observatory, especially Brian Mason, for providing historical data. Finally, the authors thank Dr. Sébastien Cormier and Dr. Philip Blanco for their guidance and mentorship, and Pat and Grady Boyce for their review of this paper.

This research was conducted as an honors project in the Physics Department of Grossmont College, El Cajon, California, USA. This research was also supported by the Institute for Student Astronomical Research (InStAR) and conducted by Boyce Research Initiatives and Education Foundation (BRIEF).

References

"00198+7518 HJ 1950." *Stelle Doppie*. Gianluca Sordiglioni, 2016. Web. 07 July 2017.

"01373+6344 MLB 383AD." *Stelle Doppie*. Gianluca Sordiglioni, 2016. Web. 07 July 2017.

Cutri, R.M. et al. 2014. *VizieR On-line Data Catalog: II/328.*

http://adsabs.harvard.edu/abs/2014yCat.2328....0C

Espin, T. E., Milburn, W., 1926, *Monthly Notices of the Astronomical Society*, **86**, 131.

http://adsabs.harvard.edu/abs/1926MNRAS..86..131E

Harshaw, Richard W., 2015, "CCD Measurements of 8 Double Stars With Binary Nature", *Journal of Double Star Observations*, **12** (4), 388-293.

Herschel, J. F. W., 1833, *Memoirs of the Royal Astronomical Society*, **6**, 1.

http://adsabs.harvard.edu/abs/1833MmRAS...6....1H

Stelle Doppie. Gianluca Sordiglioni, 2016. Web. 08 July 2017.

Urban, S. E., Corbin, T. E., Wycoff, G. L., Martin, J. C., Jackson, E. S., Zacharias, M. I., Hall, D. M., 1998, *The Astronomical Journal*, **115**, 1212. http://adsabs.harvard.edu/abs/1998AJ....115.1212U

A Comparison of Methods for Astrometric Measurements of Close Double Stars

Alex Cherney
Melbourne, Australia
alex@terrastro.com

Abstract: Off-the-shelf equipment – an 8-inch Schmidt-Cassegrain telescope and a DSLR camera - were used for observations of 18 double stars with separation in the 0.5 – 11" range.

All 18 double stars were measured with the Speckle Interferometry method. 8 double stars were also measured with the Lucky Imaging method and 5 – with the Video Drift Method. The results obtained with each method were compared with computed ephemerides from published orbits and latest precise observations.

Speckle interferometry measurements of double stars wider than 1" produced the average O-C residuals of 0.52º PA and 0.04" separation. For the Lucky Imaging method, the average residuals were 0.9º and 0.03". For the pairs wider than 4.3" Video Drift method was applicable and the residuals were 0.46º and 0.06". A potential error in the Sixth Orbit Catalog for HDO 182 (λ Scl) Grade 5 orbit was identified.

A brief historic background of double star research, methods of measurement and results are presented. Additionally, the quantitative assessment of methods with error analysis is performed.

Introduction

A variety of methods for measuring separations and position angles of double stars are readily available to the amateur astronomy community. These methods range from a micrometer eyepiece for visual observations to Speckle Interferometry, using high-speed digital video cameras for accurate diffraction-limited measurements (Argyle 2012). The main goal of this research project is to assess and compare methods for astrometric measurements of relatively close visual double stars, attainable with modest optical equipment and off-the-shelf digital video cameras.

The precision of double star measurements with a video camera depends on a number of factors, such as the resolving power and optical quality of the telescope, stability of the tracking mount, resolution of the CCD or CMOS detector and, and last but not least, distortions introduced by Earth's atmosphere. Optical, mechanical and electronic factors can be addressed by selecting the appropriate equipment, but unfortunately, favourable atmospheric seeing cannot be simply "ordered" and quite often the observations have to be performed in rather poor seeing conditions.

Speckle Interferometry (Labeyrie 1970) and Lucky Imaging (Boffin et al. 2016) methods overcome the seeing effects by using short exposures and can achieve accurate results with smaller aperture telescopes, approaching the theoretical resolution limits.

A large number of amateur astronomers own reflector telescopes on Altitude-Azimuth mounts, some with considerable resolving power (apertures of 20 inches and above). Video Drift method (Nugent & Iverson 2011) uses multiple position measurements to produce accurate results without expensive Equatorial mounts, required to support larger telescopes.

The goal of this research project is to assess double star measurement methods available to amateur astronomers with modest commercially available equipment – a telescope with an 8-inch aperture and a DSLR camera, which can also be used for day-time photography of cats, dogs and other objects of interest.

The observations were made with 8" Schmidt-Cassegrain telescope at 37.98° S latitude, 145.06° E longitude, Melbourne, Australia

History of double star observations

The term "double star" was first mentioned by Ptolemy when he described v1 and v2 Sagittarii in his star

catalog from 2nd century AD (Heintz 1978). Using modern terminology, we would call it an "optical double" because v1 and v2 Sagittarii are not gravitationally bound and have an appearance of a double star due to a coincidental line of sight alignment, as viewed from Earth.

Until late 18th century the common assumption amongst astronomers was that double stars were located close to each other in the sky by chance. That changed however, when John Mitchell used mathematical statistics and argued (Mitchell 1767) that stars did not follow random distribution on the celestial sphere and there were a lot more stars grouped in some parts of the sky, compared to the others due to some general law (perhaps gravity). Soon after Mitchell's paper, W. Herschel began to study double stars with his powerful reflecting telescopes. Over the course of 25 years he noticed a change of position in some pairs of stars and proposed that these were due to orbital motions.

In the 19th century the studies of double stars became more systematic. Wilhelm Struve used a micrometer to discover and reobserve more than 3,000 double stars (Heintz 1978). The results of his work – a number of double star catalogs – are still used for orbital calculations of long term double stars.

Application of plate photography and, later high-speed CCD imaging, revolutionised the field of double star research in the 20th century. It allowed astronomers to observe visual doubles with milli-arcsecond precision using lucky imaging and speckle interferometry and utilise innovative observational methods of double star research, such as spectroscopy and precise photometry.

Numerous catalogs with double star observations and measurements have been published since the 18th century. The United States Naval Observatory (USNO) produces the most current and widely used Washington Double Star (WDS) catalog. The measures in the catalog have been "collected, collated, and maintained since the early 1960's". As of March 24, 2018 there are 142,563 systems in the catalog (wds_web).

Telescope Resolution

Light from the stars and other celestial objects is diffracted as it passes through a circular aperture of an optical telescope. As the result of the diffraction, the light emitted by a point-like source (a star) forms a bright central disk (the Airy disk) surrounded by the series of light and dark concentric rings (Airy pattern) (Argyle 2012). The angular diameter (in radians) of the central disk, D_{Airy}, for the monochromatic point-like source of light with wavelength λ passing through an unobstructed circular aperture with the diameter D and the telescope focal length f can be approximated as

$$D_{Airy} = \frac{2.44\lambda f}{D} \quad \text{rad} \qquad [1]$$

The image of two stars is comprised of two diffraction patterns and the individual star images are considered to be just resolved, under idealized atmospheric conditions, if the center of the Airy disk of the first star coincides with the first dark ring of the second star's Airy pattern. This telescope angular resolution limit θ_{res} is called Rayleigh criterion and can be approximated as

$$\theta_{res} = \frac{1.22\lambda}{D} \quad \text{rad} \qquad [2]$$

For the 8" Schmidt-Cassegrain telescope with the 34% central obstruction and a broadband source of light, equation [2] provides a reasonable resolution estimate. Considering λ = 550 nm, the resolution limit is:

$$\theta_{res} = (1.22)\frac{\left(5.5\times10^{-7}\,\text{m}\right)}{0.2\,\text{m}} \approx 3.36\times10^{-6}\ \text{rad} \approx 0.7"$$

Atmospheric seeing effects

Using a simplified view, atmospheric turbulence causes dynamic variations in the distribution of cold and warm cells of air. The differences in temperature between the air cells result in the localized differences in pressure and contribute to the differential refractive index in the neighboring cells. This differential refraction distorts the plane wave fronts originating from a point light source in the sky (Figure 1). Such distortion is often referred to as "λ = 550 atmospheric seeing".

This distortion causes twinkling of stars when we

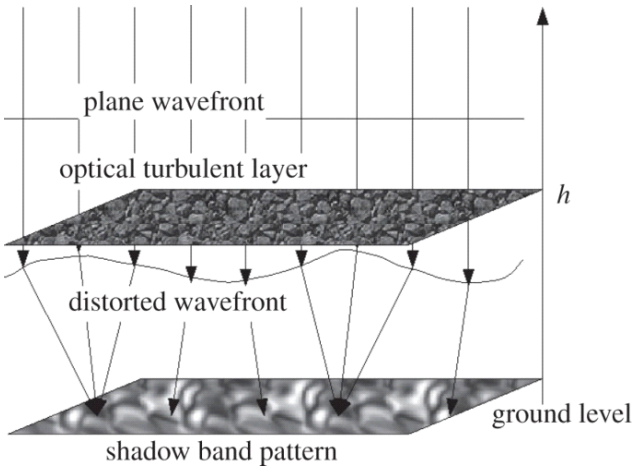

Figure 1. Propagation of light through a layer of atmospheric turbulence. Image by Sofieva et al. 2013)

look at them from Earth and also blurs the image at the telescope eyepiece or the CCD/CMOS camera. Atmospheric seeing is the most significant factor limiting resolution for all but the smallest ground-based telescopes.

The properties of the atmospheric seeing are defined by two main parameters (Boffin et al. 2016):

The atmospheric spatial coherence parameter, r_0, (Fried parameter), which defines the diameter of an average air cell.

The atmospheric coherence time, t_0, representing the interval over which the air cell of diameter r_0 affects the plane wavefront.

The Fried parameter r_0 is proportionate to the wavelength λ of the incoming light and can be expressed as:

$$r_0 = 1.009D\left(\frac{\lambda}{\theta_{seeing}}\right)^{\frac{6}{5}} \quad [3]$$

where θ_{seeing} is the full width half maximum (FWHM) diameter of the atmospheric seeing disc in radians and D is the telescope aperture diameter in metres (Argyle 2012). θ_{seeing} also increases proportionately to the zenith angle (the angle between the star and the local zenith) due to larger airmass.

The average atmospheric seeing FWHM recorded during the observing runs at the author's principal observing site in the southeastern part of Melbourne, Victoria, Australia was measured around 2". For the 8" telescope and λ = 550 nm, the Fried parameter, r_0, is approximately 4cm.

Atmospheric dispersion

Earth's atmosphere acts on the incoming light like a prism and refracts wavelengths differently, bending blue light more than red. Such refraction affects the shape and the measured position of a star.

For a double star with O5 and M5-class components, observed at 45º zenith angle (the angle between the star and the local zenith) the difference in separation is around 0.1" for the V-band filter (Rutkowski & Waniak 2005). Specialized dispersion correction devices can be employed to correct the dispersion, such as counter-rotating Risley prisms (Genet et al. 2015).

In order to minimize the atmospheric dispersion, the double stars with small difference in stellar classes were selected for observations at low zenith angles (less than 35º).

2. Equipment

The equipment used for observations in this research project included Celestron EdgeHD 800 Schmidt -Cassegrain telescope on a computer-controlled Losmandy G11 tracking German Equatorial mount and Canon 6D DSLR camera with Televue 4x Powermate image amplifier. Figure 2 shows the equipment setup and ready for an observing run.

Figure *2. Celestron Edge HD 800 with Canon 6D on Losmandy G11 mount*

Canon 6D DSLR Camera

Canon 6D is a single-shot colour camera equipped with 35.8 x 23.9 CMOS detector and DIGIC 5+ image processor. The full resolution is 5472 x 3648 pixels and the pixel size is 6.54 microns. The camera has been modified to run open source Magic Lantern software (magic_lantern_web), which allows it to record video in RAW format using the central section of the detector without scaling the image, making it particularly useful for the astrometry.

The full frame image is used to confirm the telescope pointing and to determine the image scale and camera orientation using astrometric plate-solving technique.

The ISO sensitivity (gain) range is 100 – 102400. The camera is equipped with a thermo-electric cooler, which is unregulated and achieves detector temperature of around 18º C below the temperature of ambient air.

Being a single-shot colour camera, Canon 6D includes red, green and blue colour filters located above the detector and arranged in a "Bayer" matrix. It facilitates the capture all colour information in one image but, depending on the colour, only one or two out of four pixels in each image contain signal from the specific colour. Moreover, the colour filters differ in the

(Text continues on page 655)

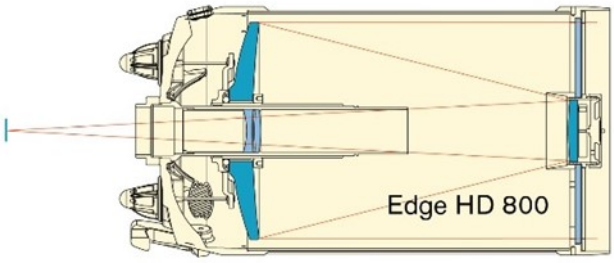

Figure 3.. Celestron Edge HD 800 telescope. (image by Celestron_EdgeHD_web)

amount of light they let through.

These limitations may potentially affect the determination of the precise position of a star, based on a point spread function fitting. In order to mitigate that effect in speckle interferometry measurements, a Gaussian lowpass spatial filter is used, and multiple images are averaged in the lucky imaging method. For the video drift method, a different technique is used and a monochrome image is constructed from the red, green and blue channels without debayering, resulting in half effective resolution.

Celestron Edge HD 800 corrected Schmidt-Cassegrain telescope and image amplifier

Celestron Edge HD 800 (Figure 3) is a Schmidt-Cassegrain telescope with aperture of 203mm and focal ratio of f/10 (Celestron_EdgeHD_web). The secondary obstruction is 68.6mm or 34%. The telescope is fitted with an optical corrector which provides a highly corrected field over 42mm diameter.

Televue Powermate 4x image amplifier was used to achieve the f/ratio of f/40 required to observe close double stars using speckle interferometry and lucky imaging methods.

Losmandy G11 German Equatorial tracking mount

Losmandy G11 computerised German Equatorial mount tracks the celestial objects and allows for computer control using ASCOM standard protocol (ASCOM_web) and permanent Periodic Error Correction (PEC). The mount was carefully polar-aligned using drift-alignment technique and periodic error was measured and corrected for, in order to keep the observed double stars in the centre of the field of view.

The mount provides excellent support for the Celestron EdgeHD 800 telescope and Canon6D camera and autoguiding is not required for the short exposures used in the observations.

3. Observational workflow

Limiting Visual Magnitude

Prior to the selection of observational targets, a number of single stars were observed in order to determine the limiting visual stellar magnitude resulting in an acceptable signal-to-noise ratio for the longest exposure limit set at 30ms.

Image Scale and Camera Orientation

In order to measure double star separation and position angle parameters it is necessary to determine the image scale in arcseconds per pixel and camera orientation in relation to North and East. To achieve statistically robust image scale and camera orientation values, the following two methods were applied:

1. Astrometric plate solving using PlateSolve2 software, developed by David Rowe (planewave_web). This method measures image scale and camera orientation with very low error values (typical errors were less than 1%).
2. Video Drift method automatically determines the plate scale and camera orientation using known Declination of the double star and precise timing from the video sequence.

The camera remained in the same position for the duration of several observing runs unless the telescope was moved into storage. Average camera orientation angle and image scale values were calculated and used for a series of observing runs when the telescope was left in the field and not disturbed.

Image Acquisition and processing workflow

Telescope pointing and tracking were performed using Sequence Generator Pro software (sgpro_web). This software provides integration with PlateSolve2 for automatic determination and adjustment of the telescope pointing position. It also keeps the log of observed targets with timestamps.

Before starting the observation of a specific double star, a 30-second exposure was taken by Sequence Generator Pro software, utilising the full frame of Canon 6D (5472 x 3648 pixels). The image centre coordinates were determined using astrometric plate solving and a slew command issued to move the telescope to the correct position if required. The same data used for telescope pointing adjustment was used for astrometric determination of the image scale and camera orientation.

Video recording. For each target, the star was centered in the Canon 6D field of view and 864 x 864 pixels video sequence was recorded using the central section of the detector. After recording of the tracked sequences was complete, the target was placed at the edge of the frame, video recording started and the telescope drive turned off. When the target drifted off the opposite edge of the frame, the telescope clock drive was turned back on. The aforementioned process was repeated twice, resulting in two tracked sequences and two video drift sequences.

During the first three observing runs the tracked sequence duration was just over 70 seconds, resulting in approx. 2,000 video frames. After the initial data reduction, it was determined that longer runs of around 180 seconds would produce 5,000 frames and allow for improved statistical analysis. Therefore, during last three observing runs longer 3-minute tracked sequences were recorded.

For each reference star, two 3-minute long tracked video sequences were recorded, resulting in approx. 5,000 frames in each sequence.

Image Conversion. The first step was to convert RAW video images produced by Magic Lantern software in MLV container format to individual Adobe DNG files. MLVMystic software program (mlvmystic_web) was used for this conversion. Then the DNG files were visually examined, first and last few hundred frames deleted to avoid any distortions due to telescope vibrations when the video recording was triggered manually. Selected DNG files were converted to monochrome FITS files in PixInsight software – without debayering for Speckle Interferometry and Lucky Imaging; and using SuperPixel method (2x2 binning) for the Video Drift method.

Image pre-processing was done in Speckle Toolbox. The FITS images were grouped into FITS cubes, with 1,000 images per cube for data reduction in Speckle Toolbox (Speckle Interferometry) and REDUC (Lucky Imaging). An observation would result in 8 cubes per double or reference star during the first three observing runs and 10 FITS cubes during the last three runs. For the Video Drift method, the converted FITS files were sorted into folders, named in accordance with the double star designation.

Data Reduction. 8 – 10 FITS cubes, pre-processed in the previous step were analyzed in Speckle Toolbox and REDUC programs (described in section 4). Average results and standard deviation values were computed in Microsoft Excel for each observed double star. The data reduction results were saved as tables for each of the measurement methods.

Drift videos, converted to 2 x 2-binned FITS sequences were reduced in Tangra3 program and measured positions saved in a text file. The drift data was pasted into VidPro Excel spreadsheet and analysed.

4. Double Star Measurements

Speckle Interferometry

Labeyrie (1970) used a laser beam to simulate a star and a silicone-sprayed glass plate, placed in front of the telescope, to simulate the atmsopheric seeing. He then developed a method for recovering the high-resolution structure from the distorted image by applying a Fourier transform to the series of speckle images and obtaining the sum of their power spectra.

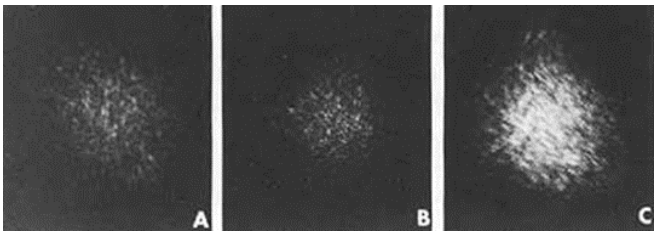

Figure 4. Speckle photographs of Betelgeuse (A), Bellatrix (B) and a close double star Capella obtained with the Kitt Peak 4-m telescope. Image by history_nasa_web

The dynamic atmospheric cells are responsible for the degradation of the telescopic image, if the image integration time is greater than atmospheric coherence time t_o (the average lifetime of the atmospheric cell). However, if the image integration time is less than the average lifetime of the atmospheric cell then the image of a star will be a combination of small spots, called "speckles" caused by the constructive and destructive interference of light, as it passes through the atmospheric cells (Figure 4).

Such speckle image preserves the diffraction limited information, which is considerably better than the size of the atmospheric seeing disk for all but the smallest telescopes.

If two components of a double star are close enough in the sky then their light passes through the same pattern of refractive cells in the atmsophere (isoplanatic patch). As the result, the same atmospheric point spread function applies to both double star components or, in more poetic terms – the two stars "twinkle" together. The maximum separation for a double star to be in the same isoplanatic patch under average atmospheric seeing is around 5" – 7". The average time for the isoplanatic patch to exhibit a significant change depends more on the wind speed than the movements of the individual air cells and is typically in the order of 10ms (Boffin et al. 2016).

The number of speckles N in the image, for the telescope with aperture D and the Fried parameter r_o can be estimated as:

$$N = \frac{D^2}{r_o^2} \qquad [4]$$

For the Celestron EdgeHD 800 telescope used for observations D = 0.2 m and r_o = 0.04 m the number of speckles N present in the image is expected to be around 25.

Figure 5 shows a magnified image with a resem-

Figure 5. 0.004 second exposure of a reference star (Fomalhaut) with 0.2m telescope

blance of the speckle pattern, in a 0.004s exposure of a reference star (Fomalhaut) obtained during an observing run on November 2, 2017. The image scale of 0.18" per pixel is too large and not all individual speckles are resolved, unlike in the image obtained with 4-meter Kitt Peak telescope (Figure 4).

Speckle data reduction was performed in Speckle Toolbox (ST) software written by David Rowe and distributed free of charge (Harshaw et al., 2017).

The data reduction in ST requires the steps outlined below.

FITS cubes pre-processing

A FITS cube with a double or reference star is loaded and a Fast Fourier Transform (FFT) of every image in the cube is computed. Subsequently all transforms are averaged and a Power Spectral Density (PSD) file is produced. The PSD file is considerably smaller in size than the FITS cube -– 1Mb vs 500MB for 1,000 image cube. ST offers a convenient feature to preprocess multiple FITS cubes in a batch.

Speckle Reduction

The double star and reference PSD files, preprocessed in the step 1, are opened and appropriate values for Low-Pass and High-Pass dimensional filters are selected.

The reference PSD is a power spectral density file of a reference single star located near the observed double star in the sky. It should be recorded using a very short exposure time (ideally less than 5 ms). It is used to sharpen the double star image by removing the effects of the telescope central obstruction and optical aberrations as well as most of the atmospheric dispersion. In ST the deconvolution process divides the double star PSD by the reference PSD (Harshaw et al. 2017)

$$\langle O \rangle = \frac{\langle I \rangle}{\langle T \rangle} \qquad [5]$$

where $\langle I \rangle$, $\langle T \rangle$, and $\langle O \rangle$, are the averages of Fourier transforms of the double star image, the reference star (representing telescope and atmospheric aberrations) and the deconvolved image, respectively. Subsequent inverse Fourier Transform of $\langle O \rangle$ produces the autocorrelation which can be measured by the ST astrometry tool.

The *Low-Pass Gaussian filter* removes the noise originating from the in-camera electronic processing circuits, sky background and photon shot noise. For the images taken with Canon 6D one-shot colour camera, the Gaussian Low-Pass filter also addresses the difference in signal passing through the individual colour filters of the Bayer matrix.

The value for the Low-Pass filter radius f_c (in pixels) should be set with a cut-off frequency slightly wider than the following value (Harshaw et al. 2017):

$$f_c = \frac{hN}{2.44 \lambda F/D} \qquad [6]$$

where λ is the wavelentgh, h is the pixel dimension and F/D is the effective focal ratio of the optical system.

For the Celestron EdgeHD 800 with 4x image amplifier, Canon 6D camera with 6.55 micron pixels, λ = 550 nm, N = 512, and f_c = 62 pixels.

Setting the Low-Pass filter value to a slightly wider value of 70 pixels empirically produced best results.

The purpose of the *High-Pass Gaussian filter* is to eliminate the effects of optical aberrations and atmospheric seeing by cutting off the wide end of the point-spread function.

The value of this filter is adjusted by inspecting the PSD image and making sure that it removes the bright central peak but does not cut off useful signal by extending beyond the zero-order fringe pattern in the PSD image (Figure 6).

During the first two observing runs the reference star images were not taken and a larger value for the Low-Pass filter was used instead. Additionally for very close double stars (separation less than 1"), the deconvolution using a reference star did not result in a resolvable image. For those double stars a symmetrised point spread function was subtracted from the image, leaving non-symmetrical part only (Harshaw et al. 2017). Reasonable results were achieved using this method for very close doubles.

Astrometry Tool

After selecting the appropriate values for the filters, ST performs another Fast Fourier Transform and produces an autocorellogram, which can be directly measured with the ST Astrometry Tool.

Figure 6. Gaussian high pass filter examples. Left - too wide (cuts off the central peak and the fringe pattern), centre - set correctly, right – too narrow (allows the central peak to be seen). Image adapted from Harsahw et al. (2017)

In the ST *Astrometry Tool*, the scale calibration values – plate scale in arcseconds per pixel and camera orientation in degrees – are entered. The measuring circle is placed around the secondary component (Figure 7). A right-click on the circle opens the context menu and "Set Target Location" is selected. Then ST computes the accurate position of the secondary component in relation to the centre, based on the centroid value. The ST Astrometry tool provides an automatic selection of the target location, but it may not always work depending on other bright parts of the image. In that case the measuring circle is placed manually.

The separation is converted from pixels to arcseconds by ST automatically, based on the plate scale. The position angle however, carries the 180° uncertainty and ST uses known information about the double star, supplied as an input parameter in order to resolve this ambiguity. The measurement results are then written to a comma-separated text file for further statistical analysis.

ST allows for semi-automatic processing of PSD files and takes a text file with input parameters to make the reduction of large number of FITS cubes less laborious.

Lucky Imaging

The lucky imaging method, like the Speckle Interferometry method, requires exposure times comparable with the atmospheric coherence time t_o, however instead of computing a power spectrum density over all exposures, the lucky imaging method uses a selection process to include only those images that match quality criteria. Typically, around 1-5% of the images are included based on the point spread function fitting.

The lucky imaging data reduction is performed in REDUC software written by Florent Losse and distributed free of charge (Harshaw et al. 2017).

The data reduction in REDUC is performed using "Easy Lucky Imaging" process. After selecting rough positions for primary and secondary double star components, REDUC uses point spread function fitting to select, align and stack the best frames, producing an image that can be more reliably measured than individual frames.

Figure 8 shows three images from an observation sequence for WDS22266-1645 double star. The typical unlucky and lucky frames were taken less than 0.2 s apart (images A and B). Image C is an aligned stack of 55 lucky images as selected by the Easy Lucky Imaging algorithm in REDUC. It demonstrates that stacking makes it possible to determine the peaks with reasonable accuracy. For close doubles, the center peaks were determined using SURFACE algorithm, which takes into account an empirical model of the atmospheric point-spread function. Pairs wider than 3" were processed using AutoReduc method, which measures posi-

(Text continues on page 659)

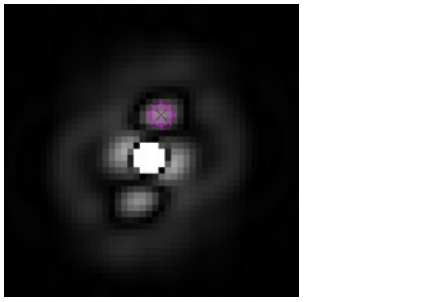

Figure 7. Autocorellogram for WDS22266-1645 with automatic peak selection circle placed by ST. Separation 1.3"

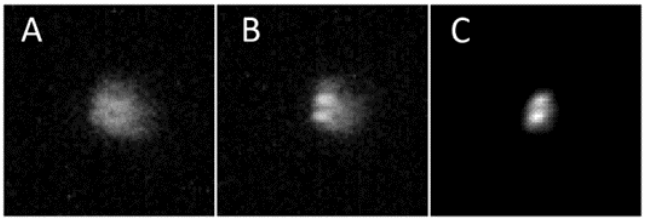

Figure 8. Magnified images of WDS22266-1645 (Exposure: 30ms, Separation 1.3"). A - Unlucky image, B – Lucky image, C – Aligned and stacked series of best 55 lucky images.

tions of each frame in the "lucky" set and calculates an average value.

Video Drift

Tangra astrometric video analysis software (tangra_web) was used to reduce 840x840 pixels video drift sequences. Tangra is a software program with open source code, developed and maintained by Hristo Pavlov. It is designed for astronomical video observations of asteroid occulations and can track and perform aperture photometry of stars, as they drift across the frame. Thanks to the program's open source code, the author of this paper was able to modify the program code and append (*x,y*) positions of the measured stars to the exported light curve data, making it suitable for double star video drift measurement method.

Tangra analyses the individual FITS files from a folder, tracks the drifting stars using Point Spread Function fitting and records their (*x,y*) positions. The values are recorded with 0.1-pixel precision. After successful tracking of the video frames, the series of positions are saved into a text file for further analysis in the VidPro Excel spreadsheet.

The VidPro Excel spreadsheet, originally developed by Nugent & Iverson (2011), was modified to accept the output from Tangra software. The orientation of the camera detector and the drift angle are determined for each video using least squares regression fitting from all measured (*x,y*) coordinate pairs. The position angle, θ is determined in VidPro (Nugent & Iverson 2011) as:

The position angle is adjusted for drift angle and quadrant position in relation to the primary star.

The separation for each video frame, ρ in pixels is calculated as:

In the above equations [7] and [8], x_p, y_p are the

$$\theta = \arctan\left(\frac{x_p - x_s}{y_p - y_s}\right) \qquad [7]$$

primary (brighter) star coordinates, x_s, y_s – secondary star coordinates and δ is the declination of the double star.

In order to convert separation ρ from pixels to

$$\rho = \sqrt{\left(x_p - x_s\right)^2 + \left(y_p - y_s\right)^2}\ \cos\delta \qquad [8]$$

arcseconds, the scale factor *S* is calculated as:

where x_b, x_e, y_b, and y_e are the coordinates of the points at the beginning and the end of the drift for each

$$S = \frac{dt 15.041068}{\sqrt{\left(x_b - x_e\right)^2 + \left(y_b - y_e\right)^2}} \qquad [9]$$

star and *dt* is the time of drift in seconds, calculated from the 29.921 frames per second video frame rate.

The pixel scale factor and drift angle are calculated for each video drift. The average pixel scale for 10 recorded video drifts with 2x binning applied was 0.357" per pixel (standard deviation σ = 0.0039").

5. Target Selection

The selection criteria were as follows:

1. Favourable positioning in the sky within the 35° zenith angle;
2. 0.6" – 10" separation in order to compare the selected methods of measurements;
3. Dimmest star on the pair brighter than 8th visual magnitude (determined during a trial run)

18 double stars were selected for observations during 6 runs, which are listed in Table 1.

The primary and secondary visual magnitude values (m1 and m2) and spectral class data were taken from the WDS Catalog, orbit grades (O G) from the Sixth Orbit Catalog (1 – 5 numeric grade, U – Uncertain double, P – Physical binary but without orbital parameters, N – Non-physical double), SEP (in degrees) and PA (in arcseconds) were calculated ephemerides, where applicable. Exposure time in milliseconds was set based on visual magnitude values and the outcome of the test run.

6. Observation Results

Speckle Interferometry results

The results of Speckle Interferometry measurements for 18 double stars with separations ranging from 0.64" to 11.45" are presented in Table 2. The errors are discussed in Section 9.

Lucky Imaging results

It was not possible to detect centroids for stars closer than 1" with the Lucky Imaging method. Double stars with orbit grades 4 or better and separations larger than 1", measured by the Speckle Interferometry method, were also measured using Lucky Imaging method for comparison. Non-physical double 02583-4018 PZ 2 was included for comparison with the Video Drift method because of its wider separation. The results of Lucky Imaging measurements for 8 double stars are presented in Table 3.

(Text continues on page 662)

A Comparison of Methods for Astrometric Measurements of Close Double Stars

Table 1. Observation targets for six observing sessions 2017-08-30 to 2017-10-15. PA and SEP are the position angle in degrees and separation in arceseconds, calculated from orbital parameters where orbits are available or last observed values from WDS where orbits are not available. OG is the orbit grade. Spectral classes are from WDS. Exposure values in milliseconds are estimated based on previous test runs.

NAME	RA+DEC	MAGS	PA	SEP	OG	Spectral Class	Exp ms	Notes
BU 391AB	00094-2759	6.13,6.24	258.12	1.301	5	F4IV-V (yellow-white)	30	
BU 395	00373-2446	6.60,6.20	117.7	0.626	1	G8V (yellow)	30	
HDO 182	00427-3828	6.60,7.01	139.37	0.513	5	A0V (white)	30	1
I 47	00519-4343	7.45,7.95	30.65	0.603	5	F2V+F5V (yellow-white/ yellow-white)	30	
SLR 1AB	01061-4643	4.10,4.19	80.64	0.616	3	G8IIIv (yellow)	8	
DUN 5	01398-5612	5.78,5.90	186.2	11.45	4	K0V+K5V (yellow-orange/ yellow-orange)	30	2,6
STF 202AB	02020+0246	4.10,5.17	265	1.8	4	A0p+A3m (white/white)	10	
PZ 2	02583-4018	3.20,4.12	90.55	8.43	N	A4III+A1V (white/white)	4	3,6
RHD 1AB	14396-6050	-0.01,1.33	313	4.1	2	G2V+K1V (yellow/yellow-orange)	0.6	
H 2 19AB	16256-2327	5.07,5.74	338	3.2	5	B2IV+B2V (blue-white/ blue-white)	30	
SHJ 243AB	17153-2636	5.12,5.12	143	5.4	4	K5Ve+K1V (yellow-orange/ yellow-orange)	30	
HJ 5014	18068-4325	5.65,5.68	363	1.8	4	A5V+A5V (white/white)	30	
HDO 150AB	19026-2953	3.27,3.48	252	0.6	1	A2III (white)	4	
HJ 5084	19064-3704	4.53,6.42	343	1.6	2	F8V+F8V (yellow-white/ yellow-white)	30	
BU 276	22008-2827	5.70,6.77	115	1.2	U	B8Ve (blue-white)	30	4
SHJ 345AB	22266-1645	6.29,6.39	78	1.3	4	G0V+G0V (yellow/yellow)	30	
DUN 251	23395-4638	6.53,7.27	279	4.1	P	A8V+F0V (white/yellow-white)	30	5
H 2 24	23460-1841	5.65,6.46	135	7	P	A9IV+F2V (white/yellow-white)	30	6

Notes:

1. Speckle Interferometry measurements show a large error in position angle compared to ephemeris. Orbit parameters are possibly incorrect (discussed in the Error Analysis Section).
2. Orbit parameters are slightly incorrect. Using last precise measurement from 2016 listed in WDS, Sca2015c (discussed in the Error Analysis Section)
3. Non-physical double. Measurements from Anton (2010).
4. Uncertain double. Measurements from Horch et al. (2010).
5. Physical double without orbital solution. Data from int4_web, Tok2006a.
6. Separation is too large for Speckle Interferometry. Speckle measurements included for comparison with Lucky Imaging and Video Drift methods.

A Comparison of Methods for Astrometric Measurements of Close Double Stars

Table 2. Speckle Interferometry results. Observed from 37.98°S latitude, 145.06°E longitude, Melbourne, Australia with 8" Schmidt-Cassegrain telescope. "PA meas" and "SEP meas" are the measured position angle in degrees and separation in arcseconds. "D PA" and "D SEP" are the residuals between the observed and computed or last observed values. "STDEV PA" and "STDEV SEP" are the standard deviation values of multiple measurements

NAME	RA+DEC	MAGS	PA	SEP	DATE	N	D	D	STDEV	STDEV
			meas	meas			PA	SEP	PA	SEP
BU 391AB	00094-2759	6.13,6.24	258.28	1.363	2017.745	1	0.16	0.062	0.225	0.007
			258.02	1.342	2017.781	1	-0.1	0.041	0.224	0.005
BU 395	00373-2446	6.60,6.20	123.88	0.875	2017.778	1	6.18	0.249	5.269	0.03
HDO 182	00427-3828	6.60,7.01	22.64	0.753	2017.742	1	-116.73	0.24	1.41	0.027
			24	0.782	2017.745	1	-115.38	0.269	0.508	0.005
I 47	00519-4343	7.45,7.95	28.52	0.832	2017.745	1	-2.13	0.229	0.562	0.039
SLR 1AB	01061-4643	4.10,4.19	73.95	0.642	2017.658	1	-6.69	0.026	0.894	0.015
			75.8	0.681	2017.742	1	-4.84	0.065	0.517	0.015
			89.19	0.74	2017.775	1	8.87	0.121	0.47	0.002
DUN 5	01398-5612	5.78,5.90	186.55	11.446	2017.775	1	0.35	-0.004	0.041	0.007
			186.59	11.441	2017.781	1	0.39	-0.004	0.03	0.005
STF 202AB	02020+0246	4.10,5.17	263.17	1.888	2017.781	1	1.63	0.054	0.155	0.008
PZ 2	02583-4018	3.20,4.12	91.45	8.373	2017.742	1	0.35	-0.257	0.054	0.007
RHD 1AB	14396-6050	-0.01,1.33	323.98	4.341	2017.658	1	0.82	0.005	0.054	0.004
H 2 19AB	16256-2327	6.30,6.80	334.13	3.023	2017.658	1	-2.91	0.158	0.13	0.012
SHJ 243AB	17153-2636	5.12,5.12	139.97	5.103	2017.658	1	-0.05	0.046	0.105	0.004
HJ 5014	18068-4325	5.65,5.68	360.56	1.797	2017.658	1	1.68	0.058	0.209	0.004
HDO 150AB	19026-2953	3.27,3.48	220.87	0.719	2017.658	1	-25.41	0.164	3.84	0.012
HJ 5084	19064-3704	4.53,6.42	338.17	1.429	2017.658	1	0.17	-0.021	0.384	0.012
BU 276	22008-2827	5.70,6.77	113.17	1.891	2017.658	1	-1.73	0.671	0.22	0.01
			113.17	1.89	2017.742	1	-1.73	0.67	0.228	0.018
SHJ 345AB	22266-1645	6.29,6.39	72.22	1.336	2017.778	1	-0.36	0.04	0.015	0.000
			71.75	1.347	2017.781	1	-0.83	0.051	0.377	0.002
DUN 251	23395-4638	6.53,7.27	277.49	3.855	2017.745	1	-1.61	-0.205	0.052	0.003
H 2 24	23460-1841	5.65,6.46	135.15	6.993	2017.658	1	-0.05	-0.018	0.014	0.001

Table 3. Lucky Imaging results. Observed from 37.98°S latitude, 145.06°E longitude, Melbourne, Australia with 8" Schmidt-Cassegrain telescope. "PA meas" and "SEP meas" are the measured position angle in degrees and separation in arcseconds. "D PA" and "D SEP" are the residuals between the observed and computed or last observed values. "STDEV PA" and "STDEV SEP" are the standard deviation values of multiple measurements

NAME	RA+DEC	MAGS	PA meas	SEP meas	DATE	N	D PA	D SEP	STDEV PA	STDEV SEP
BU 391AB	00094-2759	6.13,6.24	257.54	1.331	2017.745	1	-0.58	0.03	0.302	0.012
			258.43	1.34	2017.781	1	0.31	0.039	0.775	0.037
DUN 5	01398-5612	5.78,5.90	186.58	11.439	2017.775	1	0.03	-0.011	0.052	0.01
			186.51	11.448	2017.781	1	-0.05	-0.002	0.082	0.008
STF 202AB	02020+0246	4.10,5.17	264.32	1.781	2017.781	1	2.78	-0.053	1.118	0.083
PZ 2	02583-4018	3.20,4.12	91.44	8.376	2017.658	1	0.34	-0.254	0.069	0.009
RHD 1AB	14396-6050	-0.01,1.33	324.03	4.33	2017.658	1	0.87	-0.006	0.128	0.013
SHJ 243AB	17153-2636	5.12,5.12	140.11	5.102	2017.658	1	0.09	0.045	0.179	0.017
HJ 5014	18068-4325	5.68,5.68	360.37	1.765	2017.658	1	1.49	0.026	0.237	0.015
HJ 5084	19064-3704	4.53,6.42	338.83	1.46	2017.658	1	0.83	0.01	0.667	0.011

(Continued from page 659)

Video Drift Results

It was not possible to track double star positions with separations smaller than 4" in Tangra, due to overlapping point spread function fitting circles. Therefore, only 5 wider double stars were measured with the Video Drift method and the results are presented in Table 4.

7. Error Analysis

Speckle Interferometry errors

Overall 25 observations were made during six observing runs with the observed separations ranging from 0.64" to 11.5". 18 measurements of double stars wider than 1", produced reliable results with the Speckle Interferometry method. The average absolute separation O-C residual was 0.04" and the average absolute position angle O-C residual – 0.52º.

Six measurements of binary stars closer than 1" were less reliable – the average absolute O-C separation residual was 0.142" and average absolute O-C position angle residual was 9.02º. Two measurements of 00427-3828 HDO 182 were excluded from the statistical analysis due to suspected errors in the orbital parameters provided in the Sixth Orbit Catalog (discussed below).

Separation and position angle residuals plotted against separation (Figures 9, 10) show that separations of double stars closer than 0.6" are overestimated and position angles have larger errors. Considering that 0.6" is below the telescopes resolution limit (0.7", according

Table 4. Video Drift results. Observed from 37.98°S latitude, 145.06°E longitude, Melbourne, Australia with 8" Schmidt -Cassegrain telescope. "PA meas" and "SEP meas" are the measured position angle in degrees and separation in arcseconds. "D PA" and "D SEP" are the residuals between the observed and computed or last observed values. "STDEV PA" and "STDEV SEP" are the standard deviation values of multiple measurements.

NAME	RA+DEC	MAGS	PA meas	SEP meas	DATE	N	D PA	D SEP	STDEV PA	STDEV SEP
DUN 5	01398-5612	5.78,5.90	186.46	11.34	2017.658	1	0.25	-0.11	1	0.16
			186.51	11.34	2017.658	1	0.31	-0.11	0.905	0.105
PZ 2	02583-4018	3.20,4.12	90.07	8.325	2017.658	1	-1.03	-0.305	0.735	0.13
RHD 1AB	14396-6050	-0.01,1.33	324.34	4.243	2017.742	1	1.18	-0.093	2.11	0.153
SHJ 243AB	17153-2636	5.12,5.12	140.05	5.05	2017.775	1	0.03	-0.007	1.02	0.12
H 2 24	23460-1841	5.65,6.46	134.69	7.011	2017.658	1	-0.51	-0.014	0.728	0.095

to the Rayleigh criterion) such results are expected and these measurements were done out of curiosity to see how close the little 8-inch Celestron telescope can go.

These plots also show that negative and positive residuals are distributed reasonably evenly and there are no significant systematic errors in the measurements, other than the expected over-estimation of separation for very close doubles (1" or less)

Two residuals (compared with the original catalogue values), however stood out and prompted further investigations.

1. 00427-3828 HDO 182 (λ Scl)

The ephemeris for λ Scl predicts the position angle 139.37º and separation 0.513" but average measured values from two runs on different nights were 23.32º and 0.76" , respectively.

Further investigation suggests that the Grade 5 orbit in the Sixths Orbit Catalog is incorrect and may need adjustment. Fourth Catalog of Interferometric Measurements of Binary Stars (int4_web) contains 12 measurements of λ Scl with the position angle slowly increasing from 13.7º to 17.5º from 1989 to 1996. Two last measurements in 2008 by Tokovinin however, record the position angle of 199.6º; and are likely to be erroneous (perhaps a misplaced decimal point). Anton (2010) observed λ Scl in 2008 with 0.4m telescope using Lucky Imaging method and recorded the position angle of 21º.

Considering these errors, λ Scl was excluded from the statistical analysis.

2. 01398-5612 DUN 5 (p Eri)

The ephemeris for p Eri predicts the position angle 186.34º and separation 11.62", but average measured values from two runs on different nights were 186.57º and 11.4". The separation residual of 0.181 is too large compared with all other Speckle Interferometry residuals.

The measurements with Lucky Imaging and Video Drift methods showed results consistent with the values obtained with Speckle Interferometry method. Therefore, the last precise position measurement from 2016 (186.2º and 11.4") listed in the WDS Catalog was used as a reference instead.

Lucky imaging errors

7 binary stars with orbit grades 4 or better and one non-physical double star were measured using Lucky imaging method with 10 total measurements. The average absolute separation residual was 0.03" and the average absolute position angle residual was 0.90º.

Separation and position angle residuals plotted against separation (Figures 11, 12) show that the errors are comparable with the Speckle Interferometry method and there were no obvious systematic errors in measurements using Lucky Imaging method.

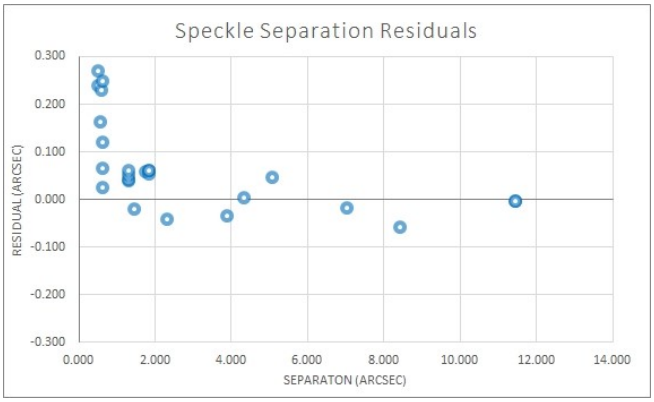

Figure 9. Speckle Interferometry – Separation O-C residuals vs Separation.

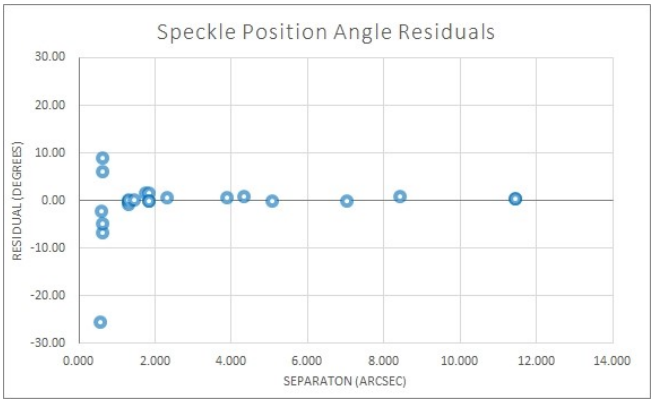

Figure 10. Speckle Interferometry – Position Angle O-C residuals vs Separation

Figure 11. Lucky Imaging – Separation O-C residuals vs Separation.

4 binary stars with orbit grades 4 or better and one non-physical double star were measured using Lucky imaging method with 6 total measurements (Figures 13, 14). The average absolute separation residual was 0.06" and the average absolute position angle residual – 0.46º.

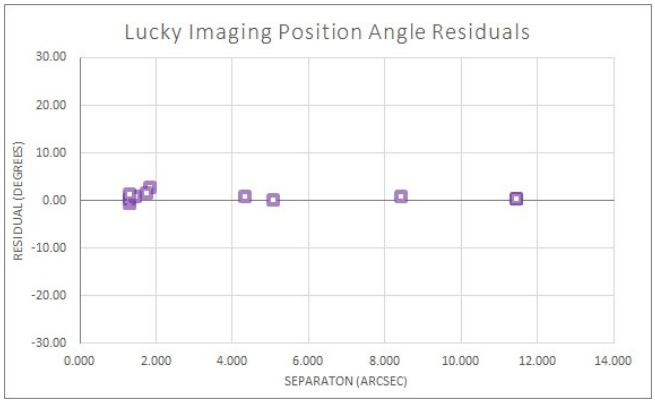

Figure 12. Lucky Imaging – Position Angle O-C residuals vs Separation

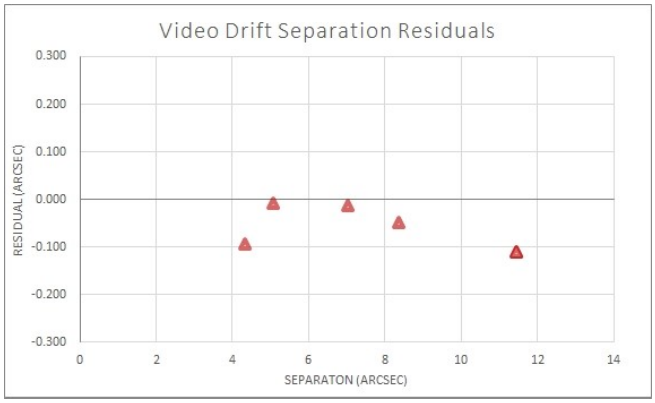

Figure 13. Video Drift – Separation O-C residuals vs Separation.

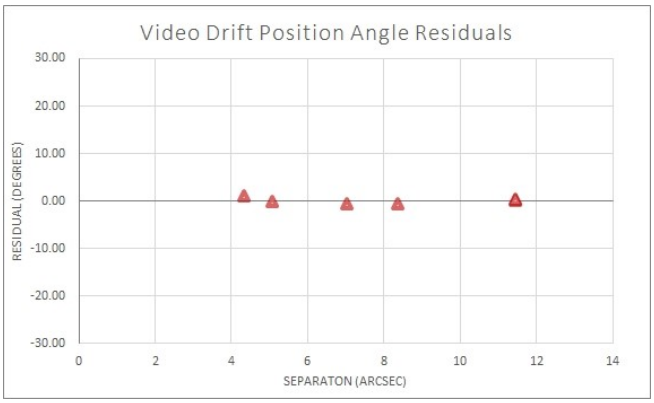

Figure 14. Video Drift – Position Angle O-C residuals vs Separation

8. Comparison of Methods

Figure 15 shows the data reduction results for RHD 1AB (Alpha Centauri, separation 4.33") using three methods:

- Lucky — the stack of 117 best frames.
- Speckle — the autocorrelogram, ready to be measured.
- Video Drift — the sum of 330 video frames without tracking. The speckle pattern is clearly visible.

The O-C residuals, computed from the Sixth Orbit Catalogue ephemerides (or last precise observations for those without orbits), were converted from polar to rectangular coordinates and plotted in Figure 16 in order to assess and compare the precision of measurements. Double stars closer than 1" were excluded from the plot because they could only be measured with the Speckle Interferometry method and the uncertainty of measurements was too large.

It is evident from the result tables and the plot, that Video Drift method produced the least accurate results with a tendency to under-estimate the separation parameters. Speckle Interferometry and Lucky Imaging methods produced results with similar accuracy, and all of the residuals were well within the one-pixel square, represented by the dotted line on the plot.

The results are summarized in Table 5

From the practical point of view, the easiest method to apply during image acquisition is the Video Drift Method, as it does not require tracking and no additional steps to determine image scale and angle. Image acquisition for the Speckle Interferometry and Lucky Imaging methods is identical and can be somewhat laborious, due the difficulties in pointing a consumer grade telescope mount with the sufficient precision, consider-

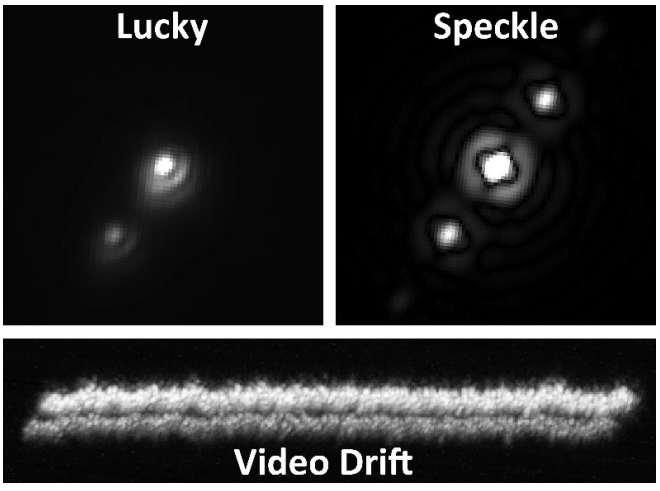

Figure 15. Data reduction of RHD 1AB (Alpha Centauri) using three methods.

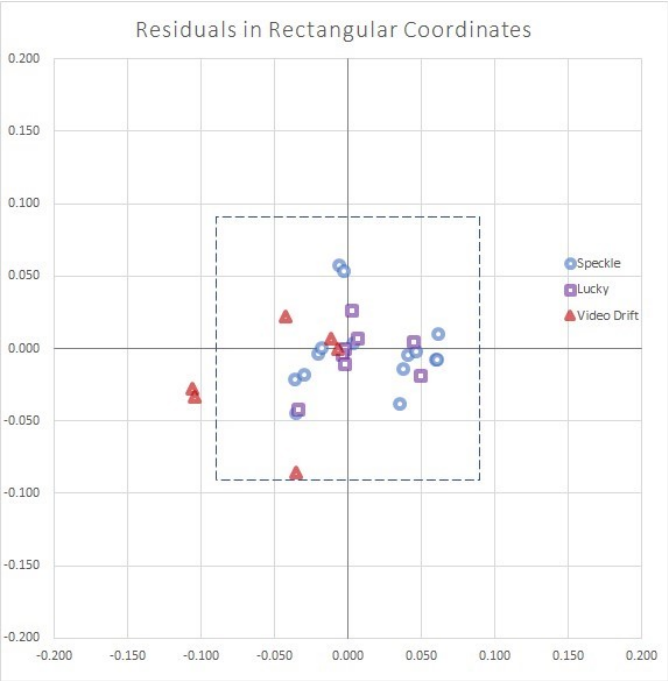

Figure 16. O-C residuals plotted in rectangular coordinates for measurements obtained with different methods. Blue circles represent Speckle Interferometry, purple rectangles – Lucky Imaging and red triangles – Video Drift results. The dash-lined square represents one pixel in the instrumental setup.

ing a very narrow field of view. Use of the full 36x24mm frame in Canon 6D camera with the Open Source Magic Lantern software for that purpose was definitely helpful. Alternatively, a second, shorter telescope can be coupled with the main instrument and used for pointing, but it requires additional hardware.

The data reduction process was the easiest and quickest with the Speckle Toolbox, thanks to semi-automated method of reduction, which after preparation of a text input file required least manual steps and waiting time to obtain the results. It was also rather difficult to measure doubles closer than 3" using Lucky imaging.

9. Conclusions

Successful series of double star observations were performed in the field using a small consumer-grade telescope and a DSLR camera. Data reduction was performed using three different methods and near diffraction-limited results were obtained using Speckle Interferometry and Lucky Imaging methods.

The Video Drift method is well suited for observations of wider pairs, separated by more than 4". It does not require reference stars and calculates image scale and orientation from the drift data automatically. This method would be most appealing to the owners of

Table 5. Summary of the results for pairs wider than 1". NS is the number of measured doubles Min SEP— minimum separation measured with the particular method; O-C PA, O-C SEP — average absolute Observed — Computed residuals; STDEV O-C PA, STDEV O-C SEP — standard deviation values for O-C residuals in Position Angle and Separation

METHOD	NS	Min SEP	O-C PA	STDEV O-C PA	O-C SEP	STDEV O-C SEP
Speckle	18	1.3	0.52	0.15	0.04	0.01
Lucky	8	1.3	0.90	0.38	0.03	0.02
Video Drift	5	4.3	0.46	1.08	0.06	0.13

"Dobsonian" telescopes and is quite easy to use.

Lucky Imaging and Speckle Interferometry allow us to measure double stars close to the telescope's resolution limit. Although the learning curve for the data reduction and analysis is steeper than with the Video Drift, the availability of well documented Speckle Toolbox and REDUC software programs makes it an enjoyable process. Overall, the measurements in Speckle Toolbox are more precise and repeatable, especially at smaller separations. The U. S. Naval Observatory uses speckle-style data reduction for even wider pairs, even when there is no isoplanicity or interference, because this method provides more precise measurements than Lucky Imaging (Harshaw et al. 2017).

Antoine Labeyrie (1970) in his pioneering paper on Speckle Interferometry concluded that it is capable of achieving 0.02" resolution but requires "the largest possible telescope and sensitive image receivers such as image intensifiers or electronographic cameras". Advances in computing bring the Speckle Interferometry method to personal computers and modern digital cameras make it available to most amateur astronomers, even with very small telescopes, by professional standards.

10. Images

The reduction process involves processing of large number of images and the working folder at the conclusion of this project contains 577,000 image and text files, with the total size of 1.2 Terabytes. Subsets of RAW videos, FITS images and FITS cubes are available upon request.

11. Acknowledgements

This research project was done as part of Swinburne Astronomy Online postgraduate program and special thanks are extended to Swinburne University of Technology and Eduardo Alvarez for the opportunity and guidance in working on the project.

Warm thanks are extended to David Rowe, Florent

Losse, Richard Nugent and Hristo Pavlov for developing and maintaining excellent free software which made this research project possible.

This research has made use of the Washington Double Star Catalog maintained at the U.S. Naval Observatory.

12. References

Double Stars, Heintz, W.D., Dordrecht, D. Reidel Publishing Co 1978.

Observing and Measuring Visual Double Stars, 2nd edition, B. Argyle, Springer-Verlag London 2012.

Boffin H., Hussain, G., Berger, J.P. & Schmidtobreick, L. 2016, *Astronomy at High Angular Resolution* (Springer International Publishing Switzerland).

Genet, R.M., Ridgely, J., Teiche, A., Foley, E., Christiansen, C., Rowe, D., Zimmerman, N., Knox, K., Hege, K., Kenney, J., *et al.*, 2015, "Speckle Interferometry of Short-Period Binary Stars", *Journal of Double Star Observations,* **11**, 151.

Harshaw, R., Rowe, D. and Genet, R., 2017, "The Speckle Toolbox: A Powerful Data Reduction Tool for CCD Astrometry*", Journal of Double Star Observations*, **13**, 52-67.

Horch, E., Franz, O.G. and Ninkov, Z., 2000, "CCD speckle observations of binary stars from the southern hemisphere. II. Measures from the Lowell-Tololo telescope during 1999", *The Astronomical Journal,* **120**, 2638.

Labeyrie, A., 1970, "Attainment of diffraction limited resolution in large telescopes by Fourier analysing speckle patterns in star images", *Astron. Astrophys*, **6**, 85-87.

Michell, J., 1767, "An inquiry into the probable parallax and magnitude of the Fixed Stars, etc.", *Phil. Trans.*, **57**, 234.

Nugent, R. and Iverson, E.W., 2010, "A New Video Method to Measure Double Stars", *Journal of Double Star Observations*, 2011, **7**, 185-194.

Rutkowski, A. and Waniak, W., 2005, "Speckle observations of binary stars with a 0.5 m telescope", *Publications of the Astronomical Society of the Pacific*, **117**, 1362.

Sofieva, V.F., Dalaudier, F. and Vernin, J., 2013, "Using stellar scintillation for studies of turbulence in the Earth's atmosphere", *Phil. Trans. R. Soc.* A, 371 .

Tokovinin, A., Mason, B.D. and Hartkopf, W.I., 2010, "Speckle Interferometry at the Blanco and SOAR Telescopes in 2008 and 2009", *The Astronomical Journal*, **139**, 743.

astroplanner_web: AstroPlanner, http://astroplanner.net/ (accessed 24 March 2018)

int4_web: Fourth Catalog of Interferometric Measurements of Binary Stars, http://www.usno.navy.mil/USNO/astrometry/optical-IR-prod/wds/int4/fourth-catalog-of-interferometric-measurements-of-binary-stars (accessed 24 March 2018)

mlvmystic_web: MLVMystic, https://github.com/GTempler/MLVMystic (accessed 24 March 2018)

planewave_web: Software and Update, http://planewave.com/downloads/software/ (accessed 24 March 2018)

reduc_web: REDUC, http://www.astrosurf.com/hfosaf/reduc/tutorial.htm (accessed 24 March 2018)

sgpro_web: Sequence Generator Pro v2.6, http://mainsequencesoftware.com/Products/SGPro (accessed 24 March 2018)

tangra_web: Tangra, http://www.hristopavlov.net/Tangra3/ (accessed 24 March 2018)

wds_web: Washington Double Star Catalogue, http://ad.usno.navy.mil/wds/ (accessed 24 March 2018)

CPM pairs from LSPM so far not WDS listed – Part V

Wilfried R.A. Knapp
Vienna, Austria
wilfried.knapp@gmail.com

John Nanson
Star Splitters Double Star Blog
Manzanita, Oregon
jnanson@nehalemtel.net

Abstract: The LSPM catalog (Lepine and Shara 2005) is a rich source for CPM pairs. We thought that after our four recent "CPM pairs from LSPM" reports – now largely exhausted – to make sure we had once again a closer look and found against our expectations that indeed nearly 200 additional potential CPM pairs so far (per March 2018) not listed in the WDS catalog. This report covers about 90 of these objects

1. Introduction

The LSPM catalog contains 61,977 high proper motion stars detected mainly by comparing POSS I (average epoch 1950) to POSS II (average epoch 1990) images using software developed specifically for locating such objects (Lépine and Shara 2005) but also by using other sources as for example Tycho II and 2MASS. The authors of this catalog also identified 1,159 common proper motion pairs to be included in this data set but only about 170 such pairs were considered new discoveries and listed in the WDS catalog with the discoverer code LEP. Yet our own research showed that the LSPM catalog contains about 3,500 pairs of objects closer than 25 arc seconds with a high probability that such pairs are very fast common proper motion pairs. About 95% of these pairs are per March 2018 already listed in the WDS catalog usually with note code "V", which means considered physical by means of common proper motion, along with a multitude of different discoverer codes, but there is still a residue of nearly 200 so far not WDS listed CPM candidates.

A bit less than half of these objects have not only GAIA DR1 data available for both components, but also from 2MASS, allowing the use of our current work-horse CPM rating procedure according to Knapp and Nanson 2017 (see description Appendix A) by comparing 2MASS to GAIA DR1 positions but also for calculating Vmag estimations from the then available G/J/H/K magnitude data procedure according to Knapp/Nanson 2018. We decided to limit this report to this subset of objects and checked also several other catalogs like UCAC4, UCAC5, URAT1, and SDSS9 by cross-matching with our list to get a solid observation history for these objects. As a reference, the LSPM catalog data is also listed even if for unknown reasons no observation date per object is provided although this data had to be available for calculating proper motion values. Finally we did a cross-match with the first data release of the most recent very large Pan-STARRS star catalog (PS1) – this resulted in the first step in a surprising large number of matched objects for some primaries as well as for some secondaries due to obvious problems of this catalog with fast moving stars leading to multiple objects for the same star along its proper motion path (as example three objects for the primary with 120180155409691210, 120180155413511309 and 120180155412340851 and two objects for the secondary with 120180155400451483 and 120180155403301508). Another side effect with the same cause seems to be in some cases a single object for fast moving stars with an imprecise star position due

to averaged different measurement results over time – at least the calculated separation and position angle from the PS1 positions seem in some cases a bit off.

2. Results of Our Research

In Table 1 we present for the selected objects as much data as we could find in the catalogs available to us. Given below is a description of the table content per column:

- Obj gives the discoverer code with a running number in the header line
- RA and Dec give the recent precise RA/DE coordinates of the A component from GAIA DR1 in the header line in decimal degrees and in the data lines for the sources referred to in the Notes column
- Sep gives separation in arcseconds in the data lines calculated from the indicated catalog positions
- PA gives position angle in degrees in the data lines calculated from the indicated catalog positions
- M1 and M2 give estimated Vmags in the header line for A and B and in the data lines values as indicated in the Notes column
- pmRA1 and pmDE1 with e_pm1 give the proper motion data for A and pmRA2, pmDE2 and e_pm2 for B in the header line calculated by comparison of 2MASS to GAIA DR1 positions as well as in the data lines directly from the catalogs specified in the Notes column if available
- CPM Score gives the estimated probability for being physical based on the CPM assessment result comparing positions between 2MASS and GAIA DR1 in the header line
- Ap indicates in the data lines the aperture used for the observation listed and Me indicates the WDS code for the used observation method (for GAIA calculated equivalent circular surface diameter)
- Date is the Julian epoch of the (averaged) observation date given in the data lines
- N gives in the header line the suggested WDS note code "V"
- Source/Notes finally indicate in the header line and in the data lines the sources used and additional explanations if considered necessary.

3. Summary

From 91 objects checked for CPM about 2/3 are most probably physical pairs indicated by very fast common proper motion and less than 10% are to be considered optical.

NSN n+15 and n+21 are objects with contradicting evidence – the comparison 2MASS to GAIA DR1 positions indicates strongly common proper motion with the caveat of a rather large 2MASS position error. But this impression is heavily supported by the visual comparison of POSS.I to POSS.II images represented also by comparison of USNO A2 to USNO B1 catalog positions – Figure 1 is an RGB-composite of these images for NSN n+21.

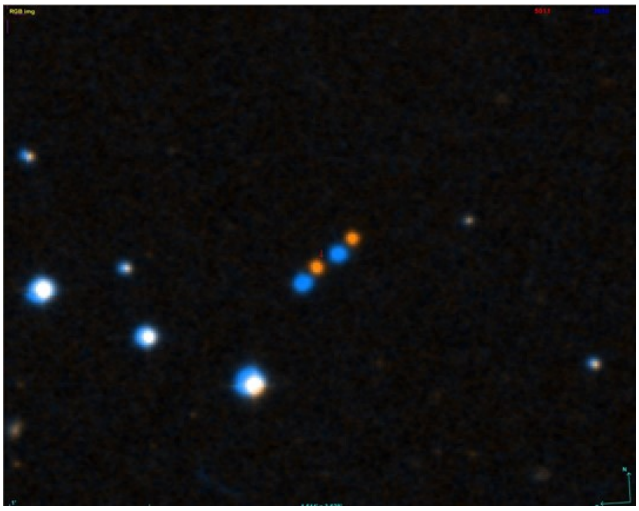

Figure 1. NSN n+21 RGB POSS.I to POSS.II composite

On the other side we have a "rather optical" CPM assessment based on quite precise UCAC5 proper motion data – this high precision is the reason for the "rather optical" rating because the difference in proper motion direction and proper motion speed is outside the range allowed by the small UCAC5 proper motion data error. We assume in both cases a potential orbit as reason for this contradicting evidence – we can only hope that future GAIA data releases provide Plx data for these stars allowing for an assessment of potential gravitational relationship.

One other object (KPP n+18) seems of special interest, as LSPM indicates here a physical triple with a third component seemingly confirmed by 2MASS and SDSS9 – but this component might rather be bogus than real.

4. Follow Up

There is a remainder of about 100 further potential CPM pairs with separation up to 25 arc seconds with currently not enough data available for a reliable CPM assessment. For these we wait for the next GAIA data release hoping for proper motion data for all these objects for both components.

None of our own images and thus our own measurements are currently available for the listed objects, but this might be a future step.

(Text continues on page 692)

Table 1. Research Results for Potential Common Proper Motion Pairs Found in the LSPM Catalog

Obj	RA	Dec	Sep	PA	M1	M2	pmRA1	pmDec1	e_pm1	pmRA2	pmDec2	e_pm2	CPM score	Ap	Me	Date	N	Source/Notes
KPP n+1	2.92609953	3.38804405	6.755	188.593	16.146	16.186	275.827	-40.624	8.819	279.426	-42.242	8.819	100	0.96	Hg	2015.000	V	GAIA DR1/2MASS. M1 and M2 estimated from G/J/H/K-mag. PM data from 2MASS to GAIA DR1 comparison. Most certainly physical
	2.92495100	3.38821200	6.738	189.114	16.100		286.000	-45.000		286.000	-45.000							LSPM J0011+0323. M1 and M2 are LSPM Vmag estimates
	2.92486200	3.38822600	6.738	189.114	14.553	14.896								1.30	E2	1998.876		2MASS. M1 and M2 estimated from J- and K-band
	2.92499830	3.38820250	6.747	189.176	15.771	15.771	286.000	-45.000	11.314	286.000	-45.000	11.314		0.20	Eu	2000.000		UCAC4. Given magnitudes are Vmags. Central epochs averaged
	2.92559500	3.38809100	6.747	188.638	17.199	17.185	330.000	273.000	9.899					2.50	Es	2008.756		SDSS9. M1 and M2 are SDSS9 gmags
	2.92583469	3.38807615	6.751	188.472	16.972	16.966								1.80	C	2011.612		Pan-STARRS release 1 (PS1) Survey - DR1. M1 and M2 are PS1 gmags
	2.92609953	3.38804405	6.755	188.593	15.130	15.216								0.96	Hg	2015.000		GAIA DR1. M1 and M2 are Gmags
NSN n+1	9.61673847	38.41643496	6.970	332.288	18.279	18.945	143.020	86.892	6.138	144.786	85.369	6.137	100	0.96	Hg	2015.000	V	GAIA DR1/2MASS. M1 and M2 estimated from G/J/H/K-mag. PM data from 2MASS to GAIA DR1 comparison. Most certainly physical
	9.61597800	38.41607300	7.001	332.189	19.120	19.080	144.000	80.000		144.000	80.000							LSPM J0038+3825. M1 and M2 are LSPM Vmag estimates
	9.61601800	38.41609200	7.001	332.189	16.992									1.30	E2	2000.791		2MASS. M1 and M2 estimated from J- and K-band
	9.61613900	38.41614400	6.993	332.311	19.487	20.108	135.000	79.000	4.243	100.000	87.000	4.243		2.50	Es	2002.764		SDSS9. M1 and M2 are SDSS9 gmags
	9.61597800	38.41607330	7.002	332.177			142.400	84.900	6.600	145.400	83.700	6.600		0.20	Eu	2013.180		URAT1
	9.61672066	38.41642576	6.971	332.333	19.239	19.818								1.80	C	2012.597		Pan-STARRS release 1 (PS1) Survey - DR1. M1 and M2 are PS1 gmags
	9.61673847	38.41643496	6.970	332.288	17.168	17.613								0.96	Hg	2015.000		GAIA DR1. M1 and M2 are Gmags
	9.61597000	38.41620900	6.618	326.500	15.560	16.110	134.000	86.000	5.657	74.000	82.000	56.886				1975.700		USNO B1. M1 and M2 are Imags
KPP n+2	12.55201620	62.58251328	20.273	112.555	16.056	16.074	-103.938	-117.697	5.608	-105.685	-118.886	5.608	97	0.96	Hg	2015.000	V	GAIA DR1/2MASS. M1 and M2 estimated from G/J/H/K-mag. PM data from 2MASS to GAIA DR1 comparison. Almost certainly physical
	12.55295800	62.58300400	20.288	112.482	16.760	17.410	-102.000	-117.000		-102.000	-117.000							LSPM J0050+6234. M1 and M2 are LSPM Vmag estimates
	12.55296500	62.58300800	20.290	112.480	14.487	14.264								1.30	E2	1999.868		2MASS. M1 and M2 estimated from J- and K-band
	12.55293390	62.58296170	20.493	111.823			-108.000	-111.200	6.522	-102.600	-106.800	5.445		0.20	Eu	1986.548		UCAC4. Given magnitudes are Vmags. Central epochs averaged
	12.55295620	62.58300360	20.291	112.479			-104.700	-116.100	5.900	-107.000	-118.300	6.000		0.20	Eu	2013.444		URAT1
	12.55224279	62.58262650	20.269	112.561	17.076	17.246								1.80	C	2011.560		Pan-STARRS release 1 (PS1) Survey - DR1. M1 and M2 are PS1 gmags
	12.55201620	62.58251328	20.273	112.555	14.865	14.808								0.96	Hg	2015.000		GAIA DR1. M1 and M2 are Gmags
	12.55601700	62.58458100	20.365	112.338	15.700	15.500								1.20	Pp	1952.708		USNO A2. M1 and M2 are Rmags
	12.55286200	62.58299500	20.254	112.775	14.140	13.190	-106.000	-124.000	6.708	-110.000	-126.000	8.944				1976.400		USNO B1. M1 and M2 are Imags
NSN n+2	15.54120051	10.15061258	3.369	284.029	13.098	13.408	155.263	15.553	10.430	155.178	13.245	10.430	95	0.96	Hg	2015.000	V	GAIA DR1/2MASS. M1 and M2 estimated from G/J/H/K-mag. PM data from 2MASS to GAIA DR1 comparison. Almost certainly physical
	15.54054300	10.15054700	3.380	284.620	13.700	15.210	160.000	18.000		160.000	18.000							LSPM J0102+1009. M1 and M2 are LSPM Vmag estimates
	15.54057600	10.15055100	3.376	284.576	12.208	12.487								1.30	E2	2000.746		2MASS. M1 and M2 estimated from J- and K-band
	15.54057240	10.15055370	3.366	283.679	12.648		160.000	18.000	11.314	23.400	42.100	6.037		0.20	Eu	1998.613		UCAC4. Given magnitudes are Vmags. Central epochs averaged
	15.54086100	10.15056600	3.312	284.477	25.114	14.024								2.50	Es	2008.825		SDSS9. M1 and M2 are SDSS9 gmags
	15.54120047	10.15061257	3.293	284.970	13.757	14.122								1.80	C	2014.209		Pan-STARRS release 1 (PS1) Survey - DR1. M1 and M2 are PS1 gmags
	15.54120051	10.15061258	3.369	284.029	12.154	12.432								0.96	Hg	2015.000		GAIA DR1. M1 and M2 are Gmags

Table 1 continues on the next page.

Table 1 (continued). Research Results for Potential Common Proper Motion Pairs Found in the LSPM Catalog

Obj	RA	Dec	Sep	PA	M1	M2	pmRA1	pmDec1	e_pm1	pmRA2	pmDec2	e_pm2	CPM score	Ap	Me	Date	N	Source/Notes
KPP n+3	16.32030711	16.33819899	7.797	8.584	14.991	17.151	180.912	13.715	4.899	183.879	17.603	4.899	100	0.96	Hg	2015.000	V	GAIA DR1/2MASS. M1 and M2 estimated from G/J/H/K-mag. PM data from 2MASS to GAIA DR1 comparison. Most certainly physical
	16.31953200	16.33814200	7.723	8.256	15.520	14.700	196.000	14.000		196.000	14.000							LSPM J0105+1620. M1 and M2 are LSPM Vmag estimates
	16.31940000	16.33813300	7.723	8.281	14.208	15.623								1.30	E2	1997.678		2MASS. M1 and M2 estimated from J- and K-band
	16.31996900	16.33817500	7.763	9.141	15.911	18.375								2.50	Es	2008.840		SDSS9. M1 and M2 are SDSS9 gmags
	16.31952190	16.33814040	7.733	8.330	15.050		181.500	11.600	5.200	185.300	15.700	5.300		0.20	Eu	2013.423		URAT1
	16.32029065	16.33819706	7.797	8.572	15.722	18.065								1.80	C	2012.251		Pan-STARRS release 1 (PS1) Survey - DR1. M1 and M2 are PS1 gmags
	16.32030711	16.33819899	7.797	8.584	14.104	16.078								0.96	Hg	2015.000		GAIA DR1. M1 and M2 are Gmags
	16.31702000	16.33810900	6.222	8.783	13.700	15.800								1.20	Pp	1953.997		USNO A2. M1 and M2 are Rmags
NSN n+3	27.80357893	81.35093457	20.716	33.170	14.016	20.114	208.076	7.193	5.934	219.125	13.454	26.325	76	0.96	Hg	2015.000	V	GAIA DR1/2MASS. M1 and M2 estimated from G/J/H/K-mag. PM data from 2MASS to GAIA DR1 comparison. Most probably physical
	27.79781200	81.35089900	20.589	32.953	13.670	18.340	209.000	26.000		178.000	14.000							LSPM J0151+8121. M1 and M2 are LSPM Vmag estimates
	27.79808300	81.35090600	20.561	32.964	13.812									1.30	E2	2000.731		2MASS. M1 and M2 estimated from J- and K-band
	27.79812930	81.35086690	20.568	32.321			-35.700	199.500	13.100	217.600	12.400	8.300		0.20	Eu	2013.467		URAT1
	27.80346620	81.35093634	20.481	31.985	14.193	20.396								1.80	C	2012.370		Pan-STARRS release 1 (PS1) Survey - DR1. M1 and M2 are PS1 gmags
	27.80357893	81.35093457	20.716	33.170	13.661	19.097								0.96	Hg	2015.000		GAIA DR1. M1 and M2 are Gmags
	27.79718900	81.35104800	20.522	32.442	13.050	18.220	-94.000	-56.000	5.000	210.000	340.000	18.601				1977.200		USNO B1. M1 and M2 are Imags
KPP n+4	34.80486862	50.64913464	9.223	50.499	14.756	16.445	119.287	100.882	5.573	118.826	102.000	5.573	100	0.96	Hg	2015.000	V	GAIA DR1/2MASS. M1 and M2 estimated from G/J/H/K-mag. PM data from 2MASS to GAIA DR1 comparison. Most certainly physical
	34.80408500	50.64871600	9.216	50.599	15.250	15.130	117.000	103.000		117.000	103.000							LSPM J0219+5038. M1 and M2 are LSPM Vmag estimates
	34.80407300	50.64870800	9.218	50.608	13.143	14.228								1.30	E2	1999.775		2MASS. M1 and M2 estimated from J- and K-band
	34.80408410	50.64871390	9.219	50.609			117.500	102.700	5.900	116.800	103.800	5.900		0.20	Eu	2013.487		URAT1
	34.80486194	50.64912750	9.192	50.458	15.563	17.558								1.80	C	2012.600		Pan-STARRS release 1 (PS1) Survey - DR1. M1 and M2 are PS1 gmags
	34.80486862	50.64913464	9.223	50.499	13.648	15.107								0.96	Hg	2015.000		GAIA DR1. M1 and M2 are Gmags
	34.80177000	50.64742000	8.387	51.067	14.000	15.000								1.20	Pp	1953.912		USNO A2. M1 and M2 are Rmags
	34.80468700	50.64922800	9.436	51.073	11.700		246.000	278.000	41.012	306.000	268.000	6.708				1978.450		USNO B1. M1 and M2 are Imags
NSN n+4	37.55648134	42.02318127	5.279	71.836	11.545	14.428	166.117	-17.101	5.708	172.177	-7.933	5.708	80	0.96	Hg	2015.000	V	GAIA DR1/2MASS. M1 and M2 estimated from G/J/H/K-mag. PM data from 2MASS to GAIA DR1 comparison. Most probably physical
	37.55545000	42.02325800	5.377	74.146	11.320		162.000	-21.000		159.000	-19.000							LSPM J0230+4201. M1 and M2 are LSPM Vmag estimates
	37.55547800	42.02325800	5.141	73.064	11.202	12.157								1.30	E2	1998.847		2MASS. M1 and M2 estimated from J- and K-band
	37.55554810	42.02325160	5.148	72.963	11.404		163.700	-19.300	5.500	166.700	-10.100	5.700		0.20	Eu	2013.514		URAT1
	37.55648134	42.02318127	5.279	71.836	10.779	13.043								0.96	Hg	2015.000		GAIA DR1. M1 and M2 are Gmags

Table 1 continues on the next page.

Table 1 (continued). Research Results for Potential Common Proper Motion Pairs Found in the LSPM Catalog

Obj	RA	Dec	Sep	PA	M1	M2	pmRA1	pmDec1	e_pm1	pmRA2	pmDec2	e_pm2	CPM score	Ap	Me	Date	N	Source/Notes
KPP n+5	44.85520482	63.65448425	8.149	85.724	15.189	19.292	-23.156	-105.463	5.936	-24.771	-101.487	6.690	95	0.96	Hg	2015.000	V	GAIA DR1/2MASS. M1 and M2 estimated from G/J/H/K-mag. PM data from 2MASS to GAIA DR1 comparison. Almost certainly physical
	44.85542300	63.65493400	8.166	86.133	15.210	18.500	-30.000	-161.000		-30.000	-161.000							LSPM J0259+6339. M1 and M2 are LSPM Vmag estimates
	44.85541200	63.65490300	8.168	86.133	14.524	17.569								1.30	E2	2000.706		2MASS. M1 and M2 estimated from J- and K-band
	44.85542250	63.65492340	8.171	86.165	15.212		-24.100	-104.800	6.300	-29.100	-99.500	6.500		0.20	Eu	2013.462		URAT1
	44.85520482	63.65448425	8.149	85.724	14.363	17.965								0.96	Hg	2015.000		GAIA DR1. M1 and M2 are Gmags
	44.85610900	63.65622000	9.030	81.009	14.400	18.100								1.20	Pp	1954.414		USNO A2. M1 and M2 are Rmags
	44.85549500	63.65496700	6.824	87.309	13.740	16.330	-20.000	-100.000	5.000	-68.000	-120.000	14.213				1976.650		USNO B1. M1 and M2 are Imags
NSN n+5	45.82886429	50.26639401	6.974	140.136	15.834	17.112	148.475	-79.716	5.278	148.829	-78.799	5.278	100	0.96	Hg	2015.000	V	GAIA DR1/2MASS. M1 and M2 estimated from G/J/H/K-mag. PM data from 2MASS to GAIA DR1 comparison. Most certainly physical
	45.82789200	50.26672700	6.979	140.278	15.700		136.000	-74.000		136.000	-74.000							LSPM J0303+5016. M1 and M2 are LSPM Vmag estimates
	45.82782700	50.26675000	6.981	140.249	14.815	15.554								1.30	E2	1998.923		2MASS. M1 and M2 estimated from J- and K-band
	45.82789720	50.26672670	6.981	140.238			150.500	-78.300	5.600	150.300	-77.100	5.600		0.20	Eu	2013.474		URAT1
	45.82882565	50.26640666	6.972	140.139	16.624	18.016								1.80	C	2012.200		Pan-STARRS release 1 (PS1) Survey - DR1. M1 and M2 are PS1 gmags
	45.82886429	50.26639401	6.974	140.136	14.863	16.033								0.96	Hg	2015.000		GAIA DR1. M1 and M2 are Gmags
KPP n+6	59.82485870	58.39459239	7.143	40.826	16.120	18.060	114.928	-184.113	5.314	115.072	-179.276	5.314	100	0.96	Hg	2015.000	V	GAIA DR1/2MASS. M1 and M2 estimated from G/J/H/K-mag. PM data from 2MASS to GAIA DR1 comparison. Most certainly physical
	59.82394000	58.39536300	7.081	41.196	14.320		105.000	-173.000		104.000	-173.000							LSPM J0359+5823. M1 and M2 are LSPM Vmag estimates
	59.82388600	58.39540900	7.083	41.219	14.427	15.876								1.30	E2	1999.033		2MASS. M1 and M2 estimated from J- and K-band
	59.82394460	58.39535950	7.089	41.202			115.600	-183.900	5.600	115.600	-179.000	5.700		0.20	Eu	2013.546		URAT1
	59.82483502	58.39461153	7.142	40.908	17.065	19.288								1.80	C	2012.871		Pan-STARRS release 1 (PS1) Survey - DR1. M1 and M2 are PS1 gmags
	59.82485870	58.39459239	7.143	40.826	15.011	16.758								0.96	Hg	2015.000		GAIA DR1. M1 and M2 are Gmags
NSN n+6	69.81833910	39.11018064	9.422	235.662	16.859	18.812	199.946	16.343	6.553	202.358	17.842	6.554	100	0.96	Hg	2015.000	V	GAIA DR1/2MASS. M1 and M2 estimated from G/J/H/K-mag. PM data from 2MASS to GAIA DR1 comparison. Most certainly physical
	69.81726100	39.11010400	9.476	235.867	17.070	19.140	192.000	-16.000		182.000	13.000							LSPM J0439+3906. M1 and M2 are LSPM Vmag estimates
	69.81717800	39.11010700	9.468	235.674	15.414	16.859								1.30	E2	1998.779		2MASS. M1 and M2 estimated from J- and K-band
	69.81726500	39.11011240	9.464	235.660			200.000	15.700	5.500	202.900	16.500	5.600		0.20	Eu	2013.523		URAT1
	69.81830282	39.11017959	9.407	235.614	17.705	19.681								1.80	C	2012.726		Pan-STARRS release 1 (PS1) Survey - DR1. M1 and M2 are PS1 gmags
	69.81833910	39.11018064	9.422	235.662	15.819	17.416								0.96	Hg	2015.000		GAIA DR1. M1 and M2 are Gmags
	69.81723900	39.11004500	9.080	238.683	14.810	16.180	232.000	-50.000	15.000	214.000	12.000	48.703				1988.700		USNO B1. M1 and M2 are Imags
KPP n+7	96.67677258	17.84302981	3.467	82.224	17.654	18.614	2.109	-160.479	7.019	-2.792	-161.465	7.059	100	0.96	Hg	2015.000	V	GAIA DR1/2MASS. M1 and M2 estimated from G/J/H/K-mag. PM data from 2MASS to GAIA DR1 comparison. Most certainly physical
	96.67677300	17.84369900	3.536	82.100	16.720		13.000	-159.000		13.000	-159.000							LSPM J0626+1750. M1 and M2 are LSPM Vmag estimates
	96.67676200	17.84379600	3.553	82.138										1.30	E2	1997.812		2MASS. M1 and M2 estimated from J- and K-band
	96.67676590	17.84369970	3.504	82.117			6.300	-158.600	5.200	-15.800	-160.800	6.600		0.20	Eu	2013.487		URAT1
	96.67677183	17.84306060	3.464	82.666	18.345	19.319								1.80	C	2011.896		Pan-STARRS release 1 (PS1) Survey - DR1. M1 and M2 are PS1 gmags
	96.67677258	17.84302981	3.467	82.224	16.802	17.643								0.96	Hg	2015.000		GAIA DR1. M1 and M2 are Gmags

Table 1 continues on the next page.

Table 1 (continued). Research Results for Potential Common Proper Motion Pairs Found in the LSPM Catalog

Obj	RA	Dec	Sep	PA	M1	M2	pmRA1	pmDec1	e_pm1	pmRA2	pmDec2	e_pm2	CPM score	Ap	Me	Date	N	Source/Notes
NSN n+7	99.90983957	23.99157254	7.504	83.797	14.115	20.545	-14.198	-166.376	6.083	-12.864	-134.732	18.289	5	0.96	Hg	2015.000		GAIA DR1/2MASS. M1 and M2 estimated from G/J/H/K-mag. PM data from 2MASS to GAIA DR1 comparison. Almost certainly optical
	99.90990400	23.99226600	7.460	87.483	14.400	19.560	-18.000	-169.000		-18.000	-169.000							LSPM J0639+2359. M1 and M2 are LSPM Vmag estimates
	99.90990500	23.99227300	7.447	87.451	14.180									1.30	E2	1999.844		2MASS. M1 and M2 estimated from J- and K-band
	99.90984168	23.99159533	7.492	84.186	14.342									1.80	C	2011.897		Pan-STARRS release 1 (PS1) Survey - DR1. M1 and M2 are PS1 gmags
	99.90983957	23.99157254	7.504	83.797	13.792	19.317								0.96	Hg	2015.000		GAIA DR1. M1 and M2 are Gmags
	99.90993100	23.99226700	6.737	83.002	12.990	17.580	-14.000	-160.000	2.236	12.000	-148.000	5.099				1980.400		USNO B1. M1 and M2 are Imags
KPP n+8	101.91494250	5.94940287	22.915	211.411	15.962	19.080	101.413	-133.283	7.027	96.589	-118.624	7.027	78	0.96	Hg	2015.000	V	GAIA DR1/2MASS. M1 and M2 estimated from G/J/H/K-mag. PM data from 2MASS to GAIA DR1 comparison. Most probably physical
	101.91452000	5.94995900	23.059	210.939	16.600	18.850	117.000	-126.000		117.000	-126.000							LSPM J0647+0556. M1 and M2 are LSPM Vmag estimates
	101.91451400	5.94996300	23.067	210.969	14.510	16.192								1.30	E2	1999.871		2MASS. M1 and M2 estimated from J- and K-band
	101.91451750	5.94995810	23.067	210.971	16.294		101.400	-136.800	6.000	102.500	-138.600	6.700		0.20	Eu	2013.526		URAT1
	101.91492940	5.94941847	22.933	211.339	16.920	19.414								1.80	C	2012.316		Pan-STARRS release 1 (PS1) Survey - DR1. M1 and M2 are PS1 gmags
	101.91494250	5.94940287	22.915	211.411	14.846	17.282								0.96	Hg	2015.000		GAIA DR1. M1 and M2 are Gmags
	101.91307500	5.95155600	23.164	210.783	15.600	17.800								1.20	Pp	1953.992		USNO A2. M1 and M2 are Rmags
	101.91409500	5.95035600	23.078	210.911	13.680	15.470										1950.000		USNO B1. M1 and M2 are Imags
NSN n+8	102.00645360	30.61126220	5.306	145.181	15.114	20.325	2.039	-150.825	5.287	3.563	-155.542	7.097	100	0.96	Hg	2015.000	V	GAIA DR1/2MASS. M1 and M2 estimated from G/J/H/K-mag. PM data from 2MASS to GAIA DR1 comparison. Most certainly physical
	102.00644700	30.61188500	5.238	144.738	15.370		13.000	-166.000		13.000	-166.000							LSPM J0648+3036. M1 and M2 are LSPM Vmag estimates
	102.00644300	30.61193700	5.230	144.927	13.841									1.30	E2	1998.893		2MASS. M1 and M2 estimated from J- and K-band
	102.00645290	30.61128438	5.326	145.426	15.965									1.80	C	2011.911		Pan-STARRS release 1 (PS1) Survey - DR1. M1 and M2 are PS1 gmags
	102.00645360	30.61126220	5.306	145.181	14.029	18.378								0.96	Hg	2015.000		GAIA DR1. M1 and M2 are Gmags
KPP n+9	103.37468250	60.75767343	4.624	130.501	11.526	15.654	-46.140	-167.369	6.269	-40.166	-172.364	7.148	100	0.96	Hg	2015.000	V	GAIA DR1/2MASS. M1 and M2 estimated from G/J/H/K-mag. PM data from 2MASS to GAIA DR1 comparison. Most certainly physical
	103.37496900	60.75832700	4.552	127.517	11.480		-56.000	-168.000		-48.000	-173.000							LSPM J0653+6045. M1 and M2 are LSPM Vmag estimates
	103.37510100	60.75841500	4.499	130.518	11.399	14.097								1.30	E2	1999.049		2MASS. M1 and M2 estimated from J- and K-band
	103.37475880	60.75780539	4.798	134.972	11.935									1.80	C	2012.090		Pan-STARRS release 1 (PS1) Survey - DR1. M1 and M2 are PS1 gmags
	103.37468250	60.75767343	4.624	130.501	10.950	14.523	-48.820	-168.094	1.044					0.96	Hg	2015.000		GAIA DR1. M1 and M2 are Gmags
NSN n+9	106.17738670	4.18083978	17.905	94.918	18.111	19.479	172.607	-225.730	5.654	173.666	-230.127	23.772	95	0.96	Hg	2015.000	V	GAIA DR1/2MASS. M1 and M2 estimated from G/J/H/K-mag. PM data from 2MASS to GAIA DR1 comparison. Almost certainly physical
	106.17665900	4.18178000	17.890	94.709	17.960	19.420	183.000	-231.000		183.000	-231.000							LSPM J0704+0410. M1 and M2 are LSPM Vmag estimates
	106.17666200	4.18178500	17.883	94.711	17.726	17.960								1.30	E2	1999.925		2MASS. M1 and M2 estimated from J- and K-band
	106.17710800	4.18122200	17.761	94.557	19.156	20.635	176.000	-242.000	4.243	179.000	-232.000	5.657		2.50	Es	2009.082		SDSS9. M1 and M2 are SDSS9 gmags
	106.17666540	4.18178030	17.881	94.709			179.200	-221.800	7.100	147.200	-212.900	10.500		0.20	Eu	2012.936		URAT1
	106.17738270	4.18084633	17.915	95.013	18.927	20.370								1.80	C	2013.873		Pan-STARRS release 1 (PS1) Survey - DR1. M1 and M2 are PS1 gmags
	106.17738670	4.18083978	17.905	94.918	17.363	18.525								0.96	Hg	2015.000		GAIA DR1. M1 and M2 are Gmags
	106.17651700	4.18187300	18.285	94.777	14.730	17.310	164.000	-240.000	19.849	182.000	-232.000	8.544				1981.250		USNO B1. M1 and M2 are Imags

Table 1 continues on the next page.

Table 1 (continued). Research Results for Potential Common Proper Motion Pairs Found in the LSPM Catalog

Obj	RA	Dec	Sep	PA	M1	M2	pmRA1	pmDec1	e_pm1	pmRA2	pmDec2	e_pm2	CPM score	Ap	Me	Date	N	Source/Notes
KPP n+10	112.14125810	89.68378631	17.589	306.903	16.223	17.429	199.128	-140.429	9.005	197.105	-134.327	9.005	100	0.96	Hg	2015.000	V	GAIA DR1/2MASS. M1 and M2 estimated from G/J/H/K-mag. PM data from 2MASS to GAIA DR1 comparison. Most certainly physical
	111.99185200	89.68442500	17.505	306.716	16.860	18.440	231.000	89.000		231.000	89.000							LSPM J0727+8941. M1 and M2 are LSPM Vmag estimates
	111.98275800	89.68440200	17.507	306.711	14.705	15.569								1.30	E2	1999.216		2MASS. M1 and M2 estimated from J- and K-band
	111.99047370	89.68436910	17.511	306.718			202.300	-146.700	6.700	199.000	-142.500	6.800		0.20	Eu	2013.101		URAT1
	112.11818190	89.68393330	17.532	306.770	17.062	18.390								1.80	C	2012.204		Pan-STARRS release 1 (PS1) Survey - DR1. M1 and M2 are PS1 gmags
	112.14125810	89.68378631	17.589	306.903	15.161	16.290								0.96	Hg	2015.000		GAIA DR1. M1 and M2 are Gmags
	111.52575600	89.68610900	17.622	305.882	15.600	16.800								1.20	Pp	1952.642		USNO A2. M1 and M2 are Rmags
	112.01254500	89.68435300	18.455	306.399	12.580	13.660	192.000	-132.000	2.236	-378.000	208.000	11.402				1981.650		USNO B1. M1 and M2 are Imags
NSN n+10	115.50143181	3.80957497	19.308	93.950	13.985	14.083	-221.775	36.552	6.120	-218.797	33.822	6.119	100	0.96	Hg	2015.000	V	GAIA DR1/2MASS. M1 and M2 estimated from G/J/H/K-mag. PM data from 2MASS to GAIA DR1 comparison. Most certainly physical
	115.50235700	3.80942300	19.257	93.837	14.680	14.210	-219.000	38.000		-219.000	38.000							LSPM J0742+0348. M1 and M2 are LSPM Vmag estimates
	115.50236200	3.80942200	19.261	93.837	13.120	13.148								1.30	E2	1999.934		2MASS. M1 and M2 estimated from J- and K-band
	115.50235830	3.80942670	19.307	93.854	14.100	14.161	-221.700	31.600	9.398	-232.100	36.200	7.948		0.20	Eu	1997.878		UCAC4. Given magnitudes are Vmags. Central epochs averaged
	115.50143535	3.80957682	19.321	93.964	14.746	14.841								1.80	C	2013.267		Pan-STARRS release 1 (PS1) Survey - DR1. M1 and M2 are PS1 gmags
	115.50143181	3.80957497	19.308	93.950	13.077	13.165								0.96	Hg	2015.000		GAIA DR1. M1 and M2 are Gmags
	115.50509500	3.80897800	19.301	93.861	13.400	13.700								1.20	Pp	1955.955		USNO A2. M1 and M2 are Rmags
	115.50255300	3.80937500	20.020	93.350	12.720	12.740				246.000	12.000	3.606				1989.100		USNO B1. M1 and M2 are Imags
KPP n+11	117.57001110	48.47250498	9.633	21.941	12.106	20.201	-52.397	-278.163	6.737	-53.353	-278.414	7.287	100	0.96	Hg	2015.000	V	GAIA DR1/2MASS. M1 and M2 estimated from G/J/H/K-mag. PM data from 2MASS to GAIA DR1 comparison. Most certainly physical
	117.57034300	48.47366300	9.648	22.055	12.060		-59.000	-274.000		-59.000	-274.000							LSPM J0750+4828. M1 and M2 are LSPM Vmag estimates
	117.57033700	48.47365200	9.642	22.011	11.609	17.043								1.30	E2	2000.155		2MASS. M1 and M2 estimated from J- and K-band
	117.57029800	48.47335500	9.642	21.781	15.299	25.112								2.50	Es	2003.886		SDSS9. M1 and M2 are SDSS9 gmags
	117.57003390	48.47259670	9.411	21.817	12.016									0.20	Eu	2013.902		URAT1
	117.57013750	48.47270459	9.688	21.016	13.545	20.988								1.80	C	2011.717		Pan-STARRS release 1 (PS1) Survey - DR1. M1 and M2 are PS1 gmags
	117.57001110	48.47250498	9.633	21.941	11.320	18.187								0.96	Hg	2015.000		GAIA DR1. M1 and M2 are Gmags
NSN n+11	120.37131110	57.98965980	3.905	277.744	13.108	15.601	-47.073	-214.138	5.759	-47.615	-214.779	5.760	100	0.96	Hg	2015.000	V	GAIA DR1/2MASS. M1 and M2 estimated from G/J/H/K-mag. PM data from 2MASS to GAIA DR1 comparison. Most certainly physical
	120.37168100	57.99055100	3.896	277.915	13.130		-50.000	-220.000		-50.000	-220.000							LSPM J0801+5759. M1 and M2 are LSPM Vmag estimates
	120.37170600	57.99061200	3.897	277.911	12.451	13.888								1.30	E2	1998.992		2MASS. M1 and M2 estimated from J- and K-band
	120.37138320	57.98982589	3.994	269.690	13.695	16.483								1.80	C	2012.471		Pan-STARRS release 1 (PS1) Survey - DR1. M1 and M2 are PS1 gmags
	120.37131110	57.98965980	3.905	277.744	12.265	14.464								0.96	Hg	2015.000		GAIA DR1. M1 and M2 are Gmags

Table 1 continues on the next page.

Table 1 (continued). Research Results for Potential Common Proper Motion Pairs Found in the LSPM Catalog

Obj	RA	Dec	Sep	PA	M1	M2	pmRA1	pmDec1	e_pm1	pmRA2	pmDec2	e_pm2	CPM score	Ap	Me	Date	N	Source/Notes
KPP n+12	136.24782794	2.43621322	10.048	68.278	13.010	13.448	-209.282	6.087	5.695	-202.926	12.616	5.730	100	0.96	Hg	2015.000	V	GAIA DR1/2MASS. M1 and M2 estimated from G/J/H/K-mag. PM data from 2MASS to GAIA DR1 comparison. Most certainly physical
	136.24870300	2.43618800	9.904	68.552	13.060	12.440	-197.000	3.000		-197.000	3.000							LSPM J0905+0226. M1 and M2 are LSPM Vmag estimates
	136.24869600	2.43618800	9.924	68.597	11.907	11.802								1.30	E2	2000.081		2MASS. M1 and M2 estimated from J- and K-band
	136.24869080	2.43619030	9.920	68.722	12.904		-197.000	3.000	11.314	-197.000	3.000	11.314		0.20	Eu	2000.000		UCAC4. Given magnitudes are Vmags. Central epochs averaged
	136.24858200	2.43614400	10.151	67.962	15.472	15.417								2.50	Es	2001.140		SDSS9. M1 and M2 are SDSS9 gmags
	136.24870070	2.43618770	9.923	68.596			-208.000	1.300	5.900	-202.200	8.300	5.900		0.20	Eu	2013.893		URAT1
	136.24782761	2.43621273	10.069	68.427		14.435								1.80	C	2013.117		Pan-STARRS release 1 (PS1) Survey - DR1. M1 and M2 are PS1 gmags
	136.24782794	2.43621322	10.048	68.278	11.967	12.244								0.96	Hg	2015.000		GAIA DR1. M1 and M2 are Gmags
NSN n+12	139.41627290	28.55545973	8.869	110.923	13.434	14.166	-204.467	-85.408	6.275	-199.308	-83.752	6.308	100	0.96	Hg	2015.000	V	GAIA DR1/2MASS. M1 and M2 estimated from G/J/H/K-mag. PM data from 2MASS to GAIA DR1 comparison. Most certainly physical
	139.41725200	28.55581900	8.802	111.271	12.750	14.330	-196.000	-70.000		-196.000	-70.000							LSPM J0917+2833. M1 and M2 are LSPM Vmag estimates
	139.41729300	28.55583400	8.802	111.271	12.243	12.704								1.30	E2	1999.224		2MASS. M1 and M2 estimated from J- and K-band
	139.41722620	28.55579620	8.682	111.624	13.342		-200.400	-79.700	8.450	-196.000	-70.000	11.314		0.20	Eu	2000.195		UCAC4. Given magnitudes are Vmags. Central epochs averaged
	139.41693400	28.55569200	8.532	113.208	14.826	15.515								2.50	Es	2004.212		SDSS9. M1 and M2 are SDSS9 gmags
	139.41646910	28.55558028	8.632	114.520	14.209	15.035								1.80	C	2011.994		Pan-STARRS release 1 (PS1) Survey - DR1. M1 and M2 are PS1 gmags
	139.41627290	28.55545973	8.869	110.923	12.354	13.016								0.96	Hg	2015.000		GAIA DR1. M1 and M2 are Gmags
KPP n+13	146.93021270	38.33563030	5.377	291.512	16.386	17.116	103.829	-298.992	5.068	104.243	-297.765	5.068	100	0.96	Hg	2015.000	V	GAIA DR1/2MASS. M1 and M2 estimated from G/J/H/K-mag. PM data from 2MASS to GAIA DR1 comparison. Most certainly physical
	146.92965700	38.33687200	5.365	291.325	15.650		110.000	-309.000		110.000	-309.000							LSPM J0947+3820. M1 and M2 are LSPM Vmag estimates
	146.92959700	38.33702100	5.376	291.282	14.943	15.363								1.30	E2	1998.255		2MASS. M1 and M2 estimated from J- and K-band
	146.92977800	38.33662200	5.373	291.540	17.503	18.263								2.50	Es	2002.999		SDSS9. M1 and M2 are SDSS9 gmags
	146.93016610	38.33571690	5.337	291.238										0.20	Eu	2013.889		URAT1
	146.93011570	38.33585597	5.366	291.385	17.281	18.051								1.80	C	2012.300		Pan-STARRS release 1 (PS1) Survey - DR1. M1 and M2 are PS1 gmags
	146.93021270	38.33563030	5.377	291.512	15.325	15.997								0.96	Hg	2015.000		GAIA DR1. M1 and M2 are Gmags
NSN n+13	148.75393853	48.57182783	9.878	303.230	12.666	13.305	158.929	-1.742	5.687	153.026	0.345	7.167	100	0.96	Hg	2015.000	V	GAIA DR1/2MASS. M1 and M2 estimated from G/J/H/K-mag. PM data from 2MASS to GAIA DR1 comparison. Most certainly physical
	148.75293000	48.57183500	9.792	303.344		12.220	150.000	-7.000		150.000	-7.000							LSPM J0954+4834. M1 and M2 are LSPM Vmag estimates
	148.75294900	48.57183500	9.788	303.359	12.206	12.355								1.30	E2	2000.169		2MASS. M1 and M2 estimated from J- and K-band
	148.75311530	48.57183420	9.774	303.286	12.442		150.000	-7.000	11.314	150.000	-7.000	11.314		0.20	Eu	2000.000		UCAC4. Given magnitudes are Vmags. Central epochs averaged
	148.75314220	48.57182000	9.846	303.261	12.308	13.094	157.300	2.300	1.697	154.900	3.400	1.697	100	0.20	Eu	2002.943		UCAC5. M1 and M2 are fmag values. Most certainly physical
	148.75312700	48.57180200	9.839	303.337	15.145	14.670								2.50	Es	2001.890		SDSS9. M1 and M2 are SDSS9 gmags
	148.75293760	48.57183490	9.787	303.362			156.500	-2.100	5.900	150.200	0.100	5.900		0.20	Eu	2013.739		URAT1
	148.75399204	48.57183862	9.963	302.639	13.312									1.80	C	2013.732		Pan-STARRS release 1 (PS1) Survey - DR1. M1 and M2 are PS1 gmags
	148.75393853	48.57182783	9.878	303.230	11.827	12.363								0.96	Hg	2015.000		GAIA DR1. M1 and M2 are Gmags

Table 1 continues on the next page.

Table 1 (continued). Research Results for Potential Common Proper Motion Pairs Found in the LSPM Catalog

Obj	RA	Dec	Sep	PA	M1	M2	pmRA1	pmDec1	e_pm1	pmRA2	pmDec2	e_pm2	CPM score	Ap	Me	Date	N	Source/Notes
KPP n+14	156.05630641	39.04302930	5.750	243.107	13.468	13.883	-94.458	94.247	5.069	-94.143	107.909	5.068	64	0.96	Hg	2015.000	V	GAIA DR1/2MASS. M1 and M2 estimated from G/J/H/K-mag. PM data from 2MASS to GAIA DR1 comparison. Probably physical
	156.05680800	39.04264500	5.850	241.071		12.650	-93.000	112.000		-93.000	112.000							LSPM J1024+3902. M1 and M2 are LSPM Vmag estimates
	156.05687200	39.04259100	5.862	241.137	11.705	12.076								1.30	E2	1998.258		2MASS. M1 and M2 estimated from J- and K-band
	156.05673860	39.04270670	5.837	241.243	13.329		-93.000	112.000	11.314	-93.000	112.000	11.314		0.20	Eu	2000.000		UCAC4. Given magnitudes are Vmags. Central epochs averaged
	156.05667800	39.04271600	5.805	241.475	14.889	15.382								2.50	Es	2003.087		SDSS9. M1 and M2 are SDSS9 gmags
	156.05681240	39.04263770	5.848	241.346	13.329		-95.800	96.700	5.200	-94.500	110.800	5.200		0.20	Eu	2013.896		URAT1
	156.05629129	39.04302762	5.652	242.593	14.468	14.912								1.80	C	2012.208		Pan-STARRS release 1 (PS1) Survey - DR1. M1 and M2 are PS1 gmags
	156.05630641	39.04302930	5.750	243.107	12.212	12.580								0.96	Hg	2015.000		GAIA DR1. M1 and M2 are Gmags
NSN n+14	158.70471058	1.97792776	8.972	125.028	14.629	14.664	125.030	-150.884	5.804	123.584	-150.998	5.839	100	0.96	Hg	2015.000	V	GAIA DR1/2MASS. M1 and M2 estimated from G/J/H/K-mag. PM data from 2MASS to GAIA DR1 comparison. Most certainly physical
	158.70419300	1.97855700	8.980	124.980	14.440	14.080	126.000	-159.000		126.000	-159.000							LSPM J1034+0158. M1 and M2 are LSPM Vmag estimates
	158.70419300	1.97855200	8.989	124.940	13.576	13.786								1.30	E2	2000.106		2MASS. M1 and M2 estimated from J- and K-band
	158.70416210	1.97856090	9.112	124.632	14.178	14.126	13.400	-57.300	3.124	126.000	-159.000	11.314		0.20	Eu	1998.508		UCAC4. Given magnitudes are Vmags. Central epochs averaged
	158.70414300	1.97853400	8.984	124.935	15.580	15.640	-18.000	-52.000	5.657	442.000	-354.000	25.456		2.50	Es	2000.343		SDSS9. M1 and M2 are SDSS9 gmags
	158.70418920	1.97855640	8.989	124.937	14.178		125.700	-151.900	5.900	124.600	-152.400	5.800		0.20	Eu	2014.110		URAT1
	158.70471087	1.97792773	8.963	125.033	15.374	15.431								1.80	C	2014.429		Pan-STARRS release 1 (PS1) Survey - DR1. M1 and M2 are PS1 gmags
	158.70471058	1.97792776	8.972	125.028	13.700	13.753								0.96	Hg	2015.000		GAIA DR1. M1 and M2 are Gmags
	158.70413900	1.97855600	8.465	124.713		11.950	-12.000	-52.000	15.652	420.000	-328.000	136.517				1988.150		USNO B1. M1 and M2 are Imags
KPP n+15	164.64075540	46.21622202	2.932	90.028	19.356	20.185	-85.542	-187.813	16.342	-82.282	-194.850	14.087	95	0.96	Hg	2015.000	V	GAIA DR1/2MASS. M1 and M2 estimated from G/J/H/K-mag. PM data from 2MASS to GAIA DR1 comparison. Almost certainly physical
	164.64128100	46.21699900	2.854	87.759	18.160		-55.000	-212.000		-55.000	-212.000							LSPM J1058+4613. M1 and M2 are LSPM Vmag estimates
	164.64130700	46.21706000	2.882	87.781										1.30	E2	1998.938		2MASS. M1 and M2 estimated from J- and K-band
	164.64104100	46.21688600	2.934	90.000	20.221	20.963								2.50	Es	2003.177		SDSS9. M1 and M2 are SDSS9 gmags
	164.64076570	46.21623877	2.910	90.452	19.956	20.672								1.80	C	2013.300		Pan-STARRS release 1 (PS1) Survey - DR1. M1 and M2 are PS1 gmags
	164.64075540	46.21622202	2.932	90.028	18.392	19.022								0.96	Hg	2015.000		GAIA DR1. M1 and M2 are Gmags

Table 1 continues on the next page.

Table 1 (continued). Research Results for Potential Common Proper Motion Pairs Found in the LSPM Catalog

Obj	RA	Dec	Sep	PA	M1	M2	pmRA1	pmDec1	e_pm1	pmRA2	pmDec2	e_pm2	CPM score	Ap	Me	Date	N	Source/Notes
NSN n+15	174.66795584	23.72994713	18.423	195.800	12.728	13.005	-224.664	-4.758	24.828	-229.721	-0.989	24.828	80	0.96	Hg	2015.000	?	GAIA DR1/2MASS. M1 and M2 estimated from G/J/H/K-mag. PM data from 2MASS to GAIA DR1 comparison. Most probably physical
	174.66897600	23.72996700	18.455	195.496	13.040	12.980	-219.000	6.000		-219.000	6.000							LSPM J1138+2343. M1 and M2 are LSPM Vmag estimates
	174.66898100	23.72996700	18.457	195.525	11.912	12.154								1.30	E2	1999.962		2MASS. M1 and M2 estimated from J- and K-band
	174.66890140	23.72997200	18.523	194.445	12.807	13.094	-219.000	6.000	11.314	-234.700	6.200	4.892		0.20	Eu	1998.493		UCAC4. Given magnitudes are Vmags. Central epochs averaged
	174.66890220	23.72993690	18.466	195.519	12.492	12.819	-225.700	2.700	1.910	-231.200	7.400	1.980	32	0.20	Eu	2001.184		UCAC5. M1 and M2 are fmag values. Probably optical. Might be effect of orbit
	174.66865400	23.72993100	18.432	195.579	15.835	16.018	-228.000	27.000	18.385	-236.000	7.000	2.828		2.50	Es	2005.096		SDSS9. M1 and M2 are SDSS9 gmags
	174.66805280	23.72995560	18.420	195.761	12.816	13.094								0.20	Eu	2013.806		URAT1
	174.66795507	23.72994725	18.423	195.793	13.613	13.717								1.80	C	2012.360		Pan-STARRS release 1 (PS1) Survey - DR1. M1 and M2 are PS1 gmags
	174.66795584	23.72994713	18.423	195.800	11.794	12.064								0.96	Hg	2015.000		GAIA DR1. M1 and M2 are Gmags
	174.67242500	23.72981400	18.385	194.651	11.800	11.600								1.20	Pp	1950.353		USNO A2. M1 and M2 are Rmags
	174.66900900	23.72993400	17.978	195.295	10.300	10.700	-210.000	12.000	81.468	-226.000	18.000	4.472				1987.800		USNO B1. M1 and M2 are Imags
KPP n+16	177.58507247	51.55428980	5.914	60.480	12.625	13.342	-133.505	-80.790	6.154	-131.989	-81.643	6.154	100	0.96	Hg	2015.000	V	GAIA DR1/2MASS. M1 and M2 estimated from G/J/H/K-mag. PM data from 2MASS to GAIA DR1 comparison. Most certainly physical
	177.58596800	51.55462600	5.901	60.263		9.970	-144.000	-66.000		-144.000	-66.000							LSPM J1150+5133. M1 and M2 are LSPM Vmag estimates
	177.58596600	51.55462600	5.901	60.263	12.526	13.075								1.30	E2	2000.019		2MASS. M1 and M2 estimated from J- and K-band
	177.58577220	51.55457370	5.775	60.260	12.117	12.456	-144.000	-66.000	11.314	-144.000	-66.000	11.314		0.20	Eu	2000.000		UCAC4. Given magnitudes are Vmags. Central epochs averaged
	177.58586700	51.55454400	5.937	60.426	15.350	14.673								2.50	Es	2001.970		SDSS9. M1 and M2 are SDSS9 gmags
	177.58596690	51.55462620	5.901	60.265	12.116		-131.500	-78.100	5.900	-131.700	-78.500	5.900		0.20	Eu	2013.757		URAT1
	177.58507247	51.55428980	6.013	61.014		13.703								1.80	C	2012.792		Pan-STARRS release 1 (PS1) Survey - DR1. M1 and M2 are PS1 gmags
	177.58507247	51.55428980	5.914	60.480	12.166	12.771				-136.087	-70.171	0.575		0.96	Hg	2015.000		GAIA DR1. M1 and M2 are Gmags
NSN n+16	177.80018110	37.13041755	4.772	10.133	11.980	16.036	-175.647	-63.850	6.821	-175.213	-62.153	6.821	100	0.96	Hg	2015.000	V	GAIA DR1/2MASS. M1 and M2 estimated from G/J/H/K-mag. PM data from 2MASS to GAIA DR1 comparison. Most certainly physical
	177.80108600	37.13063800	4.928	10.266	11.600		-176.000	-64.000		-184.000	-57.000							LSPM J1151+3707. M1 and M2 are LSPM Vmag estimates
	177.80120400	37.13071400	4.743	10.107	11.852	14.607								1.30	E2	1998.285		2MASS. M1 and M2 estimated from J- and K-band
	177.80083300	37.13059700	4.835	9.946	12.384	17.072								2.50	Es	2004.207		SDSS9. M1 and M2 are SDSS9 gmags
	177.80109930	37.13068330	4.736	10.058	11.837		-175.400	-64.300	5.200	-178.100	-67.700	7.700		0.20	Eu	2014.078		URAT1
	177.80022240	37.13041224	4.792	9.545	13.196	16.581								1.80	C	2011.963		Pan-STARRS release 1 (PS1) Survey - DR1. M1 and M2 are PS1 gmags
	177.80018110	37.13041755	4.772	10.133	11.539	15.019	-178.458	-59.330	1.300					0.96	Hg	2015.000		GAIA DR1. M1 and M2 are Gmags
KPP n+17	180.54182790	23.64545145	4.333	205.485	17.136	17.752	-158.351	-94.509	13.391	-163.703	-102.688	13.338	95	0.96	Hg	2015.000	V	GAIA DR1/2MASS. M1 and M2 estimated from G/J/H/K-mag. PM data from 2MASS to GAIA DR1 comparison. Almost certainly physical
	180.54254200	23.64584500	4.175	205.000	16.260		-165.000	-91.000		-165.000	-91.000							LSPM J1202+2338. M1 and M2 are LSPM Vmag estimates
	180.54257700	23.64586100	4.182	205.204	16.248	16.966								1.30	E2	1999.400		2MASS. M1 and M2 estimated from J- and K-band
	180.54229800	23.64570700	4.332	205.283	17.952	18.687								2.50	Es	2005.189		SDSS9. M1 and M2 are SDSS9 gmags
	180.54196310	23.64551554	4.657	208.408	17.777	18.493								1.80	C	2012.078		Pan-STARRS release 1 (PS1) Survey - DR1. M1 and M2 are PS1 gmags
	180.54182790	23.64545145	4.333	205.485	16.442	17.034								0.96	Hg	2015.000		GAIA DR1. M1 and M2 are Gmags

Table 1 continues on the next page.

Table 1 (continued). Research Results for Potential Common Proper Motion Pairs Found in the LSPM Catalog

Obj	RA	Dec	Sep	PA	M1	M2	pmRA1	pmDec1	e_pm1	pmRA2	pmDec2	e_pm2	CPM score	Ap	Me	Date	N	Source/Notes
NSN n+17	185.79160820	4.70430425	4.753	233.109	14.166	17.099	-164.487	44.909	7.620	-165.338	46.225	7.620	100	0.96	Hg	2015.000	V	GAIA DR1/2MASS. M1 and M2 estimated from G/J/H/K-mag. PM data from 2MASS to GAIA DR1 comparison. Most certainly physical
	185.79228200	4.70411700	4.746	232.751	14.100		-182.000	54.000		-182.000	54.000							LSPM J1223+0442. M1 and M2 are LSPM Vmag estimates
	185.79228900	4.70411900	4.755	232.829	13.119	15.463								1.30	E2	2000.150		2MASS. M1 and M2 estimated from J- and K-band
	185.79226300	4.70414600	4.785	232.994	15.953	18.335	-152.000	64.000	4.243					2.50	Es	2001.290		SDSS9. M1 and M2 are SDSS9 gmags
	185.79229580	4.70411690	4.754	232.828	14.358		-166.500	47.600	6.100	-173.000	42.100	6.500		0.20	Eu	2013.701		URAT1
	185.79175250	4.70425276	5.003	237.394	14.972	18.041								1.80	C	2011.894		Pan-STARRS release 1 (PS1) Survey - DR1. M1 and M2 are PS1 gmags
	185.79160820	4.70430425	4.753	233.109	13.167	15.877								0.96	Hg	2015.000		GAIA DR1. M1 and M2 are Gmags
KPP n+18	188.08654296	13.58382735	12.516	351.208	9.985	16.220	-281.900	-10.140	5.840	-284.326	-2.106	5.837	100	0.96	Hg	2015.000		GAIA DR1/2MASS. M1 and M2 estimated from G/J/H/K-mag. PM data from 2MASS to GAIA DR1 comparison. Most certainly physical
	188.08654800	13.58382900	12.470	351.600	9.860	17.110	-275.000	-6.000		-263.000	6.000							LSPM J1232+1335W and LSPM J1232+1335N. M1 and M2 are LSPM Vmag estimates. Note: There is with LSPM J1232+1335E a third component with unclear status - might be bogus
	188.08671800	13.58385700	12.735	351.299	9.800	14.900								1.30	E2	1998.039		2MASS. M1 and M2 estimated from J- and K-band
	188.08655420	13.58382920	12.539	350.251	9.920		-273.200	-3.600		-263.000	6.000			0.20	Eu	1995.500		UCAC4. Given magnitudes are Vmags. Central epochs averaged
	188.08546690	13.58381220	12.486	351.426	9.920		-274.350	-10.110	6.200	-276.530	-2.990	6.270	100	0.20	Eu	2013.915		URAT1. PM from position comparison with 2MASS
	188.08535167	13.58380921	12.470	352.100	9.714	17.055								1.80	C	2012.398		Pan-STARRS release 1 (PS1) Survey - DR1. M1 and M2 are PS1 gmags
	188.08654296	13.58382735	12.516	351.208	9.633	15.181								0.96	Hg	2015.000		GAIA DR1. M1 and M2 are Gmags
NSN n+18	189.36291460	29.87837546	9.545	263.390	13.441	17.890	-162.558	-93.597	13.550	-166.753	-98.134	13.550	95	0.96	Hg	2015.000	V	GAIA DR1/2MASS. M1 and M2 estimated from G/J/H/K-mag. PM data from 2MASS to GAIA DR1 comparison. Almost certainly physical
	189.36369300	29.87876100	9.439	263.782	13.850		-149.000	-101.000		-149.000	-101.000							LSPM J1237+2952. M1 and M2 are LSPM Vmag estimates
	189.36379100	29.87881300	9.467	263.800	12.423	15.393								1.30	E2	1998.171		2MASS. M1 and M2 estimated from J- and K-band
	189.36341400	29.87861800	9.523	263.662	15.358	19.441								2.50	Es	2004.957		SDSS9. M1 and M2 are SDSS9 gmags
	189.36369430	29.87876560	9.476	263.771	13.660		-165.100	-92.700	5.200	-170.200	-96.700	5.300		0.20	Eu	2013.678		URAT1
	189.36293300	29.87837203	9.510	263.883	14.198	19.086								1.80	C	2011.436		Pan-STARRS release 1 (PS1) Survey - DR1. M1 and M2 are PS1 gmags
	189.36291460	29.87837546	9.545	263.390	12.412	16.410								0.96	Hg	2015.000		GAIA DR1. M1 and M2 are Gmags

Table 1 continues on the next page.

Table 1 (continued). Research Results for Potential Common Proper Motion Pairs Found in the LSPM Catalog

Obj	RA	Dec	Sep	PA	M1	M2	pmRA1	pmDec1	e_pm1	pmRA2	pmDec2	e_pm2	CPM score	Ap	Me	Date	N	Source/Notes
KPP n+19	190.50561513	75.14582872	6.139	125.983	14.903	15.669	-205.945	-24.230	9.414	-195.387	-29.899	6.732	100	0.96	Hg	2015.000	V	GAIA DR1/2MASS. M1 and M2 estimated from G/J/H/K-mag. PM data from 2MASS to GAIA DR1 comparison. Most certainly physical
	190.50897200	75.14592700	5.950	126.192	16.510	15.750	-197.000	-46.000		-197.000	-46.000							LSPM J1242+7508. M1 and M2 are LSPM Vmag estimates
	190.50913900	75.14593500	5.951	126.231		14.245								1.30	E2	1999.209		2MASS. M1 and M2 estimated from J- and K-band
	190.50804650	75.14591060	6.070	126.892	14.845					-197.000	-46.000	11.314		0.20	Eu	2002.025		UCAC4. Given magnitudes are Vmags. Central epochs averaged
	190.50570568	75.14583202	6.113	126.078	15.148	16.596								1.80	C	2012.659		Pan-STARRS release 1 (PS1) Survey - DR1. M1 and M2 are PS1 gmags
	190.50561513	75.14582872	6.139	125.983	15.295	14.514								0.96	Hg	2015.000		GAIA DR1. M1 and M2 are Gmags
NSN n+19	191.46016829	63.33268625	15.045	143.997	16.897	17.143	-159.088	79.249	10.271	-158.921	80.667	10.271	95	0.96	Hg	2015.000	V	GAIA DR1/2MASS. M1 and M2 estimated from G/J/H/K-mag. PM data from 2MASS to GAIA DR1 comparison. Almost certainly physical
	191.46163900	63.33235500	15.068	144.021	16.930	16.790	-158.000	83.000		-158.000	84.000							LSPM J1245+6319. M1 and M2 are LSPM Vmag estimates
	191.46171700	63.33234000	15.061	144.056	15.695	15.908								1.30	E2	1999.271		2MASS. M1 and M2 estimated from J- and K-band
	191.46146100	63.33240700	15.071	143.978	17.917	18.205	-148.000	82.000	4.243	-151.000	83.000	4.243		2.50	Es	2001.391		SDSS9. M1 and M2 are SDSS9 gmags
	191.46164440	63.33235650	15.061	144.055			-160.100	81.600	5.600	-160.200	82.500	5.600		0.20	Eu	2013.651		URAT1
	191.46022942	63.33267161	15.038	144.012	17.694	17.982								1.80	C	2012.136		Pan-STARRS release 1 (PS1) Survey - DR1. M1 and M2 are PS1 gmags
	191.46016829	63.33268625	15.045	143.997	15.962	16.196								0.96	Hg	2015.000		GAIA DR1. M1 and M2 are Gmags
	191.46597000	63.33135000	15.176	143.483	16.200	16.600								1.20	Pp	1953.280		USNO A2. M1 and M2 are Rmags
	191.46153900	63.33246400	15.103	144.914	14.410	14.550	-146.000	86.000	2.236	-154.000	82.000	6.708				1977.400		USNO B1. M1 and M2 are Imags
KPP n+20	197.59418774	31.92089465	7.143	96.297	15.034	15.209	-204.759	-92.392	5.950	-198.112	-92.312	5.953	100	0.96	Hg	2015.000	V	GAIA DR1/2MASS. M1 and M2 estimated from G/J/H/K-mag. PM data from 2MASS to GAIA DR1 comparison. Most certainly physical
	197.59518400	31.92127800	7.038	96.373		12.100	-197.000	-94.000		-197.000	-94.000							LSPM J1310+3155. M1 and M2 are LSPM Vmag estimates
	197.59531400	31.92132600	7.032	96.408	13.571	13.682								1.30	E2	1998.193		2MASS. M1 and M2 estimated from J- and K-band
	197.59503210	31.92121920	7.190	95.689	14.755					-197.000	-94.000	11.314		0.20	Eu	2000.750		UCAC4. Given magnitudes are Vmags. Central epochs averaged
	197.59487100	31.92114400	7.076	96.485	16.192	16.365								2.50	Es	2004.362		SDSS9. M1 and M2 are SDSS9 gmags
	197.59426780	31.92091690	7.120	96.351										0.20	Eu	2013.745		URAT1
	197.59438598	31.92097635	6.942	97.736	15.918	16.130								1.80	C	2012.365		Pan-STARRS release 1 (PS1) Survey - DR1. M1 and M2 are PS1 gmags
	197.59418774	31.92089465	7.143	96.297	13.889	14.062								0.96	Hg	2015.000		GAIA DR1. M1 and M2 are Gmags

Table 1 continues on the next page.

Table 1 (continued). Research Results for Potential Common Proper Motion Pairs Found in the LSPM Catalog

Obj	RA	Dec	Sep	PA	M1	M2	pmRA1	pmDec1	e_pm1	pmRA2	pmDec2	e_pm2	CPM score	Ap	Me	Date	N	Source/Notes
NSN n+20	202.09689580	35.75677614	3.109	102.699	15.249	15.563	-183.541	-29.139	7.871	-195.966	-35.665	7.871	80	0.96	Hg	2015.000	V	GAIA DR1/2MASS. M1 and M2 estimated from G/J/H/K-mag. PM data from 2MASS to GAIA DR1 comparison. Most probably physical
	202.09783900	35.75689300	3.262	100.171	14.900	14.900	-191.000	-44.000		-191.000	-44.000							LSPM J1328+3545. M1 and M2 are LSPM Vmag estimates
	202.09789600	35.75690500	3.283	100.170	13.345	13.491								1.30	E2	1999.080		2MASS. M1 and M2 estimated from J- and K-band
	202.09767740	35.75695870	3.404	105.644			67.300	-104.900	8.773	-191.000	-44.000	11.314		0.20	Eu	2000.343		UCAC4. Given magnitudes are Vmags. Central epochs averaged
	202.09758500	35.75689600	3.209	101.323	16.628	17.085								2.50	Es	2004.209		SDSS9. M1 and M2 are SDSS9 gmags
	202.09690579	35.75678370	3.124	102.163	16.348	16.618								1.80	C	2013.380		Pan-STARRS release 1 (PS1) Survey - DR1. M1 and M2 are PS1 gmags
	202.09689580	35.75677614	3.109	102.699	13.938	14.155								0.96	Hg	2015.000		GAIA DR1. M1 and M2 are Gmags
KPP n+21	204.37606700	16.21978766	4.475	43.822	14.753	19.283	-197.703	-40.061	7.115	-199.032	-38.367	7.115	100	0.96	Hg	2015.000	V	GAIA DR1/2MASS. M1 and M2 estimated from G/J/H/K-mag. PM data from 2MASS to GAIA DR1 comparison. Most certainly physical
	204.37692300	16.21995200	4.497	44.694	14.950		-186.000	-46.000		-186.000	-46.000							LSPM J1337+1613. M1 and M2 are LSPM Vmag estimates
	204.37703500	16.21997600	4.471	44.284	13.390									1.30	E2	1998.075		2MASS. M1 and M2 estimated from J- and K-band
	204.37659000	16.21991200	4.551	43.899	15.799	25.114	-192.000	-48.000	2.828					2.50	Es	2005.364		SDSS9. M1 and M2 are SDSS9 gmags
	204.37608130	16.21979153	4.479	44.136	15.569									1.80	C	2012.429		Pan-STARRS release 1 (PS1) Survey - DR1. M1 and M2 are PS1 gmags
	204.37606700	16.21978766	4.475	43.822	13.640	17.677								0.96	Hg	2015.000		GAIA DR1. M1 and M2 are Gmags
NSN n+21	217.07528389	63.81773459	19.587	306.030	13.854	14.237	-136.935	187.102	21.956	-139.876	180.072	9.386	95	0.96	Hg	2015.000	?	GAIA DR1/2MASS. M1 and M2 estimated from G/J/H/K-mag. PM data from 2MASS to GAIA DR1 comparison. Almost certainly physical
	217.07656900	63.81695600	19.621	306.356	14.590	12.980	-154.000	181.000		-154.000	181.000							LSPM J1428+6349. M1 and M2 are LSPM Vmag estimates
	217.07664000	63.81691700	19.615	306.370	12.378	12.713								1.30	E2	1999.269		2MASS. M1 and M2 estimated from J- and K-band
	217.07663740	63.81697670	20.429	306.533	14.232		-151.500	184.200	4.118	-154.000	181.000	11.314		0.20	Eu	1999.920		UCAC4. Given magnitudes are Vmags. Central epochs averaged
	217.07635080	63.81714250	19.611	305.787	14.074	14.297	-144.600	181.900	1.838	-138.800	186.400	1.980	20	0.20	Eu	2003.279		UCAC5. M1 and M2 are fmag values. Most probably optical. Might be effect of orbit
	217.07656400	63.81699200	19.561	305.793	15.157	15.286	-146.000	182.000	4.243	-145.000	190.000	4.243		2.50	Es	2000.321		SDSS9. M1 and M2 are SDSS9 gmags
	217.07657720	63.81695570	19.617	306.345	14.232		-137.400	190.100	5.700	-145.600	183.600	5.700		0.20	Eu	2013.587		URAT1
	217.07528085	63.81773446	19.609	306.004	14.744	14.993								1.80	C	2013.290		Pan-STARRS release 1 (PS1) Survey - DR1. M1 and M2 are PS1 gmags
	217.07528389	63.81773459	19.587	306.030	12.725	13.087								0.96	Hg	2015.000		GAIA DR1. M1 and M2 are Gmags
	217.08052800	63.81472800	19.393	304.846	12.100	12.600								1.20	Pp	1956.201		USNO A2. M1 and M2 are Rmags
	217.07668100	63.81697000	19.654	305.883	11.060	11.230	-142.000	182.000	2.828	-142.000	192.000	4.243				1978.600		USNO B1. M1 and M2 are Imags

Table 1 continues on the next page.

Table 1 (continued). Research Results for Potential Common Proper Motion Pairs Found in the LSPM Catalog

Obj	RA	Dec	Sep	PA	M1	M2	pmRA1	pmDec1	e_pm1	pmRA2	pmDec2	e_pm2	CPM score	Ap	Me	Date	N	Source/Notes
KPP n+22	225.16476630	14.35798784	4.251	281.652	14.768	17.795	-167.983	-17.316	5.532	-166.464	-13.755	5.532	100	0.96	Hg	2015.000	V	GAIA DR1/2MASS. M1 and M2 estimated from G/J/H/K-mag. PM data from 2MASS to GAIA DR1 comparison. Most certainly physical
	225.16549700	14.35806000	4.281	280.711	15.130		-168.000	-19.000		-168.000	-19.000							LSPM J1500+1421. M1 and M2 are LSPM Vmag estimates
	225.16556900	14.35806800	4.264	280.803	13.853	16.016								1.30	E2	1998.335		2MASS. M1 and M2 estimated from J- and K-band
	225.16520200	14.35804600	4.278	281.060	15.977	19.053	-156.000	-10.000	2.828					2.50	Es	2005.362		SDSS9. M1 and M2 are SDSS9 gmags
	225.16478430	14.35798793	4.224	281.642	15.445	18.726								1.80	C	2012.637		Pan-STARRS release 1 (PS1) Survey - DR1. M1 and M2 are PS1 gmags
	225.16476630	14.35798784	4.251	281.652	13.846	16.640								0.96	Hg	2015.000		GAIA DR1. M1 and M2 are Gmags
NSN n+22	229.61100380	51.81334176	4.607	273.956	14.999	16.814	59.171	-184.600	5.130	60.084	-186.060	5.130	100	0.96	Hg	2015.000	V	GAIA DR1/2MASS. M1 and M2 estimated from G/J/H/K-mag. PM data from 2MASS to GAIA DR1 comparison. Most certainly physical
	229.61059600	51.81411000	4.631	274.235	13.720		53.000	-190.000		53.000	-190.000							LSPM J1518+5148. M1 and M2 are LSPM Vmag estimates
	229.61056400	51.81419000	4.624	274.242	14.604	15.694								1.30	E2	1998.458		2MASS. M1 and M2 estimated from J- and K-band
	229.61067560	51.81394280	4.466	275.204	14.843		53.000	-190.000	11.314					0.20	Eu	2001.595		UCAC4. Given magnitudes are Vmags. Central epochs averaged
	229.61065600	51.81399100	4.600	273.994	15.943	17.839								2.50	Es	2002.437		SDSS9. M1 and M2 are SDSS9 gmags
	229.61060290	51.81411180	4.620	274.187	14.843		55.900	-182.700	5.300	58.100	-186.100	5.500		0.20	Eu	2013.579		URAT1
	229.61099210	51.81336254	4.604	274.102	15.560	17.562								1.80	C	2012.560		Pan-STARRS release 1 (PS1) Survey - DR1. M1 and M2 are PS1 gmags
	229.61100380	51.81334176	4.607	273.956	14.287	15.909								0.96	Hg	2015.000		GAIA DR1. M1 and M2 are Gmags
KPP n+23	230.69858660	59.71482087	14.462	114.218	19.116	20.192	0.531	-181.598	6.361	1.445	-175.629	7.252	100	0.96	Hg	2015.000	V	GAIA DR1/2MASS. M1 and M2 estimated from G/J/H/K-mag. PM data from 2MASS to GAIA DR1 comparison. Most certainly physical
	230.69857800	59.71558000	14.499	114.575	19.840	20.800	-8.000	-171.000		-8.000	-171.000							LSPM J1522+5942. M1 and M2 are LSPM Vmag estimates
	230.69858200	59.71561400	14.488	114.580	16.817	17.792								1.30	E2	1999.277		2MASS. M1 and M2 estimated from J- and K-band
	230.69856700	59.71523900	14.457	114.119	20.178	21.650	6.000	-176.000	4.243					2.50	Es	2006.394		SDSS9. M1 and M2 are SDSS9 gmags
	230.69858260	59.71557850	14.487	114.554			1.800	-175.800	5.800	4.100	-168.100	6.400		0.20	Eu	2013.442		URAT1
	230.69858450	59.71483708	14.468	114.281	19.987	21.264								1.80	C	2012.648		Pan-STARRS release 1 (PS1) Survey - DR1. M1 and M2 are PS1 gmags
	230.69858660	59.71482087	14.462	114.218	17.600	18.662								0.96	Hg	2015.000		GAIA DR1. M1 and M2 are Gmags
	230.69852500	59.71560900	15.204	119.568	15.810	17.300	12.000	-176.000	3.162	26.000	-568.000	17.263				1980.100		USNO B1. M1 and M2 are Imags
NSN n+23	230.79185370	16.22578118	17.209	44.018	15.597	19.805	-192.405	39.518	6.742	-193.472	40.864	6.743	100	0.96	Hg	2015.000	V	GAIA DR1/2MASS. M1 and M2 estimated from G/J/H/K-mag. PM data from 2MASS to GAIA DR1 comparison. Most certainly physical
	230.79267900	16.22561800	17.241	44.225	16.210	20.360	-179.000	30.000		-179.000	30.000							LSPM J1523+1613. M1 and M2 are LSPM Vmag estimates
	230.79267100	16.22562000	17.205	44.102	14.175	16.895								1.30	E2	2000.317		2MASS. M1 and M2 estimated from J- and K-band
	230.79238100	16.22567300	17.201	44.068	16.725	21.493	-183.000	47.000	2.828					2.50	Es	2005.195		SDSS9. M1 and M2 are SDSS9 gmags
	230.79268840	16.22561680	17.206	44.107	15.841		-190.700	38.100	6.100	-192.200	37.600	6.500		0.20	Eu	2013.573		URAT1
	230.79187610	16.22577654	17.202	43.968	16.486	21.134								1.80	C	2012.731		Pan-STARRS release 1 (PS1) Survey - DR1. M1 and M2 are PS1 gmags
	230.79185370	16.22578118	17.209	44.018	14.478	17.932								0.96	Hg	2015.000		GAIA DR1. M1 and M2 are Gmags

Table 1 continues on the next page.

Table 1 (continued). Research Results for Potential Common Proper Motion Pairs Found in the LSPM Catalog

Obj	RA	Dec	Sep	PA	M1	M2	pmRA1	pmDec1	e_pm1	pmRA2	pmDec2	e_pm2	CPM score	Ap	Me	Date	N	Source/Notes
KPP n+24	231.14426330	31.78079100	5.878	253.718	14.294	18.045	-203.961	43.617	5.503	-214.159	39.578	5.503	80	0.96	Hg	2015.000	V	GAIA DR1/2MASS. M1 and M2 estimated from G/J/H/K-mag. PM data from 2MASS to GAIA DR1 comparison. Most probably physical
	231.14527900	31.78060300	5.733	254.035	14.190		-197.000	30.000		-197.000	30.000							LSPM J1524+3146. M1 and M2 are LSPM Vmag estimates
	231.14538000	31.78058800	5.695	253.890	14.262	17.194								1.30	E2	1998.245		2MASS. M1 and M2 estimated from J- and K-band
	231.14501600	31.78066300	5.856	253.941	14.605	19.025	-193.000	45.000	4.243					2.50	Es	2003.330		SDSS9. M1 and M2 are SDSS9 gmags
	231.14427290	31.78078954	5.818	253.396	14.521	18.760								1.80	C	2012.629		Pan-STARRS release 1 (PS1) Survey - DR1. M1 and M2 are PS1 gmags
	231.14426330	31.78079100	5.878	253.718	13.936	17.240								0.96	Hg	2015.000		GAIA DR1. M1 and M2 are Gmags
NSN n+24	234.78889459	54.04620925	4.844	7.570	17.562	19.564	6.280	-130.473	10.404	-20.384	-122.409	28.441	1	0.96	Hg	2015.000		GAIA DR1/2MASS. M1 and M2 estimated from G/J/H/K-mag. PM data from 2MASS to GAIA DR1 comparison. Almost certainly optical
	234.78884900	54.04675700	4.796	12.420	17.840	17.820		-159.000			-159.000							LSPM J1539+5402. M1 and M2 are LSPM Vmag estimates
	234.78885100	54.04674100	4.795	12.395	16.934									1.30	E2	2000.328		2MASS. M1 and M2 estimated from J- and K-band
	234.78895000	54.04679200	4.846	7.695	18.451	20.581	5.000	-406.000	33.941	101.000	371.000	79.196		2.50	Es	2000.261		SDSS9. M1 and M2 are SDSS9 gmags
	234.78884990	54.04675270	4.795	12.520			7.100	-128.200	6.200	-23.800	-121.300	6.200		0.20	Eu	2013.708		URAT1
	234.78889316	54.04622471	5.054	7.409	18.255	20.364								1.80	C	2013.010		Pan-STARRS release 1 (PS1) Survey - DR1. M1 and M2 are PS1 gmags
	234.78889459	54.04620925	4.844	7.570	16.883	18.711								0.96	Hg	2015.000		GAIA DR1. M1 and M2 are Gmags
KPP n+25	244.12879590	74.94402011	4.341	254.849	11.742	17.595	-146.654	65.968	7.685	-149.117	65.478	7.685	100	0.96	Hg	2015.000	V	GAIA DR1/2MASS. M1 and M2 estimated from G/J/H/K-mag. PM data from 2MASS to GAIA DR1 comparison. Most certainly physical
	244.13119500	74.94375600	4.337	254.596	11.230		-146.000	70.000		-133.000	78.000							LSPM J1616+7456. M1 and M2 are LSPM Vmag estimates
	244.13125300	74.94373300	4.301	254.814	11.442									1.30	E2	1999.332		2MASS. M1 and M2 estimated from J- and K-band
	244.12879510	74.94401932	4.290	254.375	12.342									1.80	C	2012.156		Pan-STARRS release 1 (PS1) Survey - DR1. M1 and M2 are PS1 gmags
	244.12879590	74.94402011	4.341	254.849	11.106	15.132	-144.136	67.951	1.364					0.96	Hg	2015.000		GAIA DR1. M1 and M2 are Gmags
NSN n+25	249.43491930	37.19972645	23.442	238.716	12.962	17.262	-170.213	50.406	5.530	-169.411	52.487	5.530	97	0.96	Hg	2015.000	V	GAIA DR1/2MASS. M1 and M2 estimated from G/J/H/K-mag. PM data from 2MASS to GAIA DR1 comparison. Almost certainly physical
	249.43582200	37.19951600	23.466	238.653	13.020	17.470	-158.000	48.000		-158.000	48.000							LSPM J1637+3711. M1 and M2 are LSPM Vmag estimates
	249.43590900	37.19949300	23.471	238.661	12.578	15.378								1.30	E2	1998.327		2MASS. M1 and M2 estimated from J- and K-band
	249.43566100	37.19955300	23.459	238.765	15.815	18.472	-163.000	53.000	4.243	-179.000	55.000	4.243		2.50	Es	2002.438		SDSS9. M1 and M2 are SDSS9 gmags
	249.43580990	37.19951570	23.468	238.673	12.834		-169.200	49.100	5.300	-168.800	52.200	5.300		0.20	Eu	2013.649		URAT1
	249.43491880	37.19972577	23.354	238.507		18.185								1.80	C	2011.853		Pan-STARRS release 1 (PS1) Survey - DR1. M1 and M2 are PS1 gmags
	249.43491930	37.19972645	23.442	238.716	12.245	16.138								0.96	Hg	2015.000		GAIA DR1. M1 and M2 are Gmags
	249.43851200	37.19889800	23.618	239.436	12.200	16.600								1.20	Pp	1954.400		USNO A2. M1 and M2 are Rmags
	249.43597300	37.19948100	24.090	240.727	11.110	14.540	-150.000	46.000	6.403	-200.000	50.000	40.460				1977.450		USNO B1. M1 and M2 are Imags

Table 1 continues on the next page.

Table 1 (continued). Research Results for Potential Common Proper Motion Pairs Found in the LSPM Catalog

Obj	RA	Dec	Sep	PA	M1	M2	pmRA1	pmDec1	e_pm1	pmRA2	pmDec2	e_pm2	CPM score	Ap	Me	Date	N	Source/Notes
KPP n+26	250.33374260	35.07841991	21.957	218.531	15.967	20.961	-171.430	3.654	5.942	-255.028	32.559	5.942	0	0.96	Hg	2015.000		GAIA DR1/2MASS. M1 and M2 estimated from G/J/H/K-mag. PM data from 2MASS to GAIA DR1 comparison. Almost certainly optical
	250.33462500	35.07840700	21.530	214.899	15.980	19.300	-155.000	5.000		-155.000	5.000							LSPM J1641+3504. M1 and M2 are LSPM Vmag estimates
	250.33471200	35.07840300	21.511	214.828	14.637	17.834								1.30	E2	1998.340		2MASS. M1 and M2 estimated from J- and K-band
	250.33446400	35.07839600	21.715	214.653	17.030	21.593	-161.000	3.000	4.243					2.50	Es	2002.438		SDSS9. M1 and M2 are SDSS9 gmags
	250.33391860	35.07842653	21.599	215.207	16.776									1.80	C	2012.171		Pan-STARRS release 1 (PS1) Survey - DR1. M1 and M2 are PS1 gmags
	250.33374260	35.07841991	21.957	218.531	14.974	18.969								0.96	Hg	2015.000		GAIA DR1. M1 and M2 are Gmags
	250.33706700	35.07838400	21.813	217.127	14.500	18.400								1.20	Pp	1954.400		USNO A2. M1 and M2 are Rmags
	250.33478100	35.07847300	21.984	218.517	13.590	17.370	-146.000	6.000	5.000	-156.000	8.000	12.369				1976.300		USNO B1. M1 and M2 are Imags
NSN n+26	252.74260720	27.79043888	20.997	44.154	15.227	20.497	-125.345	117.659	5.921	-126.038	117.576	5.921	97	0.96	Hg	2015.000	V	GAIA DR1/2MASS. M1 and M2 estimated from G/J/H/K-mag. PM data from 2MASS to GAIA DR1 comparison. Almost certainly physical
	252.74321000	27.78994900	20.999	44.154	15.670	21.100	-122.000	124.000		-122.000	124.000							LSPM J1650+2747. M1 and M2 are LSPM Vmag estimates
	252.74322000	27.78993000	21.006	44.173	14.015	17.279								1.30	E2	1999.430		2MASS. M1 and M2 estimated from J- and K-band
	252.74299400	27.79010500	21.005	44.284	16.275	22.307	-123.000	126.000	2.828					2.50	Es	2004.709		SDSS9. M1 and M2 are SDSS9 gmags
	252.74319780	27.78994830	21.005	44.171	15.531		-124.900	116.600	5.700	-125.000	115.800	6.300		0.20	Eu	2013.414		URAT1
	252.74262460	27.79042411	20.996	44.101	16.030	21.950								1.80	C	2011.523		Pan-STARRS release 1 (PS1) Survey - DR1. M1 and M2 are PS1 gmags
	252.74260720	27.79043888	20.997	44.154	14.136	18.503								0.96	Hg	2015.000		GAIA DR1. M1 and M2 are Gmags
	252.74339500	27.78979500	21.064	44.978		17.290										1993.400		USNO B1. M1 and M2 are Imags
KPP n+27	258.86564357	30.87188009	14.944	346.889	13.059	13.856	-216.752	-210.026	5.073	-208.629	-212.217	5.073	80	0.96	Hg	2015.000	V	GAIA DR1/2MASS. M1 and M2 estimated from G/J/H/K-mag. PM data from 2MASS to GAIA DR1 comparison. Most probably physical
	258.86673000	30.87277400	15.025	346.199	13.600	11.330	-182.000	-171.000		-182.000	-171.000							LSPM J1715+3052. M1 and M2 are LSPM Vmag estimates
	258.86681700	30.87285600	15.011	346.417	11.735	12.507								1.30	E2	1998.272		2MASS. M1 and M2 estimated from J- and K-band
	258.86659420	30.87266030	15.050	346.223		13.097	-182.000	-171.000	11.314	-182.000	-171.000	11.314		0.20	Eu	2000.000		UCAC4. Given magnitudes are Vmags. Central epochs averaged
	258.86661600	30.87268600	14.896	346.408	16.352	15.194								2.50	Es	2001.291		SDSS9. M1 and M2 are SDSS9 gmags
	258.86574970	30.87196890	14.951	346.710										0.20	Eu	2013.688		URAT1
	258.86564346	30.87187978	14.942	346.895	18.444									1.80	C	2013.713		Pan-STARRS release 1 (PS1) Survey - DR1. M1 and M2 are PS1 gmags
	258.86564357	30.87188009	14.944	346.889	11.957	12.762								0.96	Hg	2015.000		GAIA DR1. M1 and M2 are Gmags
	258.86740000	30.87355300	16.871	347.820		10.500					-10.000					1985.450		USNO B1. M1 and M2 are Imags
NSN n+27	262.14934770	13.55514513	8.175	116.113	11.056	14.322	-106.795	-104.346	6.290	-110.279	-109.618	6.362	100	0.96	Hg	2015.000	V	GAIA DR1/2MASS. M1 and M2 estimated from G/J/H/K-mag. PM data from 2MASS to GAIA DR1 comparison. Most certainly physical
	262.14984100	13.55538200	7.787	111.082	10.850		-101.000	-223.000		-121.000	-119.000							LSPM J1728+1333. M1 and M2 are LSPM Vmag estimates
	262.14979500	13.55557000	8.187	115.470	10.556	13.177								1.30	E2	2000.342		2MASS. M1 and M2 estimated from J- and K-band
	262.14979800	13.55529000	7.722	110.124	10.929		-101.000	-223.000	11.314	-121.000	-119.000	11.314		0.20	Eu	2000.000		UCAC4. Given magnitudes are Vmags. Central epochs averaged
	262.14980520	13.55557990	8.187	115.451	10.930		-103.900	-103.000	6.000	-109.200	-110.600	6.100		0.20	Eu	2013.826		URAT1
	262.14934780	13.55514513	8.172	115.828	12.006	15.167								1.80	C	2013.402		Pan-STARRS release 1 (PS1) Survey - DR1. M1 and M2 are PS1 gmags
	262.14934770	13.55514513	8.175	116.113	10.355	13.241								0.96	Hg	2015.000		GAIA DR1. M1 and M2 are Gmags

Table 1 continues on the next page.

Table 1 (continued). Research Results for Potential Common Proper Motion Pairs Found in the LSPM Catalog

Obj	RA	Dec	Sep	PA	M1	M2	pmRA1	pmDec1	e_pm1	pmRA2	pmDec2	e_pm2	CPM score	Ap	Me	Date	N	Source/Notes
KPP n+28	268.04904600	76.41071523	15.458	347.158	18.308	19.985	-69.823	126.853	6.760	-65.053	129.892	6.760	97	0.96	Hg	2015.000	V	GAIA DR1/2MASS. M1 and M2 estimated from G/J/H/K-mag. PM data from 2MASS to GAIA DR1 comparison. Almost certainly physical
	268.05029300	76.41018700	15.427	346.847	19.130	20.400	-66.000	134.000		-66.000	134.000							LSPM J1752+7624. M1 and M2 are LSPM Vmag estimates
	268.05026700	76.41019400	15.430	346.866	16.618	17.457								1.30	E2	2000.208		2MASS. M1 and M2 estimated from J- and K-band
	268.05028430	76.41018680	15.428	346.861			-68.700	123.800	6.200	-65.700	130.000	6.400		0.20	Eu	2013.387		URAT1
	268.04908570	76.41069823	15.489	347.133	19.340	20.985								1.80	C	2012.553		Pan-STARRS release 1 (PS1) Survey - DR1. M1 and M2 are PS1 gmags
	268.04904600	76.41071523	15.458	347.158	17.162	18.437								0.96	Hg	2015.000		GAIA DR1. M1 and M2 are Gmags
	268.05039800	76.41026400	14.848	348.118	15.990	16.890	-66.000	134.000	5.000							1986.250		USNO B1. M1 and M2 are Imags
NSN n+28	273.51044090	38.88264272	6.487	124.992	10.599	16.096	-45.270	147.658	5.113	-55.833	154.296	5.113	64	0.96	Hg	2015.000	V	GAIA DR1/2MASS. M1 and M2 estimated from G/J/H/K-mag. PM data from 2MASS to GAIA DR1 comparison. Probably physical
	273.51068100	38.88198100	6.581	123.728	10.580		-43.000	162.000		-37.000	154.000							LSPM J1814+3852. M1 and M2 are LSPM Vmag estimates
	273.51070900	38.88196200	6.694	124.904	10.308	14.108								1.30	E2	1998.404		2MASS. M1 and M2 estimated from J- and K-band
	273.51068430	38.88202760	6.658	124.882	10.421		-43.600	148.300	5.300	-60.500	163.300	5.300		0.20	Eu	2014.084		URAT1
	273.51044090	38.88264272	6.517	125.236	10.197	17.031								1.80	C	2011.827		Pan-STARRS release 1 (PS1) Survey - DR1. M1 and M2 are PS1 gmags
	273.51044090	38.88264272	6.487	124.992	9.966	14.769	-44.168	161.651	1.037					0.96	Hg	2015.000		GAIA DR1. M1 and M2 are Gmags
KPP n+29	279.51681920	63.68012903	3.453	134.098	18.174	18.921	13.201	196.521	6.755	9.903	193.691	6.755	100	0.96	Hg	2015.000	V	GAIA DR1/2MASS. M1 and M2 estimated from G/J/H/K-mag. PM data from 2MASS to GAIA DR1 comparison. Most certainly physical
	279.51669300	63.67931000	3.463	132.992	17.900		12.000	182.000		12.000	182.000							LSPM J1838+6340. M1 and M2 are LSPM Vmag estimates
	279.51669800	63.67932900	3.460	133.046	16.547	17.488								1.30	E2	2000.345		2MASS. M1 and M2 estimated from J- and K-band
	279.51679300	63.67966400	3.451	134.088	19.249	20.025								2.50	Es	2006.331		SDSS9. M1 and M2 are SDSS9 gmags
	279.51669440	63.67931000	3.462	133.056			15.700	196.800	6.400	11.100	200.600	6.400		0.20	Eu	2013.398		URAT1
	279.51681420	63.68010779	3.437	133.815	19.013	19.708								1.80	C	2013.053		Pan-STARRS release 1 (PS1) Survey - DR1. M1 and M2 are PS1 gmags
	279.51681920	63.68012903	3.453	134.098	17.119	17.712								0.96	Hg	2015.000		GAIA DR1. M1 and M2 are Gmags
NSN n+29	285.11483570	5.85966178	17.253	26.138	14.803	15.436	72.972	-185.252	6.905	73.070	-182.336	6.905	100	0.96	Hg	2015.000	V	GAIA DR1/2MASS. M1 and M2 estimated from G/J/H/K-mag. PM data from 2MASS to GAIA DR1 comparison. Most certainly physical
	285.11453200	5.86043300	17.187	26.028	14.930	15.530	76.000	-197.000		76.000	-197.000							LSPM J1900+0551. M1 and M2 are LSPM Vmag estimates
	285.11452200	5.86045400	17.212	26.200	13.390	13.886								1.30	E2	1999.605		2MASS. M1 and M2 estimated from J- and K-band
	285.11454500	5.86039120	17.193	26.071			76.000	-197.000	11.314	76.000	-197.000	11.314		0.20	Eu	2000.000		UCAC4. Given magnitudes are Vmags. Central epochs averaged
	285.11453060	5.86044670	17.216	26.116	15.179	15.710	76.500	-197.700	3.183	78.100	-195.600	4.950	100	0.20	Eu	2000.711		UCAC5. M1 and M2 are fmag values. Most certainly physical
	285.11452980	5.86043370	17.214	26.197	15.129		70.400	-183.900	6.200	69.900	-181.000	6.100		0.20	Eu	2013.482		URAT1
	285.11477540	5.85982840	16.889	27.428	15.693	16.396								1.80	C	2011.838		Pan-STARRS release 1 (PS1) Survey - DR1. M1 and M2 are PS1 gmags
	285.11483570	5.85966178	17.253	26.138	13.653	14.215								0.96	Hg	2015.000		GAIA DR1. M1 and M2 are Gmags
	285.11355900	5.86310900	17.345	26.064	13.800	14.700								1.20	Pp	1951.506		USNO A2. M1 and M2 are Rmags
	285.11459800	5.86058900	16.727	25.380	12.170	12.850	80.000	-182.000	5.657	70.000	-192.000	3.162				1975.100		USNO B1. M1 and M2 are Imags

Table 1 continues on the next page.

Table 1 (continued). Research Results for Potential Common Proper Motion Pairs Found in the LSPM Catalog

Obj	RA	Dec	Sep	PA	M1	M2	pmRA1	pmDec1	e_pm1	pmRA2	pmDec2	e_pm2	CPM score	Ap	Me	Date	N	Source/Notes
KPP n+30	290.59280280	4.90815445	10.125	189.500	14.196	17.558	-201.489	84.388	5.979	-182.855	83.241	15.140	76	0.96	Hg	2015.000	V	GAIA DR1/2MASS. M1 and M2 estimated from G/J/H/K-mag. PM data from 2MASS to GAIA DR1 comparison. Most probably physical
	290.59362800	4.90780000	10.150	191.186	15.240	17.520	-230.000	56.000		-196.000	81.000							LSPM J1922+0454. M1 and M2 are LSPM Vmag estimates
	290.59366900	4.90779300	10.159	191.115	12.977									1.30	E2	1999.580		2MASS. M1 and M2 estimated from J- and K-band
	290.59364580	4.90780260	10.157	191.057	14.391		-198.500	86.200	5.800	-173.600	82.500	6.500		0.20	Eu	2013.989		URAT1
	290.59297120	4.90807078	9.964	192.559	15.010	17.861								1.80	C	2011.944		Pan-STARRS release 1 (PS1) Survey - DR1. M1 and M2 are PS1 gmags
	290.59280280	4.90815445	10.125	189.500	13.147	17.430								0.96	Hg	2015.000		GAIA DR1. M1 and M2 are Gmags
	290.59652000	4.90680900	10.793	192.416	12.500	17.300								1.20	Pp	1950.611		USNO A2. M1 and M2 are Rmags
NSN n+30	290.76105470	39.41093217	7.153	9.110	15.972	16.314	-97.555	-251.069	5.554	-100.535	-251.725	5.553	100	0.96	Hg	2015.000	V	GAIA DR1/2MASS. M1 and M2 estimated from G/J/H/K-mag. PM data from 2MASS to GAIA DR1 comparison. Most certainly physical
	290.76156600	39.41197200	7.173	9.530	16.190	16.530	-111.000	-264.000		-111.000	-264.000							LSPM J1923+3924. M1 and M2 are LSPM Vmag estimates
	290.76163700	39.41209000	7.172	9.487	15.242	15.777								1.30	E2	1998.398		2MASS. M1 and M2 estimated from J- and K-band
	290.76146360	39.41177450	7.188	9.354			-111.000	-264.000	11.314	-111.000	-264.000	11.314		0.20	Eu	2000.000		UCAC4. Given magnitudes are Vmags. Central epochs averaged
	290.76149080	39.41179220	7.184	8.684	15.898	16.352	-98.400	-251.000	3.677	-94.500	-254.200	4.455	100	0.20	Eu	2002.667		UCAC5. M1 and M2 are fmag values. Most certainly physical
	290.76109190	39.41103720	7.156	9.222										0.20	Eu	2013.587		URAT1
	290.76115480	39.41114366	7.170	9.236	16.674	17.032								1.80	C	2011.951		Pan-STARRS release 1 (PS1) Survey - DR1. M1 and M2 are PS1 gmags
	290.76105470	39.41093217	7.153	9.110	15.189	15.575								0.96	Hg	2015.000		GAIA DR1. M1 and M2 are Gmags
	290.76168900	39.41228900	6.723	7.870	13.360	13.630	-92.000	-246.000	12.083	-70.000	-84.000	43.566				1979.150		USNO B1. M1 and M2 are Imags
KPP n+31	291.51384910	44.35973726	6.063	30.647	10.371	15.166	69.467	209.761	5.122	69.109	212.124	5.122	100	0.96	Hg	2015.000	V	GAIA DR1/2MASS. M1 and M2 estimated from G/J/H/K-mag. PM data from 2MASS to GAIA DR1 comparison. Most certainly physical
	291.51339700	44.35884500	6.185	32.245	10.390		73.000	207.000		79.000	198.000							LSPM J1926+4421. M1 and M2 are LSPM Vmag estimates
	291.51340200	44.35877200	6.032	30.885	10.403	14.320								1.30	E2	1998.434		2MASS. M1 and M2 estimated from J- and K-band
	291.51342800	44.35885980	6.821	30.794	10.324		73.000	207.400	5.341	79.000	198.000	11.314		0.20	Eu	2000.580		UCAC4. Given magnitudes are Vmags. Central epochs averaged
	291.51384910	44.35973726	6.063	30.647	10.113	14.351	73.716	208.123	1.502					0.96	Hg	2015.000		GAIA DR1. M1 and M2 are Gmags
NSN n+31	296.43090740	31.67938570	19.845	122.901	15.276	17.899	-6.726	158.446	5.090	-8.042	156.850	5.090	97	0.96	Hg	2015.000	V	GAIA DR1/2MASS. M1 and M2 estimated from G/J/H/K-mag. PM data from 2MASS to GAIA DR1 comparison. Almost certainly physical
	296.43093900	31.67872000	19.889	122.717	14.980	17.710	-13.000	147.000		-13.000	147.000							LSPM J1945+3140. M1 and M2 are LSPM Vmag estimates
	296.43094400	31.67865200	19.850	122.802	14.619	16.437								1.30	E2	1998.330		2MASS. M1 and M2 estimated from J- and K-band
	296.43093820	31.67872540	19.849	122.804			-9.600	158.800	5.400	-11.700	158.000	5.500		0.20	Eu	2013.361		URAT1
	296.43090870	31.67935750	19.851	122.924	15.921	18.861								1.80	C	2011.793		Pan-STARRS release 1 (PS1) Survey - DR1. M1 and M2 are PS1 gmags
	296.43090740	31.67938570	19.845	122.901	14.452	16.894								0.96	Hg	2015.000		GAIA DR1. M1 and M2 are Gmags
	296.43094800	31.67865900	19.768	122.186	13.580	15.690	20.000	46.000	2.828	18.000	180.000	7.810				1981.950		USNO B1. M1 and M2 are Imags

Table 1 continues on the next page.

Table 1 (continued). Research Results for Potential Common Proper Motion Pairs Found in the LSPM Catalog

Obj	RA	Dec	Sep	PA	M1	M2	pmRA1	pmDec1	e_pm1	pmRA2	pmDec2	e_pm2	CPM score	Ap	Me	Date	N	Source/Notes
KPP n+32	297.40514930	10.17525806	24.690	246.218	17.831	17.918	124.462	91.185	5.502	124.195	94.060	5.497	97	0.96	Hg	2015.000	V	GAIA DR1/2MASS. M1 and M2 estimated from G/J/H/K-mag. PM data from 2MASS to GAIA DR1 comparison. Almost certainly physical
	297.40463300	10.17487900	24.717	246.133	18.030	18.230	139.000	103.000		139.000	103.000							LSPM J1949+1010. M1 and M2 are LSPM Vmag estimates
	297.40460700	10.17486700	24.704	246.120	16.363	16.513								1.30	E2	1999.561		2MASS. M1 and M2 estimated from J- and K-band
	297.40478000	10.17498900	24.657	246.181	25.116	19.247	117.000	88.000	12.728	129.000	98.000	4.243		2.50	Es	2004.710		SDSS9. M1 and M2 are SDSS9 gmags
	297.40462200	10.17487840	24.704	246.120			123.200	92.700	5.700	122.600	96.500	5.900		0.20	Eu	2013.901		URAT1
	297.40504270	10.17521325	24.715	246.179	18.900	18.940								1.80	C	2012.143		Pan-STARRS release 1 (PS1) Survey - DR1. M1 and M2 are PS1 gmags
	297.40514930	10.17525806	24.690	246.218	16.618	16.698								0.96	Hg	2015.000		GAIA DR1. M1 and M2 are Gmags
	297.40469800	10.17487300	24.875	246.521	15.100	15.430	144.000	60.000	6.083	130.000	94.000	6.403				1984.700		USNO B1. M1 and M2 are Imags
NSN n+32	302.97655052	10.51794417	22.714	222.956	16.563	18.081	-138.016	-122.188	8.599	-139.966	-116.705	8.596	97	0.96	Hg	2015.000	V	GAIA DR1/2MASS. M1 and M2 estimated from G/J/H/K-mag. PM data from 2MASS to GAIA DR1 comparison. Almost certainly physical
	302.97714200	10.51845600	22.751	222.760		17.830	-151.000	-145.000		-151.000	-145.000							LSPM J2011+1031. M1 and M2 are LSPM Vmag estimates
	302.97711900	10.51843900	22.754	222.767	14.943	16.579								1.30	E2	2000.421		2MASS. M1 and M2 estimated from J- and K-band
	302.97713490	10.51845250	22.755	222.763			-134.900	-116.800	6.000	-136.000	-113.000	6.300		0.20	Eu	2013.977		URAT1
	302.97657306	10.51796497	22.741	222.961	17.360	19.053								1.80	C	2012.392		Pan-STARRS release 1 (PS1) Survey - DR1. M1 and M2 are PS1 gmags
	302.97655052	10.51794417	22.714	222.956	15.553	16.984								0.96	Hg	2015.000		GAIA DR1. M1 and M2 are Gmags
	302.97920000	10.52026200	22.843	222.982	15.600	17.400								1.20	Pp	1951.645		USNO A2. M1 and M2 are Rmags
KPP n+33	306.56056131	31.94439794	17.146	60.398	16.611	16.862	109.768	101.667	5.422	111.013	97.929	5.422	97	0.96	Hg	2015.000	V	GAIA DR1/2MASS. M1 and M2 estimated from G/J/H/K-mag. PM data from 2MASS to GAIA DR1 comparison. Almost certainly physical
	306.56002800	31.94397400	17.181	60.252	16.790	16.460	119.000	97.000		119.000	97.000							LSPM J2026+3156. M1 and M2 are LSPM Vmag estimates
	306.55999900	31.94395600	17.158	60.196	14.881	14.897								1.30	E2	1999.351		2MASS. M1 and M2 estimated from J- and K-band
	306.56002210	31.94397450	17.162	60.191			110.100	103.600	5.700	113.000	108.700	5.800		0.20	Eu	2013.468		URAT1
	306.56054264	31.94438394	17.154	60.347	17.722	17.953								1.80	C	2012.107		Pan-STARRS release 1 (PS1) Survey - DR1. M1 and M2 are PS1 gmags
	306.56056131	31.94439794	17.146	60.398	15.374	15.562								0.96	Hg	2015.000		GAIA DR1. M1 and M2 are Gmags
	306.55828700	31.94278400	17.190	60.366	16.000	16.300								1.20	Pp	1951.665		USNO A2. M1 and M2 are Rmags
NSN n+33	308.43534240	23.49770633	9.438	94.079	16.527	19.439	-44.457	-126.999	6.289	-41.451	-135.952	19.584	76	0.96	Hg	2015.000	V	GAIA DR1/2MASS. M1 and M2 estimated from G/J/H/K-mag. PM data from 2MASS to GAIA DR1 comparison. Most probably physical
	308.43554700	23.49823800	9.385	93.320	16.810	19.220	-70.000	-146.000		-70.000	-146.000							LSPM J2033+2329. M1 and M2 are LSPM Vmag estimates
	308.43554000	23.49822400	9.385	93.299	16.401									1.30	E2	2000.326		2MASS. M1 and M2 estimated from J- and K-band
	308.43554430	23.49823540	9.382	93.271			-42.600	-125.200	6.100	-33.900	-139.300	6.200		0.20	Eu	2013.572		URAT1
	308.43535050	23.49772766	9.439	94.316	17.030	20.166								1.80	C	2012.211		Pan-STARRS release 1 (PS1) Survey - DR1. M1 and M2 are PS1 gmags
	308.43534240	23.49770633	9.438	94.079	15.969	18.531								0.96	Hg	2015.000		GAIA DR1. M1 and M2 are Gmags
	308.43547500	23.49831700	9.668	92.775	15.410	17.240	-82.000	-138.000	6.708	-48.000	-126.000	11.705				1980.050		USNO B1. M1 and M2 are Imags

Table 1 continues on the next page.

Table 1 (continued). Research Results for Potential Common Proper Motion Pairs Found in the LSPM Catalog

Obj	RA	Dec	Sep	PA	M1	M2	pmRA1	pmDec1	e_pm1	pmRA2	pmDec2	e_pm2	CPM score	Ap	Me	Date	N	Source/Notes
KPP n+34	309.71614560	1.46939744	6.338	241.354	15.278	20.014	-53.123	-182.563	6.886	-56.743	-182.568	6.894	100	0.96	Hg	2015.000	V	GAIA DR1/2MASS. M1 and M2 estimated from G/J/H/K-mag. PM data from 2MASS to GAIA DR1 comparison. Most certainly physical
	309.71637000	1.47015800	6.276	241.046	16.010	19.890	-34.000	-179.000		-34.000	-179.000							LSPM J2038+0128. M1 and M2 are LSPM Vmag estimates
	309.71636000	1.47013400	6.292	241.125	13.931	17.089								1.30	E2	2000.476		2MASS. M1 and M2 estimated from J- and K-band
	309.71636700	1.47015760	6.295	241.157	15.521		-51.700	-179.700	6.300	-44.200	-179.500	6.700		0.20	Eu	2013.622		URAT1
	309.71615150	1.46942181	6.354	241.151	16.102	21.198								1.80	C	2012.603		Pan-STARRS release 1 (PS1) Survey - DR1. M1 and M2 are PS1 gmags
	309.71614560	1.46939744	6.338	241.354	14.204	18.115								0.96	Hg	2015.000		GAIA DR1. M1 and M2 are Gmags
NSN n+34	312.50910160	24.01329620	4.879	225.173	15.028	19.659	-136.557	-120.567	6.098	-97.732	-93.317	21.097	4	0.96	Hg	2015.000		GAIA DR1/2MASS. M1 and M2 estimated from G/J/H/K-mag. PM data from 2MASS to GAIA DR1 comparison. Almost certainly optical
	312.50973500	24.01380000	5.636	226.882	15.090		-122.000	-111.000		-122.000	-111.000							LSPM J2050+2400. M1 and M2 are LSPM Vmag estimates
	312.50973000	24.01380300	5.588	226.421	14.572	18.023								1.30	E2	1999.868		2MASS. M1 and M2 estimated from J- and K-band
	312.50972500	24.01379870	5.582	226.408			-129.100	-114.100	6.000	-83.900	-87.500	11.900		0.20	Eu	2013.473		URAT1
	312.50912500	24.01331578	4.928	225.220	15.180	19.976								1.80	C	2011.932		Pan-STARRS release 1 (PS1) Survey - DR1. M1 and M2 are PS1 gmags
	312.50910160	24.01329620	4.879	225.173	14.491	18.449								0.96	Hg	2015.000		GAIA DR1. M1 and M2 are Gmags
KPP n+35	314.14653172	30.79811637	10.008	200.186	13.970	14.425	197.925	84.927	5.920	194.412	85.122	5.920	100	0.96	Hg	2015.000	V	GAIA DR1/2MASS. M1 and M2 estimated from G/J/H/K-mag. PM data from 2MASS to GAIA DR1 comparison. Most certainly physical
	314.14556900	30.79776200	9.988	199.892	14.330	14.200	194.000	88.000		194.000	88.000							LSPM J2056+3047. M1 and M2 are LSPM Vmag estimates
	314.14553500	30.79774900	9.992	199.885	12.724	13.090								1.30	E2	1999.428		2MASS. M1 and M2 estimated from J- and K-band
	314.14556940	30.79774750	9.981	200.053			201.600	92.900	4.968	194.100	87.300	5.061		0.20	Eu	2001.675		UCAC4. Given magnitudes are Vmags. Central epochs averaged
	314.14557180	30.79776260	9.992	199.897			199.500	86.000	5.800	196.200	86.400	5.800		0.20	Eu	2013.660		URAT1
	314.14631966	30.79803741	10.010	200.140	14.820	15.321								1.80	C	2011.841		Pan-STARRS release 1 (PS1) Survey - DR1. M1 and M2 are PS1 gmags
	314.14653172	30.79811637	10.008	200.186	12.930	13.352								0.96	Hg	2015.000		GAIA DR1. M1 and M2 are Gmags
NSN n+35	317.00939820	31.27068296	7.618	221.610	14.496	17.562	258.960	134.099	5.565	261.568	135.697	5.565	100	0.96	Hg	2015.000	V	GAIA DR1/2MASS. M1 and M2 estimated from G/J/H/K-mag. PM data from 2MASS to GAIA DR1 comparison. Most certainly physical
	317.00814800	31.27012400	7.642	221.574	14.930	17.510	254.000	135.000		254.000	135.000							LSPM J2108+3116. M1 and M2 are LSPM Vmag estimates
	317.00811500	31.27011500	7.663	221.711	13.060	15.579								1.30	E2	1999.753		2MASS. M1 and M2 estimated from J- and K-band
	317.00926490	31.27062690	7.657	221.804	14.345									0.20	Eu	2013.464		URAT1
	317.00938080	31.27067556	7.701	221.869	15.308	18.837								1.80	C	2011.914		Pan-STARRS release 1 (PS1) Survey - DR1. M1 and M2 are PS1 gmags
	317.00939820	31.27068296	7.618	221.610	13.434	16.233								0.96	Hg	2015.000		GAIA DR1. M1 and M2 are Gmags
KPP n+36	317.25486558	36.86919785	5.223	266.947	18.368	18.543	-152.143	-158.546	6.430	-135.417	-151.420	7.698	80	0.96	Hg	2015.000	V	GAIA DR1/2MASS. M1 and M2 estimated from G/J/H/K-mag. PM data from 2MASS to GAIA DR1 comparison. Most probably physical
	317.25567600	36.86986200	5.464	265.806		18.300	-112.000	-157.000		-112.000	-157.000							LSPM J2109+3652. M1 and M2 are LSPM Vmag estimates
	317.25573900	36.86992600	5.506	265.876	17.178									1.30	E2	1998.466		2MASS. M1 and M2 estimated from J- and K-band
	317.25583390	36.86992060	6.002	264.223			179.100	-12.400	5.500	-134.100	-147.900	5.600		0.20	Eu	2013.297		URAT1
	317.25488711	36.86921846	5.223	266.942	19.064	19.368								1.80	C	2012.176		Pan-STARRS release 1 (PS1) Survey - DR1. M1 and M2 are PS1 gmags
	317.25486558	36.86919785	5.223	266.947	17.569	17.823								0.96	Hg	2015.000		GAIA DR1. M1 and M2 are Gmags
	317.25754500	36.87191200	3.858	268.503	16.800	16.700								1.20	Pp	1951.517		USNO A2. M1 and M2 are Rmags
	317.25595300	36.86992800	5.547	266.279	15.130	15.950	-14.000	-144.000	15.133	-88.000	-180.000	38.079				1979.750		USNO B1. M1 and M2 are Imags

Table 1 continues on the next page.

Table 1 (continued). Research Results for Potential Common Proper Motion Pairs Found in the LSPM Catalog

Obj	RA	Dec	Sep	PA	M1	M2	pmRA1	pmDec1	e_pm1	pmRA2	pmDec2	e_pm2	CPM score	Ap	Me	Date	N	Source/Notes
NSN n+36	317.86511102	27.30857949	6.996	210.132	15.532	16.010	-43.166	-213.272	5.623	-38.704	-199.651	5.623	80	0.96	Hg	2015.000	V	GAIA DR1/2MASS. M1 and M2 estimated from G/J/H/K-mag. PM data from 2MASS to GAIA DR1 comparison. Most probably physical
	317.86532600	27.30946900	7.221	210.008		14.150	-28.000	-209.000		-28.000	-209.000							LSPM J2111+2718. M1 and M2 are LSPM Vmag estimates
	317.86531500	27.30947500	7.208	209.773	14.119	14.055								1.30	E2	1999.884		2MASS. M1 and M2 estimated from J- and K-band
	317.86531090	27.30934370	7.245	209.948	15.137	15.137	-28.000	-209.000	11.314	-28.000	-209.000	11.314		0.20	Eu	2000.000		UCAC4. Given magnitudes are Vmags. Central epochs averaged
	317.86531350	27.30946830	7.208	209.770	15.137		-41.800	-211.800	6.000	-44.600	-211.400	6.000		0.20	Eu	2013.515		URAT1
	317.86512116	27.30861910	7.058	210.151	16.376	16.696								1.80	C	2011.987		Pan-STARRS release 1 (PS1) Survey - DR1. M1 and M2 are PS1 gmags
	317.86511102	27.30857949	6.996	210.132	14.506	14.805								0.96	Hg	2015.000		GAIA DR1. M1 and M2 are Gmags
KPP n+37	320.93176250	44.32522823	17.249	230.760	14.773	17.434	120.442	188.496	5.232	118.665	186.304	5.232	100	0.96	Hg	2015.000	V	GAIA DR1/2MASS. M1 and M2 estimated from G/J/H/K-mag. PM data from 2MASS to GAIA DR1 comparison. Most certainly physical
	320.93106100	44.32443600	17.143	230.795	15.500	18.240	129.000	169.000		140.000	202.000							LSPM J2123+4419. M1 and M2 are LSPM Vmag estimates
	320.93100400	44.32437900	17.204	230.791	13.766	15.793								1.30	E2	1998.781		2MASS. M1 and M2 estimated from J- and K-band
	320.93105980	44.32444380	17.209	230.788	14.908		119.000	191.500	5.600	116.200	189.500	5.700		0.20	Eu	2013.499		URAT1
	320.93175340	44.32521686	17.316	230.693	15.503	18.373								1.80	C	2012.005		Pan-STARRS release 1 (PS1) Survey - DR1. M1 and M2 are PS1 gmags
	320.93176250	44.32522823	17.249	230.760	13.814	16.284								0.96	Hg	2015.000		GAIA DR1. M1 and M2 are Gmags
	320.92902300	44.32197500	17.847	231.752	13.800	16.800								1.20	Pp	1953.677		USNO A2. M1 and M2 are Rmags
	320.93107500	44.32428900	16.228	233.773	12.280	14.290	118.000	178.000	8.602	138.000	210.000	3.606				1976.200		USNO B1. M1 and M2 are Imags
NSN n+37	323.54636730	28.06259448	4.132	275.085	16.116	16.894	-115.692	-112.742	5.732	-118.390	-115.034	5.731	100	0.96	Hg	2015.000	V	GAIA DR1/2MASS. M1 and M2 estimated from G/J/H/K-mag. PM data from 2MASS to GAIA DR1 comparison. Most certainly physical
	323.54693600	28.06306500	4.093	275.654	15.720	15.720	-116.000	-113.000		-116.000	-113.000							LSPM J2134+2803. M1 and M2 are LSPM Vmag estimates
	323.54695400	28.06309900	4.093	275.654	14.775	15.392								1.30	E2	1998.890		2MASS. M1 and M2 estimated from J- and K-band
	323.54656200	28.06274800	4.132	275.300	17.317	18.163								2.50	Es	2009.879		SDSS9. M1 and M2 are SDSS9 gmags
	323.54691290	28.06306470	4.091	275.656			-117.400	-111.300	5.600	-116.300	-111.300	6.600		0.20	Eu	2013.393		URAT1
	323.54639520	28.06261628	4.124	275.172	17.047	17.927								1.80	C	2011.904		Pan-STARRS release 1 (PS1) Survey - DR1. M1 and M2 are PS1 gmags
	323.54636730	28.06259448	4.132	275.085	15.073	15.766								0.96	Hg	2015.000		GAIA DR1. M1 and M2 are Gmags
KPP n+38	324.45889060	33.61480370	9.883	17.554	14.853	19.594	-5.835	-208.787	5.815	14.961	-304.682	27.659	4	0.96	Hg	2015.000		GAIA DR1/2MASS. M1 and M2 estimated from G/J/H/K-mag. PM data from 2MASS to GAIA DR1 comparison. Almost certainly optical
	324.45892300	33.61567300	11.142	13.776	14.980	16.690	10.000	-207.000		10.000	-207.000							LSPM J2137+3336. M1 and M2 are LSPM Vmag estimates
	324.45891900	33.61565000	11.148	13.896	13.383	18.095								1.30	E2	2000.408		2MASS. M1 and M2 estimated from J- and K-band
	324.45891960	33.61567390	11.060	13.984	15.146		-7.400	-208.800	6.300	5.600	6.500	6.300		0.20	Eu	2013.335		URAT1
	324.45889060	33.61480370	9.883	17.554	13.667	18.563								0.96	Hg	2015.000		GAIA DR1. M1 and M2 are Gmags
	324.45887000	33.61579800	10.786	15.361	12.000	16.420	-16.000	-208.000	13.038	36.000		14.142				1978.450		USNO B1. M1 and M2 are Imags

Table 1 continues on the next page.

Table 1 (continued). Research Results for Potential Common Proper Motion Pairs Found in the LSPM Catalog

Obj	RA	Dec	Sep	PA	M1	M2	pmRA1	pmDec1	e_pm1	pmRA2	pmDec2	e_pm2	CPM score	Ap	Me	Date	N	Source/Notes
NSN n+38	326.07432507	16.17806126	15.702	337.562	16.037	16.985	-203.373	-45.086	5.220	-206.019	-44.751	5.221	100	0.96	Hg	2015.000	V	GAIA DR1/2MASS. M1 and M2 estimated from G/J/H/K-mag. PM data from 2MASS to GAIA DR1 comparison. Most certainly physical
	326.07522600	16.17824900	15.709	337.483		16.590	-185.000	-45.000		-185.000	-45.000							LSPM J2144+1610. M1 and M2 are LSPM Vmag estimates
	326.07528200	16.17826500	15.681	337.700	14.313	15.340								1.30	E2	1998.732		2MASS. M1 and M2 estimated from J- and K-band
	326.07514980	16.17823120	15.706	337.476			-185.000	-45.000	11.314	-185.000	-45.000	11.314		0.20	Eu	2000.000		UCAC4. Given magnitudes are Vmags. Central epochs averaged
	326.07463700	16.17812700	15.673	337.662	17.023	18.134								2.50	Es	2009.789		SDSS9. M1 and M2 are SDSS9 gmags
	326.07520750	16.17824820	15.682	337.700			-203.200	-48.100	5.600	-202.500	-47.100	5.700		0.20	Eu	2013.300		URAT1
	326.07435716	16.17806743	15.703	337.578	16.769	17.845								1.80	C	2012.037		Pan-STARRS release 1 (PS1) Survey - DR1. M1 and M2 are PS1 gmags
	326.07432507	16.17806126	15.702	337.562	14.960	15.908								0.96	Hg	2015.000		GAIA DR1. M1 and M2 are Gmags
KPP n+39	327.90269177	18.09345136	5.750	139.626	14.806	14.980	51.361	-214.182	6.442	54.773	-215.319	6.433	100	0.96	Hg	2015.000	V	GAIA DR1/2MASS. M1 and M2 estimated from G/J/H/K-mag. PM data from 2MASS to GAIA DR1 comparison. Most certainly physical
	327.90246600	18.09434300	5.689	140.027	16.230	15.540	60.000	-213.000		60.000	-213.000							LSPM J2151+1805. M1 and M2 are LSPM Vmag estimates
	327.90245800	18.09437800	5.703	139.918	13.176	13.498								1.30	E2	1999.425		2MASS. M1 and M2 estimated from J- and K-band
	327.90253730	18.09423140	5.534	140.889	14.487	14.487	-126.100	27.900	10.526	60.000	-213.000	11.314		0.20	Eu	1999.403		UCAC4. Given magnitudes are Vmags. Central epochs averaged
	327.90259400	18.09375700	5.735	140.097	15.911	16.054								2.50	Es	2009.791		SDSS9. M1 and M2 are SDSS9 gmags
	327.90269509	18.09347862	5.737	139.790	15.681	15.791								1.80	C	2011.903		Pan-STARRS release 1 (PS1) Survey - DR1. M1 and M2 are PS1 gmags
	327.90269177	18.09345136	5.750	139.626	13.701	13.933								0.96	Hg	2015.000		GAIA DR1. M1 and M2 are Gmags
NSN n+39	328.08916840	28.37831202	5.101	285.417	14.171	14.265	194.320	59.450	5.822	195.913	62.585	5.821	100	0.96	Hg	2015.000	V	GAIA DR1/2MASS. M1 and M2 estimated from G/J/H/K-mag. PM data from 2MASS to GAIA DR1 comparison. Most certainly physical
	328.08825700	28.37806300	5.196	284.650	13.090		182.000	62.000		182.000	62.000							LSPM J2152+2822. M1 and M2 are LSPM Vmag estimates
	328.08827300	28.37807100	5.112	284.853	12.876	12.943								1.30	E2	2000.405		2MASS. M1 and M2 estimated from J- and K-band
	328.08836830	28.37809250	5.152	285.041	13.674		182.000	62.000	11.314					0.20	Eu	2000.940		UCAC4. Given magnitudes are Vmags. Central epochs averaged
	328.08885000	28.37825500	5.104	285.211	15.833	15.475								2.50	Es	2009.878		SDSS9. M1 and M2 are SDSS9 gmags
	328.08826710	28.37805990	5.174	284.827	13.674		44.300	98.300	8.000	194.400	64.700	6.500		0.20	Eu	2013.354		URAT1
	328.08910200	28.37826480	4.988	287.665	14.948	15.049								1.80	C	2012.060		Pan-STARRS release 1 (PS1) Survey - DR1. M1 and M2 are PS1 gmags
	328.08916840	28.37831202	5.101	285.417	13.139	13.234								0.96	Hg	2015.000		GAIA DR1. M1 and M2 are Gmags
KPP n+40	330.39145070	45.46347885	7.878	292.972	11.331	15.893	149.958	102.082	5.828	149.296	100.127	5.829	100	0.96	Hg	2015.000	V	GAIA DR1/2MASS. M1 and M2 estimated from G/J/H/K-mag. PM data from 2MASS to GAIA DR1 comparison. Most certainly physical
	330.39056400	45.46305100	7.881	293.189	11.380		145.000	107.000		148.000	111.000							LSPM J2201+4527. M1 and M2 are LSPM Vmag estimates
	330.39058600	45.46306600	7.881	293.189	11.191	14.462								1.30	E2	2000.441		2MASS. M1 and M2 estimated from J- and K-band
	330.39059310	45.46304950	7.710	296.233	11.111		143.600	105.500	1.281	148.000	111.000	11.314		0.20	Eu	1998.570		UCAC4. Given magnitudes are Vmags. Central epochs averaged
	330.39097500	45.46323100	7.518	294.619	14.638	17.144								2.50	Es	2006.394		SDSS9. M1 and M2 are SDSS9 gmags
	330.39055980	45.46305290	7.881	293.193	11.111		149.800	105.500	6.200	150.000	102.700	6.200		0.20	Eu	2013.501		URAT1
	330.39117420	45.46335087	7.699	294.874		16.779								1.80	C	2012.032		Pan-STARRS release 1 (PS1) Survey - DR1. M1 and M2 are PS1 gmags
	330.39145070	45.46347885	7.878	292.972	10.885	14.820	142.538	103.856	1.623					0.96	Hg	2015.000		GAIA DR1. M1 and M2 are Gmags

Table 1 continues on the next page.

Table 1 (continued). Research Results for Potential Common Proper Motion Pairs Found in the LSPM Catalog

Obj	RA	Dec	Sep	PA	M1	M2	pmRA1	pmDec1	e_pm1	pmRA2	pmDec2	e_pm2	CPM score	Ap	Me	Date	N	Source/Notes
NSN n+40	334.83818280	66.66483484	20.655	13.779	16.922	17.397	154.805	85.167	5.563	150.470	83.828	5.588	97	0.96	Hg	2015.000	V	GAIA DR1/2MASS. M1 and M2 estimated from G/J/H/K-mag. PM data from 2MASS to GAIA DR1 comparison. Almost certainly physical
	334.83654800	66.66448200	20.691	13.995	17.040	17.620	150.000	97.000		150.000	97.000							LSPM J2219+6639. M1 and M2 are LSPM Vmag estimates
	334.83652700	66.66447400	20.690	13.943	15.871	16.211								1.30	E2	1999.747		2MASS. M1 and M2 estimated from J- and K-band
	334.83655460	66.66447980	20.690	13.942			156.200	83.900	6.000	152.400	83.100	6.000		0.20	Eu	2013.300		URAT1
	334.83810900	66.66481866	20.662	13.802	17.801	18.295								1.80	C	2012.235		Pan-STARRS release 1 (PS1) Survey - DR1. M1 and M2 are PS1 gmags
	334.83818280	66.66483484	20.655	13.779	15.917	16.347								0.96	Hg	2015.000		GAIA DR1. M1 and M2 are Gmags
	334.83157000	66.66334200	20.713	13.989	16.400	17.100								1.20	Pp	1952.631		USNO A2. M1 and M2 are Rmags
	334.83655900	66.66458400	20.434	15.183	14.720	15.300	152.000	92.000	4.123	206.000	60.000	16.643				1984.600		USNO B1. M1 and M2 are Imags
KPP n+41	337.85463780	38.17525829	6.232	22.423	16.270	16.836	-165.980	-123.666	6.159	-166.500	-124.049	6.159	100	0.96	Hg	2015.000	V	GAIA DR1/2MASS. M1 and M2 estimated from G/J/H/K-mag. PM data from 2MASS to GAIA DR1 comparison. Most certainly physical
	337.85553000	38.17577400	6.253	22.737	15.990	16.660	-173.000	-118.000		-173.000	-118.000							LSPM J2231+3810. M1 and M2 are LSPM Vmag estimates
	337.85559000	38.17581600	6.241	22.473	14.715	15.125								1.30	E2	1998.765		2MASS. M1 and M2 estimated from J- and K-band
	337.85515200	38.17552300	6.241	22.558	17.407	18.029								2.50	Es	2006.708		SDSS9. M1 and M2 are SDSS9 gmags
	337.85551750	38.17577340	6.241	22.464			-166.100	-123.600	5.700	-166.500	-123.700	5.700		0.20	Eu	2013.263		URAT1
	337.85467510	38.17527764	6.239	22.471	17.155	17.777								1.80	C	2012.355		Pan-STARRS release 1 (PS1) Survey - DR1. M1 and M2 are PS1 gmags
	337.85463780	38.17525829	6.232	22.423	15.143	15.670								0.96	Hg	2015.000		GAIA DR1. M1 and M2 are Gmags
	337.85843100	38.17742500	4.923	23.619	15.300	15.300								1.20	Pp	1953.608		USNO A2. M1 and M2 are Rmags
NSN n+41	340.27575290	39.14694958	19.873	315.897	14.937	17.395	228.120	146.325	5.681	231.554	143.910	14.815	95	0.96	Hg	2015.000	V	GAIA DR1/2MASS. M1 and M2 estimated from G/J/H/K-mag. PM data from 2MASS to GAIA DR1 comparison. Almost certainly physical
	340.27450600	39.14634300	19.914	315.774	15.530	17.630	227.000	159.000		214.000	128.000							LSPM J2241+3908. M1 and M2 are LSPM Vmag estimates
	340.27442700	39.14629000	19.941	315.859	13.691	17.977								1.30	E2	1998.772		2MASS. M1 and M2 estimated from J- and K-band
	340.27560470	39.14688330	19.859	315.847	15.200									0.20	Eu	2013.303		URAT1
	340.27546360	39.14680772	19.859	315.842	15.810	17.612								1.80	C	2011.417		Pan-STARRS release 1 (PS1) Survey - DR1. M1 and M2 are PS1 gmags
	340.27575290	39.14694958	19.873	315.897	13.866	17.397								0.96	Hg	2015.000		GAIA DR1. M1 and M2 are Gmags
	340.27458700	39.14636200	19.940	315.936	12.620	17.220	230.000	154.000	5.000	232.000	148.000	51.546				1984.050		USNO B1. M1 and M2 are Imags
KPP n+42	342.54227670	88.11576919	15.291	332.507	17.902	18.076	238.467	63.504	6.992	237.193	66.766	6.992	100	0.96	Hg	2015.000	V	GAIA DR1/2MASS. M1 and M2 estimated from G/J/H/K-mag. PM data from 2MASS to GAIA DR1 comparison. Most certainly physical
	342.51217700	88.11550100	15.242	332.455	18.830	19.180	298.000	53.000		298.000	53.000							LSPM J2250+8806. M1 and M2 are LSPM Vmag estimates
	342.51165200	88.11550100	15.242	332.459	15.851	15.801								1.30	E2	1999.797		2MASS. M1 and M2 estimated from J- and K-band
	342.54024220	88.11575000	15.284	332.526										0.20	Eu	2013.774		URAT1
	342.54136840	88.11576419	15.286	332.534	19.050	19.275								1.80	C	2012.222		Pan-STARRS release 1 (PS1) Survey - DR1. M1 and M2 are PS1 gmags
	342.54227670	88.11576919	15.291	332.507	16.561	16.624								0.96	Hg	2015.000		GAIA DR1. M1 and M2 are Gmags
	342.42018100	88.11477300	14.779	331.832	17.200	17.700								1.20	Pp	1952.642		USNO A2. M1 and M2 are Rmags
	342.50337300	88.11545600	15.115	335.914	15.270	15.180	-242.000	-84.000	7.280	228.000	64.000	6.325				1983.100		USNO B1. M1 and M2 are Imags

Table 1 continues on the next page.

Table 1 (continued). Research Results for Potential Common Proper Motion Pairs Found in the LSPM Catalog

Obj	RA	Dec	Sep	PA	M1	M2	pmRA1	pmDec1	e_pm1	pmRA2	pmDec2	e_pm2	CPM score	Ap	Me	Date	N	Source/Notes
NSN n+42	343.18392920	34.98832024	5.590	127.457	15.843	16.006	144.223	117.236	5.134	144.134	116.077	5.134	100	0.96	Hg	2015.000	V	GAIA DR1/2MASS. M1 and M2 estimated from G/J/H/K-mag. PM data from 2MASS to GAIA DR1 comparison. Most certainly physical
	343.18319700	34.98783100	5.554	127.446	15.080		136.000	118.000		136.000	118.000							LSPM J2252+3459. M1 and M2 are LSPM Vmag estimates
	343.18312100	34.98778200	5.579	127.291	14.581	14.454								1.30	E2	1998.472		2MASS. M1 and M2 estimated from J- and K-band
	343.18330500	34.98790480	5.551	127.411	15.616		136.000	118.000	11.314	136.000	118.000	11.314		0.20	Eu	2000.000		UCAC4. Given magnitudes are Vmags. Central epochs averaged
	343.18319540	34.98783270	5.581	127.323			144.300	119.300	5.600	143.200	117.700	5.500		0.20	Eu	2013.457		URAT1
	343.18389620	34.98829842	5.588	127.452	16.701	16.973								1.80	C	2012.367		Pan-STARRS release 1 (PS1) Survey - DR1. M1 and M2 are PS1 gmags
	343.18392920	34.98832024	5.590	127.457	14.800	14.883								0.96	Hg	2015.000		GAIA DR1. M1 and M2 are Gmags
KPP n+43	345.68282570	65.32317386	20.616	88.449	15.578	19.028	221.261	110.528	7.936	217.250	105.538	9.367	100	0.96	Hg	2015.000	V	GAIA DR1/2MASS. M1 and M2 estimated from G/J/H/K-mag. PM data from 2MASS to GAIA DR1 comparison. Most certainly physical
	345.68063400	65.32271600	20.649	88.252	15.250	19.890	220.000	96.000		220.000	96.000							LSPM J2302+6519. M1 and M2 are LSPM Vmag estimates
	345.68059200	65.32270800	20.679	88.244	14.789	18.107								1.30	E2	1999.826		2MASS. M1 and M2 estimated from J- and K-band
	345.68275650	65.32315962	20.660	88.385	16.255	19.912								1.80	C	2012.023		Pan-STARRS release 1 (PS1) Survey - DR1. M1 and M2 are PS1 gmags
	345.68282570	65.32317386	20.616	88.449	14.821	18.030								0.96	Hg	2015.000		GAIA DR1. M1 and M2 are Gmags
	345.68022500	65.32326700	21.115	93.118	12.790	17.610	216.000	148.000	5.000	226.000	114.000	7.280				1976.800		USNO B1. M1 and M2 are Imags
NSN n+43	346.25622120	31.27200337	17.320	141.911	15.638	18.996	138.516	4.175	7.098	89.080	-16.158	8.041	0	0.96	Hg	2015.000		GAIA DR1/2MASS. M1 and M2 estimated from G/J/H/K-mag. PM data from 2MASS to GAIA DR1 comparison. Almost certainly optical
	346.25555400	31.27198600	17.514	139.548	15.260	19.070	152.000	5.000		152.000	5.000							LSPM J2305+3116. M1 and M2 are LSPM Vmag estimates
	346.25554700	31.27198600	17.554	139.395	14.401	17.890								1.30	E2	2000.023		2MASS. M1 and M2 estimated from J- and K-band
	346.25598400	31.27201200	17.414	140.995	16.631	19.892				95.000	-16.000	4.243		2.50	Es	2009.796		SDSS9. M1 and M2 are SDSS9 gmags
	346.25554570	31.27198570	17.554	139.391	15.730		137.800	6.400	6.100	88.300	-11.900	6.300		0.20	Eu	2013.269		URAT1
	346.25608070	31.27200878	17.571	140.916	16.389	19.668								1.80	C	2012.100		Pan-STARRS release 1 (PS1) Survey - DR1. M1 and M2 are PS1 gmags
	346.25622120	31.27200337	17.320	141.911	14.572	17.963								0.96	Hg	2015.000		GAIA DR1. M1 and M2 are Gmags
	346.25547300	31.27192800	17.294	138.038	12.120	16.150	142.000	2.000	7.211	96.000	-14.000	6.083				1976.200		USNO B1. M1 and M2 are Imags
KPP n+44	352.21036390	7.05686160	14.909	325.553	14.447	15.222	144.810	-37.514	6.814	148.650	-36.498	6.814	100	0.96	Hg	2015.000	V	GAIA DR1/2MASS. M1 and M2 estimated from G/J/H/K-mag. PM data from 2MASS to GAIA DR1 comparison. Most certainly physical
	352.20974700	7.05701800	14.936	325.299	14.740	15.700	151.000	-35.000		151.000	-35.000							LSPM J2328+0703. M1 and M2 are LSPM Vmag estimates
	352.20977500	7.05701300	14.928	325.344	13.781	14.373								1.30	E2	2000.471		2MASS. M1 and M2 estimated from J- and K-band
	352.20974860	7.05702200	14.841	325.585			146.800	-31.700	15.164	151.000	-35.000	11.314		0.20	Eu	1999.630		UCAC4. Given magnitudes are Vmags. Central epochs averaged
	352.20978580	7.05701190	14.962	325.465	14.371	15.334	144.800	-37.900	2.052	148.200	-40.100	3.124	80	0.20	Eu	2000.733		UCAC5. M1 and M2 are fmag values. Most probably physical
	352.20999900	7.05697800	14.886	325.433	15.656	16.203	149.000	-35.000	2.828	147.000	-35.000	2.828		2.50	Es	2005.698		SDSS9. M1 and M2 are SDSS9 gmags
	352.20975610	7.05701760	14.929	325.334			142.200	-36.000	6.600	146.700	-35.700	6.600		0.20	Eu	2013.096		URAT1
	352.21036840	7.05687107	14.943	325.282	15.129	15.986								1.80	C	2012.178		Pan-STARRS release 1 (PS1) Survey - DR1. M1 and M2 are PS1 gmags
	352.21036390	7.05686160	14.909	325.553	13.579	14.293								0.96	Hg	2015.000		GAIA DR1. M1 and M2 are Gmags
	352.20773700	7.05755000	14.778	325.798	13.500	14.500								1.20	Pp	1951.604		USNO A2. M1 and M2 are Rmags
	352.20974500	7.05710600	14.771	325.413	12.320	12.910	146.000	-30.000	3.606	146.000	-32.000	4.472				1976.200		USNO B1. M1 and M2 are Imags

Table 1 concludes on the next page.

Table 1 (conclusion). Research Results for Potential Common Proper Motion Pairs Found in the LSPM Catalog

Obj	RA	Dec	Sep	PA	M1	M2	pmRA1	pmDec1	e_pm1	pmRA2	pmDec2	e_pm2	CPM score	Ap	Me	Date	N	Source/Notes
NSN n+44	352.08999150	47.69552823	11.306	236.241	14.906	18.361	169.512	-21.501	5.237	168.725	-20.226	5.237	100	0.96	Hg	2015.000	V	GAIA DR1/2MASS. M1 and M2 estimated from G/J/H/K-mag. PM data from 2MASS to GAIA DR1 comparison. Most certainly physical
	352.08895900	47.69561800	11.311	236.131	15.540	18.770	170.000	-24.000		170.000	-24.000							LSPM J2328+4741. M1 and M2 are LSPM Vmag estimates
	352.08885800	47.69562500	11.307	236.117	13.523	16.192								1.30	E2	1998.797		2MASS. M1 and M2 estimated from J- and K-band
	352.08918700	47.69561000	11.289	236.188	16.014	20.037	168.000	-20.000	4.243	168.000	-23.000	4.243		2.50	Es	2003.738		SDSS9. M1 and M2 are SDSS9 gmags
	352.08894060	47.69561890	11.306	236.123	15.164		167.000	-18.600	5.500	166.500	-16.900	5.500		0.20	Eu	2013.485		URAT1
	352.08980520	47.69554707	11.020	234.929	15.780	19.692								1.80	C	2012.493		Pan-STARRS release 1 (PS1) Survey - DR1. M1 and M2 are PS1 gmags
	352.08999150	47.69552823	11.306	236.241	13.751	16.869								0.96	Hg	2015.000		GAIA DR1. M1 and M2 are Gmags
	352.08578100	47.69588400	11.369	236.219	14.500	17.700								1.20	Pp	1954.583		USNO A2. M1 and M2 are Rmags
	352.08892300	47.69570000	10.946	236.639	12.690	15.620	170.000	-18.000	2.828	178.000	-14.000	11.705				1977.000		USNO B1. M1 and M2 are Imags
KPP n+45	352.82567080	46.12333687	3.853	342.549	18.340	21.380	-18.695	-205.448	5.246	-14.997	-207.474	10.938	95	0.96	Hg	2015.000	V	GAIA DR1/2MASS. M1 and M2 estimated from G/J/H/K-mag. PM data from 2MASS to GAIA DR1 comparison. Almost certainly physical
	352.82580600	46.12419100	3.904	341.786	19.100		-25.000	-216.000		-25.000	-216.000							LSPM J2331+4607. M1 and M2 are LSPM Vmag estimates
	352.82579200	46.12426000	3.902	341.856	16.256	18.007								1.30	E2	1998.824		2MASS. M1 and M2 estimated from J- and K-band
	352.82576000	46.12397800	3.790	342.294	19.553	22.877	-17.000	-211.000	4.243					2.50	Es	2003.738		SDSS9. M1 and M2 are SDSS9 gmags
	352.82567910	46.12336324	3.795	342.016	19.298									1.80	C	2012.503		Pan-STARRS release 1 (PS1) Survey - DR1. M1 and M2 are PS1 gmags
	352.82567080	46.12333687	3.853	342.549	17.220	19.585								0.96	Hg	2015.000		GAIA DR1. M1 and M2 are Gmags
NSN n+45	357.10645337	22.89507867	4.945	18.428	14.801	15.221	-97.317	-128.538	8.263	-98.378	-128.509	8.263	95	0.96	Hg	2015.000	V	GAIA DR1/2MASS. M1 and M2 estimated from G/J/H/K-mag. PM data from 2MASS to GAIA DR1 comparison. Almost certainly physical
	357.10687300	22.89561700	4.959	19.049	14.900	13.890	-99.000	-143.000		-99.000	-143.000							LSPM J2348+2253. M1 and M2 are LSPM Vmag estimates
	357.10688100	22.89559900	4.949	18.599	13.754	14.303								1.30	E2	2000.427		2MASS. M1 and M2 estimated from J- and K-band
	357.10682450	22.89555920	4.955	19.144		14.384	-99.000	-143.000	11.314	-99.000	-143.000	11.314		0.20	Eu	2000.000		UCAC4. Given magnitudes are Vmags. Central epochs averaged
	357.10659600	22.89530300	4.964	18.461	16.076	16.368								2.50	Es	2009.794		SDSS9. M1 and M2 are SDSS9 gmags
	357.10689340	22.89561380	4.950	18.611	14.384	14.384	-99.200	-124.900	6.500	-101.100	-126.000	6.200		0.20	Eu	2013.517		URAT1
	357.10646396	22.89509024	4.953	18.395	15.540	15.948								1.80	C	2012.346		Pan-STARRS release 1 (PS1) Survey - DR1. M1 and M2 are PS1 gmags
	357.10645337	22.89507867	4.945	18.428	13.803	14.260								0.96	Hg	2015.000		GAIA DR1. M1 and M2 are Gmags
KPP n+46	358.15647930	27.33472770	6.037	133.989	14.635	17.777	-156.741	-96.813	8.886	-152.362	-100.517	8.886	100	0.96	Hg	2015.000	V	GAIA DR1/2MASS. M1 and M2 estimated from G/J/H/K-mag. PM data from 2MASS to GAIA DR1 comparison. Most certainly physical
	358.15719600	27.33512900	5.960	133.898	14.190		-156.000	-104.000		-156.000	-104.000							LSPM J2352+2720. M1 and M2 are LSPM Vmag estimates
	358.15726900	27.33516100	5.944	134.048	13.902	15.866								1.30	E2	1998.888		2MASS. M1 and M2 estimated from J- and K-band
	358.15673300	27.33487700	6.032	134.293	15.534	19.230								2.50	Es	2009.792		SDSS9. M1 and M2 are SDSS9 gmags
	358.15721550	27.33513090	5.949	134.065	14.725		-153.300	-96.700	5.700	-152.900	-100.700	5.900		0.20	Eu	2013.354		URAT1
	358.15649570	27.33473693	6.038	133.696	15.355	18.837								1.80	C	2011.995		Pan-STARRS release 1 (PS1) Survey - DR1. M1 and M2 are PS1 gmags
	358.15647930	27.33472770	6.037	133.989	13.715	16.466								0.96	Hg	2015.000		GAIA DR1. M1 and M2 are Gmags

CPM Pairs from LSPM so far not WDS Listed – Part V

(Continued from page 668)

5. Acknowledgements

The following tools and resources have been used for this research:

- Washington Double Star catalog
- 2MASS All Sky catalog
- GAIA DR1 catalog
- UCAC4 catalog
- UCAC5 catalog
- URAT1 catalog
- SDSS9 catalog
- LSPM catalog
- Aladin Sky Atlas v9 and 10
- SIMBAD, VizieR, TAP Vizier, X-Match
- AstroPlanner V2.2

6. References

Knapp, Wilfried R. A., Nanson, John, 2017, "A New Concept for Counter-Checking of Assumed CPM Pairs", *Journal of Double Star Observations*, **13** (1), 31-51.

Knapp, Wilfried R. A., Nanson, John, 2017, "CPM Pairs from LSPM so far not WDS Listed – Part I", *JDSO*, **13** (2), 140-161.

Knapp, Wilfried R. A., Nanson, John, 2017, "CPM Pairs from LSPM so far not WDS Listed – Part II", *JDSO*, **13** (4), 447-464.

Knapp, Wilfried R. A., Nanson, John, 2017, "CPM Pairs from LSPM so far not WDS Listed – Part III", *JDSO*, **13** (4), 538-552.

Knapp, Wilfried R. A., Nanson, John, 2017, "CPM Pairs from LSPM so far not WDS Listed – Part IV", *JDSO*, **14**, (2), 367-388.

Knapp, Wilfried R. A., Nanson, John, 2018, "Estimating Visual Magnitudes for Wide Double Stars", *JDSO*, **14** (3), 503-520.

Knapp, Wilfried R. A., 2018, "A New Concept for Counter-Checking of Assumed Binaries", *JDSO*, **14** (3), 487-491.

Lépine, Séastien, Shara, Michael M., 2005, "A Catalog of Northern Stars with Annual Proper Motion Larger than 0.15" (LSPM-North Catalog)", *The Astronomical Journal*, **129**, 1483-1522.

Discovery of a New Optical Double Star in the Constellation Gemini

Joerg S. Schlimmer
Seeheim-Jugenheim, Germany
Email: js@epsilon-lyrae.de

Abstract: During observations in constellations Geminorium an optical companion of TYC1937-692-1 in a distance of about 5.7 arc seconds could be found.

Report

TYC1937-692-1 is not listed as double star in SIMBAD astronomical database or in WDS catalog. It is located 2 degrees east of 75 Geminorium. Its brightness is 11.23 magnitudes; the companion has an estimated brightness of 14 magnitudes. There is only a small proper motion of 9.5 in R.A and -12.2 in declinations [SIMBAD].

Two observations were made with a 12-inch Newtonian telescope in combination with a QHY 5LII-C CMOS Camera. Focal length was 1500 mm. Reproduction scale was about 0.52 as/pixel. For telescope control the planetary software Redshift 7 was used. The data analyses were done with the software program REDUC [Losse] and are given in Table 1.

Figure 1 shows the double star ES 421 (WDS07523+2842) and TYC1937-692-1. Distance between both is only 133 arc seconds. For the image 100 frames were stacked.

Acknowledgments

This research has made use of the SIMBAD database, operated at CDS, Strasbourg, France

This research has made use of the Washington Double Star Catalog maintained at the U.S. Naval Observatory.

References

SIMBAD, CDS, Centre de Données astronomiques de Strasbourg, SIMBAD Astronomical Database, http://simbad.u-strasbg.fr/simbad/

Losse, Florent, http://www.astrosurf.com/hfosaf/uk/tdownload.htm#reduc

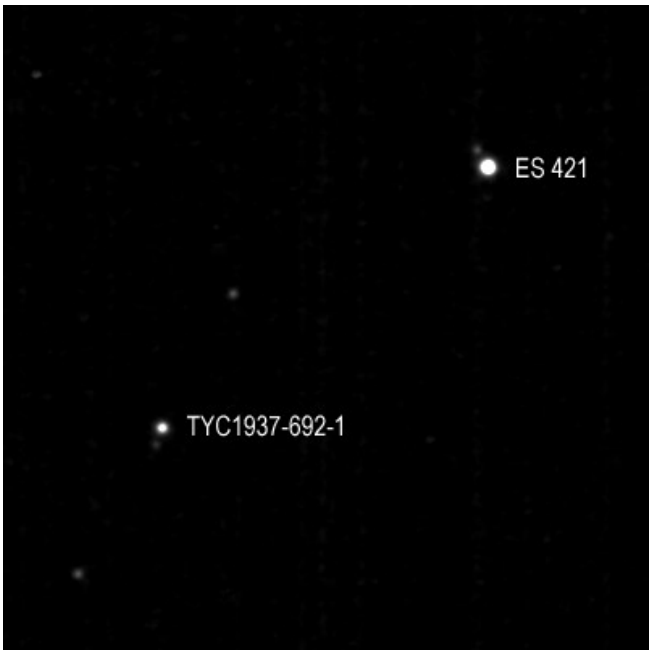

Figure 1.

Table 1. Measurements of New Double

Name	RA+Dec	Mag	PA	Sep	Date	N
TYC1937-692-1	07 52 10.6 +28 43 19.46	11.23	345.3	5.66	2018.279	2

Comparison and CCD Measurements of Four Double Star Systems: WDS 03003+1432, 03009+5221, 03001+3911, 08165+7930

Jack Cahill[1], Zoe Boysen[1], Mac Clark[2], Grace Wagner[3], Kalée Tock[4]

[1]University School of Nashville, Nashville, Tennessee
[2]Wilmington Friends School, Wilmington, Delaware
[3]Fort Worth Country Day School, Fort Worth, Texas
[4]Stanford Online High School, Stanford, California

Abstract: As a class, we examined the double star systems WDS 03003+1432, 03009+5221, 03001+3911, and 08165+7930. CCD measurements made using the Skynet robotic telescope network are in good agreement with the historical trends for these stars. For 08165+7930, we confirm a curved trend-line suggestive of an elliptical orbit, validating its current status as a short-arc binary system. For the other systems, there is not yet enough data to infer a relationship, gravitational or otherwise.

Introduction

Understanding the orbits of stars that are gravitationally bound to each other was the genesis of the field of astrophysics, in which the laws of physics are applied to astronomical systems. Since the 1700's, astronomers have been studying stars that appear close together, looking for evidence of gravitational relationships. Given the orbital parameters governing the motion of such binary stars, it is possible to calculate the mass of the system. Together with other data, individual star masses can be determined, which helps to constrain the mass-luminosity relationship for stars in general (Wikipedia, 2018). Because the mass-luminosity relationship is fundamental for many applications of astronomy, the continuing study of double stars remains essential.

Since the orbital periods of binary star systems can span millennia, even historical data that stretches very far back does not always include all or even most of the orbit. Sometimes, only a tiny fraction of the arc is visible over multiple hundreds of years. Such systems are called Short-Arc Binaries, or SAB's. In such cases, it is sometimes possible to estimate orbital parameters, with the caveat that these have a high uncertainty. Careful and persistent collection of data is necessary to ensure that astronomers of the future are able to calculate the orbital parameters with greater accuracy.

Four star systems were selected for this study. Three are double star systems with unknown classification, and the fourth has been classified as an SAB. In this paper, we compare and contrast the data for these four systems, and the inferences that can be drawn about each. We also contribute a measurement of three of the four systems for inclusion in the Washington Double Star Catalog.

Target Selection

The stars for this study were chosen to be 5 arcseconds or more apart so they could be resolved in the image. They were chosen to have a magnitude difference of no more than 3 so that the same exposure time would be appropriate for both. These constraints came about because of the limitations of the telescopes on the Skynet Robotic Telescope Network.

History of the Stars

The four chosen star systems are shown in Table 1. Interestingly, the change in position angle and separation between the first and most recent observation does not distinguish the SAB from the other systems.

The immediate surroundings of each of the stars is shown in Figure 1. The small red squares represent other stars in the field, some of which are too dim to be visible in the image.

A brief synopsis of the discovery and historical ob-

Table 1: WDS data for the double star systems in this study

Star	Number of Past Observations	Observation Timespan	Change in Separation From First to Most Recent Observation (as)	Change in Position Angle From First to Most Recent Observation (deg)	Classification
WDS 03001+3911	14	1928-2014	0.1	1	Uncertain
WDS 03003+1432	20	1897-2018	1.59	2.1	Uncertain
WDS 03009+5221	92	1793-2018	2.1	4	Uncertain
WDS 08165+7930	95	1832-2018	-0.16	4.74	Short-Arc Binary

servations of each system follows.

WDS 03001+3911 ST Per

WDS 03001+3911 ST Per was discovered by Dr. Akbar Ali on October 24, 1928, when the stars were measured to have a separation of 11.6″ and a position angle of 6.2°. Dr. Ali was the director of the Nizamiah Observatory, which is located on the campus of Osmania University in Hyderabad, India. He died on February 7, 1960. This double star system is in the constellation Perseus, and whether a gravitational relationship exists between the stars is currently uncertain.

WDS 03003+1432 AG 60

WDS 03003+1432 AG 60 is also a double star system with an uncertain nature. Its discovery was first published in 1897 in a periodical called the "Astronomische Gesellschaft" (Astronomische Gesellschaft, 2016). This star is in the constellation Aries.

WDS 03009+5221 STF 331

WDS 03009+5221 STF 331 was discovered in 1793 and the last measurement prior to this work was made in 2016, with a total of 75 observations taken. This double star is in the constellation Perseus. Despite substantial changes in both position angle and separation, the nature of the double star is uncertain. The spectral class of the stars is B7V+B9V, and their magnitude difference is 0.96.

This double was first officially studied by Friedrich Georg Wilhelm Von Struve, a German-Russian astronomer. He was born on April 15, 1793 in Altona, Germany, and died on November 23, 1864 in St. Petersburg, Russia. Struve grew up in a family of astronomers, and became known for studying double stars (Encyclopedia Britannica, 2015). He discovered 03009+5221 STF 331 in 1837. During this time Struve was working at the Dorpat Observatory, in Tartu, Estonia. In this same year, he published his findings on multiple star systems in *Mensurae Micrometricae* (Encyclopedia of World Biography, 2010). His study on multiple star systems demonstrated that such systems are not rare, and their abundance exemplified Isaac Newton's law of gravitation operating outside the solar system (Encyclopedia Britannica, 2015).

WDS 08165+7930 STF 1169AB

Friedrich Georg Wilhelm von Struve was also the discoverer of WDS 08165+7930 STF 1169AB, and the discovery of this star was also made during his research at the University of Dorpat (Tartu, Estonia) in 1832. His first measurements were made on a telescope with

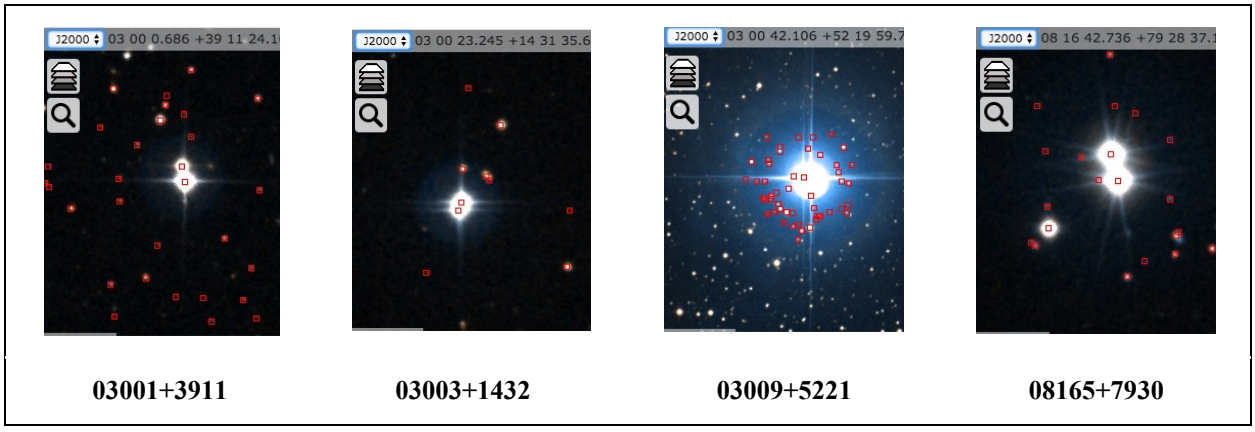

Figure 1: Double star systems in the study, screenshots from Aladin

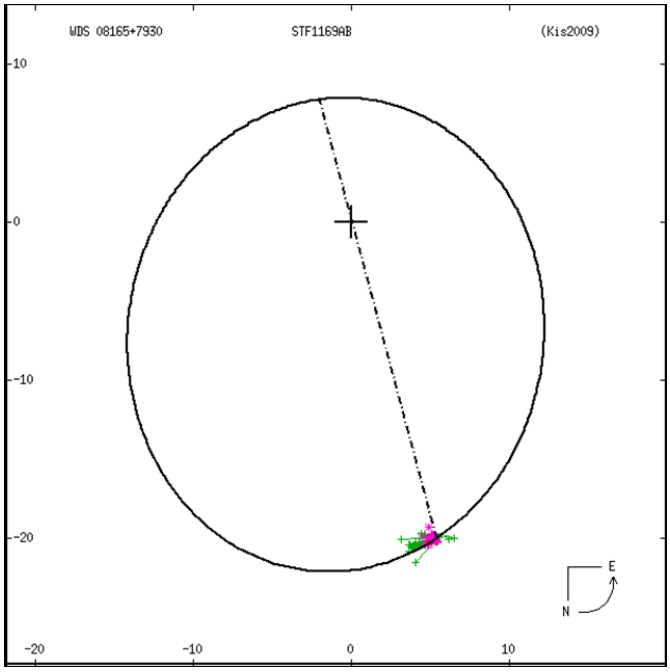

Figure 2: WDS orbital solution for 08165+7930AB STF1169AB

an aperture of 0.3m, the position angle to be approximately 10.1°, and the separation to be 20.74" (Encyclopedia Britannica, 2015). As time progressed, the observed PA rose steadily from Struve's initial measurement of 10° to approximately 14.84°. The star is located in Camelopardalis.

WDS 08165+7930 was classified as an SAB in 2009. As with all SABs, the data points that potentially form an arc make such a slight and small curve relative to the hypothetical orbit that it is challenging to evaluate the accuracy of the proposed orbit. For example, the arc that is currently visible for WDS 08165+7930 could fit into several different elliptical solutions. This is because only approximately 3-5% of the orbit has been observed, contributing to a proposed period of 200c (See Figure 2). Given the paucity of the observations, it is even possible that this orbit may be premature, and that this is not even a binary.

Gaia DR1

The Gaia DR1 database on VizieR was used to find information about each of the stars using their coordinates. The Gaia telescope is a European Space Agency telescope launched in 2013. It is equipped with a dual telescope system with a common structure and a common focal plane, blue and red photometers, and a radial velocity spectrometer. From the magnitudes presented and the configuration of the Aladin Lite images, the desired stars were determined to be the two brightest stars out of their respective fields. The proper motion of the secondary star was only available for 08165+7930 (see Table 2). Parallax data was only available for the primary star in each pair.

Our Measurements

We used the Skynet Robotic Telescope Network for this study. The telescopes used were the Athabasca University Robotic Telescope (AURT) in Canada and the 17-inch telescope at the Dark Sky Observatory in North Carolina.

AURT

The Athabasca University Robotic Telescope, or AURT, is located at Athabasca University in Alberta, Canada. It is used to take detailed images of the northern night sky. The telescope has an aperture of 0.4 meters and is remotely controlled. The focal length is 3868.0 mm and the f-ratio is 10.9. We used the Lum filter, which blocks the infrared and ultraviolet rays. It has a field of view of 24.6 x 16.4 arcminutes. Stars

Table 2: Available Data on Targets from Gaia DR1

	03003+1432	03009+5221	03001+3911	08165+7930
Precise coordinates	030020.97+143152.5	030052.18+522106.5	030005.70+391124.9	081631.05+793003.5
Primary Magnitude	9.56 (WDS), 9.406 (Gaia)	5.21	9.63	8.40
Secondary magnitude	10.0 (WDS), 9.946 (Gaia)	6.17	11.99	8.64
Parallax (mas)	3.78 ± 0.36	6.77 ± 0.44	3.11± 0.29	13.82 ± 0.45
Distance (ly)	863 ± 82.2	482 ± 31.96	1049 ± 97.5	236 ± 7.68
Primary PM (mas/yr)	12.927, -2.614	27.129, -24.901	-4.412, -21.319	-50.676, -65.684
Secondary PM (mas/yr)	not known	not known	not known	-48.095, -66.258
Spectral class (from WDS)	G5 (primary)	B7V+B9V	A3V	G0 (primary)

03003+1432 and 03001+3911 had exposure times of 10 seconds, and stars 03009+5221 and 08165+7930 had exposure times of 5 seconds.

DSO-17

The Dark Sky Observatory 17, or DSO-17 is a telescope located in North Carolina. The telescope has an aperture of 0.4 meters and is remotely controlled. The focal length is 2951.0 mm and the f-ratio is 6.8. We used the Lum filter for this also. Stars 03003+1432 and 03001+3911 had exposure times of 10 seconds, and stars 03009+5221 and 08165+7930 had exposure times of 5 seconds. These were the lowest exposure times that gave good images.

After collecting images from the AURT and DSO-17, the image analysis software AstroImageJ was used to reduce the data. The aperture size was selected as 6-pixels. Some of the images were blurry and some were out of frame. Possibly the images were distorted by a cloud in the field of view or movement of the telescope while the images were being taken. An example of the "swishy stars" is shown in Figure 3. There may have been a collimation problem with the telescope, which caused the centroid to be spread out off-center (Harshaw, 2018). Values highlighted yellow in Table 3 came from images of these stars. As is evident from Table 4, the yellow highlighted values are generally in poorer agreement with the historical values.

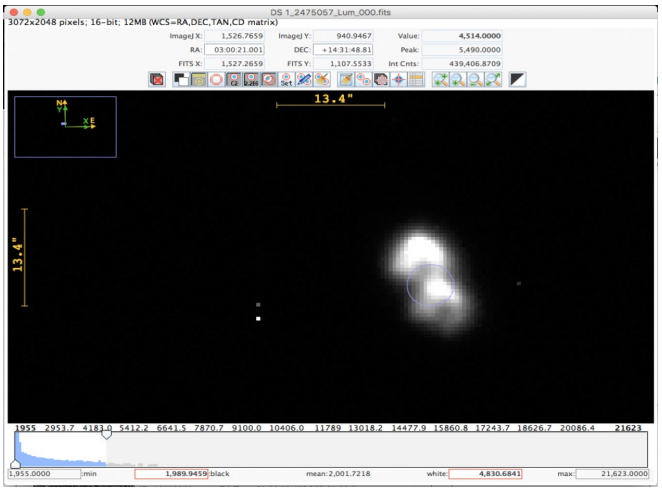

Figure 3. Distorted stars for which it was difficult to locate a centroid.

Analysis

Comparison with Historical Data

As is shown in Table 5, the position angle for WDS 03009+5221 remains relatively constant over time, with no big increases or decreases (bar the few early data points that are likely due to obsolete instruments). Similarly, the graph for WDS 03001+3911 also seems to

(Text continues on page 701)

Table 3: Measurements of the four systems with yellow values indicating stars that appear distorted

System	03001+3911		08165+7930		03003+1432		03009+5221		03001+3911		08165+7930	
Date	Feb 06, 2018		Feb 06, 2018		Feb 06, 2018		Feb 09, 2018		Feb 06, 2018		Feb 06, 2018	
Telescope	DSO-17		DSO-17		AURT		AURT		AURT		AURT	
Measure	PA	Sep	PA	Sep	PA	Sep	PA	Sep	PA	Sep	PA	Sep
Image 1	10.47	12.13	14.92	20.75	161.68	5.79	84.3	11.86	16.64	10.54	15.06	20.64
Image 2	10.38	12.15	14.95	20.83	159.61	5.82	84.48	11.93	10.07	12.16	14.97	20.66
Image 3	10.28	12.15	15.03	20.77	157.97	5.9	83.75	11.83	9.54	12.08	15	20.16
Image 4	10.28	12.08	14.97	20.69	159.77	5.9	84.75	11.94	9.76	12.08	15.14	20.69
Image 5	10.39	12.06	14.97	20.78	159.54	5.94	84.73	11.8	10.27	12.1	15.04	20.61
Average	10.36	12.14	14.97	20.76	159.71	5.78	84.40	11.87	11.26	11.30	15.04	20.55
Std Error	0.036	0.019	0.018	0.023	0.59	0.028	0.183	0.027	1.352	0.313	0.029	0.099

Table 4: Comparison of average measurement to most recent measurement for each system, where yellow shading indicates some image distortion

System	03001+3911		08165+7930		03003+1432		03009+5221		03001+3911		08165+7930	
Measure	PA	Sep	PA	Sep	PA	Sep	PA	Sep	PA	Sep	PA	Sep
Most recent measurement	11	12.2	15	20.8	160	6.4	86	12	11	12.2	15	20.8
Average	10.36	12.14	14.97	20.76	159.71	5.78	84.40	11.87	11.26	11.30	15.04	20.55

Table 5: Position angle vs time and separation vs time, our observation in red

System	Position Angle Versus Date	Separation Versus Date
03009+5221	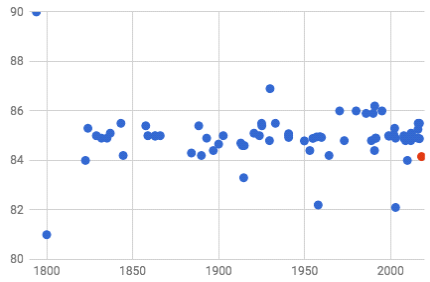	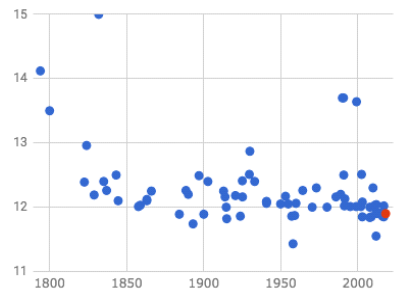
03001+3911	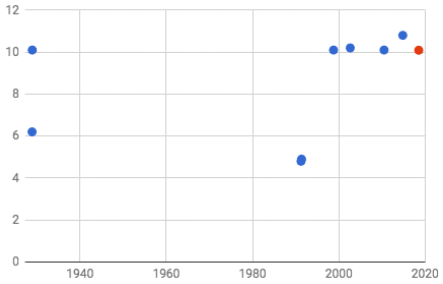	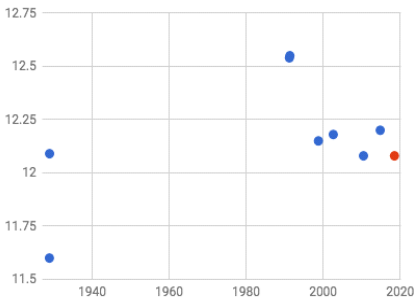
08165+7930	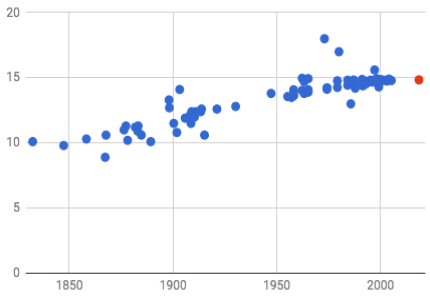	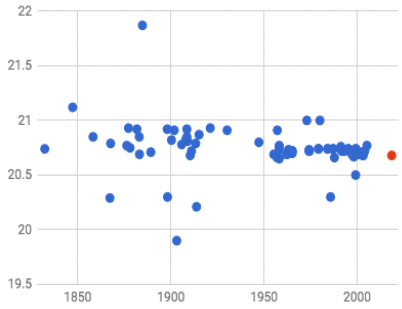
03003+1432	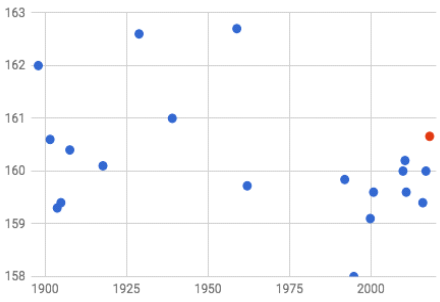	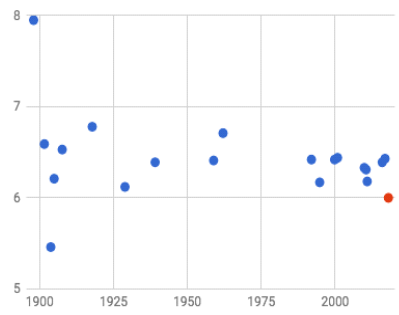

Table 6. Relative position of the secondary star relative to the primary: our measurement in red, historical measurements in blue.

System	Secondary Star Position Relative to Primary
03009+5221	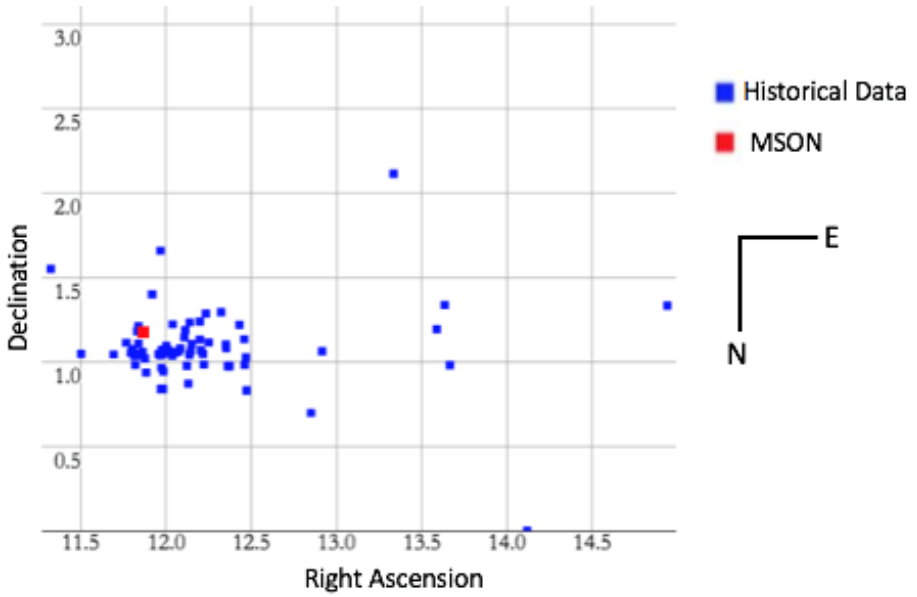
03001+3911	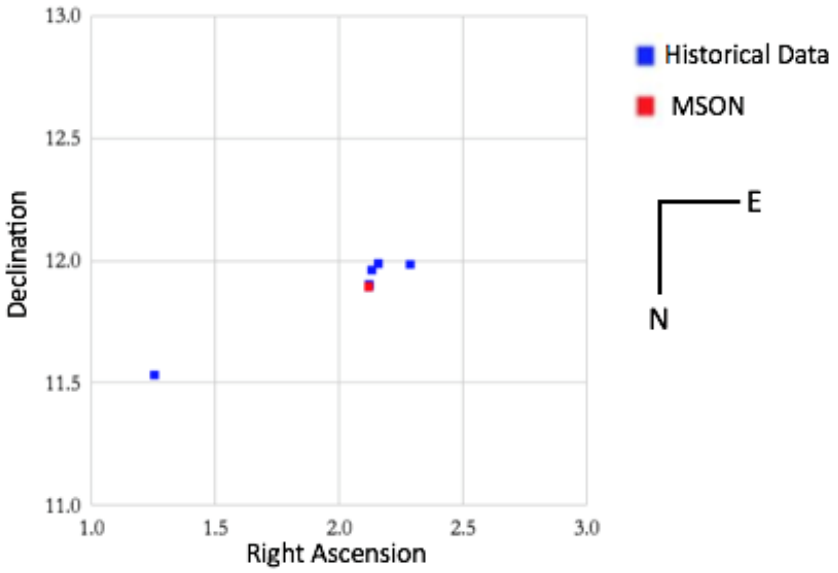

Table 6 concludes on the next page.

Table 6 (conclusion). Relative position of the secondary star relative to the primary: our measurement in red, historical measurements in blue.

System	Secondary Star Position Relative to Primary
08165+7930	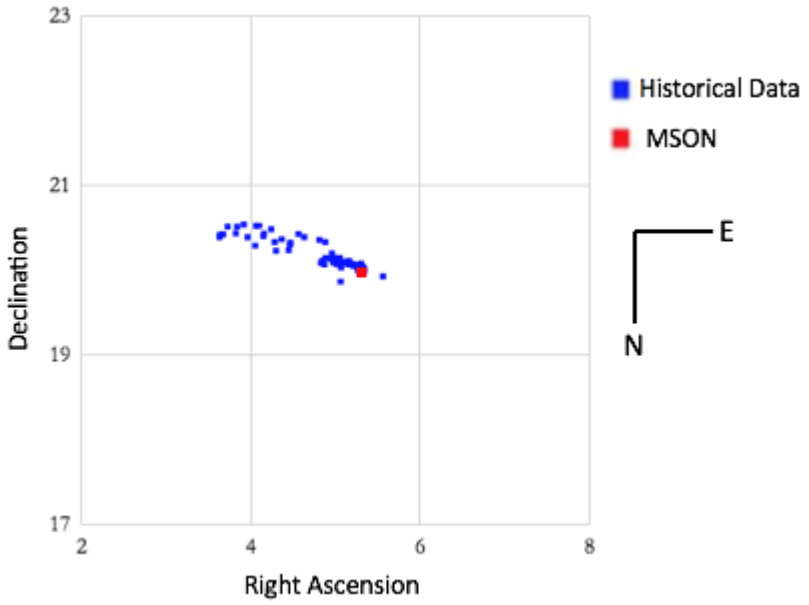
03003+1432	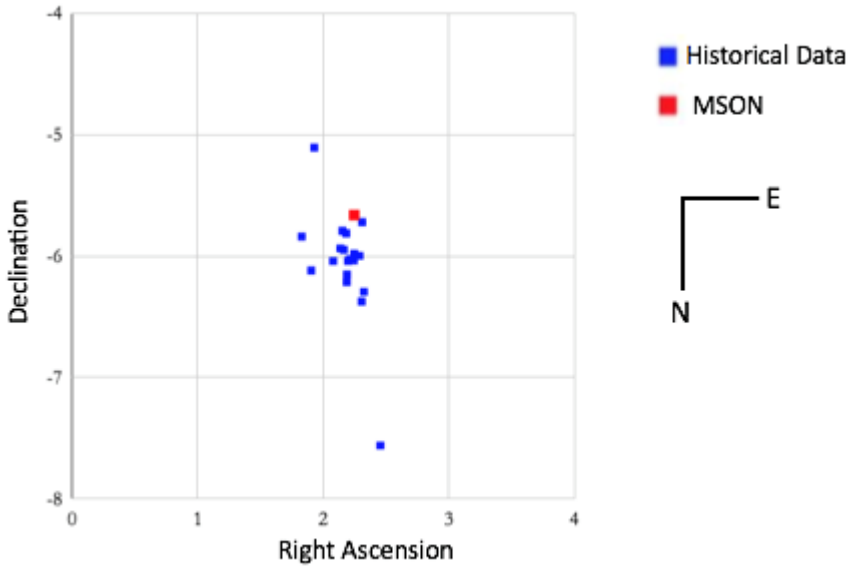

(Continued from page 697)

have a position angle that relatively remains the same, with no big increases or decreases. It is possible that the position angle of WDS 03001+3911 could potentially be increasing slightly, but there are not enough historical observations to make this conclusion definitive. The separations for these systems exhibit similar features: a separation that becomes clustered to a certain value as the observations become more recent. For some of the systems, there may be an indication that the measurements could one day exhibit a curved path, but there are too few observations to conclude this with certainty.

For 08165+7930, our measurement of 14.88° reflects and confirms the historical trend of increasing position angle. The historical measurements for separation have remained at a relatively constant 20.6-20.7"; thus, our observation of 20.66" is consistent with past observations. Also for the other systems, the average measurements from the non-distorted images are consistent with historical position angle and separation observations. This is expected, because the stars have shown little relative movement in the past. As is evident from Table 5, the only noticeable trend in the historical data is the increasing position angle for 08165+7930.

Plots of the historical observations along with our observation (in red) are shown in Table 6. WDS 08165+7930 shows evidence of the beginnings of an arc, traced out over almost 200 years of observations.

Proper Motion of 08165+7930

Since Gaia has data on the proper motion of both stars in 08165+7930, it is possible to graph the primary and secondary motions as vectors on the Cartesian plane, as is done in Figure 4.

When the smaller vector is subtracted from the larger vector, the magnitude of the resulting vector can be found using this equation:

$$|v| = \sqrt{(x_2 - x_1)^2 + (y_2 - y_1)^2}$$

The magnitude of the difference vector was divided by the magnitude of the largest proper motion vector (in this case the primary proper motion vector). The result of these calculations was (2.236)/(82.961)= 0.02. Any ratio less than 0.2, as this one is, indicates that the movement of the stars relative to each other is small compared to their movement across the sky (Harshaw 2016). This is strong evidence that the stars are moving together, as they must be if they are gravitationally bound to each other.

Fitting in Excel: Line Versus Curve

When making a scatterplot of 08165+7930, the data points indicate that the separation has remained relatively constant throughout historical observations,

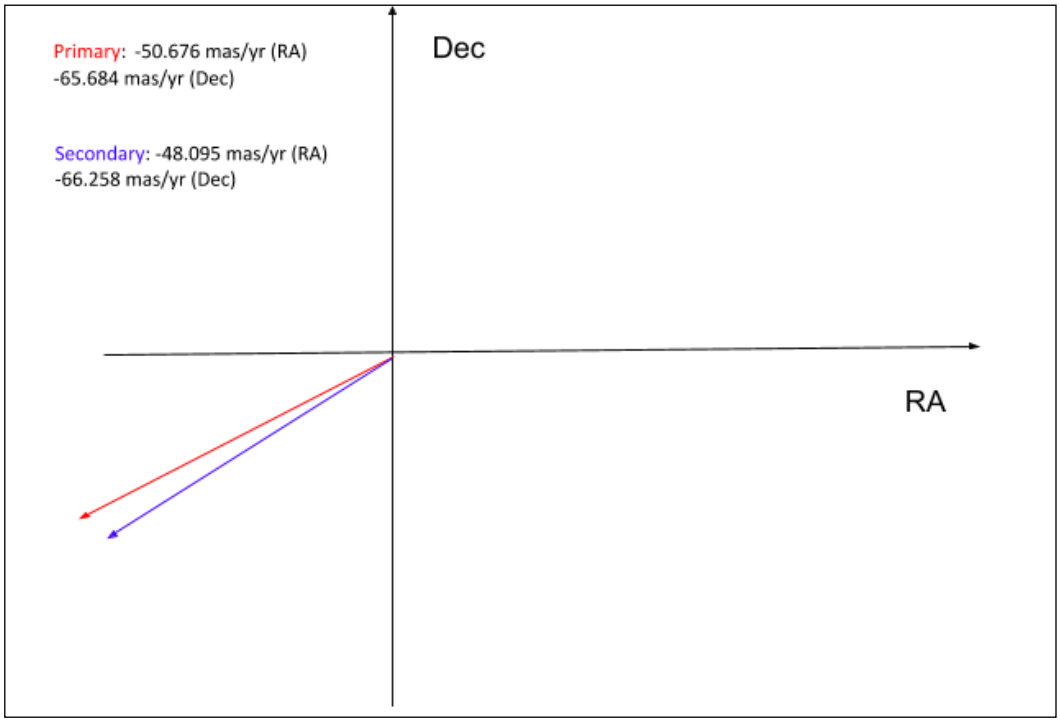

Figure 4: Proper motion vectors for WDS 08165+7930

while the position angle has steadily increased from approximately 10 degrees in 1832 to nearly 15 degrees in 2018. Using Google Sheets, the r-squared values were compared for both linear and polynomial trendlines from the plot. Given that r-squared is a statistical measure of accuracy to a given regression line, a higher value for the polynomial line than the linear one indicates that a curve describes the stars' relative motion better than a line. The actual determined value for the curved trendline is 0.851, while the determined value for the linear trendline is 0.835; thus, the secondary star appears to be taking a curved path relative to the primary. The trendlines are shown in Figures 5 and 6.

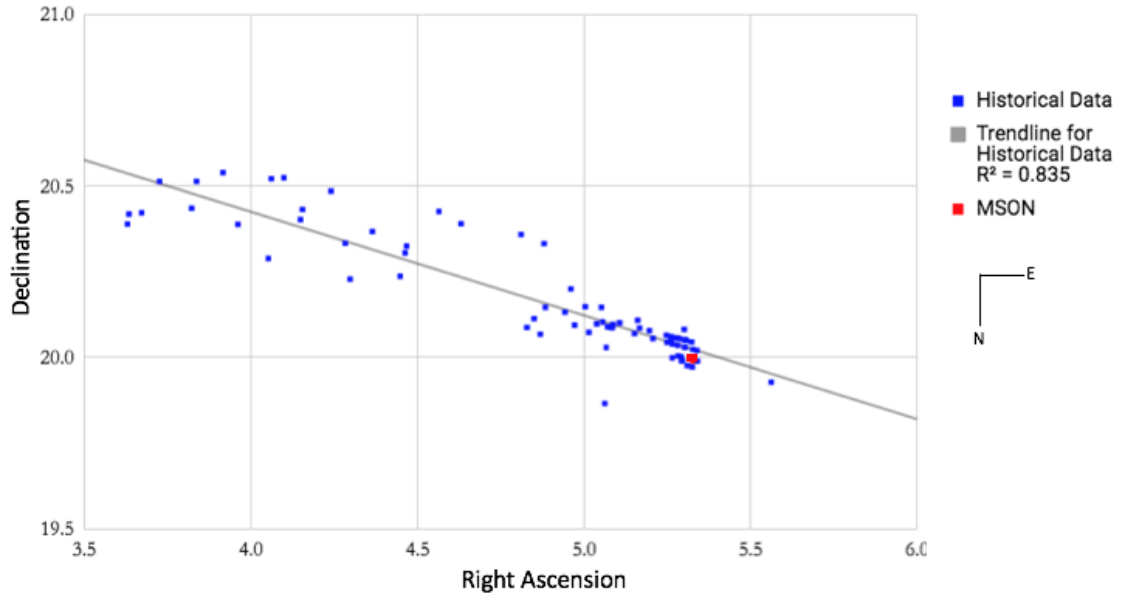

Figure 5: Linear trendline for WDS 08165+7930

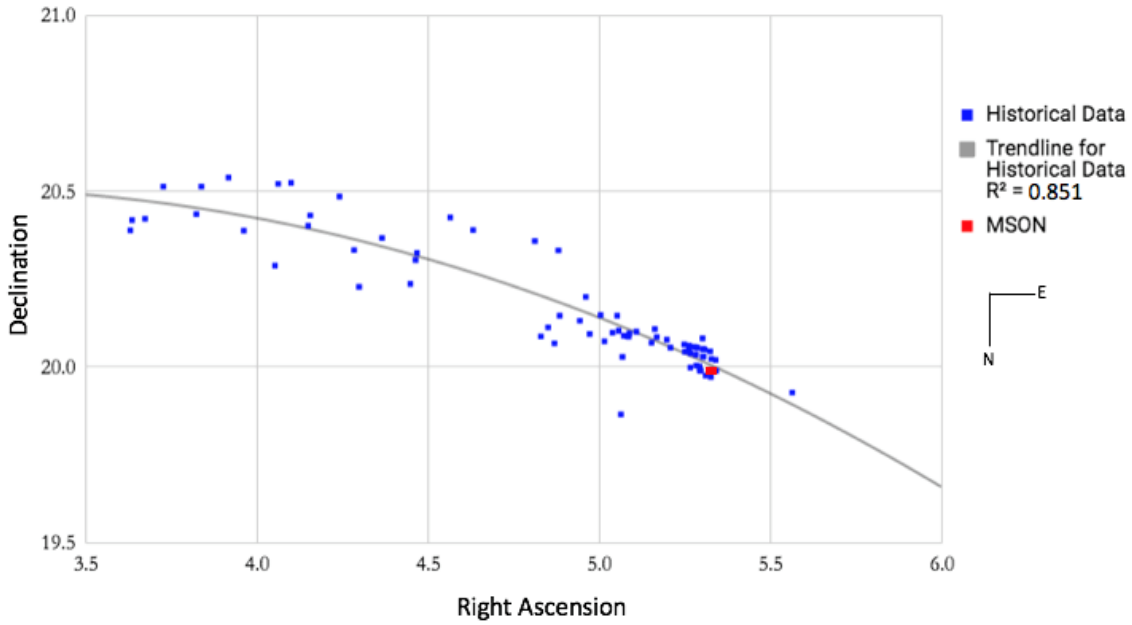

Figure 6: Polynomial trendline for WDS 08165+7930

Table 7: Desmos fit parameters for 50-point subsets of data for WDS 08165+7930

	Jack	Zoe	Grace	Mac	Kalée	Published Solution
a	15	15	15	15	15	15
e	0.651	0.615	0.615	0.618	.615	0.48
i	147	149	149	149	149	3
Ω	257	260	260	257	260	15
ω	88	91	91	88	91	157
M	191	192	189	193	550	8800
p	4950	3500	4550	3500	4400	20,000
R^2	0.76	0.68	0.83	0.86	0.89	--
Link	http://tiny.cc/08165_1	http://tiny.cc/08165_2	http://tiny.cc/08165_3	http://tiny.cc/08165_4	http://tiny.cc/08165_5	--
Fig	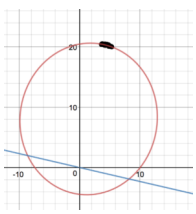	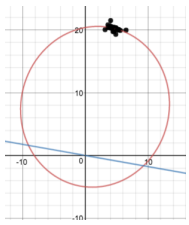	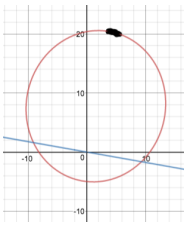	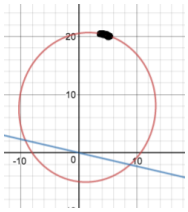	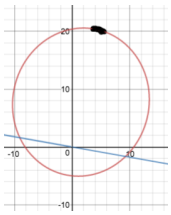	--

Desmos fits

The Desmos orbital plotting tool authored by Hensley was used in order to estimate the orbit for 08165+7930 (Hensley, 2018). Each team member selected 50 points from the data on 08165+7930, making sure that the spread between individual years was not too great (i.e. no 7+ year gaps between points). These points were then inserted into the plot tool and the parameters were adjusted to find the best R^2 value. It should be noted that this Desmos analysis was unweighted according to the criteria outlined in the *Sixth Catalog of Orbits of Visual Binary Stars*. A full orbital solution for the system would entail evaluating the data using these criteria. However, a full orbital solution is superfluous given the large period of this system and the fact that it was only 9 years ago that the solution was published (Kisselev, 2009, Van den Bos, 1962, Dommanget, 1994). As is evident from Table 7, it is possible to achieve respectable fits with varying parameters. Notably, the five spatial parameters (a, e, i, Ω, and ω) appear to be more stable than the time-dependent parameters, M and p, which also vary relative to the published solution (Kisselev, 2009). The seemingly large discrepancies in the spatial parameters between Desmos and the published solution arise from choice of coordinate axes.

Conclusion

Most of the systems studied in this paper seem to have separations and position angles that have remained relatively constant, with no big increases or decreases. The early data shows characteristic evidence of noise, while the later data becomes more tightly clustered. We contribute a measurement for three of these four systems for 2018: WDS 03009+5221, 03001+3911, and 08165+7930. The distortion of the stars in the images of the fourth system (WDS 03003+1432) calls our measurement into question, despite the fact that our measured values seem plausible based on historical data. Among the systems, 08165+7930's position angle versus time graph shows a definite trend over time, consistent with its status as a Short-Arc Binary. In all four cases, more time is needed to reveal the nature of the relationship between the stars.

Acknowledgements

This research has made use of the Washington Double Star Catalog maintained at the U.S. Naval Observatory, the SkyNet Robotic Telescope Network, the Stelledoppie catalogue maintained by Gianluca Sordiglioni, the SIMBAD database, operated at CDS, Strasbourg, France, and AstroImageJ software written by Karen Collins and John Kielkopf at the University of

Louisville, updated for double star astrometry by Karen Collins.

Special thanks to Richard Harshaw for inspiring us with his presentation to our class and patiently answering our numerous scientific questions. Thanks also to Brian Mason of the U.S. Naval Observatory for providing the data on past observations of these star systems.

References

Abhyankar, K. D. Nizamiah Observatory, Hyderabad (Reports of Observatories). Vol. 2, Royal Astronomical Society, 1961. Retrieved from http://adsabs.harvard.edu/full/1961QJRAS...2..267, February, 2018.

Astronomische Gesellschaft, 2016. Retrieved from https://en.wikipedia.org/wiki/Astronomische_Gesellschaft in February, 2018.

Dommanget, J. "Is This Orbit Really Necessary? (III)." *Astronomy and Astrophysics*, 9 Dec. 1994, http://articles.adsabs.harvard.edu/cgi-bin/nph-iarticle_query?1995A%26A...301..919D&data_type=PDF_HIGH&whole_paper=YES&type=PRINTER&filetype=.pdf.

Encyclopedia of World Biography, 2010 The Gale Group. "Friedrich Georg Wilhelm von Struve Facts" Retrieved from http://biography.yourdictionary.com/friedrich-georg-wilhelm-von-struve in Feb, 2018.

"Fact Sheet." *ESA Science & Technology: Home Page*, http://sci.esa.int/gaia/47354-fact-sheet/.

Editors of Encyclopedia Britannica. "Friedrich Georg Wilhelm von Struve." Encyclopedia Britannica. October 20, 2015. Accessed January 28, 2018. https://www.britannica.com/biography/Friedrich-Georg-Wilhelm-von-Struve.

"Friedrich Georg Wilhelm von Struve." YourDictionary, n.d. Web. 28. Retrieved in Feb 2018 from http://biography.yourdictionary.com/friedrich-georg-wilhelm-von-struve#0aewWx21yryv2b6k.99.

Harshaw, Richard W. "CCD Measurements of 141 Proper Motion Stars: The Autumn 2015 Observing Program at the Brilliant Sky Observatory, Part 3." *Journal of Double Star Observations*, vol. 12, 22 Apr. 2016.

Harshaw, Richard, 2018. Personal communication.

Hensley, Hagan, 2018. "The Double Star Orbit Initial Value Problem", *Journal of Double Star Observations*, vol. 14, 2 Apr. 2018.

Kiselev, A.A., Romanenko, J.G., & Kalinichenko, O.A. ARep 53, 126, 2009.

"Sixth Catalog of Orbits of Visual Binary Stars." *Sixth Orbit Catalog*, http://ad.usno.navy.mil/wds/orb6/orb6text.html#grading.

Van den Bos, W. H. "IS THIS ORBIT REALLY NECESSARY?" , 1962. Retrieved in Feb 2018 from http://iopscience.iop.org/article/10.1086/127812/pdf.

Wikipedia contributors. (2018, March 6). Binary star. In *Wikipedia, The Free Encyclopedia*. Retrieved 19:55, March 7, 2018, from https://en.wikipedia.org/w/index.php?title=Binary_star&oldid=828996809.

Two New Probable Proper Motion Pairs

T. V. Bryant III
Little Tycho Observatory
703 McNeill Road, Silver Spring MD 20910
rkk_529@hotmail.com

Abstract: Two pairs of stars, observed at the Little Tycho Observatory, have been investigated using Gaia DR2 data, and found to be probable common proper motion pairs. They are currently not listed in the Washington Double Star Catalog.

Two pairs of stars, observed at the Little Tycho Observatory, have been investigated using Gaia DR2 data, and found to be probable common proper motion pairs. They are currently not listed in the Washington Double Star Catalog.

These two pairs were chosen as the direction of the proper motions of each component were within a degree of one another given the reported errors in the proper motion as reported by the two catalogs.

The data for each pair are taken from the UCAC5 and Gaia DR2 Source catalogs, as rendered by the Aladin tool:

The UCAC5 data are given in Table 1. The Gaia DR2 source data are given in Table 2.

Column explanation:

RA, Dec: The J2000 position of the primary.

UCAC5/Gaia DR2 PM RA, Dec A & B: The proper motions of both the primary and secondary stars, in mas/yr.

UCAC5/Gaia DR2 PM RA, Dec err A & B: The errors in proper motion of both the primary and secondary stars, in mas/yr.

Position angle: The position angle (theta) of the pair, in degrees, as measured by the Aladin "dist" tool.

Sep: The separation of the pair (rho), in arc seconds, again as measured by the Aladin "dist" tool.

Note: The Gaia DR2 Source proper motions of the A component were not given in the Aladin data readout for the star. The Gaia DR2 proper motions are based on Gaia observations, and if no suitable observations of a given star were made, the results were not published. See https://www.aanda.org/articles/aa/pdf/forth/aa32727-18.pdf for more details.

These two pairs were chance discoveries made visually at the Little Tycho Observatory. It is to be expected that in the future discoveries like this will be made by computer searches of ever more accurate and extensive surveys such as that recently released by the ESA Gaia team.

Table 1

	RA	Dec	UCAC5 G mag A	UCAC5 PM RA A	UCAC5PM RA err A	UCAC5 PM Dec A	UCAC5PM Dec err A	UCAC5 G mag B	UCAC5 PM RA B	UCAC5PM RA err B	UCAC5 PM Dec B	UCAC5 PM Dec err B	Position Angle	Sep
1	15:32:44.64	12:44:27.5	9.397	-41.6	1.3	-16.1	1.3	9.98	-37.2	1.1	-13.3	1.0	183.3	10.24
2	14:28:43.44	33:03:54.1	9.997	-5.5	1.2	-14.2	1.2	11.070	-7.3	1.2	-17.2	1.2	317.3	49.35

Table 2.

	RA	Dec	GaiaDR2 G mag A	GaiaDR2 PM RA A	GaiaDR2 PM RA err A	Gaia DR2 PM Dec A	Gaia DR2 PM Dec err A	Gaia DR2 G mag B	Gaia DR2 PM RA B	Gaia DR2 PM RA err B	Gaia DR2 PM Dec B	Gaia DR2 PM Dec err B	PA	Sep
1	15:32:44.59	12:44:27.2	9.5069	--	--	--	--	10.0598	-34.170	0.078	-13.853	0.114	180.0	10.02
2	14:28:43.44	33:03:54.1	10.0895	-4.993	0.023	-14.357	0.048	11.1010	-7.605	0.024	-17.594	0.049	317.4	49.51

Acknowledgements

Thanks to Brian Mason of the USNO for paring down a list of probable common proper motion pairs to the two described in this short paper. William Hartkopf and Thomas Corbin, both USNO emeritus staff, corrected grammar and offered technical suggestions which were incorporated into this final version.

This work has made use of data from the European Space Agency (ESA) mission Gaia (https://www.cosmos.esa.int/gaia), processed by the Gaia Data Processing and Analysis Consortium (DPAC, https://www.cosmos.esa.int/web/gaia/dpac/consortium). Funding for the DPAC has been provided by national institutions, in particular the institutions participating in the Gaia Multilateral Agreement.

References

The Washington Double Star Catalog, 2018, Mason, B.D., Wycoff, G.L. and Hartkopf, W.I., http://ad.usno.navy.mil/proj/WDS/

Aladin web site, http://aladin.u-strasbg.fr/

Zacharias, N.; Finch, C.; Frouard, J., 2017, "UCAC5: New Proper Motions Using Gaia DR1", *The Astronomical Journal*, **153**, 166.

Lindegren et al, 2018, "Gaia Data Release 2", *Astronomy and Astrophysics*, **616A**, 2. https://www.aanda.org/articles/aa/pdf/forth/aa32727-18.pdf

WDS 00049+3005 STT 548AC, Ignored for 156 Years?

Lucy Conover[1], Saskia Onggo[1], Savannah Pluma[1], Bryce Belshin[1], Brian Delgado[1], Pat Boyce[2], and Grady Boyce[2]

1. High Tech High School, San Diego, CA
2. Boyce Research Initiatives and Education Foundation (BRIEF)

Abstract: 00049+3005 STT 548AC was first interpreted as a triple system by Otto Struve in 1861, in its only historical measurement on record. Using iTelescope T11, known for its accurate astrometry, and T24, the largest iTelescope system in the northern hemisphere, we postulate that 00049+3005 STT 548 is not a gravitationally linked triple star system. In addition, we suggest that Otto Struve likely measured a high proper motion star, the A component, and mistook another for a third star in the system. In several more recent photos, it appears that the AC pairing may be categorized incorrectly and that there is actually no C component found near the A position.

Introduction

WDS 00049+3005, a star measured only once in the Washington Double Star Catalog (WDS) since its discovery in 1861, interested the researchers because it has only the single measurement. WDS 00049+3005 is cataloged as a triple system where the B component is only 0.9 arc seconds away from the A component, making the system a challenge to measure.

History of 00049+3005 STT 548AC

The only historical measurement for 00049+3005 AC determined theta at 64 degrees and rho at 28.6 arc seconds. The primary star in the system is magnitude 8.22 with a spectral type of F7V, meaning it is a yellow -white star on the Main Sequence (Struve 1861).

The original observer of 00049+3005 was Otto Wilhelm von Struve, the second director of the Pulkovo observatory in St. Petersburg, Russia (Abalakin 2009). He was a very prestigious astronomer and won the Gold Medal of the Royal Astronomical Society.

There is only one measurement of 00049+3005 (Mason and Hartkopf, 2015) which used Struve's fifteen-inch refractor and a micrometer. Another "measurement" is outlined in the historical data in 2014. The annotation on this date was not a measurement of the star but was a reference to a paper explaining how to access and use the Washington Double Star Catalog. No data for theta and rho was imputed. This means 00049+3005 was truly not measured in the WDS in 156 years, Table 1.

Materials and Methods

The star system has an RA of 00 04 51.96, and DEC of +30 05 09.4. The declination places the system above the celestial equator; thus it was most practical to acquire images from the iTelescope network using telescope eleven (T11), Figure 1, in Mayhill, New Mexico, and telescope twenty-four (T24), Figure 2, in Auberry, California. T11, equipped with an FLI Proline PL11002M CCD camera, has a resolution of 0.81 arc seconds/pixel. The reason T11 was used for research was based on the location, separation, and magnitude of 00049+3005 which is 8.22 on the A component and an unknown magnitude on the C component which may be much dimmer. Images were later gathered from T24 for similar reasons. T24, equipped with an FLI PL09000 camera, and a resolution of 0.62 arc seconds/pixel made it a candidate to photograph 00049+3005. Fourteen images were captured from the iTelescope network (telescopes used are indicated after the filters in parentheses), Table 2. Additionally, three more images we gathered from the 2MASS infrared sky survey with H, J and K band filters.

Table 1. *Historical data reference.*

Epoch	**Theta**	**Rho**
1861.9	64	28.6
2014	No Data	No Data

WDS 00049+3005 STT 548AC, Ignored for 156 years?

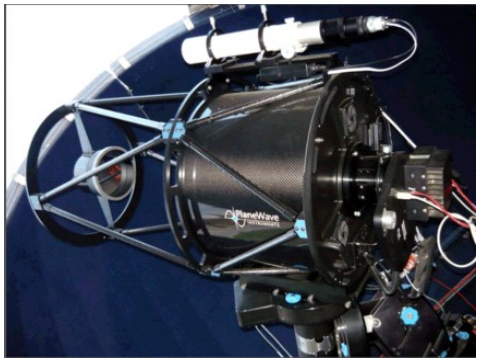

Figure 1. Telescope 11 - New Mexico.

Images were calibrated for the World Coordinate System (WCS) using Maxim DL. This establishes which way is north through identification of the target star using "PinPoint Astrometry" and comparison of the images to those in sky surveys matching the coordinates in our image. Images were then imported into Mira Pro x64 to be measured.

Data and Results

The AB components are separated by less than an arcsecond. Therefore, the pair was not resolvable for measure. The C component of 00049+3005 was not found in or near the same location as the 1861 entry in the WDS image. Measurements were conducted of nearby stars and it was found that the separation was much wider than the cataloged separation for 00049+3005. Additionally, images from the 2MASS (1997) sky survey presented some candidate stars but did not yield a star that could be identified as the C component. Therefore, new data for 00049+3005 was not possible.

Analysis and Discussion

In the images acquired, none of the surrounding stars proved to be candidates for the C component. In the images acquired from the 2MASS survey, Figure 3, there were two close stars that were not present in the iTelescope images. Each candidate was measured yet the results were inconsistent with what would be expected as the C star.

Table 2. *Overview of images acquired in 2017 and the telescopes used.*

Exposure Time	H α Filter	Luminance Filter	Blue Filter	Red Filter
30s		3 (T24)	3 (T24)	3 (T24)
60s	2 (T11)	3 (T11)	3 (T24)	3 (T24)
120s	2 (T11)	3 (T11)	3 (T24)	3 (T24)

Figure 2. Telescope 24 - California

An option was explored that Struve measured C close to the A star in 1861 and given the high proper motion of the A star (SIMBAD Web) it had moved far enough to provide a significantly different theta and rho in 2017 than was expected. The proper motion of A is listed as +066-033 indicating an eastward movement of 66 arc seconds and southern movement of 33 arc seconds in 1,000 years. Thus, A would have moved approximately 9.9 arc seconds east in RA and 4.95 south in declination. Noting this estimated 1861 position in the 2MASS image, Figure 4, measurements were recalculated to the two candidates shown (NOTE: both candidates are assumed to have zero proper motion during the last 150 years). The measurements were not in the vicinity of the 1861 measurements. The dot in Figure 4 shows the estimated position of A in 1861 with the dashed line indicating its proper motion vector.

In order to further confirm Struve's measurement was not of a binary star, data was gathered from the Gaia DR2 survey using Aladin 10. Two data sets were collected, one of 63 stars nearest to the A component's current location (set 1), and one of 55 stars nearest to the location of the A star 156 years ago (set 2). Stars were measured based on their location relative to the A star but some further away stars with fast proper motions were added to the set, as they may have crossed paths with the A star 156 years ago. The data (RA, DEC, proper motion, and their error values) were entered into an Excel spreadsheet that calculated total

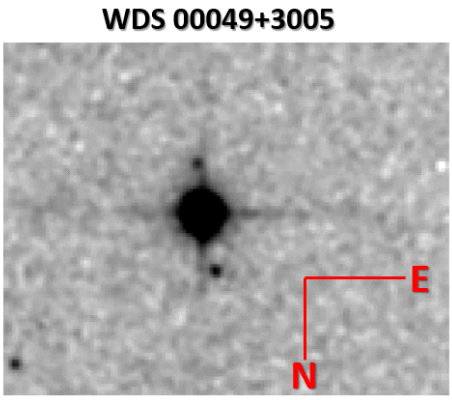

Figure 3. *00049+3005 from the 2MASS catalog (3' field of view).*

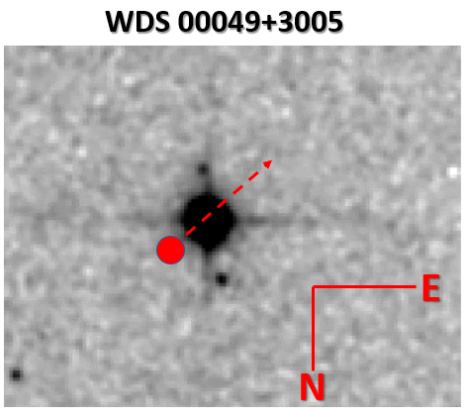

Figure 4. *00049+3005 from the 2MASS catalog (3' field of view).*

movement of the stars over 156 years, and their distances away from the A star. The proper motion of the A component was also taken into account. The data set 1 presented three stars that were 68 to 84 arcseconds away from the A component 156 years ago. The data set 2 yielded no stars that would have been close enough to the A star 156 years ago to be potential candidates.

Consideration was given to the possibility that the position and proper motion errors reported in Gaia DR2, when applied to a 156 year period, could allow old positions to vary somewhat and fall within the potential area that Struve observed. The A star has a rather high proper motion, and the other three stars in set 1 generally do not. When extrapolating the position and proper motion errors for A to 1861, we found less than one arcsecond potential position variation. The variation would be even smaller for the three candidates in set 1. Thus, none of these three, which are 68 to 84 arcseconds separated from A, could have been at the reported 28.6 arcsecond separation needed to be the C star.

We then considered the possibility that Struve had mistakenly measured a nearby double star with similar magnitudes and separations. STF 3058, which is about 15 arcminutes away, was the only comparable nearby candidate with an A star magnitude of 7.81 vs. STT 548 A's magnitude of 8.22. Its B component is a magnitude 9.21 star at a current separation of 12.6 arcseconds per the WDS. There is no reported magnitude for Struve's STT 548 C (which in itself is unusual). A similar 156-year extrapolation of the two stars' positions and proper motions established that the AB pair would have had a separation of 14 arcseconds and B would have been in the wrong quadrant in 1861. A 156-year extrapolation of STF 3058 A's neighbors found no potential C star closer than 45 arcseconds. Further Struve could not have missed the B star so a third C star is quite improbable.

We briefly considered one other possibility: that an extremely high proper motion star passed by the A star in 1861 and was not seen later when it had moved further away. We viewed the proper motion vectors from Gaia DR2 in Aladin 10 over an area of one-degree radius around the A star. Barnard's Star, which has the highest proper motion of any star, would have traversed slightly under a half of a degree over 156 years. No star with the necessary rate of motion to fulfill this scenario could be found in the one-degree radius area around STT 548 A.

Conclusion

We were unable to locate any stars matching similar criteria to 00049+3005 STT 548C that existed around the A star using 2MASS sky survey, Gaia DR2 sky survey, and current images. The data strongly suggest that it is most likely that an error occurred in the measurement process and we are unable to infer the nature of that error.

Acknowledgments

We would like to thank Pat and Grady Boyce for their dedication and support throughout this process and Brian Delgado for giving us this opportunity to do this research. Additionally, we would like to thank Brian D. Mason at the US Naval Observatory for data on our star and the iTelescope Network for providing imaging services. Finally, the group would like thank the Boyce Research Initiatives and Education Foundation (B.R.I.E.F.) for giving us the opportunities to write this paper.

References

Mason, B. and Hartkopf, W., 2015, The Washington Double Star Catalog, U.S. Naval Observatory. http://ad.usno.navy.mil/proj/WDS

NASA, Caltech, JPL, IPAC, 1997, *2MASS Image Services*

Otto Struve, 1861, *Washington Double Star Journal*

Simbad WEB: http://simbad.u-strasbg.fr/simbad/sim-id?Ident=%405471864&Name=HD%20225260A&submit=submit (Accessed 3/26/2018)

Viktor K. Abalakin, 2009 *The Pulkovo Observatory on the Centuries' Borderline*, 61-73

UDS/CNRS, 2018, SIMBAD Astronomical Database, *"HD+225260A."*

About the Authors: *Lucy Conover, Saskia Onggo, Savannah Pluma, and Bryce Belshin are students at the Gary and Jerri-Ann Jacobs High Tech High. Their "Team name" for this project is Photon Soup. Brian Delgado is a physics teacher at High Tech High. Pat Boyce is the executive director of the Boyce Research Initiatives and Research Foundation and Grady Boyce is the Vice President of B.R.I.E.F.*

Bispectrum-based Measurements of Close Large-Differential-Magnitude Visual Double Stars

J. Sérot
Clermont-Ferrand, France

Rick Wasson
Orange County Astronomers, Murrieta, California

Dave Rowe
PlaneWave Instruments, Rancho Dominguez, California

Russell Genet
California Polytechnic State University, San Luis Obispo, California

Abstract: This paper reports results of a collaborative project for assessing: (1) whether small-aperture telescopes might be used to collect reliable images of close visual double stars with large differential magnitudes (up to Δm=7) and faint late secondaries; and (2) whether bispectrum-based analysis techniques could be applied to the collected data in order not only to determine their position angles and separations, but also to obtain reliable estimations of differential magnitudes with different filters, with the ultimate objective of estimating the spectral type of the faint secondaries.

1. Introduction

Triple correlation (also known as bispectrum analysis) has been routinely used by professional astronomers in the field of close binary star observations (Horch *et al*. 2004). Relying upon speckle interferometry, this technique allows accurate measurements below the seeing limit. But, unlike classical auto-correlation-based analysis, it produces a fully reconstructed image of the observed pair. Therefore, in addition to identifying the correct quadrant of the secondary star, it also allows estimating the difference in magnitude (Δm) between the two components. Rowe has recently added a module performing bispectrum analysis to his *Speckle Toolbox* (STB) software (Harshaw, Rowe, and Genet, 2017) and experiments have shown that it can produce astrometric results on a par or better than those obtained with lucky imaging or auto-correlation (Sérot 2018b, Sérot 2018c). But these results are preliminary and, more importantly, do not address the issue of obtaining reliable estimations of Δm.

Obtaining reliable measurements of differential magnitudes for short-period visual binary stars is important, as it can provide information on the stellar types of the components and hence help in refining the models of stellar evolution. It is well known, in particular, that while the masses of stars in the middle of the main sequence are known with good accuracy from eclipsing binaries (Anderson 1991), this is not true for M-type stars. Dupuy *et al*. have shown that inferred masses for these stars can be off by a factor of two (Dupuy *et al.* 2012). A more direct, and potentially more accurate, way of computing these masses is to derive them from the orbit of binary stars. Close, short-period, visual double stars are good candidates for this because the separation between their components may be close enough to allow a significant portion of the orbit to be obtained in a relatively short period of time, but not so close (as with spectroscopic binaries for instance) that mass exchange affects their evolution.

There are two practical obstacles to the approach of using short-period visual binary stars with M-type companions for determining stellar masses. First, such pairs are difficult to observe because they generally exhibit small separation (usually below the atmospheric seeing

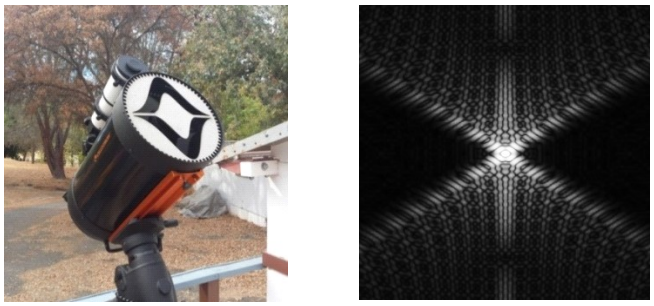

Figure 1. Foley's mask (left, here mounted on a C11 telescope) is based on the Spergel–Kasdin prolate-spheroidal mask originally described by Kasdin et al. (2003). It produces the diffraction pattern (right) plotted on a nonlinear brightness scale. Note the two triangular secondary star "discovery zones" that are relatively free of diffracted light from the primary star

limit for ground-based telescopes) and very large differential magnitudes (which implies that the light from the brighter star often overwhelms the light from the dimmer star). Second, of the many close double stars listed in the Washington Double Star (WDS) Catalog with large differential magnitudes (LDM), the spectral type of most of the secondaries is not known, primarily because it is difficult to determine using normal spectroscopic techniques. Thus, we don't know whether the secondary is a chance, more distant early star (and hence an optical double of little interest), or a nearby late star (a potential binary with a late-M star secondary and hence of great interest).

In late 2016, the authors embarked on a collaborative project for assessing whether small-aperture telescopes might be used to: (1) collect reliable images of close visual double stars with large differential magnitudes (up to $\Delta m=7$) and faint late secondaries, and (2) whether bispectrum-based analysis techniques could be applied to the collected data not only to determine (and follow) their position angles and separations, but to also obtain reliable estimations of differential magnitudes with different filters so that the spectral type of the faint secondaries could be roughly estimated. Because the available values for differential magnitudes were either lacking or imprecise (and because we had little previous experience with bispectrum reduction techniques) it was agreed to work on a common list of target stars to minimize, or at least identify, potential biases. Three observers were engaged in this campaign: R. Wasson (RW), J. Sérot (JS), and R. Harshaw (RH). The results reported in this paper are those obtained by RW and JS.

2. Previous and related work

As mentioned above, observing close doubles with large differential magnitude is challenging because the light from the bright primary simply swamps the light from the faint secondary. There are several ways this problem can be circumvented.

Shaped aperture masks can be used to diffract the bright light from the primary star away from "discovery zones," allowing faint secondaries to be observed. Many shaped masks have limited-angle discovery regions, so one must rotate these masks to fully survey the neighborhood of a star (Kasdin *et al.* 2003). Other mask species provide full 360-degree visibility around a star but do so at the expense of throughput or resolving power (Vanderbei *et al.* 2003). In general, larger discovery zones are associated with poorer contrast.

Other mask varieties have been proposed in the context of high-contrast imaging, including Lyot coronography and apodized masks. Lyot coronographs use a series of lenses and masks to isolate and remove centrally-incident light from the image (Sivaramakrishnan *et al*. 2001). These systems require accurate manufacturing techniques and precise positioning to function properly (Sing *et al*. 2013). Apodized masks, also called gradated masks, are used much like shaped aperture masks but feature a continuous transmission profile rather than either complete transparency or opaqueness. The smooth patterns theoretically can provide results superior to shaped aperture masks, but these results are difficult and expensive to achieve in practice.

Foley et al. (2015) developed a shaped aperture mask that shows some promise. While such a single, full-aperture, shaped pupil mask can help with large delta-mag close doubles, additional masks of various sorts can be placed at the image plane or Lyot stop. Adding such masks increases the degrees-of-freedom in the design space, which should allow a larger contrast ratio to be reached and therefore difference in magnitude. Although these additional masks would be much smaller, with tighter manufacturing and alignment tolerances, the contrast-ratios sufficient for double star research (approximately 10^2 to 10^3) are more modest than those for exoplanet imaging and so such additional masks may be within reach. There are a number of young giant planets (such as the HR 8799 system, to give the most famous example) that are within reach of 10^5 contrast, and have been imaged from the ground with AO systems at Keck, Palomar, and GPI (Gemini Planet Imager). A contrast ratio of 10^8 is the design figure being used for space-based science goals.

Another approach for easing the detection of close, late-M secondaries is to observe at longer wavelengths. This potentially reduces the light from an earlier primary while enhancing the light from the later secondary, thus reducing the differential magnitude. A short-wave

Bispectrum-based Measurements of Close Large-Differential-Magnitude Visual Double Stars

Figure 2. The OCA Kuhn 22-inch Cassegrain telescope instrumented for Speckle Interferometry. Camera, power, control and image acquisition are through the single blue USB3.0 cable to the laptop computer at lower right, running FireCapture software.

infrared (SWIR) InGaAs camera operating in the Y, J, and H bands (0.9-1.7μ) could work well. Sérot (2018a) has made a few initial observations with a Raptor Owl SWIR camera but the cost of these cameras still precludes their generalized use in the amateur community (though the situation may change in the very near future with the rapid development of a market for such cameras in the surveillance domain).

3. Instrumentation

The observations reported in this paper were conducted by two observers in two different locations : R. Wasson (RW) in Southern California and J. Sérot (JS) in France.

Wasson used a 22-inch classical Cassegrain telescope (Fig. 2), owned by the Orange County Astronomers astronomy club (OCA). This equipment, located at 4500 feet elevation in the foothills 15 miles east of Mount Palomar Observatory in Southern California, is described by Wasson (2018) and has been used for speckle interferometry since 2015. The results reported in this paper were obtained with a 2x Barlow lens and a

Figure 3. – Instrumental setup in Clermont-Ferrand. Left : C11 on equatorial mount. Right : optical train (flip mirror, centering eyepiece, filter wheel, projecting eyepiece and ADC – inside the tube between the filter wheel and the camera – and Raptor Kite EM-CCD

ZWO ASI290MM back-illuminated CMOS camera. The low-read-noise camera was not cooled; dark-subtraction processing would probably have improved the results but was not employed. The STB "interference" filter option was used in all processing, to suppress residual CMOS "read" noise, which otherwise causes a bright horizontal line through the images. No Atmospheric Dispersion Corrector (ADC) was used, restricting observations to zenith angles of less than about 35 degrees with moderate bandwidth near IF filters.

Because the back-illuminated CMOS camera has good QE in the near IR, an IR-pass filter (Astronomik Pro Planet 807) was used for observations of LDM pairs. It was assumed that when the primary star is a main sequence dwarf, a much fainter binary companion must be a later-type dwarf, most likely a late K or M dwarf. Therefore, the IR-pass filter was used for these initial observations. Even though the longer IR wavelength reduces the resolvable separation slightly, it should significantly reduce the magnitude difference and the required camera dynamic range.

Another benefit of near-IR observations is that the seeing is much better ("slower") than at shorter wavelengths, permitting longer exposures to record faint red stars. Exposures of 200 to 500 milliseconds were used by RW for these stars; this is about 10 times longer than usually achievable for visible wavelengths.

Sérot's observatory is located in the observer's garden at the periphery of Clermont-Ferrand, a mid-sized town in the center of France (45°47'N Lat., 3°04'E Long.) (Figure 3). The results reported in this paper

have been obtained using a Schmidt-Cassegrain reflector (Celestron C11) and a Raptor Kite EM-CCD camera (Sérot 2015, Sérot 2016a). The native focal length of the telescope (2.8 m, F/D=10) was augmented using 10 mm and 12 mm projecting eyepieces leading to pixel scales of 0.09''/pixel and 0.13''/pixel respectively. A wide-band L filter (400-700 nm) and exposures of 40-80 ms were used. An atmospheric dispersion corrector was inserted in the optical path to compensate for the effects of atmospheric dispersion.

4. Bispectrum analysis

Bispectrum analysis (BSA) – also known as triple-correlation – is an extension of the auto-correlation (AC) technique which has been used by professional astronomers for many years and is now used by several amateurs to obtain astrometric measurements of double stars below the seeing limit†.

Classical AC-based analysis operates by computing and summing the power spectrum of the images in the input sequence (taking the square of the modulus of the Fourier transform of each image) and then computing the inverse Fourier transform of the sum. In the resulting image, called an *auto-correlogram*, each secondary component gives two identical and symmetric peaks, located 180° apart from the central peak corresponding to the primary component. This technique works remarkably well for recovering the full resolution of an instrument, especially when used in conjunction with a deconvolution process, which reduces the effect of the *seeing halo* by dividing the accumulated power spectrum by that obtained for a single reference star under the same conditions.

Auto-correlograms, however, have two inherent limitations. First, since each companion gives two identical peaks in the auto-correlogram, there is always a 180° uncertainty in the measured position angle (known as the "quadrant ambiguity problem"). This is not a problem when the position of the companion is already known, at least approximately (from orbit ephemerids for instance) but is problematic for stars with few previous observations. Second, and more importantly in the context of this paper, the auto-correlogram does not allow estimation of the differential magnitude of the double star, because the intensity of the auto-correlation peaks is not related to the actual magnitudes of the components.

Bispectrum analysis (BSA) aims at overcoming the limitations of AC-based techniques. Technically, the *bispectrum* of an image is a four-dimensional complex matrix embodying the triple correlation of this image. Unlike the simple auto-correlation, the bispectrum retains the complex amplitude and hence makes it possible to recover the original image phase in the Fourier domain that is lost when the power spectrum is computed by squaring the modulus of the Fourier amplitude (as with auto-correlation). In practice, the final image phase is calculated from the bispectrum by an iterative procedure; the complex Fourier amplitude of the final image is calculated from the square root of the power spectrum, and the phase determined from the bispectrum. This allows a representation of the original set of images to be reconstructed with atmospheric distortion removed.

As with simple AC techniques, BSA is more effective when used with a reference (single) star. The power spectrum and bispectrum are computed for the reference star and are then used to compensate the power spectrum and bispectrum of the target double star.

The latest version of the Speckle ToolBox software (1.13) contains the modules necessary to reconstruct the image using BSA. The work described in this paper partly served as a test bench to assess the provided functions. The procedure is executed in two steps. One first constructs the bispectrum from the average of the triple correlation of each image in the ensemble. This process is computationally intensive, typically taking 10 times more CPU time than the computation of the power spectrum alone. The second step is the reconstruction of the final image from the power spectrum and bispectrum. This step, which iterates the image phase until convergence, is usually quite fast. During this step, the user can apply filters and photon bias removal in the Fourier domain to improve the SNR of the final image.

5. Targets

The eleven observed stars are listed in Table 1 with their characteristics obtained from the WDS catalog (Mason *et al.*, 2015). Columns 1-2 give the star identification (WDS number and discoverer code, respectively). Columns 3, 4, and 5 give the year of the first and last measurement and the total number of measurements. Columns 6-9 give the measurement values (PA=position angle in degrees, SEP=angular separation in arcsec) for the first (1) and last (2) measurement. Columns 10-12 give the magnitudes of the two components (Johnson V band is typical in WDS) and the corresponding ΔM value. Column 13 gives the spectral type of the primary component. Unfortunately, for the

† *AC-based reduction techniques are often referred to as "speckle interferometry" though, strictly speaking, the latter term should only be used when the acquired images show a sufficiently high number of fully resolved speckles, which only happens in practice for high D/R0 ratios. For small instruments, the technique should rather be called pixel auto-autocorrelation because the correlation is computed on raw pixels instead of speckles, which are either absent or too faint*

Table 1 – List of Target Stars Observed

WDS	DISC	DATE1	DATE2	NOBS	PA1	PA2	SEP1	SEP2	M1	M2	DM	SP
13122+1608	A 2225	1910	1997	7	69	74	3.0	2.5	7.52	13	5.48	F3V
14046+3425	HU 646	1903	2010	4	26	24	2.0	2.2	8.05	14.5	6.45	A3IV
14122+4225	HO 57	1883	2014	8	207	204	1.8	2.7	8.2	13.2	5.0	K5
14171+5433	BU 1271	1892	1996	13	355	355	2.8	1.8	7.1	12.3	5.2	G1IV
14525+2348	COU 305	1968	1998	3	66	66	3.2	3.6	7.37	12.5	5.13	K0
15190+2541	LDS6304	1960	2007	2	185	191	4.0	3.6	7.96	13.7	5.74	G8V
15483+1400	A 1637	1907	1975	4	256	257	2.2	2.8	9.69	14.9	5.21	K2
15536+1604	A 2079	1909	1991	6	61	59	3.5	3.4	6.26	12.5	6.24	F3V
16315+3331	BU 816	1881	1998	18	224	222	5.0	4.6	7.12	12.2	5.08	A2V
16335+3030	BU 818	1881	2009	9	34	38	3.3	4.0	6.9	13.5	6.6	A9IV
16529+4608	A 1869	1908	1945	4	214	226	2.3	2.3	9.02	15.1	6.08	G0

selected stars, the spectral types of the companions are not listed in the WDS, probably because they have not been spectroscopically observable in the glare of the nearby primary star.

The selection was based upon the magnitude, separation, spectral types of the components (as published in the WDS), and the visibility from both observatories. As announced in the introduction, the most salient feature exhibited by these pairs is their high ΔM values (ranging from 5.0 to 6.6) and the relatively close separations (from 1.7 to 4.6 arcsec). As can be expected – because of the large reported ΔM – these pairs have not been measured often (less than 10 times, on average, since their discovery). Three of the target stars are subgiants (spectral class IV) according to the WDS. These primaries are much brighter than a dwarf of the same type. Therefore, the companion may not be a late-type dwarf, but could be a normal dwarf of any type.

6. Results

All targets were observed between May 24, 2017 and Jun 1, 2017 (mean date: 2017.397). Results are listed in Tables 2 and 3.

Table 2 gives, for each target, the measured values for the position angle PA and the separation SEP obtained by the two observers (RW and JS) using two reduction methods: classical auto-correlation (AC) and bispectrum analysis (BSA). All AC and BSA values were obtained using the STB software (version 1.12 and 1.13).

The post-reduction images, from which these measurements were obtained, are given in Plates 1-11. In these plates, the first and second column show the autocorrelogram (top) and bispectrum-reconstructed image (bottom), both computed by STB, by the two observers (col 1: RW, col 2: JS). The last column shows an image of the pair obtained using the classical *lucky stacking* (LS) method, *i.e.* by co-adding the 10-30 best images of the acquisition sequence. This image was obtained by JS using the REDUC software (version 5.03) from F. Losse (Losse, 2017).

Table 2 shows that for each observer, the AC and BSA techniques give very consistent astrometric results: the mean and standard deviation of the difference in PA and SEP are μ=-0.28°/σ = 0.23° and μ = 4 mas σ = 62 mas for JS, and μ = 0°/σ = 0.40° and μ = 1 mas σ = 24 mas for RW. Moreover, the results obtained by both observers for each method are also very consistent: the mean and standard deviation of the difference for PA and SEP are μ = -0.4°/σ = 0.72° and μ = 13 mas σ = 43 mas for AC and μ = -0.19°/σ = 0.78° and μ = 20 mas σ = 63 mas for BSA respectively.

Table 3 gives the measurements of the differential magnitude Δm (m2-m1) obtained by both observers from the bispectrum-reconstructed images (as shown in the second row of Plates 1-11) and also, for JS, from the lucky stacked images (LS, as shown in the last column of Plates 1-11).

The LS values were obtained using the *Surface* algorithm provided by *Reduc*, which operates by fitting a mathematical profile on the non-saturated images of the stars.

The BSA values were obtained with STB using the method classically used for photometric measurements on CCD images. The *Speckle ToolBox* software uses three circular apertures to measure differential magnitude of the two stars simultaneously: an aperture for the primary star, one for the secondary star, and one for the background. The background aperture is placed in a "dark" area, away from both stars, and its average pixel value is subtracted from every pixel within the two star apertures.

Image calibration by JS was limited to dark and bias subtraction, but no flat fielding was done. No cali-

Bispectrum-based Measurements of Close Large-Differential-Magnitude Visual Double Stars

Table 2 – Measurements (PA and SEP)

Target	PA (°)				SEP (arcsec)			
	AC		BSA		AC		BSA	
	JS	RW	JS	RW	JS	RW	JS	RW
A 2225	72.1	72.5	72.5	72.5	3.00	2.98	2.99	2.95
HU 646	22.7	25.0	23.5	25.8	2.10	2.06	2.06	2.08
HO 57	204.8	204.6	205.0	204.5	2.56	2.57	2.57	2.56
BU 1271	353.9	354.0	354.3	354.0	1.68	1.67	1.64	1.67
COU 305	64.8	65.2	64.8	64.6	3.70	3.72	3.70	3.67
LDS6304	157.5	157.6	157.6	157.6	3.24	3.32	3.34	3.33
A 1637	n/a	258.3	257.4	257.7	n/a	2.66	2.78	2.68
A 2079	61.2	60.7	61.3	60.6	4.00	3.97	4.03	4.00
BU 816	220.4	221.0	220.5	221.0	5.05	5.05	5.07	5.03
BU 818	36.1	36.2	36.4	36.3	4.17	4.11	4.02	4.14
A 1869	219.4	220.1	219.8	220.6	2.18	2.10	2.22	2.09

Table 3 – Measurements (Δm)

Target	Δm		
	JS (center WL 530nm)		RW (center WL 885nm)
	BSA	LS	BSA
A 2225	4.7	4.6	3.9
HU 646	4.2	3.7	2.6
HO 57	4.1	4.0	4.0
BU 1271	3.9	3.1	3.1
COU 305	5.2	5.3	4.7
LDS6304	5.2	5.2	3.3
A 1637	3.7	3.2	3.3
A 2079	6.3	6.2	4.7
BU 816	4.8	5.2	3.5
BU 818	6.2	7.2	5.3
A 1869	5.0	4.4	3.5

bration was made to the RW images.

For JS, the Δm values obtained from the bispectrum -reconstructed images on the one hand and the lucky stacked images on the other hand are reasonably consistent, with a difference showing a mean value of -0.10 and a standard deviation of 0.46.

The values obtained by both observers using the same BSA method differ more significantly, with a mean value of 0.95 and standard deviation of 0.60 for the difference. This is not surprising since each observer used a different camera-filter combination. JS used a broad band "L" filter ($\lambda c \approx 550$ nm, $\Delta\lambda \approx 300$ nm), while RW used an IR-pass filter and a camera with relatively higher QE in the 800-1050 nm range. Since no attempt was made to transform the reported "raw instrumental" magnitudes to a "standard" photometric system†, the conclusions drawn from the observations must be made with care. Rough comparisons can still be made, however. In Figure 4 the Δm values obtained by both observers using the BSA method are plotted against filter center wavelength. Also shown as colored bars are the approximate filter pass bands used by each observer. It might be noted that the magnitude difference is always smaller at longer wavelength, generally indicating that the secondary star is redder than the primary.

The spectral type of each star is noted in the legend, with early types at top of the legend, and later types at

†*Such a transformation would be difficult and uncertain, because of large differences (in both center wavelength and band width) from any standard photometric filter set.*

Table 4 - Filters Used for Multi-Band Observations of High-Delta-Magnitude Double Stars with the OCA 22" Cassegrain and ZWO ASI290MM CMOS Camera

Filter Code	Manufacturer	Name	Type	Center WL (nm)	50% Transmission (nm)
G	Baader	G (LRGB Series0	Interference	534	495 to 575
R	Baader	R (LRGB Series)	Interference	636	582 to 690
IR742	Astronomik	ProPlanet 742	Interference	844*	736 to *
IR807	Astronomik	ProPlanet 807	Interference	885*	800 to *
* Indicates long-pass filter. Wavelength cutoff is determined by camera Quantum Efficiency. "Center" wavelength is weighted average of filter transmission times camera QE.					

bottom. It should be noted that the spectral type is likely dominated by the primary star alone, because it is much brighter; it is very difficult to get a spectrum for a faint star without contamination from such a bright nearby companion. Indeed, no spectra apparently exist for the faint secondary stars. There is no consistent trend in the delta magnitude slopes (i.e., color difference) with spectral type. The three K stars – the reddest primaries – all have relatively "flat" delta magnitudes, indicating that the primary and secondary stars are both reddish. But other stars of similar spectral type are not so consistent.

6.1. Multi-band Observations

As an extension of the work presented here, two stars listed in Table 1 were observed again by RW in multiple filters with the OCA 22-inch telescope. The filters employed are shown in Table 4, where the "cutoff" wavelength of the IR-pass filters was assumed to be 1050 nm (the approximate end of response for the back-illuminated silicon CMOS detector). The "center" wavelength is the weighted average of filter transmission times detector QE.

The idea was to check whether faint companions can be observed at shorter wavelengths and, if so, how the observed Δm varies with wavelength. Filters on hand were used for this initial exploration. Results obtained from auto-correlation (STB 1.05) and bispectrum analysis (STB 1.13) are given in Table 5. The faint red companions, down to V = 13.7, were successfully observed in all filters, even the G filter (center 534 nm). The PA and Separation data are quite consistent for both stars; standard deviations are small, even combining all filters and both analysis methods. This confirms that the AC and Bispectrum techniques both give valid astrometric results independently of the observing

Table 5 - Results of Multi-Band Observations of High-Delta-Magnitude Double Stars with the OCA 22" Cassegrain and ZWO ASI290MM CMOS Camera, on date 13 July 2017 (2017.531)

Double Star					Θo (deg)		ρo (")		
WDS	Discovery	WDS (V) m1 / m2	WDS DMag	Filter	AC	BS	AC	BS	DMag
15190+2541	**LDS6304**	7.96/13.7	5.74	G	157.76	157.65	3.339	3.357	5.31
				R	157.76	158.51	3.341	3.292	4.50
				IR742	157.63	157.46	3.323	3.321	3.21
				IR807	157.56	157.43	3.326	3.327	3.08
Average					157.72		3.328		
Standard Deviation					0.34		0.019		
16315+3331	**BU816**	7.12/12.2	5.08	G	221.01	221.05	5.067	5.076	4.22
				R	220.94	221.03	5.062	5.071	3.75
				IR742	221.00	221.08	5.054	5.043	3.41
				IR807	221.05	221.11	5.048	5.034	2.90
Average					221.03		5.057		
Standard Deviation					0.05		0.015		

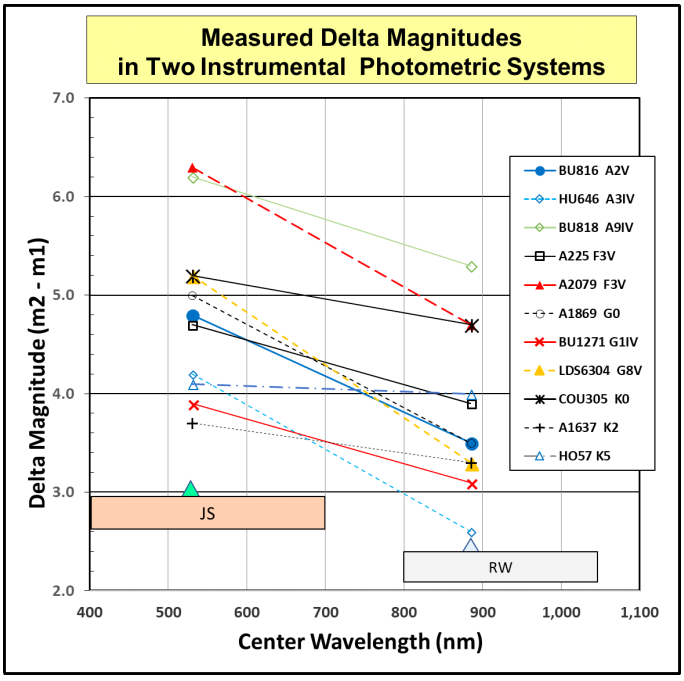

Figure 4. Measured Delta Magnitudes (Secondary – Primary) in two instrumental photometric systems.

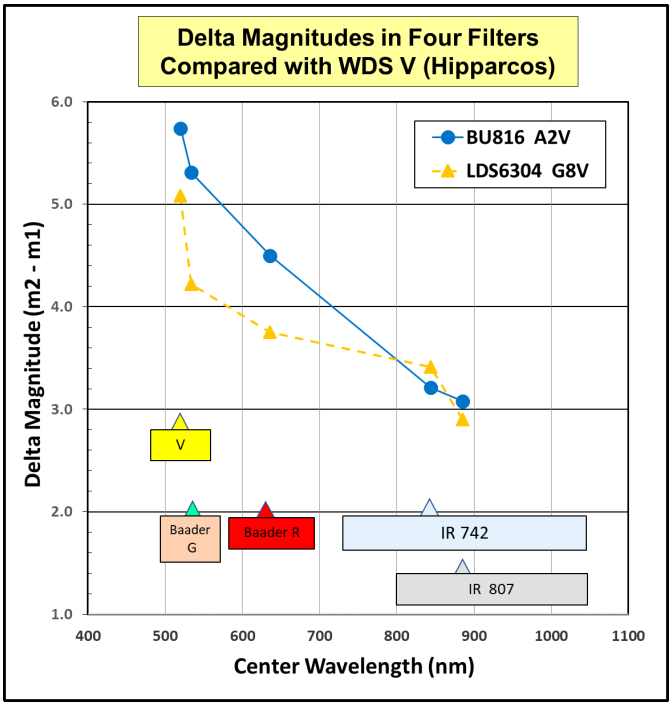

Figure 5. Measured Delta Magnitudes of two double Stars in four filters, compared with WDS V magnitudes.

wavelength.

The delta magnitude results of Bispectrum analysis are plotted in Figure 5 for the two stars observed. The bars at bottom indicate the filter passbands and center wavelengths. The left-most point and yellow bar indicate the WDS value, assumed to be the Johnson V band. There is a clear trend that the companion becomes relatively brighter (reduced delta magnitude) as wavelength increases, indicating that both secondary stars are quite red. The delta magnitude of the G filter approaches, but does not reach, that of WDS (V). The G filter is similar in center WL and 50% transmission to V; however, the G interference filter has sharp edges, without the red "tail" of the colored-glass V filter. No attempt was made to transform these magnitudes to a standard system.

In Figure 5, the early-type star BU816 (primary spectral type A2V) has a much steeper slope than the later-type star LDS6304 (primary type G8V). This trend would be expected if both secondary stars were of similar late spectral type, such as red dwarfs. This trend is also different from that in the previous comparison of Figure 4, where both stars had similar slopes. In Figures 4 and 5, the IR807 filter observations of RW were on different dates, and are shifted by about 0.4 magnitude. This could possibly be caused by variability in one or both stars, but more likely indicates uncertainty in measuring delta magnitude for such faint secondary stars. In Figure 4, the wide effective filter passband used by JS may also contribute to large differences in delta magnitude for different spectral types, because the dominant blue or red colors of the primary star can both be recorded, effectively shifting the "center" wavelength for each star.

6.2. Gaia Satellite Observations

The Gaia astrometric / photometric / radial velocity satellite, launched in late 2013, has completed a large portion of its planned observations. Exhaustive documentation is available on-line at http://sci.esa.int/gaia/. The second of four planned data releases - DR2 - became available to the public in April 2018. Although DR2 is a preliminary release, it contains a great deal of useful information having unprecedented accuracy (https://www.cosmos.esa.int/web/gaia/dr2).

Author Dave Rowe wrote code to download and access the 1.3 TB database. He then searched it for all stars in the WDS Catalog with separation less than 30", successfully identifying two components for over 76,000 doubles. Those with very high proper motion were difficult to locate. He built a file containing parameters of particular interest to double star observers; this file is in .csv spreadsheet format, for easy access, and is available for download by request.

Both components of all 11 double stars observed in

this paper were observed by Gaia, and DR2 parameters are summarized in Table 6. For each double, the first line is for the primary, and the second line for the secondary. The epoch of DR2 is given as 2015.5. The number of significant digits has been arbitrarily rounded to moderate precision in Table 6 - adequate for our purposes, but still much higher accuracy than heretofore available.

The columns of Table 6 contain the following data: WDS numerical designation, Discovery designation, Proper Motion in RA (milli-arcseconds/year), Proper Motion in Dec (milli-arcseconds/year), Parallax (milli-arcseconds), Distance (calculated from parallax, light-years), G, G_{BP}, and G_{RP} magnitudes, derived Radius (solar radii), derived Temperature (K), measured Radial Velocity (km/sec), derived Luminosity (sun=1), Separation (arcseconds), and Position Angle (degrees), both calculated from absolute position.

The G magnitudes are derived from the entire white light response (330-1050 nm) of the optics and astrometric CCD arrays, while G_{BP} (330-680 nm) and G_{RP} (640-1050 nm) magnitudes are the product of low-resolution spectrophotometer (prism) instrumentation (Pancino, 2010). A number of other parameters, not included in Table 6, are contained in DR2. But for any given star, some parameters may not be included, perhaps because sufficient analysis has not yet been performed.

A number of significant conclusions can be drawn from review of Table 6:

1. Based on very similar Proper Motion (direction and speed), Parallax (distance), and Radial Velocity (in only one case), the two components of each system are very near each other in space, and we conclude that all 11 double stars we observed are true binaries.
2. Unfortunately, because none is closer than 110 L-Y, their separation is several arcsec, and they have shown very little movement since discovery (4 to nearly 14 decades), they all probably have very long orbits.
3. All available prior observations were obtained courtesy of Brian Mason of the USNO. Some of these double stars were discovered over 100 years ago, but all have very few observations. Along with Gaia and the current observations, no systematic changes in separation or PA indicating orbital motion were seen.
4. Comparison of Tables 2 and 6 shows that our observations agree well with the Gaia separation and PA; the epochs are only about two years apart.
5. Gaia variability data were not available for any of the components; at this stage of the mission, variables may not have been evaluated in detail yet.

Table 6 - Summary of Preliminary Properties from Gaia Satellite DR2, Epoch 2015.5

WDS	Dicovery	PM RA (mas/yr)	PM Dec (mas/yr)	Parallax (mas)	Distance (l-y)	Gmag	BPmag	RPmag	Radius (sol)	Teff (K)	RV (km/s)	Lum (sol)	G Sep (")	G PA (deg)
13122+1608	**A2225**	-22.45	69.32	8.43	383	7.360	7.592	7.031	2.56	6673	-17.3	11.66	2.957	72.38
		-21.01	64.66	9.10	355	12.189	-	-	-	-	-	-		
14046+3425	**HU646**	-18.54	10.01	6.59	490	8.045	8.137	7.900	-	8157	-	-	2.087	23.80
		-16.99	10.59	6.63	487	11.882	-	-	-	-	-	-		
14122+4225	**HO57**	-38.54	-3.57	3.83	844	7.887	8.530	7.160	9.85	4697	-53.0	42.53	2.552	204.41
		-38.45	-2.69	3.58	903	11.971	-	10.303	-	-	-	-		
14171+5433	**BU1271**	-169.90	-57.35	19.18	168	6.836	7.219	6.332	2.09	5573	-45.6	3.79	1.697	353.24
		-168.55	-67.18	18.75	172	10.763	-	-	-	-	-	-		
14525+2348	**COU305**	-21.15	23.05	3.95	818	6.948	7.518	6.278	13.82	**4806**	-52.3	91.84	3.692	65.32
		-21.01	23.65	3.92	823	11.982	11.718	10.783	-	**5096**	-55.6	-		
15190+2541	**LDS6304**	-564.57	-125.14	29.42	110	7.798	8.198	7.272	0.94	5402	-30.9	0.676	3.330	158.41
		-544.13	-113.37	29.33	110	12.091	12.451	10.727	-	4947	-	-		
15483+1400	**A1637**	-1.52	-64.31	4.73	683	9.280	9.801	8.638	3.67	4941	-7.6	7.22	2.670	257.74
		-3.22	-64.74	5.53	584	12.736	13.164	11.804	0.69	4797	-	0.228		
15536+1604	**A2079**	20.20	-22.55	11.83	273	6.095	6.332	5.757	3.42	6513	-0.6	19.02	3.973	60.73
		20.19	-24.38	12.41	260	11.830	11.383	10.519	-	5096	-	-		
16315+3331	**BU816**	-25.28	-11.23	7.03	459	7.082	7.148	7.011	2.50	7982	-	22.94	5.044	221.08
		-20.47	-10.15	7.10	455	11.477	11.897	10.869	0.79	5173	-17.1	0.405		
16335+3030	**BU818**	-38.12	-2.79	5.79	558	6.818	6.959	6.624	3.71	7624	-	41.88	4.120	36.35
		-35.97	-3.83	5.93	545	12.681	12.566	11.749	-	5096	-	-		
16529+4608	**A1869**	1.95	-45.45	8.83	366	8.802	9.111	8.364	1.60	5924	3.8	2.85	2.139	221.34
		1.27	-43.97	8.75	369	12.995	-	-	-	-	-	-		

6. For those secondary stars that have Teff listed, the range is ~4800K to ~5200K. Based on the Gaia H-R diagram, using the (G_{BP} - G_{RP}) color index, this temperature range corresponds roughly to spectral types G8 through K2; therefore, these are apparently common dwarfs. None of these secondaries are red dwarfs (cooler than ~3800K), but later releases may include more red dwarfs.
7. The large Radius and Luminosity of several of the primary stars indicate that they are giants or subgiants.
8. In most binary systems, the secondary star is cooler than the primary, but the secondary star of COU305 is hotter. The cooler primary appears so much brighter (G ~ 5) because it is likely a red giant, almost 14 times the size of the sun.

7. Discussion

While conducting the photometric measurements on the bispectrum-reconstructed images, several questions arose regarding the accuracy of the inferred values. This section summarizes these questions.

As stated in Sec. 6, estimation of the magnitude of each component is carried out using a small circular aperture centered around the component. A question naturally arising is how "small" this aperture should be.

In "classical", single star, photometry, the aperture size is generally simply chosen to include the seeing disk and exclude any other nearby star. For close double stars the situation is more complicated because the involved plate scales generally make the instrumental diffraction pattern – Airy disk and rings – apparent, as evidenced in Plates 1-11.

At first sight, and since the goal of photometry is to capture all the star's light in the aperture, it could seem that the bigger the aperture is the more accurate the measurement is. But large apertures create two problems. First, for faint stars, as the aperture increases, the background soon starts adding noise faster than captured starlight. Second, for very close stars, the diffraction rings of both components are overlapping, so that measuring the magnitude of a companion with an aperture too large may include some light from the bright primary star's rings.

This suggests using an aperture no bigger than the Airy disk. Using the Airy disk of the primary star for sizing the aperture appears reasonable. After all, the theory says that the angular diameter of this disk only depends on the telescope aperture and the observed wavelength and hence is the same for all stars in the same image. In practice, it appears smaller for faint stars because, in this case, only the central, brightest area emerges from the noisy background. This means that using an aperture derived from the Airy disk of the brightest component for measuring the faintest could lead to contamination by the background noise and/or the light of the primary.

As a result, we chose to size the measurement aperture using the image of the faintest star. In practice, we brighten the image until the background becomes visible, to identify the region where the faint star merges into it. And we use the same size aperture for the brightest star. This way we obviously measure *less than all* the light for both stars, but still the *same proportion* for each one.

An extra complication arises when the faint companion sits on (or partly on) a diffraction ring from the primary. In this case it will appear artificially brighter because of that contaminating light, making the delta magnitude smaller than it should be. To address that problem, we might, in the future, use a two-step sequence. First, the instrumental magnitude of the faint star alone could be obtained using the same size aperture for both star and background, but with the background located on the same ring nearby. Then the bright star could be measured in the usual way, with its background aperture in a dark region, to get its instrumental magnitude separately. The final measurement would be obtained by just taking the difference. We have not used this procedure yet. It might be a useful technique, but it is difficult to know whether it would really improve the accuracy of the differential magnitude.

8. Conclusion and Perspectives

The results reported in this paper confirm that bispectrum analysis, as supported by the latest versions of the *Speckle ToolBox* software, not only gives astrometric results on a par with those provided with autocorrelation based methods, but also solves the classical quadrant ambiguity problem.

Results for photometric measurements, in the case of large differential magnitudes pairs, are also encouraging, although requiring further investigation. Concerning the measurement process itself, the influence of the various noise sources and distortions on the shape of the reconstructed PSFs and, in turn, on the accuracy of the final measure remains to be quantified, as does the optimal aperture (in terms of a fraction of the Airy disk) used for measuring the individual magnitudes. The use of a standard photometric system (e.g., Johnson -Cousins or Sloan) may also be necessary to achieve more consistent and astro-physically meaningful results.

Automation of multi-band speckle interferometry

(Text continues on page 726)

Bispectrum-based Measurements of Close Large-Differential-Magnitude Visual Double Stars

AC	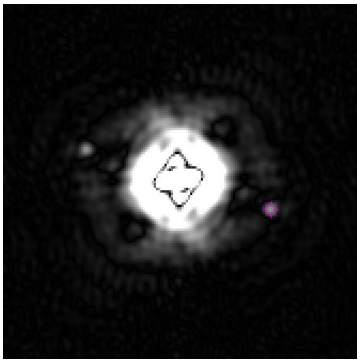	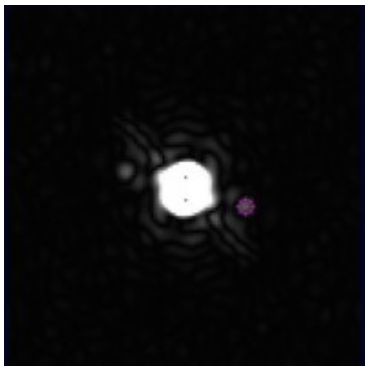	Plate 1 WDS 13122+1608 A 2225
BS	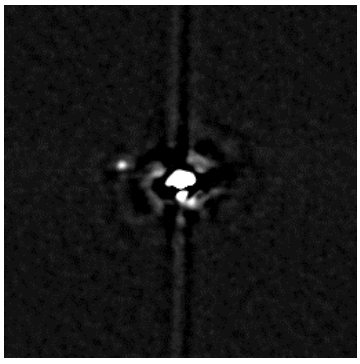	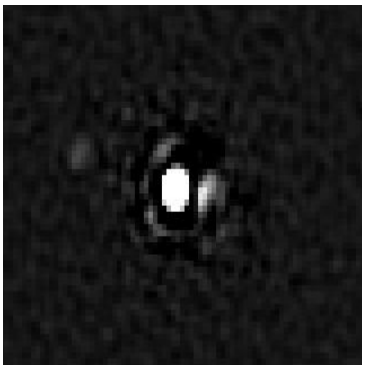	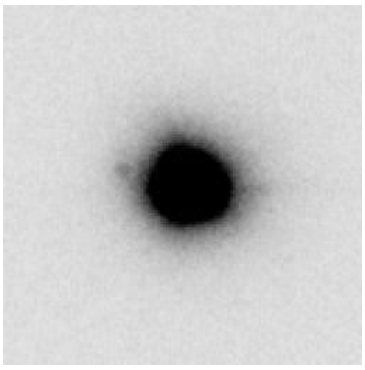
	RW	JS	LS

AC	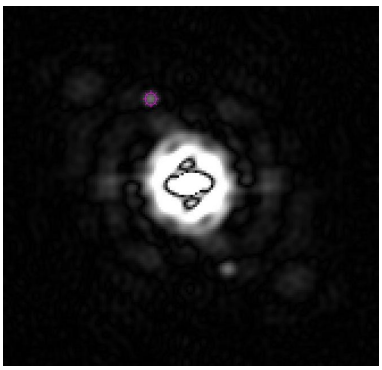	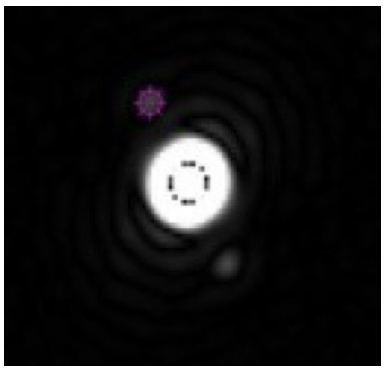	Plate 2 WDS 14122+4225 HO 57
BS	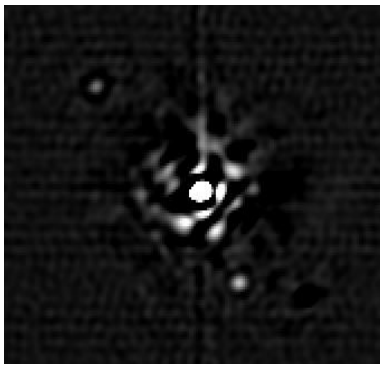	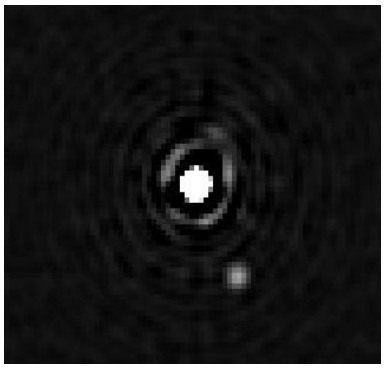	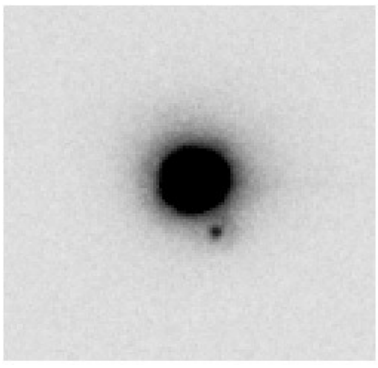
	RW	JS	LS

Bispectrum-based Measurements of Close Large-Differential-Magnitude Visual Double Stars

AC	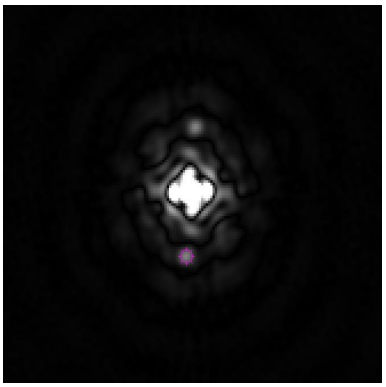	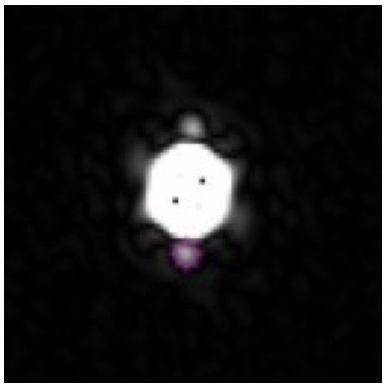	Plate 3 WDS 14171+5433 BU 1271
BS	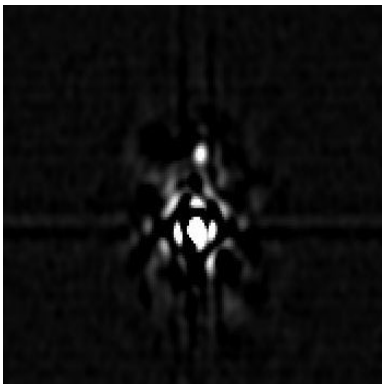	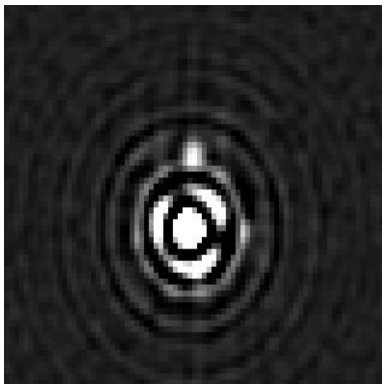	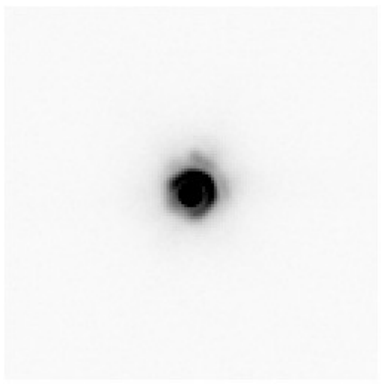
	RW	JS	LS

AC	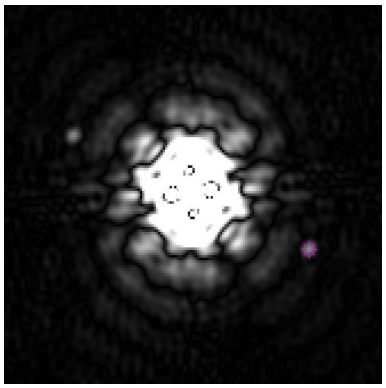	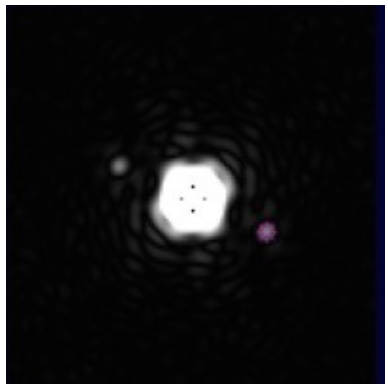	Plate 4 WDS 14525+2348 COU 305
BS	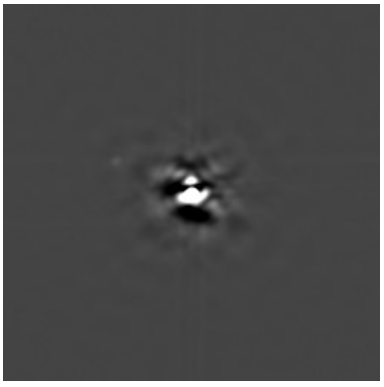	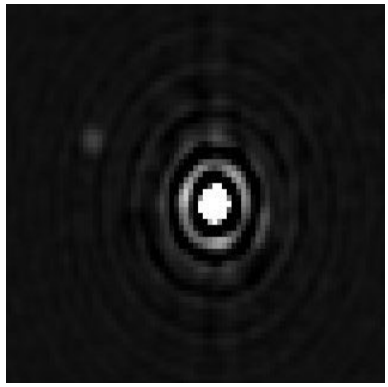	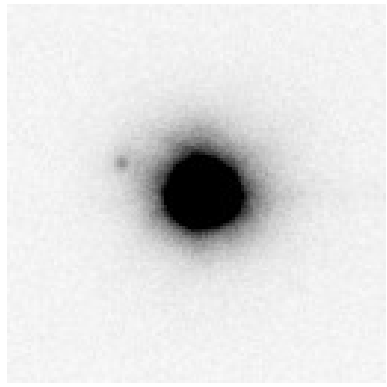
	RW	JS	LS

Bispectrum-based Measurements of Close Large-Differential-Magnitude Visual Double Stars

AC	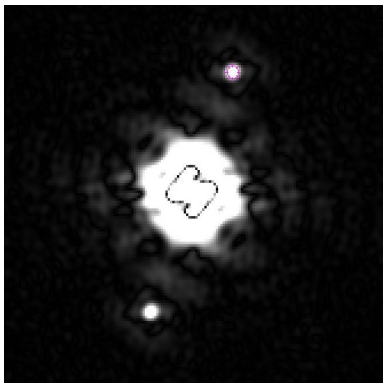	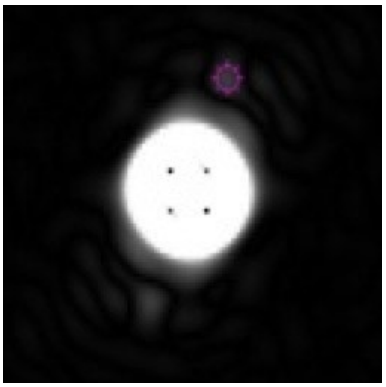	Plate 5 WDS 15190+2541 LDS6304
BS	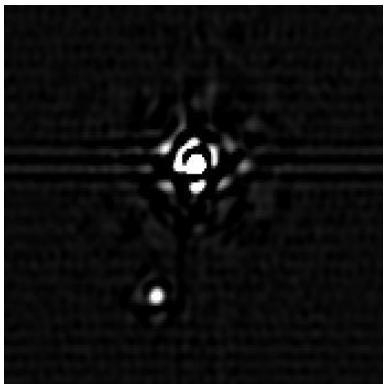	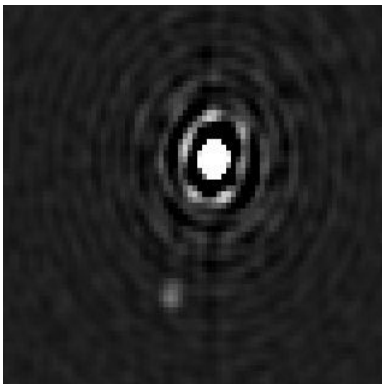	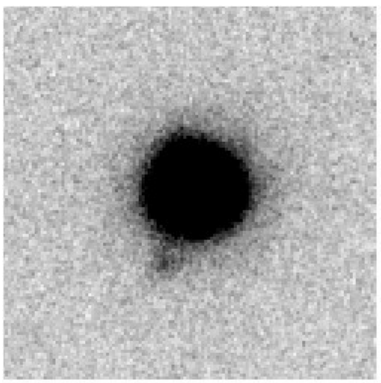
	RW	JS	LS
AC	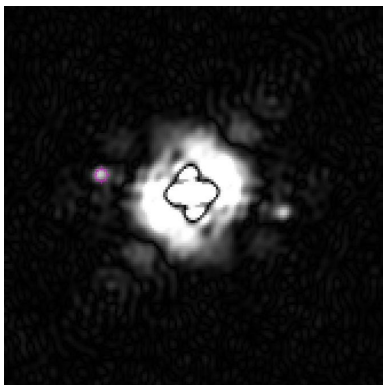	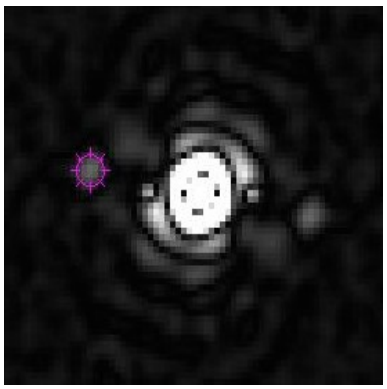	Plate 6 WDS 15483+1400 A 1637
BS	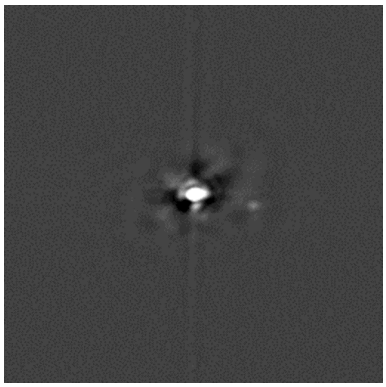	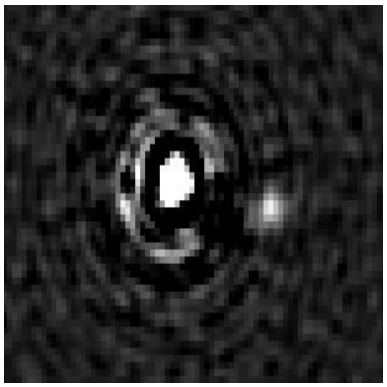	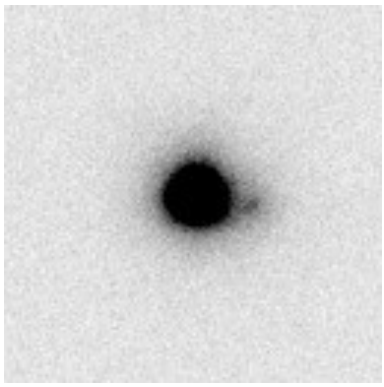
	RW	JS	LS

Bispectrum-based Measurements of Close Large-Differential-Magnitude Visual Double Stars

AC	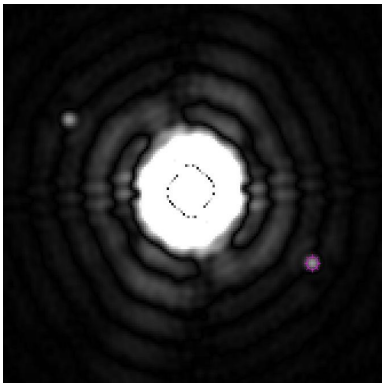	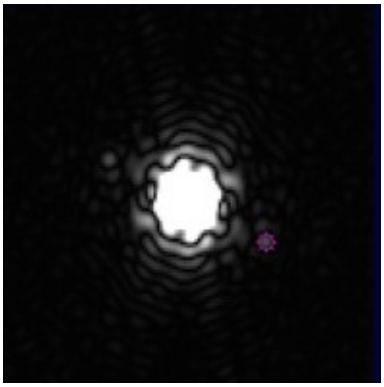	Plate 7 WDS 15536+1604 A 2079
BS	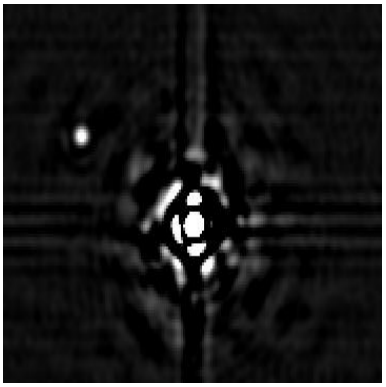	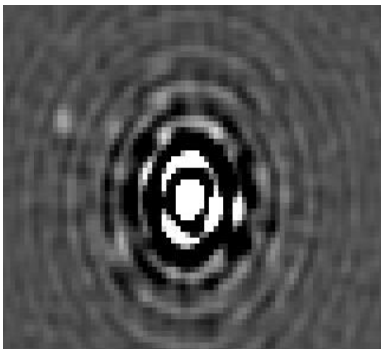	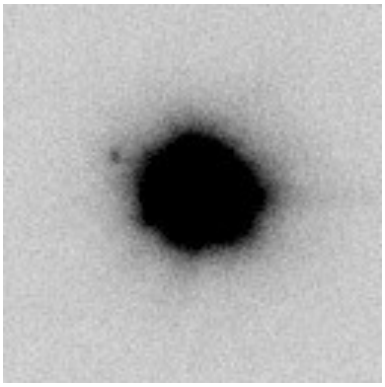
	RW	JS	LS

AC	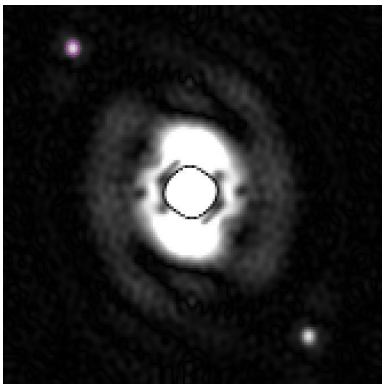	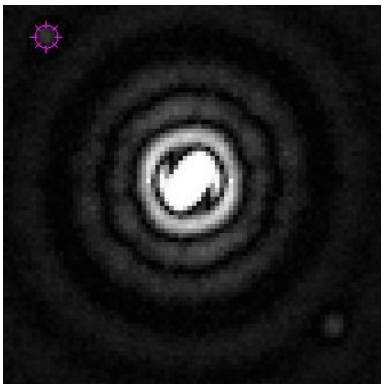	Plate 8 WDS 16315+3331 BU 816
BS	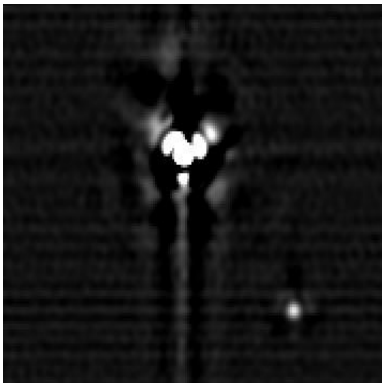	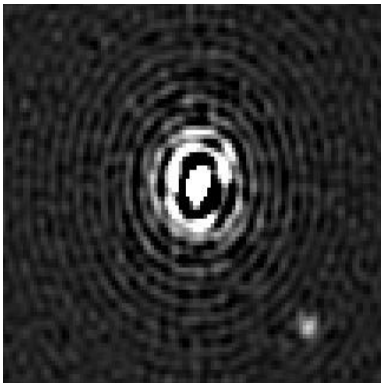	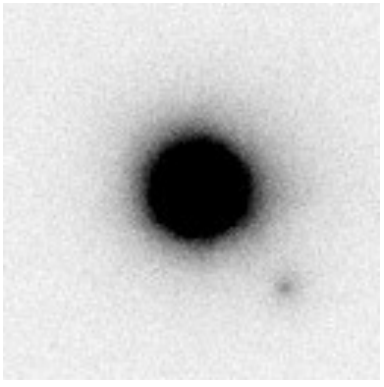
	RW	JS	LS

Bispectrum-based Measurements of Close Large-Differential-Magnitude Visual Double Stars

AC	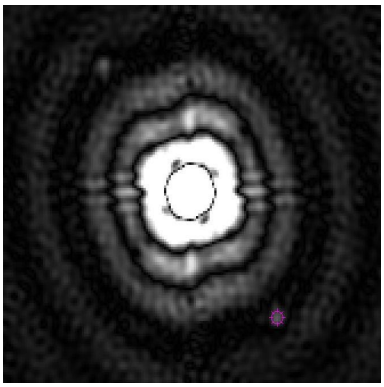	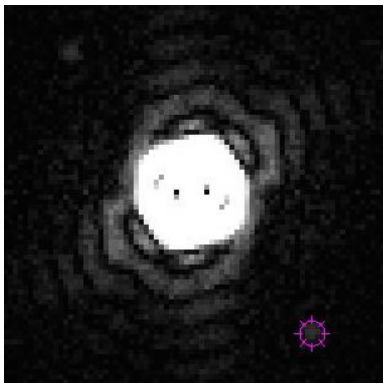	Plate 9 WDS 16335+3030 BU 818
BS	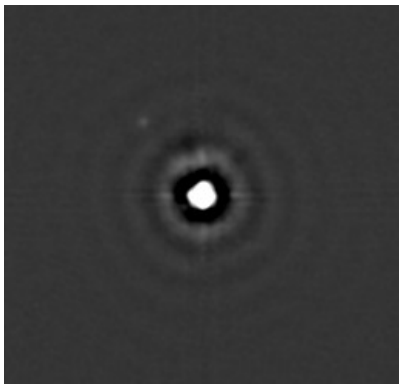	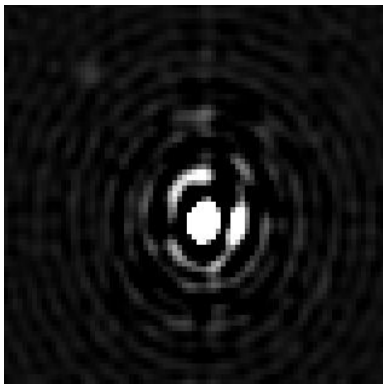	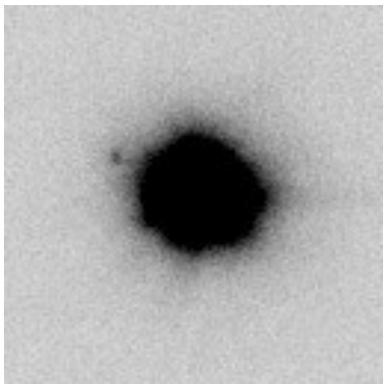
	RW	JS	LS

AC	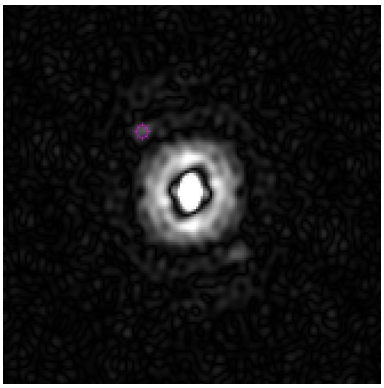	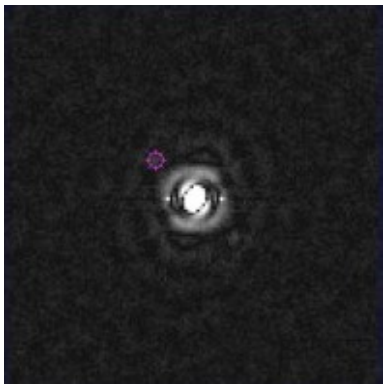	Plate 10 WDS 16529+4608 A 1869
BS	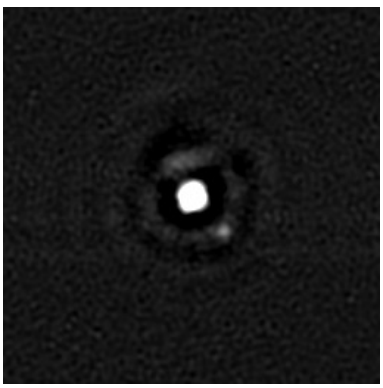	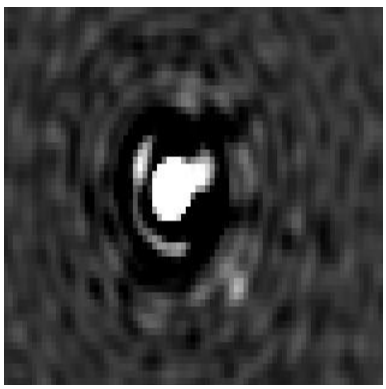	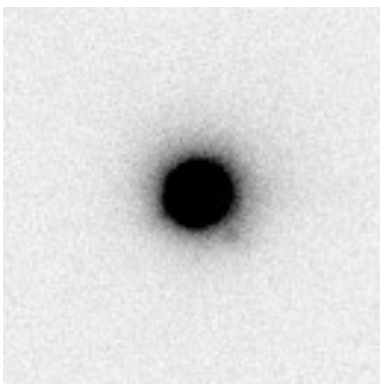
	RW	JS	LS

Bispectrum-based Measurements of Close Large-Differential-Magnitude Visual Double Stars

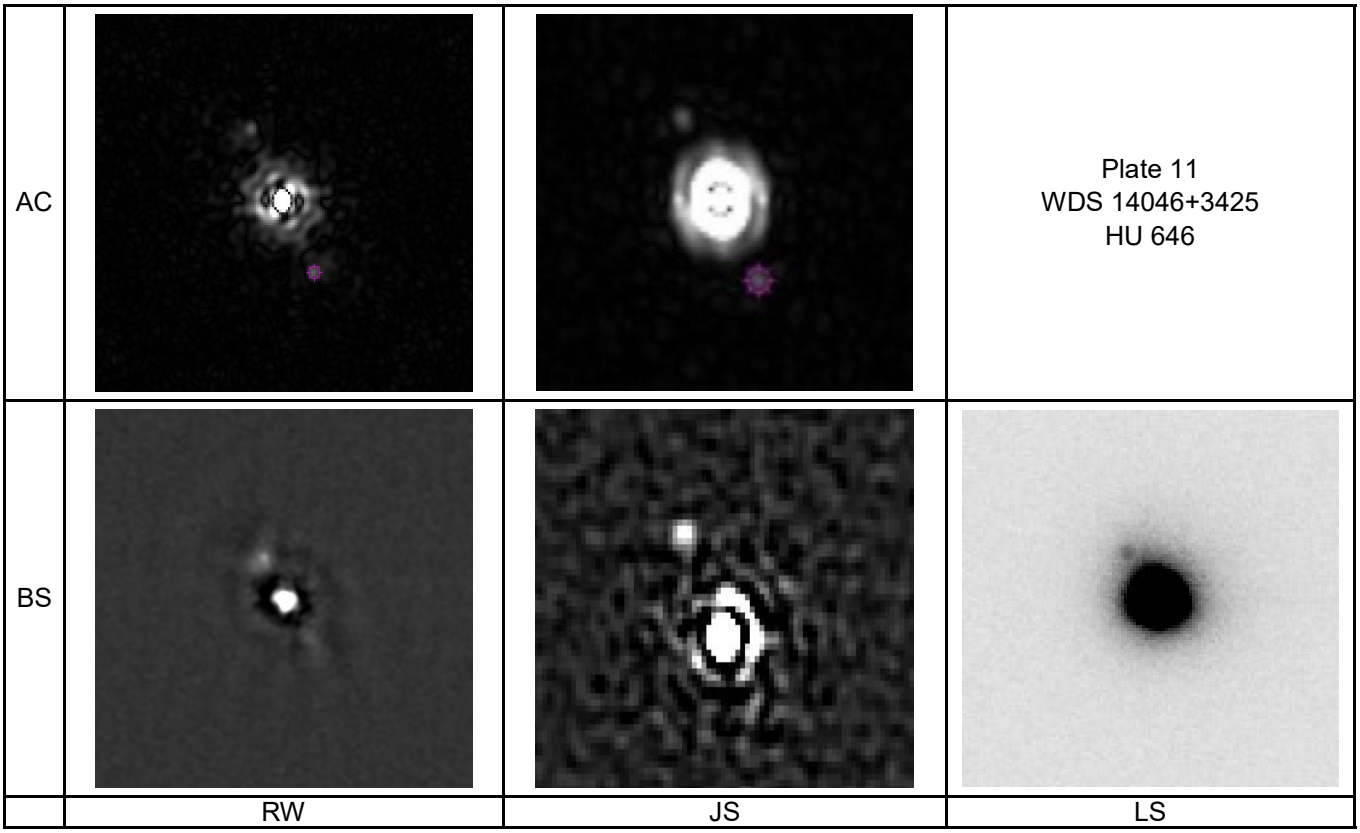

(Continued from page 720)

and bispectrum analysis should facilitate large-scale observational programs that could result in the discovery and subsequent follow-up observations of double stars with faint, late-M companions. This appears to be feasable, and efforts are underway to achieve full automation.

9. Acknowledgements

This research made use of the Washington Double Star Catalog, maintained by the U.S. Naval Observatory, of the REDUC software, developed and maintained by F. Losse, and the Speckle ToolBox software developed by D. Rowe. The authors would like to thank V. Wallen for her careful proof-reading of the final manuscript and R. Harshaw for the very interesting discussions we had throughout the project and his suggestions.

This work has made use of data from the European Space Agency (ESA) mission Gaia (https://www.cosmos.esa.int/gaia), processed by the Gaia Data Processing and Analysis Consortium (DPAC, https://www.cosmos.esa.int/web/gaia/dpac/consortium). Funding for the DPAC has been provided by national institutions, in particular the institutions participating in the Gaia Multilateral Agreement.

10. References

Anderson, J., 1991, "Accurate masses and radii of normal stars", *A & Arv,* **3**, 91.

Dupuy, T., Liu, M., & Ireland, M., 2012, "Testing theory with dynamical masses and orbits of ultracool binaries", ASP Conference Series, in press.

Edward L., Genet, R., Ridgely, J, Rowe, D., Zimmerman, N., "Observation of Large-Delta-Magnitude Close Binaries with Shaped Aperture Masks", 2015, *Journal of Double Star Observations,* **11**, 343.

Foley, E., Genet R., Ridgely J., Rowe D., Zimmerman N., 2015, "Observation of Large Delta Magnitude Close Binaries with Shaped Aperture Masks",

JDSO, 11(1s), pp 343-360.

Harshaw, R., Rowe, D., and Genet, R., 2017, "The Speckle Toolbox: A Powerful Data Reduction Tool for CCD Astrometry", *Journal of Double Star Observations*, **13**, 52-67.

Horch, E.P., Meyer, R.D. and van Altena, W.F., 2014, "Speckle Observations of Binary Stars with the WIYN Telescope-IV-Differential Photometry", *AJ* **127**, 1727-1735.

Kasdin, J., Vanderbei, R., Spergel, D., and M. Littman, 2003, "Extrasolar planet finding via optimal apodized-pupil and shaped-pupil coronographs." *ApJ*, **582**, 1147. http://adsabs.harvard.edu/abs/2003ApJ...582.1147K

Losse, F. Reduc, v5.0, 2017, http://www.astrosurf.com/hfosaf

Mason,D.B., Wycoff G.L., Hartkopf, W.I. Washington Double Star Catalog, 2015. http://www.usno.navy.mil/USNO/astrometry/optical-IR-prod/wds/WDS

Sérot, J., 2015, "Measurements of double stars using a 280 mm reflector and an EM-CCD: 2014-2015 report", *JDSO*, **11**(1s), 361-380.

Sérot, J., 2016a, "Speckle Interferometry of Close Visual Binary Stars with a 280 mm Reflector and an EM -CCD", *JDSO*, **12**(5), pp 488-499.

Sérot, J., 2017, "Measurements of Close Visual Binaries with a 280 mm Reflector and the ASI 290MM Camera", *JDSO*, **13**(2), 268-284.

Sérot, J., 2018a, "Measurements of visual binary stars with M-type companions with a SWIR camera and a 280 mm reflector", *JDSO*, **14**(1), 78-82.

Sérot, J. and Communal, J.E., 2018b, "Measurements of close visual binary stars at the Observatory of Saint-Véran", *JDSO*, **14**(3) 476-486.

Sérot, J., 2018c, "Measurements of Aitken visual binary stars : 2017 report", *JDSO*, **14**(3), 527-537.

Sivaramakrishnan, A., Koresko, C., Makidon, R., Berkefeld, T., & Kuchner, M., 2001, "Ground-based coronography with high-order adaptive optics", *AJ*, **552**, 397.

Singh, G., Martinache, F., Baudoz, P., Guyon, O., Matsuo, T., & Clergeon, C., 2013, "Lyot-based ultra-fine pointing control system for phase mask coronagraphs", *Proceedings of AO4ELTs3 Conference*: Paper 12667.

Vanderbei, R., Spergel, D., & Kasdin, J., 2003, "Spiderweb masks for high-contrast imaging", *AJ*, **590**, 593.

Wasson, R., 2018, "Speckle Interferometry with the OCA Kuhn 22" Telescope", *JDSO*, **14**(2), 223-241.

CCD Astrometric Measurements of WDS 04346-7015 GL 203 AB

Jeremy Ha[1], Alex Falatoun[2], Shannon Detwiler[1], Sean Gillette[2], Pat Boyce[2], and Grady Boyce[2]

1. San Dieguito Academy HS, Encinitas, California
2. Boyce Research Initiatives and Education Foundation (BRIEF), California, USA

Abstract: The multi-star system 04346-7015 GL 203 AB was observed during the fall of 2017. It contains a primary and 2 secondaries. Our 2018 measurement of the AB system indicated a position angle of 347.8° and a separation of 6.77", compared to the most recent prior measurement in 2005 with a position angle of 351° and a separation of 6.5". We attempted to measure the AC pair but were unsuccessful.

Introduction

DoubleSTARS is a project offered through Boyce Research Initiatives and Research Foundation (BRIEF) for high school and community college students to gain hands-on experience in the scientific process.

Within the context of double stars, there are two types: optical double star and those that are gravitationally bound, known as binary stars. Optical doubles are stars that visually appear close to one another, however may be hundreds or thousands of lightyears apart without a gravitational connection. If, however, it can be determined that the stars are close enough together that there is a gravitational association, the stars are considered a binary star system. A method of detecting a physical association between stars is by measuring their position angle, θ, and separation distance, ρ, over time to determine their relative motions and determine whether a gravitational link exists.

The star system WDS 04346-7015 GL 203 AB (henceforth referred to as GL 203) was selected because it has only two measurements from 1999 and 2005, Table 1, and it has been more than 10 years since the last measurement, so another measurement would be beneficial to see possible changes that could lead to a determination of the nature of this star system. GL 203 is a triple star system in Dorado. The A, B, and C components have a magnitude of 14.71, 18.9, and 19.55 respectively.

Table 1. Historical measurements for WDS 04346-7015 GL 203 AB. Position angle is measured in degrees and separation distance in arcseconds.

WDS 04346-7015GL 203 AB			
Epoch	Components	θ (°)	ρ (")
1999	AB	352	6.4
2005	AB	351	6.5

The goal of this study was to measure the current separation distance and position angle from the selected double star systems. In obtaining these measurements, we can provide supporting evidence whether or not these systems are either physically associated or just aligned by chance along our line of sight.

Equipment, Observations, and Data Analysis Procedures

Equipment

CCD images were taken using the T27 (Figure 1) and T13 (Figure 2) telescopes, part of the iTelescope network. T27 is located in New South Wales, Australia and is the largest telescope on the iTelescope network. T27 is a Corrected Dall-Kirkham Astrograph with an aperture of 700 mm, a focal length of 4351 mm and a focal ration of f/6.6. Coupled with the FLI PL9000 CCD, it takes images at 0.53 arc-secs/pixel, a high resolution necessary for finding closely spaced stars.

Additional images were taken using the T13 telescope because its lower resolution allows for stars with separations greater than 900 arcseconds. Located in New South Wales, Australia, T13 is an Apochromatic Refractor with an aperture of 90mm, a focal length of 504 mm and a focal ratio of f/5.6. The CCD for the T13 is a SBIG ST2000 XMC with a resolution of 3.02 arc-secs/pixel housing an array of 1600 by 1200 pixels with a FOV of 60.5 x 80.7 arc-mins.

Results

Multiple images were taken with T27 for the close-

Figure 1. Planewave 27" (0.7m) CDK700WF. CDK Astrograph with TEL 0.70-m f/6.6 reflector and CCD in Siding Spring, Australia

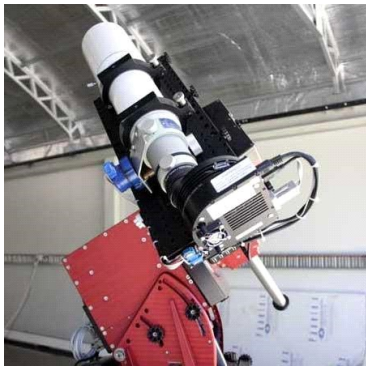

Figure 2. Takahashi SKY90. Apochromatic Refractor

ly spaced AB pair, and T13 for the significantly wider AC pair. We were unable to locate the AC pair with T13, and therefore these images were not used in this paper. The results of the images acquired with T27 are outlined in Table 2.

Analysis Procedures

All images were calibrated (flat-fielded and dark subtracted) by the iTelescope network. Each image was checked for oversaturation. After assessing the quality of the images, they were imported to MaximDL in order to assign World Coordinate System (WCS) positions using the Pinpoint Astrometry program, which compares the image to the Naval Observatory's Catalogue (UCAC4). Then, they were opened using Mira Pro x64, an astronomical image opening program. The AB stars acquired with T27 are outlined in Figure 3.

Discussion

Although there are only two recorded measurements for the AB pair, a small change in theta of 4° was observed with little change in rho since the initial 1999 measurement. These results are consistent with the existing trend of the AB pair.

The separation of the AC pair at 856.7" provided a challenge to measure. Imaging through T13 was unsuccessful at detecting the C component and it was not possible to identify in any image. An additional possible factor in failure to locate the C component is its reported magnitude of 19 and crowded star field. Thus, the AC component was not measured for this pair.

Table 2. *Position angle, separation distance, and uncertainties for GL 203 AB*

WDS 04346-7015 GL 203 AB					
Epoch	Number of Images	Mean θ (°)	σ_θ (°)	Mean ρ (″)	σ_ρ (″)
2017.87	2	347.82	0.715	6.77	0.018

Conclusion

The new data seems reasonable when referenced to past data. None of the images were able to clearly show the location of the C component. This was expected given it's extreme separation and minimal magnitude. More observations are needed for further confirmation of this assumption.

Acknowledgements

We would like to thank Pat and Grady Boyce of the Boyce Research Initiatives and Education Foundation (B.R.I.E.F.) for their nonstop encouragement, instructional support, and financial sponsorship that allowed us to use the iTelescope robotic telescope system and Mira Pro x64 software tools. This research has made use of the Washington Double Star Catalog maintained by the U.S. Naval Observatory and the telescopes of the Siding Spring Observatory, Australia. This research made use of data provided by Stelle Doppie.

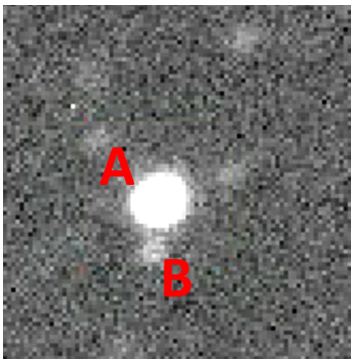

Figure 3. *T27 telescope with Luminance Filter at 270 seconds; captured using Mira Pro x64. This image shows the primary star and B component.*

References

Polski, R., Soszynski, I., Udalski, A., Szymanski, M.K.. Kubiak, M., Pietrzynski, G.,Wyrzykowski, L., Ulaczyk, K, 2012, "The Optical Gravitational Lensing Experiment. The Catalog of Stellar Proper Motions toward the Magellanic Clouds", *Acta Astr.* **62**, 1. Retrieved December 23, 2017 from https://arxiv.org/pdf/1203.2649.pdf

Shattow, G., Loeb, A., 2013, "Implications of Recent Measurements of the Milky Way Rotation for the Orbit of the Large Magellanic Cloud", *Monthly Notices of the Royal Astronomical Society: Letters,* 392: L21. Retrieved December 23, 2017 from https://arxiv.org/pdf/0808.0104.pdf

The Washington Double Star Catalog, 2012, retrieved Ocotber 06, 2017, from http://www.usno.navy.mil/USNO/astrometry/optical-IR-prod/wds/WDS

Astrometry of STF 1985 Shows Continued Off-Orbit Path

Beckett Andersen[1], Jon-Paul Ewing[1], Adrian Griffin[1], Beatriz Lopez[1], Kate Reupold[1], Katherine Pham[1], Rachel Freed[2], Richard Harshaw[3], and Russell Genet[4,5]

1. Paso Robles High School, CA
2. Sonoma State University, CA
3. Brilliant Sky Observatory, AZ
4. Cuesta College, San Luis Obispo, CA
5. Cal Poly State University - San Luis Obispo, CA

Abstract: A team of high school students from Paso Robles observed the double star STF 1985 which had an orbital plot that did not fit the most recent observations. The student team's observational data point continued the off orbital plot path.

Introduction

There are two types of double stars. The first type, an optical double, are two stars that appear to be close together but in actuality are separated by vast distances (upwards of several hundred light years). From the perspective of Earth, however, they line up and appear as a double star. The second type of double stars are gravitationally bound binaries that orbit each other.

The binary we observed was STF 1985. It was discovered in 1823 by John Herschel. However, in 1831, Friedrich Georg Wilhelm von Struve made multiple observations with a larger telescope and is credited as the discoverer of the binary. It has been observed 182 times since its discovery. In the early 1990's, STF 1985 was observed by the Hipparcos space telescope and the most recent observation was in 2015. Recent observations of STF 1985 seem to be creating a path that is veering off the orbit (Figure 1) calculated by Josef Hopmann (1973).

Earlier measurements (green data points) were visual observations with micrometers and are widely scattered. The pink points are photographic measurements.

Our research question: When we add another observation, will our measurements lend support to the current published orbit or will it provide more evidence that the orbital path of STF 1985 needs revision? To answer the research question, we needed to measure the separation (in arc seconds) and position angle (in degrees) of the dimmer secondary star with respect to the brighter primary star.

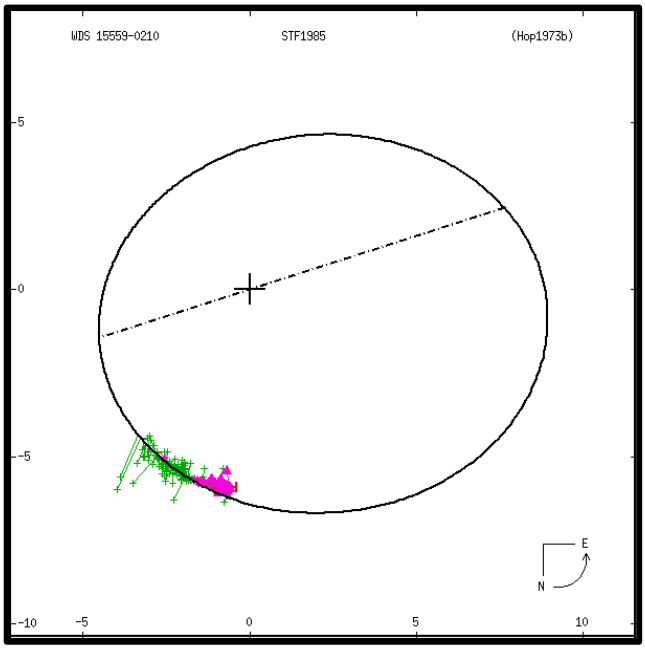

Figure 1. STF 1985 orbital plot.

Equipment and Procedures

To gather data on this binary we used the Las Cumbres Observatory (LCO) worldwide network of robotic telescopes. There are eight LCO sites that, together, host 21 telescopes. The geographic spread of the sites allow continuous observation of the night sky. All our

Astrometry of STF 1985 Shows Continued Off-Orbit Path

observations were made with the 0.4 meter LCO telescope in Siding Spring, Australia. Although several different exposures were used, we found that 0.785 seconds gave the most consistent results and we used images with these exposures.

When we selected this close binary star for observation, we were unaware that LCO used 2x2 binning, which created some difficulties for image processing due to the low resolution. The images were analyzed using AstroImageJ (Collins, 2017).

Results

Five CCD observations were obtained on April 18th, 2018 (2018.296). We found, probably due to the small separation of the two stars and 2x2 binning, that AstroImageJ did not provide precisely the same astrometric solution for an image if a second solution was obtained. To reduce this variance, we obtained five solutions for each image and averaged them. The five solutions for our first image are provided in Table 1. The variance in the other four images were similar.

The average values of the separation and position angles for each image are provided in Table 2, along with the final average of the averages, which was a measured separation of 6.00 arcseconds and the position angle of 356.87 degrees.

Discussion

The measured values for position angle and separation are close to the expected linear trend line for past observations, see Figure 2. We did notice that the position angle of our observation was a little off the trend line. This may be due to the difficulty AstroImageJ had with the poor resolution of the binned images.

Future student teams should be careful when requesting images for binaries that are closer than 10 arcseconds. If they are, be sure to request unbinned images to increase resolution.

Table 1: Repeated solutions of the same image (#355) using AstroImageJ

Trial #	Separation (as)	Position Angle (deg)
1	5.91	358.10
2	5.43	357.53
3	5.43	357.53
4	5.91	358.10
5	5.91	358.10
6	5.91	358.10
Average	5.75	357.91
Standard Deviation	0.25	0.29
Error	0.10	0.12

Table 2: Average separation and position angles of STF 1985 from 5 images

Image #	Separation (as)	Position Angle (deg)
355	5.75	357.91
356	5.92	357.98
357	5.85	356.11
358	6.01	356.79
359	6.22	356.60
Average	6.00	356.87
Standard Deviation	0.18	0.83
Error	0.08	0.37

The observations were plotted on the orbital plot using the procedure outlined by Robert Buchheim (2017). Unfortunately, the image we used had been

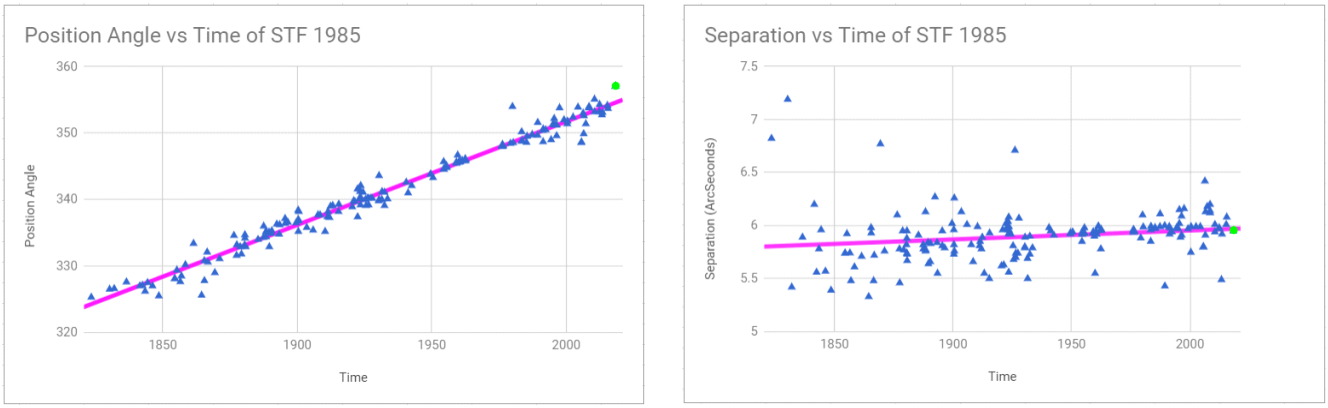

Figure 2. Position angle and separation versus time using historical data on STF1985. A linear trend line is shown for reference. The round green dot is our observation.

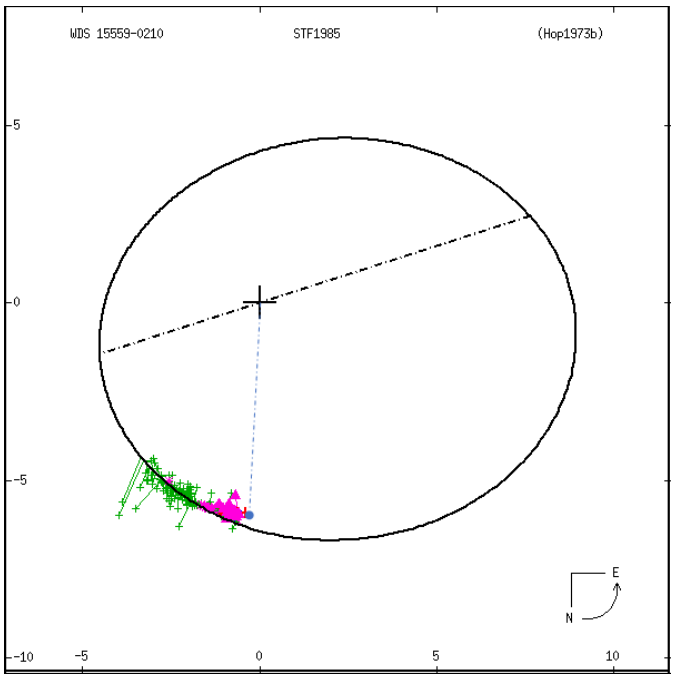

Figure 3. Correctly scaled orbital plots for STF 1985. Accidental re-sizing almost led to an inaccurate conclusion regarding our observation.

stretched horizontally by a team member when resizing for this paper. We then noticed the scale on the Y-axis was smaller than the scale on the X-axis so we returned to the original image downloaded from the WDS Catalog. Our corrected plot of our observation then aligned well with past observations, including the most recent observation in June 2017 (Musegades, 2018). The revised graph is shown in Figure 3.

Conclusion

The objective of this research was to collect observational data on a well-studied binary and measure its position angle and separation. Even with poor resolution, the image analysis software was able to give fairly consistent results and the objective was met.

Acknowledgements

We acknowledge Las Cumbres Observatory for making the observations. Brian Mason at the US Naval Observatory supplied us with past observations of STF 1895. Karen Collins' AstroImageJ was used for our image analysis. We thank Cuesta College for offering Astronomy 299 Seminar to high school students this Spring and Paso Robles High School for their ongoing support of science education and getting students out in the field to do real scientific research. Finally, we thank Vera Wallen for her review of this paper.

References

Buchheim, R., 2017, "Displaying New Measurements on WDS Orbit Plots", *Journal of Double Star Observations,* **13** (2), 233.

Collins, K., Kielkopf, J., Stassun, K, and Hessman, F., 2017, "AstroImageJ: Image processing and Photometric extraction for ultra-precise astronomical light curves", *The Astronomical Journal,* **153**, 77.

Hopmann, J., 1973, Untersuchungen IV, Sitzungsber, Österr. Akad. Wiss., Math.-Naturwiss. Kl., Abt. II, Band 181, p. 301 – 328.

Musegades, L., Niebuhr, C., Graham, M., Poore, A., Freed, R., Kenney, J.W., and Genet, R. M., 2018, "An Astrometric Observation of Binary Star System WDS 15559-0210 at the Great Basin Observatory", *Journal of Double Star Observations,* **14** (2), 197-200.

Gaia DR2 and the Washington Double Star Catalog: A Tale of Two Databases

Richard Harshaw
Brilliant Sky Observatory, Cave Creek, AZ
rharshaw51@cox.net

Abstract: A large-data extraction of the Washington Double Star Catalog (WDS) from Gaia's Data Release 2 (DR2) was done in early 2018. This data was read into an Excel spreadsheet and calculations on distance, relative motion through space, R2 fit to trend lines in the data, and relative radial velocities vis a vis system escape velocity were done. The process generates "weighting factors" for each of these four areas. Actual binaries will score high in the overall weighting of these factors, while optical pairs will score low. The result reveals that less than half of the WDS (42%) is actually physical with a very large group (33%) of unknown status (due to a lack of good data to perform the necessary calculations).

1. Introduction

The release of Gaia DR2 in April of 2018 bears seeds that will revolutionize double star astronomy forever. From the mission's home page, we find this statement of vision: "Gaia is an ambitious mission to chart a three-dimensional map of our Galaxy, the Milky Way, in the process revealing the composition, formation and evolution of the Galaxy." [ESA,2018] And we can define "ambitious" as details on 1,692,919,135 stars! Launched on Dec. 19, 2013, the mission is planned to run to late 2019. To date, there have been two releases of data (DR1, released Sept. 14, 2016; and DR2, released Apr. 25, 2018). Two more are planned (DR3 slated for release late 2020, and DR4 slated for release at the end of 2022. The content of DR2 was about 3 orders of magnitude denser than DR1, while DR3 and DR4 will be refinements to the already incredible data in DR2.

2. The Gaia Instrumentation

Gaia was placed in a Lissajous orbit around point L2. Figure 1 gives a rough idea of where Gaia has been parked.

Missions parked at any of the Lagrangian points (the "L" points in Figure 1) will reside in places that require a minimum of expenditure of propellant to maintain mission orientation and stability and represent areas of space relatively clear of space debris by the gravitational balancing points of the earth and sun. (The James Webb Space Telescope is also planned for insertion at L2.)

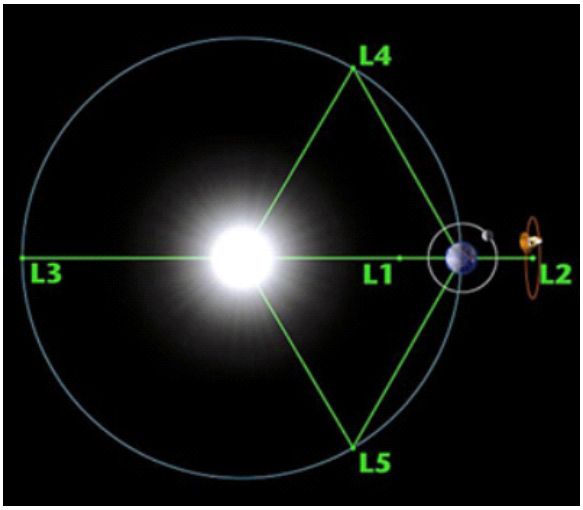

Figure 1. Gaia's Parking Station at L2

Instruments aboard the Gaia spacecraft include two star imaging systems (employing rectangular mirrors of large size), two photometers (red and blue), and a radial velocity spectrometer. These instruments are of exquisite precision and have given us literally an astronomical cache of data points about the stars surveyed.

3. Contents of DR2

One may access DR2 through the VizieR portal of the CDS service maintained by the Université de Strasbourg in France. I use this URL as my launching point for VizieR:

http://vizier.u-strasbg.fr/viz-bin/VizieR

Gaia DR2 and the Washington Double Star Catalog: A Tale of Two Databases

Currently, there is an icon at the top of the VizieR opening page that directs you to DR2 with a single mouse click (see Figure 2), but should the page design change after this paper is published, you can still retrieve DR2 by typing I/345/gaia2 into the catalog call window at the top of the page.

Once you click the Gaia DR2 hyperlink (or type the catalog call code), a menu of options fills the page. Besides the main DR2 catalog, there are 19 extractions that can be called for special research projects, but none of these falls under the domain of double star astronomy.

I therefore normally use the first entry on the selection form, "I/345/gaia2" by clicking the box in front of its listing and then clicking "Query Selected Tables".

That action opens the selection panel for what data you wish to view in DR2—and the list is very extensive! (The list extends over 5 screens down on my oversized monitor!)

You should then check the boxes for all the data you wish to retrieve. After that, you are ready to call up data on any star by using the Target Position input window at the top of the page. Here is where having the *precise* position of a double star is critical (and thankfully, the WDS does offer that datum on any star it lists). I usually open a downloaded version of the WDS and select the Precise Position for the star I want to research and paste it into the Target window.

Before you press the "Submit" button, I suggest you change the search radius from its default (2 arc minutes) to 1 arc minute, as you may well get data returned on hundreds of stars around the position you designate (depending, of course, on where your target lies with respect to galactic longitude and latitude). Clicking "Submit" will then return all the data for the stars within 1 arc minute of the precise position you designate.

As a safety check (to be sure I have the right stars in my query), I also click the "Start Aladin Lite" hyperlink above the results table to view a digitized image of the sky at this position.

DR2 can return data to you on a large number of parameters, including (but not limited to) the DR2 identifying number, precise position in the sky, parallax (and its error), proper motion vectors (and their errors), G magnitude (roughly equivalent to the visual magnitude; this number is *derived* from the R and B photometer data), B (blue) magnitude, R (red) magnitude, radial velocity and its error (in km/sec), and the effective surface temperature (T_{eff}, derived from the color photometers and estimates of distance based on the parallax). Data that is also reported (but derived from parallax and magnitudes) includes estimates of the star's radius and luminosity (both in solar equivalents). There is a lot more available than this, but these are the main items of interest to most double star researchers.

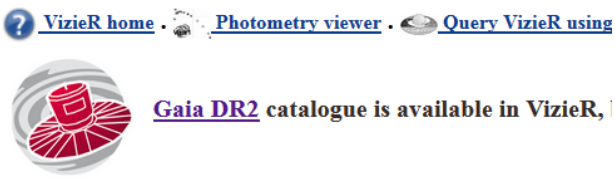

Figure 2: Link to DR2 at the top of the VizieR landing page.

The inclusion of estimates of stellar radii and luminosity based on parallax, magnitudes and temperature are also helpful as a second check on what the data might suggest. For instance, if the data show that the parallaxes of two stars are too different to permit the conclusion that the stars are binary, then a check of the luminosity for each star may help confirm that. If the companion star (usually fainter than the primary) is, in fact, quite a lot more luminous than the primary, this would confirm the suggestion that the stars are at vastly different distances.

4. The Power of Querying Large Databases

David Rowe, chief technical officer of PlainWave Instruments, is an expert on large databases. Soon after its release, he downloaded the entire DR2 database (it runs almost 8 TB!). After informing a team of us who use his Speckle Tool Box to do data reductions on our speckle measurements, we asked Dave if he could extract the Washington Double Star Catalog (WDS) from DR2? Within 24 hours, we had our catalog!

Rowe's extraction of the WDS from DR2 gives us extremely powerful tools to use in our research and saves us untold hours of time using the standard VizieR search process to get data on the stars we select for research.

Within a day or two of downloading a copy of Dave's WDS extraction, I had written routines that allowed my Excel version to compute distances to the stars (given their parallaxes and error estimates, when available, using the weighted parallax method I describe in Harshaw 2018. I had also developed subroutines that analyzed the proper motion data to compare how much the stars should have moved over a given time due to PM alone (and hence know if the PM vectors were accurate or not), and even derive estimates of the minimum distance between the members of a pair (the distance in parsecs times the separation in arc seconds) and stellar mass using the mass/luminosity relationship and DR2's B-R color indexes.

5. Factors That May Indicate Physicality

Let us define "physicality" as the likelihood that a given pair is traveling together through space, may have a common origin, and may, in fact, be in orbit around a common center of gravity. What things must be true for a pair to be physical?

First, the stars must have the same (or nearly the same) **parallax**. Rarely do both stars of a pair have the exact same parallax. So that is why it is necessary to estimate the likelihood that two stars are close enough to be gravitationally bound together by computing the total distance each parallax and its error projects and seeing if the distance "windows" overlap.

For example, suppose that two stars of a pair have parallaxes of 5.68 mas ± 0.06 mas for the primary star and 5.81 mas ± 0.05 mas for the companion. The parallaxes are not exactly equal, but what are the distance windows suggested by the parallaxes and the errors? For the primary star, the parallax could be anywhere from 5.68 + 0.06 = 5.74 mas to 5.68 – 0.06 = 5.62 mas. The distance in parsecs is simply the reciprocal of the parallax in arc seconds (not mas, so to do the calculation we must divide the parallax by 1000), giving us, for the primary star, 174 parsecs to 178 parsecs. For the companion, the parallax limits are 5.86 mas and 5.76 mas, resulting in distances of 171 parsecs to 174 parsecs. Since each star's distance window shares a common bound (174 parsecs), there is a significant chance (although not 100%) that the stars are within a parsec of each other. Is this close enough for gravitational binding?

On the surface, probably not. A survey of the 2,500+ orbits and their parameters from the 6th Orbit Catalog shows that very few known binaries have separations that exceed 3,000 AU, and most are closer than 1,000 AU. A parsec is approximately 192,000 AU, so two stars one parsec apart are probably too far apart to be gravitationally bound, even if they are very massive stars.

In a case like this, I use the weighted parallax method (cited earlier) to determine a weighted parallax (which yields 174 parsecs). If we know the separation (rho), we can easily estimate the *minimum* separation by multiplying the distance in parsecs by the separation in arc seconds. For example, if our sample pair had a value of rho of 1.26", the minimum separation would be 219 AU, well within the binding range of a physical pair. (We say *minimum separation* since we do not know the exact orientation of the system to our line of sight. The rho value we measure is a *projected* value on the plane of the sky. More than likely, the stars are not oriented orthogonal to our line of sight.)

In the analysis of the WDS extraction from DR2, I used a simple formula to assess how strong the parallax data might be in establishing physicality. That expression is given in Equation 1:

$$P_{px} = 1 - \left| \frac{P_d - C_d}{\frac{1}{2}\left(P_d + C_d\right)} \right| \qquad [1]$$

where P_d is the distance to the primary (in parsecs) and C_d is the distance to the companion. Thus, two stars with the same parallax will evaluate P to 1.00, while two stars with different parallaxes will evaluate P to something less than 1.00.

Once the parallax factor has been computed, we can move on to the analysis of the **proper motion vectors**. Two stars that are in orbit around one another should have identical, or very nearly identical, proper motions. Large differences in proper motion would suggest the stars are not gravitationally related. I evaluate the proper motion vectors with this rather complex expression (Equation 2):

$$P_{pm} = \left| 1 - \frac{\sqrt{\left(P_{pmra} - C_{pmra}\right)^2 + \left(P_{pmdec} - C_{pmdec}\right)^2}}{\sqrt{P_{pmra}^2 + P_{pmdec}^2} + \sqrt{C_{pmra}^2 + C_{pmdec}^2}} \right| * 0.15 \qquad [2]$$

where P_{pmra} is the primary star's PM vector in RA, P_{pmdec} is the primary's PM vector in DEC, and C_{pmra} and C_{pmdec} are the corresponding vectors for the companion. The 0.15 factor at the end is a weighting factor that I will explain in more detail shortly.

Thus it can be seen that two stars with exactly the same proper motion evaluate P_{pm} to 0.15 while stars with different proper motions will evaluate to something less than 0.15.

A third factor to consider is the line of best fit **R^2 value** for what appear to be linear and short arc traces on a plot of the data returned by a datarequest submitted to the USNO. I import all datarequest text files into an Excel spreadsheet I created that evaluates a number of items and plots the measurements on Cartesian coordinates, corrected for precession of the equinoxes. Most of the time, a plot of the data produces a scattered grouping of data like the one in Figure 3.

However, sometimes a data plot resembles Figure 4.

Here, the data clearly lies along a line. (The orange line is the proper motion resultant for the period between the first and last observations.) If we then click

Gaia DR2 and the Washington Double Star Catalog: A Tale of Two Databases

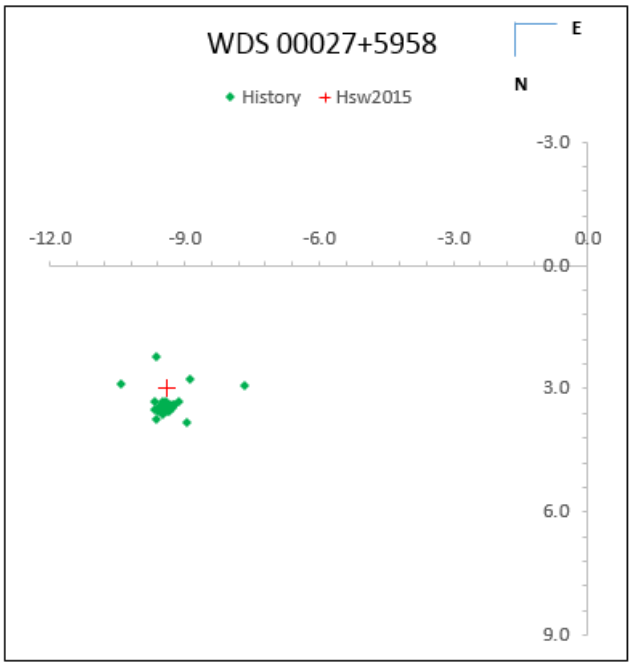

Figure 3. Plot of scattered measurements

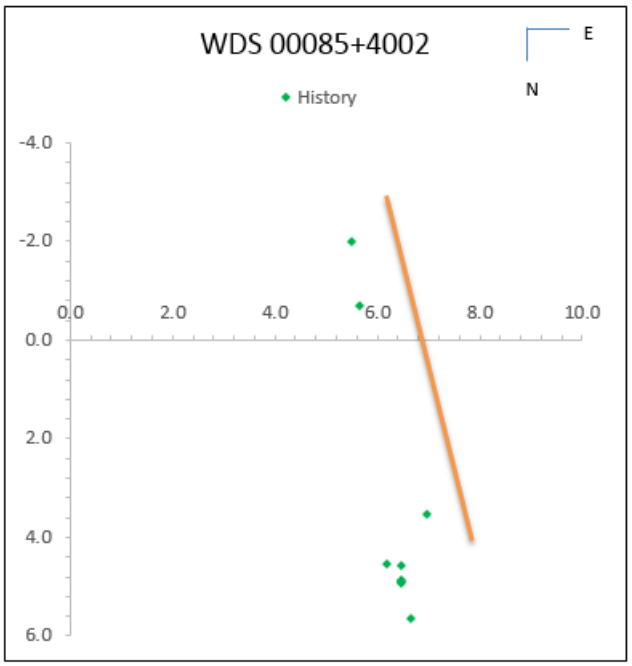

Figure 4. Plot of a linear nature

on any of the data points and ask Excel to generate a linear trend line, the graph looks like the one in Figure 5:

The closer the R^2 value is to 1.00, the better the fit of the data. 0.7135 is not a bad fit, but I have plots with values as high as 0.9989.

Similarly, an *exponential* trend line can be generated for cases that show an arc developing, like Figure 6.

When generating short arc trend lines, it is important that the projected curve enclose the (0,0) point of the graph. If the curve does not "wrap around" (0,0), the stars are not likely bound in an orbit.

However, extreme caution must be used when using the Excel Insert Trendline function with the request to see the R^2 value. By default, Excel assigns *equal weight to every measurement* while in practice, we need to assign varying weights to the measurements based on criteria covered already by the USNO at the 6th Orbit Catalog web page [USNO 2018].

The factor I use for R^2 values is only computed for those cases where I have generated graphs and have an R^2 value. If the plot shows a linear pattern, 10% of the R^2 value is *subtracted* from the final weight; if the pattern is of a short arc, 10% of the R^2 value is *added* to the final weight.

A fourth criteria to consider when determining physicality is the relative **radial velocities** of the stars compared to the escape velocity of the system. If the

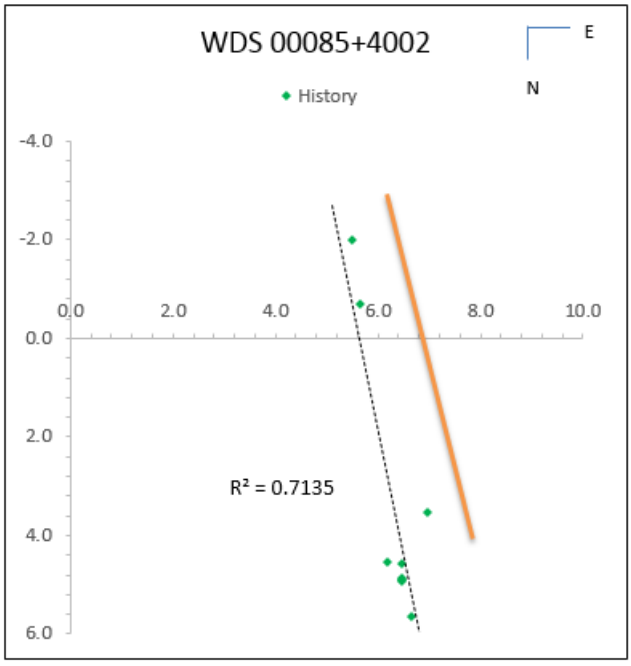

Figure 5. Plot with a linear trend line and R^2 value shown

stars are close enough by parallax to be physical, we can assess the probable masses of the stars using the mass/luminosity equations and determine a rough estimate of the masses of each star knowing their tempera-

Gaia DR2 and the Washington Double Star Catalog: A Tale of Two Databases

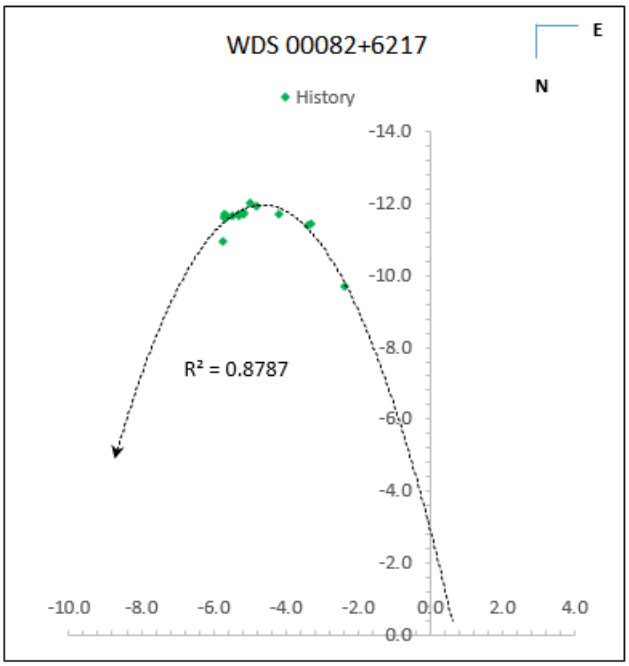

Figure 6. Plot of a short arc with high R^2 value

ture and luminosity. (The radius is also a helpful factor, but for DR2, the radius is a *derived* factor, not a directly -measured one like T_{eff}. Or course, DR2's luminosity figures are also derived from the measured magnitudes and distances as suggested by the parallaxes.)

To determine the escape velocity we use Equation 3:

$$V_{esc} = \frac{\sqrt{2GM_{Tot}}}{r} \qquad [3]$$

where G is the gravitational constant, M_{Tot} is the total mass of the binary system, and r is the distance between the two stars in parsecs [Wiley and Rica, 2015].

Meanwhile, the orbital velocity can be approximated by Equation 4:

$$V^2 = GM_{Tot}\left(\frac{2}{R} - \frac{1}{a}\right) \qquad [4]$$

Where G is the gravitational constant, M_{Tot} is the total system mass, R is the separation in AU, and a is the semi-minor axis in AU. To be on the safe side, I assume the system is not orthogonal to our line of sight and assume that the result of the equation is the absolute *maximum* possible for the system. Clearly if the difference in the radial velocities measured by Gaia exceeds this value, the pair will not be physical for long.

Estimating the total mass is tricky for cases where we do not have an orbital solution. We can estimate the masses based on the assumed values for luminosity, T_{eff}, and radius. Luminosity is related to mass by Equation 5:

$$\frac{L}{L_\odot} = \left(\frac{M}{M_\odot}\right)^n \qquad [5]$$

where L is the luminosity of the star in question, $L_\odot$ is the luminosity of the sun, M is the mass of the star in question, $M_\odot$ is the mass of the sun, and n is an exponent that varies with the luminosity class of the star. For bright massive stars, n averages 3; for sun-like stars, it runs closer to 4; and is about 2.5 for dim red dwarfs of low mass. But this holds for the Main Sequence only.

A second handle on the mass, possible with DR2's T_{eff} data, is given by Equation 6:

$$L \propto M^{3.5} \qquad [5]$$

where L is luminosity and M is mass, both relative to the sun.

A final approach to the mass problem can be derived by using the new Gaia DR2 H-R Diagram, shown in tiny form in Figure 7, and available on-line at https://physics.stackexchange.com/questions/402299/what-is-this-clump-of-hot-and-dim-stars-gaia-h-r-diagram and other URLs.

Here, one would need to enter the bottom of the chart using the B-R color index and then move up to the luminosity function to get an estimate on the star's spectral and luminosity classes. This is tedious work and the rough scaling on the vertical axis makes accuracy a challenge.

6. Combining Weight Factors

So we now have four weight factors that can be combined to give us an indication of the physicality of a pair:

1. Parallax analysis
2. Proper motion analysis
3. R^2 Fit analysis
4. Relative Radial Velocity analysis

Using parallax as the chief arbiter of physicality, I assign a relative weight of 75% to the parallax factor. I assign 10% weight each to the proper motion and R^2 factors, and 5% to the radial velocity factor, for a total of 100%.

Building the factor equations and weighting process into my Excel version of the WDS extraction from DR2 quickly yields estimates of physicality for all the stars in the WDS catalog. The closer to 1.00 the total weights

Gaia DR2 and the Washington Double Star Catalog: A Tale of Two Databases

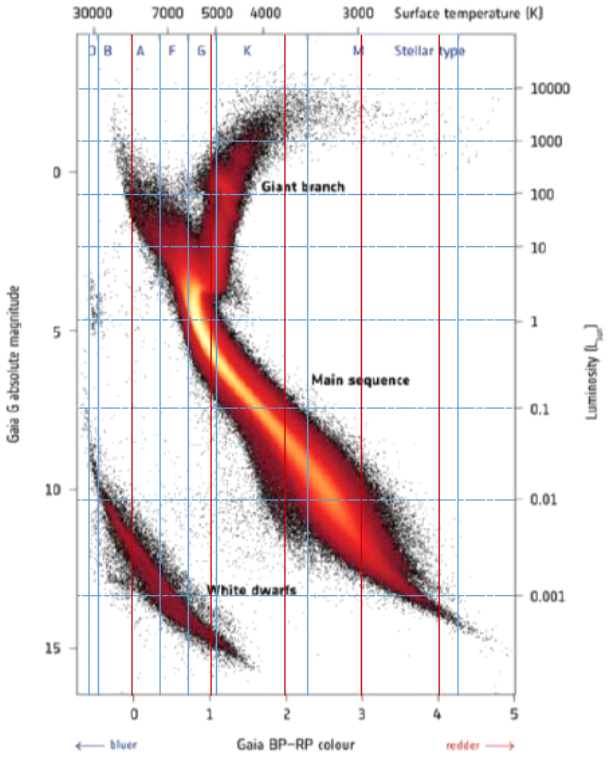

Figure 7. The Gaia DR2 H-R Diagram

are, the more likely the pair is to be physical. Conversely, as values drop towards 0.00, the pair is less and less likely to be physical.

I am currently working now on obtaining mass estimates for the 6,500 pairs I have datarequest graphs on, but have weights (less the radial velocity factor) for all the pairs in the WDS.

In Excel, one can format any cell to draw a bar graph of the value of another cell. Figure 8 shows what a section of those bar graphs looks like.

In Figure 8, stars 1, 2, 4, 5 and 6 all show fairly high values indicating physicality. Star 3 is somewhere in the middle of the range, while the last two stars lack enough critical data from DR2 to enable us to make a calculation.

7. Results

Once probability estimates had been made for all the stars in the WDS, it was a simple matter to create a data filter and view how many pairs had high probability (over 85%, class "Y") of being physical, how many had medium-high probability (65% to 85%, class "Y?"), how many might be physical (50% to 65%, class "Maybe"), how many were questionable (35% to 50%,

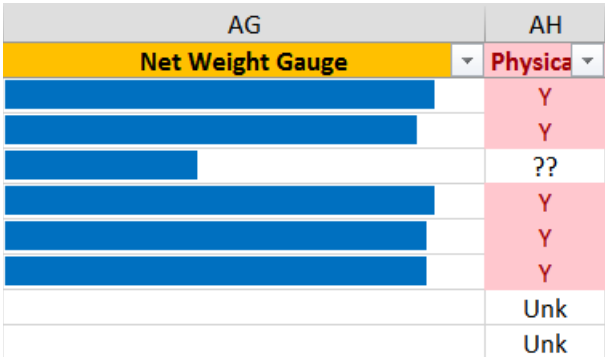

Figure 8. New Weight Average "Gauge"

class "??"), and not physical (< 35%, class "No"), with a class of "Unknown" when two or more of the weight factors could not be calculated. The numbers could then be used to create a pie chart showing the overall results. Here is what was returned (Figure 9).

Because the chart is small, I will place the results

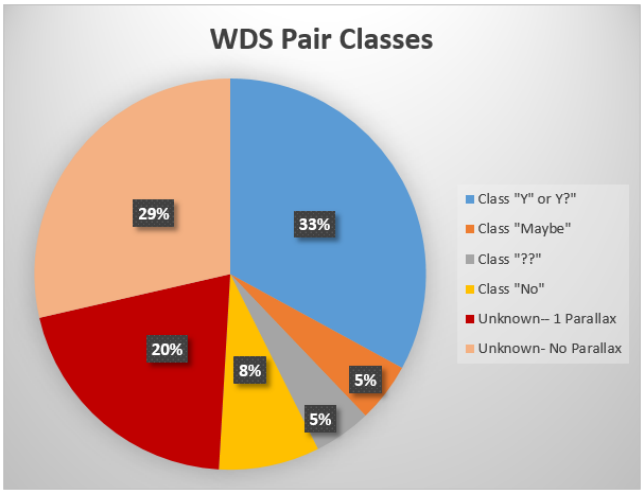

Figure 9. Pie Chart showing the makeup of the WDS

Table 1. Results of WDS / DR2 Extraction

Type of Pair	Number	Percentage
Definitely physical (Y, Y?)	46,061	33%
Maybe	6,871	4.5%
??	6,613	4.5%
No	11,642	8%
Unknown	68,595	49%

into a table (Table 1).

To my surprise, only 33% of the 139,781 WDS records extracted from DR2 show definite signs of physicality while a solid factor (8%) do not, with a further 49% of unknown status due to a lack of good data.

8. Discussion

The Excel spreadsheet is large (38 MB) and will be available to readers of this journal by clicking this link: http://www.jdso.org/volume14/number4/Harshaw_vol14_pg734/WDSGaiaDR2_Ver3.xlsx.

It is recommended that before a program of observing and measuring a double star is begun, the database should be consulted to see if the selected star is physical or not. Since it is the goal of the research to advance us towards *orbital solutions*, then non-physical pairs should not be high on the priority list.

The author will continue working on mass estimates for cases where DR2 shows radial velocities for both stars. There will also be future reports on suspected linear cases that as yet have no solutions as well as strong short arc candidates that may be ready for an orbital solution.

9. Conclusion

Gaia DR2 is a game changer for double star astronomy. Rather than make observational astrometry obsolete, on the contrary, DR2 gives us solid information to help us plan and direct our research. Look how far we have come in 250 years with hit-or-miss observation programs. Think what we can do going forward knowing now exactly where to look for new data!

10. Acknowledgements

The author wishes to thank Dave Rowe for his rapid response to team inquiries for a WDS extraction from Gaia DR2. Of course, the Washington Double Star Catalog was used to build the DR2 extraction, so special thanks to the United States Naval Observatory. And a tremendous debt of gratitude is owed the European Space Agency (ESA) for the Gaia mission and the treasure trove of data being supplied to us about our stellar neighbors in the galaxy.

11. References

ESA 2018, http://sci.esa.int/gaia/

Harshaw, Richard, 2018, "Measurements of 427 Double Stars With Speckle Interferometry: The Winter/Spring 2017 Observing Program at Brilliant Sky Observatory, Part 1", *JDSO,* **14**-2, 284-330.

USNO 2018: http://ad.usno.navy.mil/wds/orb6/orb6text.html#grading

Wiley, E. O. and Rica, F. M., 2015, "Dynamic Studies of Struve Double Stars: STF4 and STF 236AB Appear Gravitationally Bound", *JDSO*, **11**-1, 2-8.

Double Star Measurements with a 12-inch Newtonian Telescope, Annual Report of 2017

Joerg S. Schlimmer
64342 Seeheim-Jugenheim, Germany
js@epsilon-lyrae.de

Abstract: This report shows the results on 259 double star measurements from 2017; minimum separation is 0.48 as (BU 525), maximum separation is 171.7 as (STFA 37AD). The mean value of all measurements is about 20 as.

In 2017 a total of 259 double stars were measured. Observations were done with a 12-inch Newtonian telescope in combination with a CMOS QHY5L II Color camera. Reproduction scale was about 0.52 a.s. per pixel. In some cases the focal length was increased with different Barlow lenses. Observations in M44 Praesepe were done with a 5-inch refractor.

As in the previous year, double stars with large magnitude differences were of special interest (Schlimmer, 2018).

Figure 1 shows the 259 measurements sorted by separation. In 188 cases (72%) the separation is smaller than or equal to 7.5 arc seconds.

Figure 2 shows the differences in magnitudes of the measured double star components. In 199 cases (77%) the difference is greater than or equal to 2 magnitudes.

Table 1 shows the measurements of separation and position angle of 259 components from 2017. Brightness and coordinates are from Washington Double Star catalog (Mason, 2016). Date is given in Besselian years.

References

Mason, B.D., Wycoff, G.L. and Hartkopf, W.I, 2016, *The Washington Double Star Catalog*, Astrometry Department, U.S. Naval Observatory, http://ad.usno.navy.mil/proj/WDS/.

Schlimmer, S. Joerg, 2018, "Double Star Measurements Using a Webcam and CCD Camera, Annual Report of 2016", *Journal of Double Star Observations*, **14**-1, 23-29.

Acknowledgements

This research made use of the Washington Double Star Catalog maintained at the U.S. Naval Observatory.

This research made use of the SIMBAD database, operated at CDS, Strasbourg, France

Double Star Measurements with a 12-inch Newtonian Telescope, Annual Report of 2017

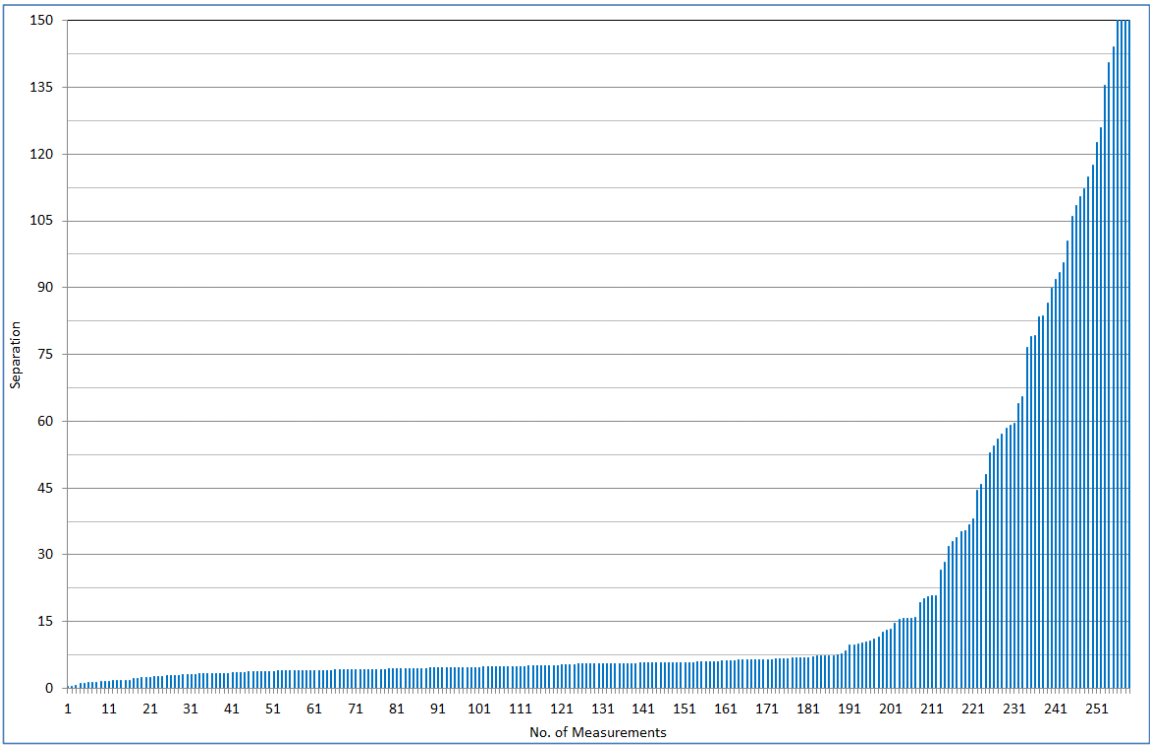

Figure 1: Separation of the 259 measurements

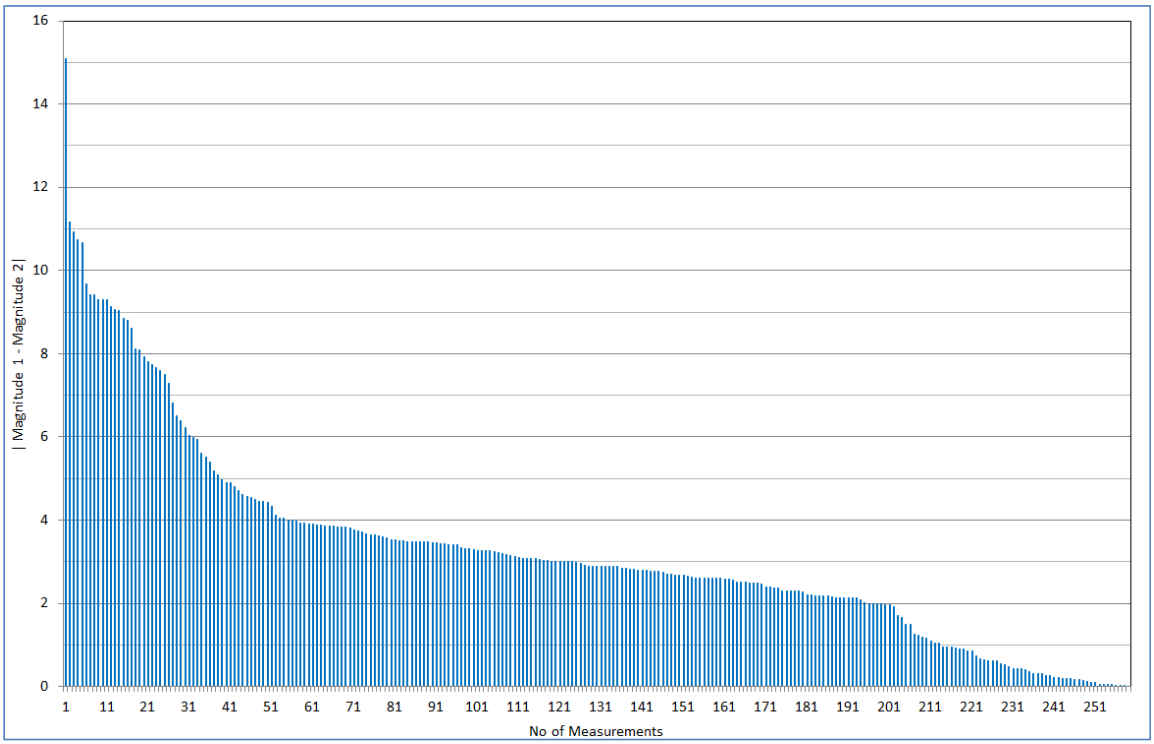

Figure 2: Differences in magnitudes of 259 measurements

Double Star Measurements with a 12-inch Newtonian Telescope, Annual Report of 2017

Table 1. Measurements

RA + Dec	Name	Mag 1	Mag 2	PA	Sep	Date	N	Note
00313+6321	BU 107AB	11.14	11.73	356.0	5.73	2017.894	1	
00337+6247	STI 97	8.41	10.55	7.7	13.17	2017.887	2	
00346+6254	BU 108AB	7.81	10.60	7.9	3.85	2017.894	1	
01226+1245	BU 1360	9.62	11.76	23.9	5.68	2017.015	1	
01535+1918	STF 180AB	4.52	4.58	1.8	7.35	2017.015	1	
02091+5104	STF 213AB	9.06	9.50	327.3	1.67	2017.017	1	2xBarlow
02172+5555	STF 235	9.60	9.81	48.4	1.78	2017.017	1	2xBarlow
02217+3923	STF 251	9.02	9.63	267.1	2.15	2017.017	1	2xBarlow
02331+5828	STF 272	8.33	8.36	217.6	1.81	2017.017	1	2xBarlow
02357+4411	A 1528	9.44	9.62	194.2	1.40	2017.017	1	2xBarlow
02388+3325	STF 285	7.48	8.14	167.5	1.51	2017.017	1	2xBarlow
02389+1526	AG 43	9.9	9.9	63.4	2.90	2017.017	1	2xBarlow
02589+2137	BU 525	7.47	7.45	273.8	0.48	2017.015	1	5xBarlow
02592+2120	STF 333AB	5.17	5.57	210.7	1.32	2017.015	1	5xBarlow
03396+1823	TOK 14AB	6.2	11.0	245.8	10.01	2017.015	1	
03446+2754	STTA 38AB	6.78	6.91	53.0	135.40	2017.015	1	Wolf 1268
03446+2754	BU 1041BC	6.91	12.42	320.8	35.09	2017.015	1	
03356+3141	BU 533AB	7.55	7.74	220.1	1.01	2017.015	1	2xBarlow
04231+3613	ES 239	10.13	13.1	240.6	4.57	2017.121	1	
04246+3358	STT 81AB	5.84	9.25	12.5	4.17	2017.121	1	
04337+4128	ES 570	10.21	14.1	186.6	4.07	2017.121	1	
04384+5455	ES 884	9.56	13.2	252.2	3.13	2017.121	1	
04522+4244	ES 1525	10.1	12.7	87.0	5.63	2017.121	1	
04537+2333	BU 1237	7.5	10.1	55.7	4.54	2017.121	1	
04581+3116	ES 330	10.68	13.5	159.3	4.46	2017.121	1	
04594+2012	A 2427	8.49	11.98	263.5	4.04	2017.121	1	
05003+3924	STT 92AB	6.02	9.50	285.0	4.08	2017.121	1	
05044+4032	ES 1719	10.37	12.9	23.1	3.90	2017.121	1	
05098+4240	BU 751AB	8.22	10.2	243.4	4.57	2017.121	1	
05098+4240	BU 751AC	8.22	11.5	104.2	12.98	2017.121	1	
05103+4040	ES 1721	8.95	11.8	168.1	6.20	2017.121	1	
05120+4154	ES 1722AB	8.63	11.91	302.9	5.61	2017.121	1	
05145+3142	A 211	9.1	13.1	134.3	4.61	2017.121	1	
05145-0812	STF 668A,BC	0.3	6.8	204.0	9.73	2017.121	1	
05145-0812	BU 555AD	0.3	15.4	0.7	44.54	2017.121	1	
05320-0018	STFA 14AC	2.41	6.83	1.0	52.91	2017.121	1	
05354-0555	STF 752AB	2.77	7.73	142.4	11.42	2017.121	1	
05355-0422	STF 750	6.43	8.39	61.0	3.84	2017.121	1	
05357-0451	HLD 173AB	5.26	14.3	170.5	20.59	2017.121	1	
05407-0157	STF 774AC	1.88	9.55	10.4	58.46	2017.121	1	

Table 1 continues on the next page.

Double Star Measurements with a 12-inch Newtonian Telescope, Annual Report of 2017

Table 1 (continued). Measurements

RA + Dec	Name	Mag 1	Mag 2	PA	Sep	Date	N	Note
05474+2939	BU 560	7.77	8.24	125.1	1.67	2017.190	1	
05546+1530	BU 563	8.1	11.1	185.8	6.73	2017.190	1	
05556+3315	ES 337	10.64	13.5	304.3	5.64	2017.190	1	
06121+2930	STF 862	7.55	10.84	337.9	6.88	2017.228	1	
06150+4858	ES 581	9.64	12.3	63.7	4.06	2017.228	1	
06194+3718	ES 287	9.81	13.3	258.7	6.23	2017.228	1	
06298+3636	STF 912	8.76	10.90	27.8	3.44	2017.228	1	
06425+3902	ES 2097AB	8.2	10.7	28.4	15.48	2017.228	1	
06502+3957	STF 966	8.21	10.96	112.0	5.17	2017.228	1	
06563+3227	STF 984	8.67	10.8	155.4	3.31	2017.228	1	
07094+3634	STF1022	6.78	10.05	128.2	5.48	2017.228	1	
07135+3209	STT 167AB	7.44	10.86	162.7	5.11	2017.228	1	
07307+3343	A 2125	9.31	12.0	105.3	4.09	2017.228	1	
07332+3252	BU 22AB	8.36	10.50	150.7	6.15	2017.228	1	
07346+3153	STF1110AB	1.93	2.97	54.3	5.13	2017.302	1	
07487+5339	A 1331	8.99	12.9	253.7	5.33	2017.228	1	
08014+5657	STF1160	8.71	11.54	31.8	6.08	2017.228	1	
08027+3211	ES 291	8.64	11.8	347.6	6.38	2017.228	1	
08081+5627	A 1334AB	9.23	13.0	246.9	4.83	2017.228	1	
08122+1739	STF1196AB	5.30	6.25	8.8	1.01	2017.302	1	Z Cnc, 2X Barlow
08122+1739	STF1196AB,C	4.92	5.85		5.84	2017.228	1	
08122+1739	STF1196AC	5.30	5.85	61.6	6.32	2017.302	1	Z Cnc, 2X Barlow
08148+4302	STT 189	6.87	10.73	293.3	4.38	2017.228	1	
08310+5920	A 1337	9.3	11.6	234.7	3.26	2017.228	1	
08358+0637	STF1245AB	5.98	7.16	24.9	10.08	2017.231	1	M44, ES 127
08358+0637	STF1245AC	5.98	10.70	109.3	100.38	2017.231	1	M44, ES 127
08358+0637	STF1245AD	5.98	11.91	291.5	110.34	2017.231	1	M44, ES 127
08358+0637	STF1245AE	5.98	9.60	206.6	114.80	2017.231	1	M44, ES 127
08399+1933	S 571AC	7.31	7.47	156.5	45.74	2017.231	1	M44, ES 127
08399+1933	S 571AD	7.31	6.67	240.9	91.78	2017.231	1	M44, ES 127
08399+1933	BKO 34DE	6.67	11.75	3.2	35.39	2017.231	1	M44, ES 127
08404+1940	STF1254AB	6.44	10.37	54.7	20.81	2017.302	1	
08404+1940	STF1254AC	6.52	7.61	343.3	64.03	2017.302	1	
08404+1940	STF1254AD	6.52	9.20	44.3	83.50	2017.302	1	
08404+1940	SMR 30AE	6.52	12.5	155.7	15.64	2017.302	1	
09013+1516	STF1300AB	9.47	9.73	176.8	4.98	2017.302	1	
09014+3215	STF1298AB	5.95	8.56	136.7	4.42	2017.228	1	
09169+3702	HO 362AB	8.60	12.45	149.2	4.63	2017.343	1	
09188+3648	STF1334AB	3.92	6.09	229.3	2.51	2017.343	1	
09207+5116	STT 199AB	6.19	10.0	141.8	5.63	2017.343	1	

Table 1 continues on the next page.

Double Star Measurements with a 12-inch Newtonian Telescope, Annual Report of 2017

Table 1 (continued). Measurements

RA + Dec	Name	Mag 1	Mag 2	PA	Sep	Date	N	Note
09412+2706	A 2052	9.29	12.27	317.8	5.15	2017.302	1	
09422+4921	ES 600	9.52	13.0	62.7	4.56	2017.302	1	
09533+5037	STT 209	7.41	10.31	309.8	4.90	2017.302	1	
10085+1206	BRT1267	10.6	12.9	1.6	4.16	2017.343	1	
10200+1950	STF1424AB	2.37	3.64	126.7	4.66	2017.302	1	
10251+5328	ES 721AB	9.97	13.5	134.3	4.07	2017.343	1	
10251+5328	ES 721AC	9.97	12.24	288.3	32.88	2017.343	1	
10293+4233	ES 1395	9.46	12.14	79.3	4.36	2017.343	1	
10339+4158	ES 1396AB	9.91	13.0	192.0	5.43	2017.343	1	
11088+4815	ES 922AB	9.64	12.87	62.3	4.87	2017.343	1	
11218+1811	STF1534	8.08	11.14	314.7	5.11	2017.343	1	
11398+2811	A 560	9.16	12.5	358.6	4.94	2017.343	1	
11436+1042	BU 917	8.70	11.59	175.9	4.08	2017.343	1	
11527+5647	ES 1826	8.95	12.8	217.5	5.62	2017.371	1	
11567+4102	STF1585	8.79	11.08	105.5	5.48	2017.371	1	
11578+4518	A 1778	9.6	11.8	218.9	3.02	2017.371	1	
12052+3851	ES 307	9.11	13.6	353.6	4.47	2017.371	1	
12077+5841	ES 1787	10.89	13.4	140.6	5.73	2017.371	1	
12089+2147	LDS 930AB	9.45	14.63	39.1	15.59	2017.343	1	Wolf 1432
12269+2816	SMR 58	4.4	12.	207.2	16.0	2017.343	1	
12272+2701	STF1643AB	9.03	9.45	2.0	2.62	2017.343	1	
12282+3641	STF1646	10.3	12.9	260.1	5.56	2017.371	1	
12392+1420	STF1666	8.15	10.30	192.3	7.38	2017.371	1	
12417-0127	STF1670AB	3.48	3.53	4.1	2.47	2017.373	1	g Vir 2xBarlow
12429+2555	ES 438	8.89	12.33	80.4	5.74	2017.371	1	
12542+2930	LDS1341	10.89	14.3	179.1	7.32	2017.371	1	
12560+3819	STF1692AB	2.85	5.52	229.2	19.33	2017.371	1	
12587+2728	STF1699	8.74	8.77	12.3	1.66	2017.417	1	2xBarlow
13003+3047	BU 1081AB	4.90	13.0	350.2	5.26	2017.343	1	
13076+2927	A 683	9.32	13.2	327.7	3.72	2017.343	1	
13125+2255	HU 573	9.83	12.30	184.5	4.12	2017.417	1	
13175+3649	HU 1146	8.75	11.84	28.3	5.55	2017.343	1	
13211+2228	HDS1873	9.24	12.70	183.5	4.36	2017.343	1	
13239+5456	STF1744AB	2.23	3.88	152.8	14.57	2017.464	1	Mizar
13287+2335	AG 188	9.60	13.1	247.0	4.65	2017.343	1	
13291+2211	STF1748AB	8.26	10.85	184.1	6.07	2017.417	1	
13407+2804	BUP 151	6.36	12.40	224.0	89.80	2017.436	1	
13407+1957	STF1772AB	5.76	9.60	133.9	4.40	2017.441	2	
13425+2812	ES 442	8.45	12.9	255.8	4.19	2017.417	1	
13447+1255	HDS1934	9.46	13.59	168.6	4.89	2017.435	2	

Table 1 continues on the next page.

Double Star Measurements with a 12-inch Newtonian Telescope, Annual Report of 2017

Table 1 (continued). Measurements

RA + Dec	Name	Mag 1	Mag 2	PA	Sep	Date	N	Note
13563+3438	BU 936	9.77	12.8	96.5	4.35	2017.453	1	
14089+4608	STF1809	9.42	11.98	195.7	4.12	2017.453	1	
14138+4111	HO 58	8.16	11.35	229.5	4.03	2017.453	1	
14161+5643	STF1831AB	7.16	9.56	137.7	5.79	2017.464	1	
14161+5643	STF1831AC	7.16	6.73	219.1	112.20	2017.464	1	
14161+5643	STF1830EF	9.33	10.28	312.4	10.56	2017.464	1	
14203+4830	STF1834	8.09	8.29	101.5	1.42	2017.507	1	2xBarlow
14224+5225	ES 738	9.94	12.9	311.0	5.51	2017.464	1	
14318+3022	HJ 2728	3.58	11.5	343.4	33.84	2017.436	1	
14325+4911	STT 283A,BC	8.08	12.62	130.2	5.87	2017.64	1	
14336+3535	STF1858AB	8.13	8.98	39.4	2.96	2017.507	1	2xBarlow
14397+4152	ES 1250	9.56	13.0	174.5	5.49	2017.464	1	
14401+5841	A 1108	8.61	12.10	116.0	4.69	2017.464	1	
14403+4843	STT 284	7.91	11.56	102.5	7.22	2017.466	1	
14416+5124	STF1871	8.02	8.07	314.1	1.64	2017.507	1	
14484+2422	STF1884	6.58	7.48	55.9	2.27	2017.510	1	2xBarlow
14497+4843	STF1890	6.31	6.67	46.3	2.59	2017.498	4	2xBarlow
14514+1906	STF1888AB	4.76	6.95	300.0	5.48	2017.466	1	
14527+0746	HLD 120AB	8.05	10.84	225.2	15.72	2017.464	1	
14560+3218	STT 289	6.2	11.1	109.2	4.78	2017.466	1	
14575+4010	STF1895	8.27	8.88	42.3	12.65	2017.466	1	
14577+4011	ES 1251	9.45	13.9	58.1	6.67	2017.466	1	
14583+4106	A 1628	8.56	11.63	97.2	5.14	2017.507	1	
15038+4739	STF1909	5.20	6.10	76.4	0.56	2017.475	3	5xBarlow, 44 Boo
15054+4809	BU 1086	5.57	13.3	253.3	6.82	2017.507	1	
15096+4142	A 572	9.4	11.4	3.5	4.14	2017.507	1	
15151+3318	SMR 32AB	12.76	11.21	334.9	26.64	2017.453	1	
15151+3318	SMR 32AC	12.76	12.90	72.4	36.75	2017.453	1	
15151+3318	SMR 32BC	11.21	12.90	105.7	48.09	2017.453	1	
15155+3319	STFA 27AB	3.56	7.89	78.3	105.95	2017.453	1	
15155+3319	SMR 31AC	3.56	14.30	4.5	93.46	2017.453	1	
15162+3418	A 1366	9.3	12.2	78.6	3.88	2017.507	1	
15166+3339	STF1929	9.79	11.8	7.5	6.51	2017.507	1	
15183+2650	STF1932AB	7.32	7.41	268.2	1.43	2017.510	1	
15232+3017	STF1937AB	5.64	5.95	230.0	0.53	2017.468	1	n CrB
15300+2530	STF1950	8.07	9.23	92.5	3.39	2017.510	1	2xBarlow
15364+3723	HU 1166AB	8.50	13.4	144.6	4.16	2017.518	1	
15379+3006	STF1963AB	8.54	8.85	298.2	5.34	2017.518	1	
15394+3638	STF1965	4.96	5.91	306.8	6.38	2017.518	1	
15462+4228	STT 301	7.50	10.38	27.4	3.97	2017.510	1	

Table 1 continues on the next page.

Double Star Measurements with a 12-inch Newtonian Telescope, Annual Report of 2017

Table 1 (continued). Measurements

RA + Dec	Name	Mag 1	Mag 2	PA	Sep	Date	N	Note
15469+4736	ES 1087	10.5	12.5	173.8	6.83	2017.518	1	
16051+5426	ES 743	9.71	12.8	13.4	5.73	2017.510	1	
16052+2211	BU 811AB	8.71	11.84	216.5	3.41	2017.510	1	
16117+3321	STT 305AB	6.44	10.17	263.0	5.67	2017.510	1	
16126+5748	ES 1793	8.74	11.52	57.1	5.66	2017.576	1	
16197+5135	HU 662	9.75	13.8	223.4	4.03	2017.576	1	
16199+5146	ES 628	13.9	13.8	265.8	3.97	2017.576	1	
16206+5150	ES 629	8.52	13.1	100.5	10.95	2017.576	1	
16240+2024	A 25	8.28	10.8	112.6	5.47	2017.576	1	
16362+5255	STF2078AB	5.38	6.42	105.1	3.07	2017.576	1	
16389+2028	STT 314	8.2	11.2	236.1	3.46	2017.576	1	
16462+4649	A 1865	9.81	12.69	296.6	4.38	2017.598	1	
16473+5218	ES 970	10.02	12.2	300.9	3.39	2017.598	1	
17046+3900	HJ 2804AB	11.00	13.3	235.8	6.41	2017.598	1	
17117+4945	STF2142AB	6.18	9.35	110.3	4.77	2017.598	1	
17146+1423	STF2140AB	3.48	5.40	102.8	4.70	2017.598	1	
17165+3448	POP 77AB	10.91	13.6	322.8	5.50	2017.598	1	
17165+3448	POP 77CD	11.43	13.7	81.0	10.42	2017.598	1	
17173+3306	STT 328	4.7	10.3	56.1	4.47	2017.598	1	
17246+1536	STF2160	6.40	9.28	66.2	3.90	2017.598	1	
17275+4716	ES 1256	10.41	13.4	329.6	4.20	2017.598	1	
17284+4822	ES 1091	10.63	13.2	308.9	6.51	2017.598	1	
17316+3601	ES 2229	10.67	13.4	31.1	3.73	2017.601	1	
17317+3604	ES 2230	10.54	11.03	92.0	9.62	2017.601	1	
17322+5236	ES 777	8.15	12.2	349.4	6.03	2017.601	1	
17353+5210	ES 635	9.50	12.6	241.5	5.84	2017.601	1	
17479+3417	BU 632AB	6.58	12.8	344.1	5.75	2017.598	1	
17503+2517	STF2232	6.71	8.85	138.7	6.34	2017.598	1	
17512+4454	STF2242	8.14	8.28	327.2	3.37	2017.598	1	
17561+2130	STT 339	8.37	10.76	171.1	3.78	2017.598	1	
17566+5129	BU 633AB	2.23	13.4	151.2	20.81	2017.598	2	
17566+5129	BU 633AD	2.23	12.9	11.1	59.50	2017.598	1	
17566+5129	BU 633AE	2.23	11.9	234.6	95.58	2017.598	2	
17566+5129	BU 633AF	2.38	11.67	113.8	126.01	2017.598	2	
17566+5129	BU 633AG	2.38	11.23	27.2	143.99	2017.598	1	
18049+4808	STT 343	7.63	10.51	82.7	3.14	2017.598	1	
18065+4022	STF2282AB	7.93	9.43	82.6	2.67	2017.598	1	
18094+4319	ES 1418	9.81	13.7	304.0	3.99	2017.598	1	
18193+4724	ES 1158	8.74	12.2	201.9	4.83	2017.598	1	
18239+5848	STF2323AB	5.06	8.07	346.3	3.77	2017.598	1	

Table 1 continues on the next page.

Double Star Measurements with a 12-inch Newtonian Telescope, Annual Report of 2017

Table 1 (continued). Measurements

RA + Dec	Name	Mag 1	Mag 2	PA	Sep	Date	N	Note
18267+3610	ES 2173	8.48	11.9	304.4	6.45	2017.598	1	
18324+4510	ES 1261	9.66	12.3	208.7	7.64	2017.598	1	
18369+3846	H 5 39AB	0.09	9.5	184.4	83.65	2017.661	2	
18369+3846	STFB 9AE	0.09	9.5	39.2	86.63	2017.661	2	
18399+5815	A 251AB	8.10	11.62	52.7	4.03	2017.598	1	
18438+5654	BU 465	9.2	11.2	297.9	2.97	2017.658	1	
18443+3940	STFA 37AD	5.15	5.38	171.7	210.48	2017.598	1	
18466+1659	STF2385AB	8.42	10.8	29.5	5.5	2017.598	1	
18471+5356	A 1382	9.58	12.9	226.1	4.62	2017.658	1	
18484+2544	A 255	9.23	12.9	69.3	4.89	2017.658	1	
18484+3612	ES 2023	8.73	12.0	245.9	6.36	2017.674	1	
18490+2110	STF2401AB	7.27	9.27	38.0	4.11	2017.658	1	
18517+5116	ES 788	9.41	11.99	319.4	3.36	2017.661	2	
18521+5120	STF2416AB	8.67	11.17	158.5	20.18	2017.658	1	
18521+5120	STF2416AC	8.67	9.41	40.7	122.66	2017.658	1	
18534+3728	HO 89	8.89	12.9	170.0	5.96	2017.674	1	
18545+3719	HO 90	8.72	12.7	227.5	3.98	2017.674	1	
18569+3112	ES 2422	8.96	12.0	178.5	5.55	2017.674	1	
18569+5645	STF2433AB	7.17	10.09	121.6	7.43	2017.674	1	
18581+3813	STF2427AB	9.61	9.93	59.4	55.91	2017.674	1	
18581+3813	CTT 11AD	9.61	11.8	290.5	57.19	2017.674	1	
18581+3813	SP 2AE	9.61	5.87	350.3	162.29	2017.674	1	
18581+3813	STF2427BC	9.93	10.20	78.9	7.19	2017.674	1	
18591+2730	A 261	9.07	12.9	192.6	3.70	2017.674	1	
18599+1454	STF2428AB	8.22	10.31	285.8	6.87	2017.674	1	
19010+5311	A 1388	9.51	12.83	262.2	5.23	2017.658	1	
19021+5216	STF2450A,BC	6.50	9.51	298.4	5.12	2017.674	1	
19037+3545	STF2448	8.75	8.80	192.7	2.39	2017.658	1	2x Barlow 0,254
19050+2114	HDS2708	8.22	11.79	3.3	5.95	2017.699	2	
19074+3230	STF2461AB	5.26	9.1	281.1	3.20	2017.731	2	17 Lyr
19083+5520	STF2479AB,C	7.49	9.68	28.6	6.54	2017.674	1	
19088+2825	ES 348	8.78	11.3	252.9	5.41	2017.724	1	
19100+5124	ES 790	9.32	12.1	116.1	4.64	2017.724	1	
19147+5946	ES 192	9.82	12.2	100.3	4.73	2017.737	1	
19151+5946	ES 193	9.12	11.9	134.7	8.44	2017.737	1	
19169+4711	ES 128	8.38	11.98	283.6	4.79	2017.737	1	
19170+3332	ES 351	9.4	11.9	264.1	5.98	2017.737	1	
19189+4952	ES 1095AB	8.88	12.82	134.6	6.71	2017.737	1	
19208+3427	ES 352	9.16	12.4	139.8	4.80	2017.737	1	
19213+5549	STF2516	8.27	9.50	233.6	4.13	2017.740	1	

Table 1 concludes on the next page.

Double Star Measurements with a 12-inch Newtonian Telescope, Annual Report of 2017

Table 1 (conclusion). Measurements

RA + Dec	Name	Mag 1	Mag 2	PA	Sep	Date	N	Note
19216+3018	A 268	9.11	12.6	103.1	3.60	2017.737	1	
19257+3658	ES 2179	8.98	11.5	132.6	6.94	2017.737	1	
19307+2758	WAL 114AC	3.19	10.99	340.8	65.60	2017.740	1	
19307+2758	CTT 17AD	3.19	12.24	32.9	108.44	2017.740	1	
19307+2758	CTT 18AE	3.19	11.81	206.5	76.66	2017.740	1	
19307+2758	SMR 34AF	3.19	12.	46.0	59.19	2017.740	1	
19307+2758	SMR 34AH	3.19	12.5	119.2	54.54	2017.740	1	
19307+2758	SMR 34AI	3.19	12.5	132.4	37.95	2017.740	1	
19307+2758	SMR 34AJ	3.19	10.	140.6	140.57	2017.740	1	
19310+3359	ES 2295	3.0	9.40	204.8	3.55	2017.739	2	
19351+3412	STT 376	7.56	10.41	236.7	2.94	2017.740	1	
19563+3505	BU 980AB	3.89	12.0	206.3	7.15	2017.740	1	
20462+3358	STT 594AB	2.46	11.6	261.3	79.20	2017.724	1	
20462+3358	BU 676AC	2.46	13.40	269.0	78.97	2017.724	1	
21069+3845	STF2758AB	5.20	6.05	153.2	31.93	2017.724	1	61 Cyg
21069+3845	STF2758AH	5.35	9.97	268.4	117.51	2017.724	1	
21069+3845	SMR 1AI	5.35	10.74	238.9	28.26	2017.724	1	
21069+3845	SMR 40AO	5.35	12.65	280.6	163.42	2017.724	1	
21069+3845	SMR 40AP	5.35	12.84	285.2	159.58	2017.724	1	

Image Reconstruction Using Bispectrum Speckle Interferometry: Application and First Results

Roberto Maria Caloi
Unione Biellese Astrofili, Italy
robime@iol.it

Abstract: Speckle interferometry yields diffraction-limited information from sequences of atmospherically-degraded short-exposure images. Sophisticated algorithms have been proposed by astronomers to reconstruct the actual image of an object. The reconstructed images allow one to measure the relative positions and the magnitude differences of the stars in a multiple star system up to the resolving power of the available instrumentation. Here I report on the main measurements and analysis required to apply one of these techniques, the building block method using the bispectrum. Preliminary results obtained with simulations and using a small telescope are shown.

1. Introduction

The atmospheric turbulence limits the resolving power of a telescope, including the smaller ones usually available to amateur astronomers, when observing with typical seeing conditions. In the last decades, professional astronomers have developed several techniques to extract as much information as possible from their sophisticated instrumentation, with speckle interferometry and recently adaptive optics most commonly used. While the latter technique is available only in the most advanced observatories in the world, the former can be applied by a much broader community, including amateur astronomers in the most simple set-ups, both for scientific and educational purposes (Genet, 2015).

In my previous paper on this subject (Caloi, 2008), I reported on an application of speckle interferometry to the estimation of the separation and position angle of double stars using the Directed Vector Autocorrelation method (Bagnuolo et al., 1992). Regarding the relative brightness of the two components in a binary star, methods that are essentially parametric are also available (Glindemann et al., 1992). As an amateur astronomer, I have been nevertheless attracted by the idea of getting a full image of the object under study. Even if parametric methods require much less computing time and yield all the information as well, when the nature of the object under study is well known, as in the case of a binary star, an image is necessary when dealing with more complex or simply unknown objects, as in the case of multiple star systems or diffuse structures.

After reviewing the existing literature and, I must say, significantly underestimating the effort needed to understand all the steps required to replicate the algorithm, I decided to implement the iterative building block method (Hofmann and Weigelt, 1993). This data reduction technique is based on the statistical properties of the bispectrum of the atmospherically degraded optical transfer function of a telescope (Lohmann et al., 1983). For a detailed review on the state of the art in the more general field of optical interferometry applied to the image reconstruction problem, I refer the reader to the recent tutorial of Thiébaut and Young (2017).

The main purpose of this paper is to highlight the key aspects as well as some of the issues that, at least for me, were initially quite difficult to familiarize with, so that other amateur astronomers could have a starting point before reading the original papers, where the theory and limitations of the methods and formulas reviewed here are covered in detail.

For rapid prototyping and deployment of all required calculations, I have used Matlab, which has provided me a very good compromise between performance and ease of development.

2. Image Formation

The image reconstruction process is essentially an inverse problem, since the main task is to recover the

Image Reconstruction Using Bispectrum Speckle Interferometry: Application and First Results

original image based on the result of observations. Several noise sources make the recovering process subject to uncertainties and biases. In order to appreciate all the data and assumptions necessary to deal with these aspects, it helps to review the main physical processes involved in the image formation on the detector that are later considered to recover the original image. Other refinements could be evaluated, in particular on how to model the actual functioning of a real detector, but they are not considered here.

The near axis image formation process can be described as follows (Klein and Furtak, 1986). Let us consider a point-like monochromatic optical source, like a single star observed using a narrow-band filter, located in the ideal source plane at position (x', y') at a large distance R'_0 from the telescope, thus forming a small angle

$$\frac{\sqrt{x'^2 + y'^2}}{R'_0}$$

with respect to the telescope optical axis. The resulting electric field intensity on the image plane, where the detector is located, is proportional to the Fourier transform of the transmission function $\tau(\tilde{x}, \tilde{y})$ defined on the telescope aperture plane. The transmission function summarizes the combined effects of the telescope aperture, its aberrations and the atmospheric disturbances. The resulting intensity distribution on the image plane can be represented as a function $PSF^{\lambda}(x, y)$ (the so called *point spread function* at wavelength λ) centered on $(fx'/R'_0, fy'/R'_0)$, where f is the actual focal length of the telescope. The image formed by the telescope on the detector is thus located in the position that is expected by geometrical optics, and spread according to the PSF. In the case of an extended incoherent optical source with an intensity distribution $o(x,y)$ according to geometrical optics, the actual image intensity distribution $i^{\lambda}(x, y)$ is the convolution of $o(x, y)$ with the point spread function $PSF^{\lambda}(x,y)$.

$$i^{\lambda}(x,y) = o(x,y) * PSF^{\lambda}(x,y) \qquad [1]$$

Equation 1 holds in the isoplanatic approximation, i.e. when the spread function does not change in the region of interest, and if the emission from the source object is not coherent, as is the case with the light emitted from a star. Under ideal conditions the point spread function for a given wavelength λ would depend on the telescope only but, due to the atmospheric turbulence, the transmission function $\tau(\tilde{x}, \tilde{y})$ changes rapidly both in time and space and, as a consequence, the same happens to $PSF^{\lambda}(x,y)$. Thus, the actual intensity distribution $i_t^{\lambda}(x, y)$ at each time t depends on a different point spread function $PSF_t^{\lambda}(x,y)$ such that

$$i_t^{\lambda}(x,y) = o(x,y) * PSF_t^{\lambda}(x,y) \qquad [2]$$

Given the incoming intensity distribution $i_t^{\lambda}(x, y)$, the actual number of photons detected per pixel will depend also on the quantum nature of light and on the actual detector used, whose main characteristics are the following: level of dark current generation, quantum efficiency, electronic read-out noise, electronic biases, presence of defects and hot pixels. These effects are particularly important when the average total number of detected photons per speckle N^{ph} is low, some hundreds or thousands to give an order of magnitude, and must be dealt with in order to avoid estimation biases (which do not disappear by simply increasing the number of recorded images used in the data reduction process).

If $i_t^{\lambda}(x, y)$ is normalized so that its total value over the image plane is one, the expected number of photoelectrons $i_t^{phe}(x,y)$ is then given by

$$i_t^{phe}(x,y) = N^{ph}\left[o(x,y) * PSF_t^{\lambda}(x,y)\right] + n_{th} \qquad [3]$$

where n_{th} represents the contribution of thermally generated electrons, here assumed to be independent from the pixel location.

The actual number of generated photoelectrons $P(i_t^{phe}(x,y))$ follows a Poisson distribution with average given by $i_t^{phe}(x, y)$. The subsequent mechanism of charge shift and amplification typical of CCDs, introduces an additional noise component, the so called read-out noise, which can be represented by a random variable normally distributed with zero mean and variance σ_e^2, indicated in what follows by $N(0, \sigma_e^2)$. An additional time invariant bias $b_{DC}(x, y)$ and a spatial dependent sensitivity factor $l(x, y)$ are also normally taken into account (due to electronic bias, defects and hot pixels, dust, etc.). The final digital value (ADU) recorded for each pixel is obtained by summing all three previous components and dividing by the detector gain G,

$$i_t^{ADU}(x,y) = \left[\begin{matrix} P\left(i_t^{phe}(x,y)\right) l(x,y) + N\left(0,\sigma_e^2\right) + \\ b_{DC}(x,y) \end{matrix}\right]\left(\frac{1}{G}\right) \qquad [4]$$

where $i_t^{ADU}(x,y)$ represents the detected specklegram at time t.

Equations 3 and 4 provide a simplified representation of the detection process, and they have been used for the actual implementation of the data-reduction process of this work. In the following sections, position (x,y) will be denoted by x to simplify expressions, with the understanding that x is the pixel bi-dimensional position.

3. Power Spectrum Estimation

A data cube $\{i_t^{ADU}(x)\}_{t=1}^{M}$ of M short exposure frames (specklegrams) of the object is the starting point of the analysis. A similar data cube $\{d_t^{ADU}(x)\}_{t=1}^{L}$ obtained with the telescope aperture covered is needed. The first step in the image reconstruction process requires the computation of the power spectrum, both its average and variance. Each frame $i_t^{ADU}(x)$ is first corrected for the gain, G, the bias $b_{DC}(x)$ and the flat field $l(x)$, to yield the actual photo-electrons plus read-out noise per pixel

$$i_t(x) = \frac{G i_t^{ADU}(x) - b_{DC}(x)}{l(x)}$$

It is subsequently cropped within a square frame centered at the position corresponding to the speckle moving average maximum intensity. The frame size is chosen large enough to contain the entire speckle, with each side made by a number of pixels equals to a power of two, in order to reduce the computation time of subsequent applications of the Fast Fourier Transform algorithm. The total number of photo-electrons and thermal electrons per frame $N_t = N_t^{ph} + N_t^{th}$ is also computed. The same cropped regions are used with the dark frames sequence to compute the total dark current due to the thermally generated electrons N_t^{dth} per frame. Here we assume that N_t^{th} and N_t^{dth} have the same expected values.

The discrete Fourier transform $I_t(u) = DFT(i_t(x))$ where u indicates the bi-dimensional frequency component, is performed for each specklegram. It has been shown (Goodman et al., 1976) that at low light levels, a typical situation in speckle interferometry, the computed power spectrum must be compensated for biases due to the photon noise inherent in the detection process. Gordon and Buscher (2012) derived a formula for a bias-free power spectrum estimator $S_t(u)$, when photon noise, thermal noise (dark current), and read-out noise are all taken into account. The main stated assumption in their study is that the various noise sources considered are independent and additive. Moreover the overall noise on different pixel positions is assumed to be statistically independent.

Under discrete Fourier transform conditions, which hold in our case, their proposed estimator becomes

$$S_t(u) = |I_t(u)|^2 - \sum_x \left(i_t(x) + \sigma_e^2(x) \right) \qquad [5]$$

where x indicates the pixel position, $i_t(x)$ the recorded intensity, and $\sigma_e^2(x)$ is the read-out noise variance. Under the additional assumption that the read-out noise does not depend on the detector position, i.e. $\sigma_e(x) = \sigma_e$, equation 5 becomes

$$S_t(u) = |I_t(u)|^2 - N_t - N_{pix}\sigma_e^2 \qquad [6]$$

where $N_t = N_t^{ph} + N_t^{th}$ is the total number of photo-electrons and thermal electrons per frame and N_{pix} is the total number of pixels. By averaging $S_t(u)$ we obtain an unbiased estimate of the power spectrum

$$S = \left\langle |I(u)|^2 \right\rangle - \langle N \rangle - N_{pix}\sigma_e^2 \qquad [7]$$

where the operator ‹› represents averaging over the entire sequence of specklegrams. The sample variance of such estimate $var(S)$ is then used to calculate the frequency dependent power spectrum standard deviation $\sigma_S(u)$,

$$\sigma_S(u) = \sqrt{\mathrm{var}\left(S(u)\right) / M} \qquad [8]$$

where M is the number of frames. The resulting power spectra has a central peak which is given by $(\tilde{N}^{ph} + \tilde{N}^{th})^2$ where $\tilde{N}^{ph}$ is the average number of photo-electrons per frame and $\tilde{N}^{th} = \tilde{N}^{dth}$ is the average number of electrons generated by the thermal noise. By correcting the central peak component for the thermal noise, the final estimate of the power spectrum $S(u)$ is obtained. No further correction is necessary outside the central peak if the thermal noise is spatially uncorrelated, so that its power spectrum is negligible for spatial frequencies different from zero.

The same analysis just described is repeated for a nearby reference star, which must be observed with similar seeing conditions as the object under study. Once we have estimated the object power spectrum $S_{obj}(u)$ and its variance $\sigma^2_{Sobj}(u)$ as well as the reference star's power spectrum $S_{ref}(u)$ and its variance $\sigma^2_{Sref}(u)$, we can apply the standard procedure of speckle interferometry (Labeyrie, 1970) which yields an estimate of the true object power spectrum $|O(u)|^2 = S_{obj}(u)/S_{ref}(u)$ up to the telescope cut-off frequency, and its variance $\sigma^2_{|O(u)|^2}$

$$\frac{\sigma^2_{|O(u)|^2}}{|O(u)|^2} = \left[\frac{\sigma_{S_{obj}}(u)}{S_{obj}(u)}\right]^2 + \left[\frac{\sigma_{S_{ref}}(u)}{S_{ref}(u)}\right]^2 \quad [9]$$

The power spectrum $|O(u)|^2$ does not contain any information regarding the phase $\varphi(u)$ of an object visibility $O(u) = |O(u)|\ e^{i\varphi(u)}$, from which the image could be reconstructed by applying the inverse Fourier transform. As a consequence, it cannot be used alone to recover an object image without some prior information about the object itself. The bispectrum is one observable quantity that contains such information.

4. Bispectrum Estimation

Let us first recall its definition. Given an intensity distribution $i(x)$ and its Fourier transform $I(u)$, the bispectrum is defined as $I^{(3)}(u,v) = I(u)I(v)I^*(u+v)$, where $I^*(u)$ indicates the complex conjugate of $I(u)$. Similarly, for the true object intensity distribution $o(x)$ we have $O^{(3)}(u, v) = O(u)O(v)O^*(u + v) = |O^{(3)}(u,v)| \exp[\beta_{O(3)}(u,v)]$. It has been shown by Lohmann et al. (1983) that the phase of the time-averaged bispectrum of the atmospheric transfer function is close to zero while its modulus is not and, as a consequence, the phase of the observed average bispectrum $\beta_{I(3)}(u,v)$ is equal to the phase of the object bispectrum $\beta_{O(3)}(u,v)$. This relation holds for $|u|$, $|v|$, and $|u + v|$ smaller than the telescope cut-off frequency. They also describe an iterative computation to recover $\varphi(u)$ from $\beta_{O(3)}(u,v)$. This property highlights the importance of the bispectrum for image reconstruction.

Astronomers have also investigated in detail how to take into account the effects of the photon noise (Wirnitzer, 1985) on its measurement. These effects lead to a bias that is significant at low light levels, when the number of photons detected per frame is of the order of less than some thousands. A bias cannot be overcome by simply increasing the number of detected interferograms. If compared to the variance, its significance becomes greater when the number of samples used to compute the average increases.

In what follows, I report the formulas presented by Gordon and Busher (2012). They extend the original results of Wirnitzer for the bispectrum, to the case where several additive noise sources are significant at the same time in the general framework of optical interferometry.

In our case, the DFT conditions stated in their paper apply. Moreover, assuming that the read-out noise does not depend on the pixel position, the given unbiased estimator reduces to

$$B_t(u,v) = I_t(u)I_t(v)I_t^*(u+v) - |I_t(u)|^2 - |I_t(v)|^2 - |I_t(u+v)|^2 + 2N_t + 3N_{pix}\sigma_e^2 + C*\delta(u,v) \quad [10]$$
$$C = -3N_tN_{pix}\sigma_e^2$$

where, following the same convention used in the previous section, $N_t = \Sigma_x\, i_t(x)$ is the total number of photoelectrons and thermal electrons recorded per frame, N_{pix} is the total number of pixels, and σ_e^2 is the read-out noise variance. By averaging (10) over t, we obtain an unbiased estimate of the bispectrum.

Finally, taking into account (6), we get

$$\langle B(u,v)\rangle = \langle I(u)I(v)I^*(u+v)\rangle - |S(u)|^2 - |S(v)|^2 - |S(u+v)|^2 - \langle N\rangle + C*\delta(u,v) \quad [11]$$

We can now combine the object's visibility modulus $|O(u)|$, obtained as described in the previous section, and the bispectrum phase (also called closure phase) $\beta(u, v) = arg(< B(u, v) >)$ to obtain our estimate of the object's bispectrum

$$O^{(3)}(u,v) = |O(u)||O(v)||O(u+v)|e^{i\beta(u,v)} \quad [12]$$

5. Image Reconstruction

We can now proceed to search for the object's image, whose bispectrum shows the best agreement with the unbiased average bispectrum obtained as described in the previous section.

The algorithm used here is the *building block method* (BBM) and the details are provided in the original paper by Hofmann and Weigelt (1993). An improved algorithm for the same purpose and based on similar considerations was proposed later by the same authors (Hofmann et al., 2014)

The main idea of the building block method is to reconstruct the object's image iteratively, by modifying the initial guess by adding one block at a time. Each new block position is chosen in such a way to reduce the distance d_k, also called cost function, between the bispectrum of the new image after k iterations $O_k^{(3)}(u, v)$ and the measured bispectrum $O^{(3)}(u, v)$. The process is repeated until the distance is minimized according to a given stopping rule.

In the building block method the user can choose among different metrics in order to define a goodness of fit. The approach followed here does not include any regularization technique and implements the following definition of distance d_k.

$$d_k = \int \frac{\left| O_k^{(3)}(u,v) - O^{(3)}(u,v) \right|^2}{\sigma^2_{O^{(3)}(u,v)}} du\, dv \qquad [13]$$

which assigns a greater weight to those regions where the variance in the measured data is lower and where the integral represents summation over the 4-dimensional bispectrum support. As given in Appendix A of Hofmann et al. (2014), one source of uncertainty depends on the estimated power spectrum and it translates into an uncertainty in the bispectrum modulus as

$$\sigma_{|O^{(3)}(u,v)|} = 0.5\sqrt{S(u)S(v)S(u+v)} \cdot \sqrt{\frac{\sigma_S^2(u)}{S^2(u)} + \frac{\sigma_S^2(v)}{S^2(v)} + \frac{\sigma_S^2(u+v)}{S^2(u+v)}} \qquad [14]$$

which holds for small relative errors.

The second source of uncertainty comes from the phase of the estimated object bispectrum, whose variance $\sigma^2_{\beta(u,v)}$ can be calculated conveniently as described in Glindemann et al. (1992) and Gordon et al. (2012) as the variance of the projection of each frame's bispectrum on a direction perpendicular to their average, divided by the square of their average modulus and the number of frames. I have considered other angular dispersion measures based on directional statistics, as well as an approach based on the bootstrap method, but a preliminary investigation has not resulted in improved results so far.

Regarding the value of the variance required by the weight factor in the cost function used in the building block method, several approaches are possible. The approach used here is to consider the bispectrum modulus and phase as two independent random variables. In this case, the bispectrum variance can be approximated by

$$\sigma^2_{O^{(3)}(u,v)} = \sigma^2_{|O^{(3)}(u,v)|} + \left| O^{(3)}(u,v) \right|^2 \sigma^2_{\beta(u,v)} \qquad [15]$$

which holds when both modulus and phase variances are relatively small. A better approximation, which takes into account the wrapping effect in the complex plane, is presented in Hofmann et al. (2014), but has not been used for the preliminary results reported in the following sections.

Pauls *et al*., (2005) propose a different model, where $\sigma^2_{|O^{(3)}(u,v)|}$ and $\sigma^2_{\beta(u,v)}$ are reported and used separately in order to arrive to a more general error model for the bispectrum.

As a matter of fact, I found the analysis of the quality of the reconstructed image as a consequence of different choices of the cost function to be an active field of research among professional astronomers in general and not only for the BBM. After initially trying several different versions of the building block cost function, with some changes in the final outcome of the reconstructed image, I have chosen expressions 13 to 15 for the actual implementation of the algorithm, mainly to reduce at the minimum the overall complexity needed to get a satisfactory outcome with the objects considered in this study, i.e. triple and binary stars.

Because the image is built by changing one pixel at a time, some details that are not consistent with the actual maximum resolving power of the telescope can be generated. To correct this outcome, the image resulting from the optimization process is smoothed by convolution with the known theoretical PSF of the telescope.

To sum up, the main steps required to carry out the image reconstruction by bispectrum speckle interferometry are:

- Estimate the object power spectrum and from that the modulus of the object visibility $|O(u)|$
- Estimate the object's bispectrum phase $\beta(u, v)$
- Combine the two previous results to get the object bispectrum $|O(u)||O(v)||O(-u - v)|e^{i\beta_{(u,v)}}$ and its variance
- Fit the object bispectrum, the iterative building block is used here, to recover the object image taking into account the estimated uncertainty in the bispectrum according to a suitable cost function
- Smooth the resulting image with the theoretical PSF of the telescope to avoid super-resolution artifacts

6. Simulation

In order to verify the reconstruction procedure under controlled conditions, simulated specklegrams have been generated assuming a monochromatic source by replicating the main physical processes introduced in section 2. The simulation starting point is a multiple star system, represented by a bi-dimensional normalized intensity function $o(x)$,

$$o(x) = \frac{\sum_{i=1}^{n} A_i \delta(x - x_i)}{\sum_{i=1}^{n} A_i} \qquad [16]$$

where x_i represents the position and A_i the intensity of each star's component i. Imaging equation 1 is then used. The PSF of each simulated frame is generated using a complex transmission function with a modulus defined by the geometry of the telescope aperture (primary and secondary mirror diameters) and a phase $\varphi(\tilde{x},\tilde{y})$ dependent on the position in the entrance pupil, the phase screen, which represents the effect of the atmospheric turbulence. The algorithm used to generate the phase screen is based on the Fast Fourier Transform method (McGlamery, 1976). The FFT method computes the phase screen by means of the inverse Fourier transform of the product of a circular complex Gaussian random noise with zero mean and unit variance and the square root of the phase power spectrum density $W_\varphi(f)$. For this purpose we can use Kolmogorov's law for energy dissipation in a viscous medium

$$W_\varphi(f) = \frac{0.023}{r_o^{5/3} f^{11/3}} \qquad [17]$$

where r_o is the Fried's parameter. This model is assumed to hold for spatial frequencies $1/L_o < f < 1/l_o$, where L_o is the outer scale and l_o is the inner scale of turbulence. Other expressions for W_φ, for example the von Krmn model, as well as other improved methods have been proposed (Lane et al., 1992; Sedmak, 2014) to avoid some shortcomings of the Kolmogorov formula and to obtain simulations in better agreement with the actual effect of the atmospheric turbulence. I have not tried to implement them because their complexity would have taken me too far from the already challenging objective of this study, i.e. to replicate the image reconstruction algorithm using data acquired with an instrumentation setup typically accessible to an amateur astronomer.

For each frame a new random phase screen is generated and, from that, a new normalized PSF is obtained, which is then convolved with the object distribution intensity given by expression 16. Photon, thermal and read-out noise are subsequently added according to the processes already described in section 2. Finally, the image is modified according to a given uniform bias and divided by the detector gain to get a final specklegram according to expression 4.

7. Comparison to Simulated Data

The application of the previous simulation and data analysis steps to known objects through simulations, as well as the comparison with the results obtainable with other analysis methods in the special case of binary stars, has been very helpful to correct initial coding errors and to check the actual performance of my implementation of the image reconstruction algorithm.

The entire data reduction process can be roughly divided into two phases, i.e. power spectrum and bispectrum estimation, followed by the application of the building block method. When the object is known to be a binary star, the resulting separation (ρ), position angle (θ) and magnitude difference (Δm) can also be compared with the same parameters obtained by least mean square (LMS) fitting the power spectrum or the bispectrum. In these cases the weight factor is chosen to be equal to the reciprocal of, respectively, the variance of the power spectrum $\sigma^2_{S}(u)$ and the variance of the bispectrum $\sigma^2_{O^{(3)}(u,v)}$. For details on a similar method used for LMS fitting the bispectrum phase of a binary star, see Glindemann et al.(1992). The results of four simulations with known binary stars are given in Table 1. For each case, the known parameters are compared to those obtained using the building block method (BBM) and the parametric fitting of the power spectrum (PS) and bispectrum (BS). For reconstructed images, the luminosity of each star component is measured by summing the values of all the pixels surrounding the pixel with the maximum intensity. Telescope, filter and detector parameters are kept fixed and assumed equal to those given in Tables 2 and 3.

The results reported in Table 1 are not intended to be comprehensive, rather they give an idea of the many factors that influence the measurement outcome, in particular under extreme conditions (very close pairs, low brightness, bad seeing, high detector thermal and/or readout noise). Even changing the data analysis method has a substantial influence on the estimated values in these cases. When the simulated conditions are more favorable, the agreement among the different methods increases significantly. In general, I found the magnitude difference subject to a greater relative uncertainty compared to the separation and position angle. This observation is in agreement with similar considerations generally reported in the literature.

Considering that the main purpose of these comparisons was to check the correctness of the implemented data-reduction algorithm, and not to investigate the effectiveness and limits of an established image reconstruction technique, I found the agreement among different methods encouraging.

As an additional test and in order to verify the performance of the reconstruction algorithm with a more complex object, I considered also the case of a triple star with components AB and AC separated by 1.2 and 0.8 arcsec respectively, position angles θ_{AB}=23°,

Image Reconstruction Using Bispectrum Speckle Interferometry: Application and First Results

Table 1. Binary star parameters estimated from 200 frames generated under different simulation conditions: (a) N^{ph}=30000, n_{th}=15, σ_e=10, b_{DC} =10, r_0=2.5 cm; (b) N^{ph}=3000, n_{th}=5, σ_e=7, b_{DC} =15, r_0=2.5 cm; (c) N^{ph}=1000, n_{th}=5, σ_e=7, b_{DC} =15, r_0=5.0 cm; (d) N^{ph}=500, n_{th}=2, σ_e=2, b_{DC} =5, r_0=5.0 cm

#	ρ (″)	θ (°)	Δm	ρ_{BBM} (″)	θ_{BBM} (°)	Δm_{BBM}	ρ_{PS} (″)	θ_{PS} (°)	Δm_{PS}	ρ_{BS} (″)	θ_{BS} (°)	Δm_{BS}
(a)	1.2	23	0.55	1.16	21.7	0.71	1.17	22.1	0.63	1.17	21.9	0.59
(b)	1.3	210	0.25	1.25	210.7	0.27	1.30	206.0	0.41	1.23	208.1	0.0
(c)	1.3	210	0.25	1.21	211.1	0.21	1.26	211.2	0.32	1.26	211.1	0.13
(d)	0.8	125	1.0	0.80	124.2	0.98	0.81	121.3	0.87	0.80	121.5	0.76

θ_{AC}=125°, and with a magnitude difference Δm_{AB}=0.55 and Δm_{AC}=0.99. An example of a specklegram simulated by using these parameters is shown in Figure 1. The estimated power spectrum, after bias subtraction and calibration is shown in Figure 2. As can be seen, the actual usable region is smaller than the theoretical maximum one given by the telescope cut-off frequency - which in this case corresponds to a circle with radius of about 15 pixels. It is the measured variance that gives the weight to assign to different regions when the data reduction process is carried out. The result is in any case sufficiently defined to be somewhat different, as expected, from the typical fringe pattern of a simple binary star. The image reconstructed using the building block method is shown in Figure 3. The estimated values of the magnitude differences from the reconstructed image are Δm_{AB}=0.54 and Δm_{AC} =0.97, which are very close to the actual values of the simulated object.

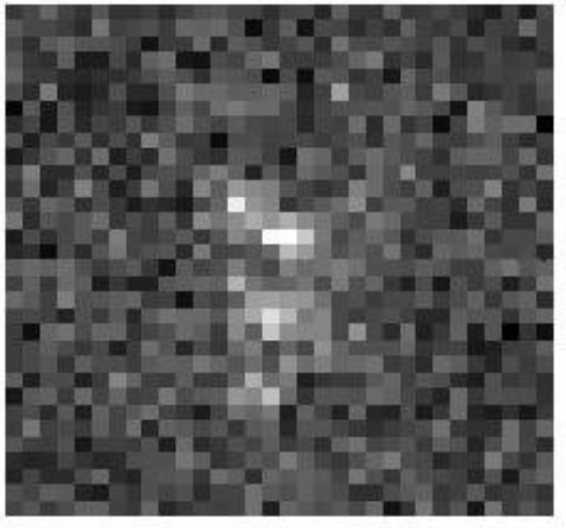

Figure 1: Example of specklegram of a triple star generated with simulation parameters N^{ph}=3000, n_{th}=10, σ_e=5, b_{DC} =15, r_0=3.0 cm. Image scale is 0.2171 arcsec per pixel.

8. Experimental Setup and Calibration

Speckle observations have been conducted with a 9.25" Schmidt-Cassegrain Celestron fitted with a JMI focuser and a Powermate 2.5X focal extender. The detector is an Imaging Source DMK 21AU04.AS based on a Sony ICX 098 BL chip, fitted with a Green Astronomik Type IIc filter. Nominal specifications for each component are summarized in Table 2.

The image reconstruction requires some input parameters that must be calibrated before the algorithm is executed. These estimates are given in Table 3.

The drift method (Caloi, 2008) is used to estimate the image scale and its orientation. Based on this calibration, the theoretical image cut-off frequency f_c is found to be 0.4594

$$f_c = \frac{D\Delta x}{\lambda f} = K\frac{D}{\lambda}$$

where D is the telescope primary diameter, Δx is the pixel size, f is the telescope effective focal length, λ is the effective transmission bandwidth center, which

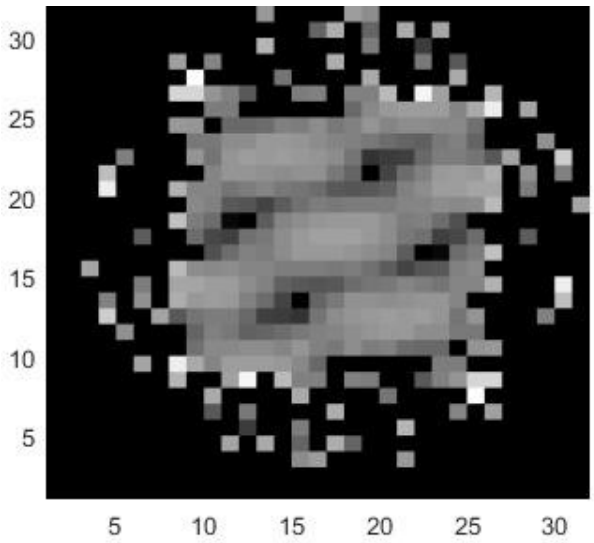

Figure 2: Estimated power spectrum (log scale) of a triple star from a sequence of 200 simulated specklegrams.

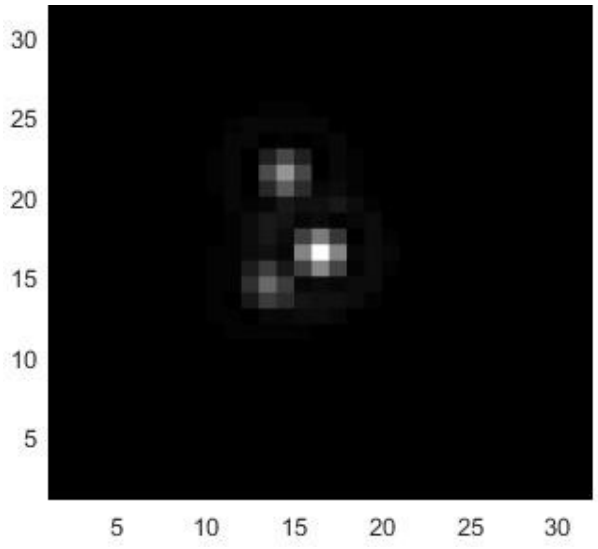

Figure 3. Reconstructed image of a simulated triple star.

combines the nominal filter properties and the frequency dependent quantum efficiency of the detector, and K is the image scale in rad/pixel. The cut-off frequency is less than 0.5, so this setup fulfills the Nyquist condition for digital image sampling.

Regarding the gain G of the CCD camera used in this study, the only related information I found on the producer website is the amplification scale which has a linear working range of 0 to 1023 corresponding to a 0 - 36 dB range (20 dB corresponds to an amplification factor of 10). Lacking such information, which is required if we want to apply the image reconstruction algorithm under low light conditions, I followed two different methods to estimate G as a function of the actual detector settings used during observations.

The first and less accurate method is based on the relation between the variance of a Poisson process with its mean, which gives

$$G\left(e^{-} / ADU\right) = \frac{\mu_c}{\sigma_c^2}$$

where μ_c and σ_c^2 are the mean and the variance respectively of the total counts, per given time interval, in a selected region of the detector with bright and uniform illumination, when photon noise is the main source of noise and the bias is negligible. The second method is less sensible to other noise sources or biases and requires measurement of μ_c and σ_c^2 as before under different light conditions. The gain is estimated as the slope of the linear regression of μ_c vs σ_c^2.

In addition, flat field images have been obtained

Table 2. Observation Nominal Parameters

Parameter	Symbol	Value
Telescope diameter	D	0.235 m
Telescope secondary obstruction	d	0.085 m
Transmission bandwidth	$\lambda \pm \Delta\lambda$	538 nm ± 40 nm
Pixel size (square shape)	$\Delta x \cdot \Delta x$	5.6 μm · 5.6 μm

Table 3. Calibrated parameters. Gain G is estimated for a nominal setting of 1023 on the DMK21AU04.AS CCD camera.

Parameter	Symbol	Value
Image scale	K	0.217 as/pixel
Detector gain	G	2.26 e^{-}/ADU
Theoretical cut-off frequency	fc	0.4594

to correct raw frames for non-homogenous spatial sensitivity, biases, or for the presence of dust on the detector's chip. Similarly, read-out and thermal noise have been estimated with the telescope aperture covered and with the same exposure time and CCD detector temperature of the actual observations of the target object and the reference star. A typical observing session requires, for each target object, obtaining several sequences of some hundreds of frames of both the target and the reference star, followed by similar sequences to estimate bias, dark current and read-out noise. I have used single frame exposure times in the 20-40 ms range, to *freeze* the speckle pattern, depending on seeing conditions and object brightness. The presence of a filter, the very short exposure time, and other practical considerations reduces significantly the possibility to successfully reconstruct the image of objects with a magnitude higher than 8 with the experimental setup used in this study.

9. Comparison to Measured Data

I have applied the image reconstruction procedure to video sequences captured during three different nights with the equipment already described in section 8. Due to the small size of the telescope, all objects considered have been binary stars. More complex objects, like close triple stars could become interesting targets if at least a medium size telescope with an aperture greater than 40 cm were used.

Even if seeing conditions were rather poor, 2 to 4 arcsec and windy, during all three observing

Image Reconstruction Using Bispectrum Speckle Interferometry: Application and First Results

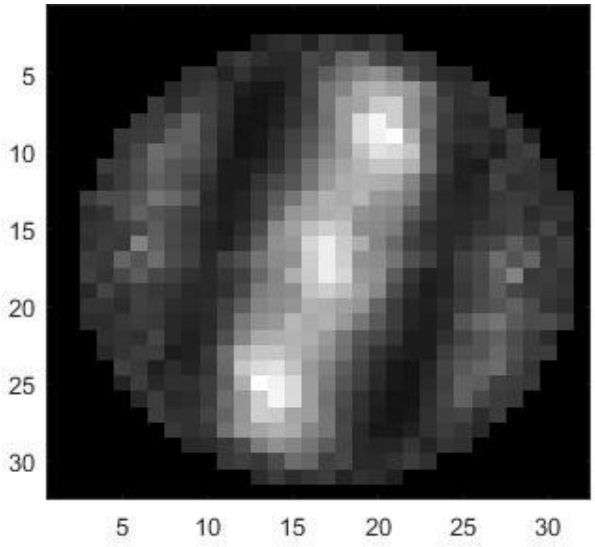

Figure 4: Average power spectrum of STF1909.

sessions, the high degree of atmospheric turbulence has facilitated the test of the performance of the reconstruction process, because speckles angular sizes were significantly greater than the resolving power of the telescope.

For each target, sequences of 200 up to 500 frames have been recorded and the measurements repeated during the same night. The dark current contribution was found to be negligible, while actual read-out noise was estimated to be between $3e^-$ and $7e^-$ depending on the chosen detector parameters and frame rate. Comparative results are given in Table 4 similarly to what has been done in Section 7 for simulated objects. Separations, position angles, and magnitude differences are extracted from the WDS catalog using the online search engine available at http://stelledoppie.goaction.it (Sordiglioni, 2012). Comparisons of measured magnitude differences to the known values must be considered indicative because the bandpass and center wavelength of the optical filter used in this study are just a proxy of a V-band standard filter. Moreover, the results obtained by model fitting the power spectrum (PS) and bispectrum (BS) are based on simple gradient descent minimization with a starting point given by the values obtained using the DVA method. As a consequence, the actual results could have been influenced by the presence of local minima in the optimization process.

Overall, the dispersion around known values for the magnitude differences is significantly greater than the errors in the separation and position angle, regardless of the method used. Nevertheless, these preliminary results confirm that the BBM yields reasonable estimates when compared to other methods applied to the same input data without *a priori* assumptions on the nature of the object under study.

The standard deviation of the error in the magnitude differences based on all 25 measurements of the nine binary stars in Table 4 is 0.62 mag for the BBM, and is slightly less than the values 0.76 mag and 0.73 mag obtained by least-square fitting the power spectrum (PS) and the bispectrum (BS) respectively. The results appear consistent with the known difficulties in performing photometry of close binary stars. At the same time, some improvement is to be expected with a fine tuning of the detector parameters used during observations - shutter speed, detector gain and frame rate - and by performing measurements under less severe conditions, i.e. with a better and more stable seeing.

To give an example of the outputs of the reconstruction process for STF1909, Figure 4 shows the average power spectrum after calibration with the reference star. In this case, the typical fringes of a double star, with separation very close to the maximum resolving power of the telescope, are clearly visible. The reconstructed image, not corrected for the actual detector orientation, is shown in Figure 5 after convolution with the telescope theoretical PSF.

On a desktop PC with an Intel(R) i3-4130 @ 3.40 GHz processor the required computation time for a selected region of 32 x 32 pixels is less than 5 minutes for 200 iterations, but increases significantly for images of a larger size. In all cases considered,

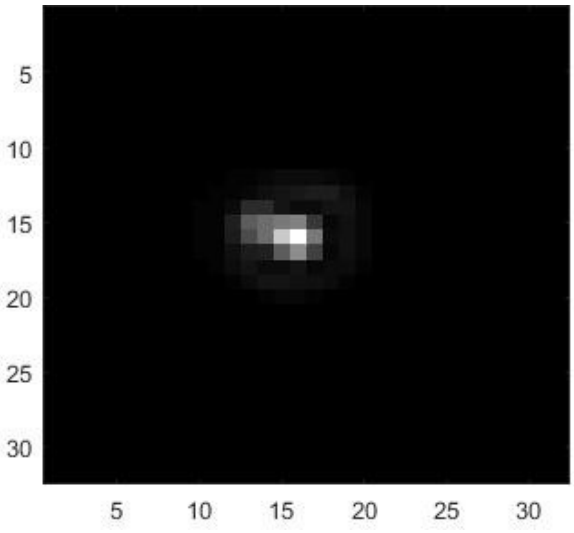

Figure 5: Reconstructed image of STF1909.

Image Reconstruction Using Bispectrum Speckle Interferometry: Application and First Results

Table 4: Estimated binary star parameters vs. known values from the WDS catalog using image reconstruction (BBM) and model fitting both the power spectrum (PS) and bispectrum (BS). The number of observations per night N_{obs} is given in the last column.

Disc	Date	WDS			BBM			PS			BS			Nobs
		ρ(")	θ(°)	Δm	ρ(")	θ(°)	Δm	ρ(")	θ(°)	Δm	ρ(")	θ(°)	Δm	
STT 413AB	2016.479	0.92	359.5	1.53	0.9	359.2	1.63	0.94	1.44	1.36	0.92	1.26	1.13	6
STF1998AB	2016.479	1.09	6.3	0.29	1.09	4.9	0.2	1.11	6.6	0.31	1.09	6.2	0.01	4
STF3050AB	2016.83	2.41	340.6	0.26	2.44	340.8	0.85	2.44	340.8	0.99	2.44	340.9	0.84	2
STF 228	2016.83	0.68	302.1	0.65	0.66	305.8	1.53	0.63	303.6	1.11	0.63	303.4	1.1	2
STF 228	2018.078	0.64	304.6	0.65	0.62	304.2	1.62	0.7	305.1	1.22	0.71	303.5	0.74	2
STF 333AB	2018.078	1.33	209.9	2.65	1.23	209.7	2.24	0.88	205.8	0	0.89	204.48	0	2
STT 215	2018.078	1.57	177.89	0.21	1.5	175.1	1.5	1.54	173.7	1.28	1.48	174.8	1.21	2
STF1687AB	2018.078	1.18	200.16	1.93	1.16	197.7	2.36	1.08	194.1	0.72	1.08	199.8	0.58	2
STF1909	2018.078	0.52	80.84	0.9	0.48	80	0.8	0.41	77.7	0.29	0.44	77.5	0.29	2

less than 50 iterations were required. The plot in Figure 6 shows how the value of the cost function d_k decreases after several iterations in the building block method for STF1909. As a general rule the reconstruction can be stopped once the rate of decrease of d_k reduces significantly.

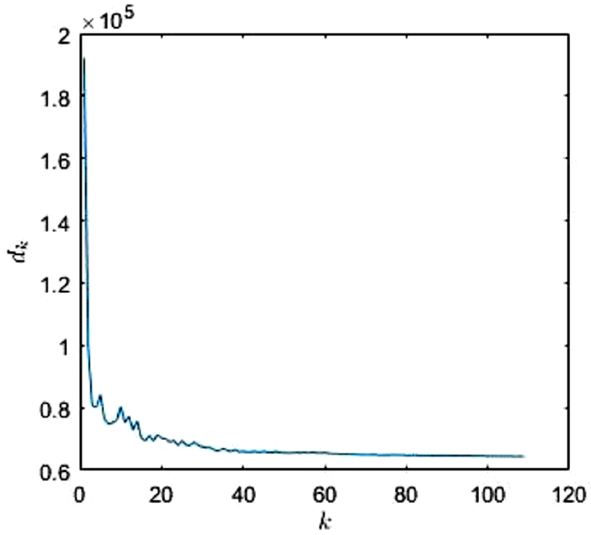

Figure 6. Residual value of the cost function d_k at iteration k in the building block method.

10. Conclusions

The main concepts involved in the recovery of an image from speckle interferometric data have been reviewed, with some details on how to correct for biases in the power spectrum and bispectrum and on how to calculate the frequency dependent variance of each estimated quantity. The building block method using the bispectrum has been successfully replicated, initially with simulated data and later with the estimate of the separation, position angle and magnitude difference of a number of close binary stars. The obtained accuracy for the magnitude differences is found to be about 0.6 mag with the equipment and the small telescope used in this report, even if some improvement is to be expected under more favorable observing conditions.

Finally, I hope this study and the listed bibliography will also provide a useful starting point to other amateur astronomers interested in the reconstruction of an image from speckles data using the bispectrum.

11. Acknowledgements

The author wishes to thank Carlo Perotti for his support during observations and Karl-Ludwig Bath for useful discussions in the early stages of this work. This research has made use of Cartes du Ciel, the Washington Double Star Catalog, and the double star database Stelle Doppie.

12. References

Bagnuolo, W. G. Jr., Mason, B.D., Barry, D.J., Hartkopf, W.I., and McAlister, H.A., 1992, *Astron. J.*, **103**, 4, 1399-1407.

Caloi, R. M., 2008, *Journal of Double Star Observations*, **4**-3, 111-118.

Genet, R. M., 2015, *Journal of Double Star Observations*, **11**-1S, 266-276.

Goodman, J. W., and J. F. Belsher, 1976, Technical Reports RADC-TR-76-50.

Gordon, J. A., and Buscher, D. F., 2012, *Astron. Astrophys.*, **541**, A46.

Glindemann, A., Lane, R.G., and Dainty, J.C., 1992, *J. Opt. Soc. Am. A*, **9**, 543-548.

Hofmann, K.-H. and Weigelt, G., 1993, *Astron. Astrophys.*, **278**, 328.

Hofmann, K.-H., Weigelt, G. and Schertl, D., 2014, *Astron. Astrophys.*, **565**, A48.

Klein, M.V., and Furtak, T.E., 1986, *Optics*, Wiley.

Labeyrie, A., 1970, *Astron. Astrophys.*, **6**, 85.

Lane, R. G., Glindemann, A., and Dainty, J.C., 1992, *Waves in Random Media*, b (1992), 209-224.

Lohmann, A.W., Weigelt, G., and Wirnitzer, B., 1983, *Appl. Opt.*, **22**, 4028.

McGlamery, B. L., 1976, *Proc. SPIE 0074 Image Processing.*

Pauls, T.A., Young, J.S. Cotton, W.D. and Monnier, J.D., 2005, PASP, **117**, 1255.

Sedmak, G., 2014, *Astron. Astrophys.*, **4**, 155.

Sordiglioni, G., 2012, *Il Bollettino delle Stelle Doppie*, 2.

Thiébaut, É. and Young, J., 2017, *J. Opt. Soc. Am. A*, **34**, 6.

Weigelt, G., 1977, *Opt. Commun.*, **21**, 55.

Wirnitzer, B., 1985, *J. Opt. Soc. Am. A*, **2**,14.

The Southern Double Stars of Carl Rümker III: Quantified Probability of Boundedness and Preliminary Grade 5 Orbits for Some Very Long Period Doubles

Roderick R. Letchford[1]
Graeme L. White[2]
Allan D. Ernest[3]

1. Vianney College Seminary, NSW Australia, rodvianney@yahoo.com.au
2. Astrophysics Group, Computational Engineering and Science Research Centre, University of Southern Queensland, Toowoomba, Australia QLD 4350, graemewhiteau@gmail.com
3. Charles Sturt University, NSW Australia, aernest@csu.edu.au

Abstract: All of the Southern double star pairs published by Carl Rümker in 1832 may be classified as very wide and measures have been obtained for only a small fraction of a single orbit. We attempt to find orbital elements of some Rümker doubles, and give an objective probability as to their binary status. Of the 28 pairs discovered by Rumker, we show some evidence for orbital (bound) movement for pairs RMK 4 and 8 and propose grade 5 orbits for them.

1. Introduction

In 1990 Charles E. Worley published an article with the rather provocative title "Is this Orbit really Necessary?" (Worley, 1990). It followed an earlier article by Willem H. van den Bos (1962) with the same title and argument. Both authors criticised the publication of orbits that were either unreliable or useless. Unreliable because they were based on too few observations over too short an arc, or useless because the quality of recalculated orbits rarely increases.

Notwithstanding the opinions of these eminent astronomers, we wish to offer a justification and a new simple method for attempting to find orbital parameters of wide binaries that have been observed over a short arc.

The justification is easily stated. If the residuals from an elliptical orbit are smaller than those obtained from a presumed rectilinear motion then it can be said that it is more likely than not that the pair are true binaries rather than optical doubles. Distinguishing between optical and binary doubles has important ramifications for many aspects of astrophysics especially stellar formation models (Guinan, Harmanec, & Hartkopf, 2007). Indeed there has been renewed interest in wide binary systems because of their potential to distinguish between the mainstream-accepted WIMP-based hypothesis of dark matter, and Modified Newtonian Dynamics (Chanamé & Gould, 2004; Longhitano, Binggeli, & Zejda, 2010; Németh et al., 2016).

Various methods have been proposed to extract orbital information from short arcs. Two in particular are used regularly in publications.

The first is the so-called "Kovole" method which is the Kowalski method modified for short-arcs (see for example, Catović, Olević, & Hartkopf (1992), Catović & Olević (1995), and Olević & Cvetković (2004, 2005)). The second is a method based on the more well-known Thiele-Innes-Van-den-Bos method (see for example, Docobo (1985) and Docobo and Hestroffer (2012)). Neither of these two methods are satisfactory when applied to a single very short arc and we outline our method for optimising an elliptical fit to very short arcs in the next section.

We also present here Paper III of a study of the double stars identified nearly two hundred years ago at Sir Thomas Brisbane's observatory at Parramatta, Australia by Carl Rümker (see Paper I, Letchford, White, and Ernest 2017, and Paper II, 2018, and references therein). In the present study we present the orbital elements of five pairs from Rümker's double star list. Sec-

tion 2 is our method for the computation of the elements of orbital motion, Section 3 discusses the validity of the claim that the stars are in a binary system, and Section 4 presents the elements and the Appendix the diagrammatic results for the five pairs.

2. Computation of Orbital Parameters for Very Short Arcs

As with all techniques of orbit fitting to the astrometric observations of double stars, we start with the fundamental step of fitting of an ellipse to the projection of the orbit onto the plane of the sky (the *apparent orbit*). Standared orbital elements follow from the satisfactory fitting of the ellipse.

The fundamental problem in finding an optimum ellipse from a small fraction of a potential ellipse is that the family of possible solutions can be very large with large variations of measured parameters and large uncertainties. We maintain however, that this difficulty can be mostly, but not completely, overcome by introducing into the calculations as many constraints on the solutions as possible.

Apart from making the initial assumption that the doubles are possibly binaries, we have identified and incorporated into our calculations the following constraints:

a) The orbit (defined by the motion of the secondary stars relative to the primary) must cross to all sides of the primary star. That is, in a projection on the sky, the N-S and E-W axes will be crossed in (only) two places for each axis, one either side of the origin (0,0).
b) Because the secondary is slow moving the positions obtained from the space-based HIPPARCOS and GAIA missions will be relatively close together. Thus the rectilinear line passing through these two positions (see Paper II, Letchford, White, & Ernest, (2018)) can be considered as approximating a tangential to the orbit. Therefore the elliptical orbit will only exist on the side of this line containing the primary. The space on the other side of the rectilinear line can be eliminated from consideration.
c) The fixed primary star must appear inside the apparent relative obit of the secondary.
d) In most double star work the ultimate aim is to obtain direct measures of the stellar masses using Kepler's third law,

$$M_1 + M_2 = \frac{a_{''}^3}{\prod_{''}^3 P_{yrs}^2}$$

where M_1 and M_2 are the masses of the primary and secondary in solar masses, respectively; a is the semi-major axis of the real apparent orbit in arcseconds; Π is the parallax of the system (the primary star) in arcseconds; and P is the orbital period in years. Here we reverse the exercise and with the sum of the masses obtained from their spectral types, and their parallax from an online catalogue (see Paper I and the reference to ASCC 2.5 in that Paper) provide an additional constraint on P and a.
e) The calculated positions at 1991.25 and 2015.0 must be within the uncertainty ellipses of the HIPPARCOS and GAIA positions respectively, and close as possible to all other (historic) measures considered. All historic observational data are included and unweighted. No outliers were discarded.

A Monte Carlo approach was used to incorporate four random positions along the axes into the observed positional data (constraints a) and b)). An orbit was obtained using the Kowalski method along with Kepler's equation. The orbit was then tested to see if it fulfilled constraints c), d) and e). If it did, the resulting residual and orbital elements were calculated and binned and compared with subsequent possible orbits. We limited the outer boundary of the random axial points to 4 minutes from the fixed star, noting that in the 6th Orbit catalog, only two pairs have a semi-major axis greater than 180 arcseconds and a period measured in centuries. This approach was repeated until 16 orbits were recovered whose residuals (sum of the squares of distances between the observed and calculated positions) varied by no more than 0.04 square arcseconds from the lowest residual ellipse. The best orbit is the orbit that produces the lowest residual.

The elements of the best orbit are accepted and given in Table 1. They have been rounded to their significant figures on the basis of their uncertainties.

As the best orbit was not the average of the resulting orbits, but the one with the lowest residual, we estimated the uncertainty of the orbital parameters of the best orbit using the square root of its variance:

$$\sigma_{OE} = \pm\sqrt{(OE - OE_{mean})^2} = |OE - OE_{mean}|$$

3. Orbits or Rectilinear Motion – Bound or Unbound Systems

We return to the differentiation of the orbital motion displayed by a bound binary system and the physically unbounded motion that displays straight (rectilinear) relative motion.

We assert, as above, that if the residuals from an elliptical orbit are smaller than those obtained from a rectilinear motion then the pair are more likely to be a binary rather than an optical double. In paper II in this series (Letchford, White and Ernest, 2018) the rectiline-

ar motion of 14 Rümker pairs was presented. In that work, the rectilinear motion was computed based on the two precise astrometric positions at ICRS and epoch 1991.25 and 2015.0 respectively obtained from the HIPPARCOS and GAIA space-based missions, where the precision in position is typically 5 milli-arcseconds for HIPPARCOS and 0.4 milliarcseconds for GAIA in the pairs under consideration. Ground-based historic observations extending over ~200 years are ignored in that analysis as the associated uncertainties are estimated to be ~0.3 to ~0.5 arcseconds, two orders of magnitude greater than those of the HIPPARCOS and GAIA uncertainties.

The published rectilinear models of the Rümker pairs in paper II are therefore not compatible with computed orbits presented here. To compare like-with-like, we recalculated the rectilinear motion of the pairs in Table 1 using a Monte Carlo method, similar to that used for the computation of the orbit parameters, so that the rectilinear fit results in the lowest residual but the rectilinear motion passes within the formal uncertainties of the HIPPARCOS and GAIA positions. To keep the calculations as objective as possible, we have not weighted nor discarded any historic data. This reanalysis results in a rectilinear fit which is close to but not identical to that of Paper II.

The like-with-like comparison of the residuals resulting from the orbit computation, and the residuals resulting from the rectilinear fit, are presented in Table 1, last two columns, and the percentage probability that the pair represent a gravitationally bound pair in an elliptical orbit is given by:

$$\exp\left[\frac{orbit\ residual}{linear\ residual}\ln(0.5)\right]\times 100\%$$

which is defined such that if, for example, the orbital residual equals the rectilinear residual (percentage probability = 50%), the binary nature of the pair (or their possible rectilinear nature) remains unknown. Values greater than 50% (orbital residual < linear residual) imply the increasing validity of a bound pair, while values less than 50% (orbital residual > linear residual) imply an increasing probability of an unbound system.

4. Results

The orbital elements, their uncertainties, along with the resulting residual of orbital and (recalculated) rectilinear motion are presented in Table 1. The associated plots are in the Appendix.

5. Discussion

From Paper II, only RMK 1, 3, 4, 5, 6, 8, 10, 11, 12, 17, 20, 25, 27 and 28 had both full HIPPARCOS and GAIA DR1 data. Of those only 1, 3, 4, 6, 8, yielded potential orbits given the constraints of Sections 2 and 3. We conclude from this that either the remaining pairs are optical doubles or that the secondary is moving too slowly with respect to the primary for even our brute-force method to detect (as yet) any curvature in their astrometric motion.

For the five orbits reported here, the orbital period are all long, ranging from 2400 years up to one million years. The average period is some 330000 years, and the formal errors are, on average 60% of the period. The largest semi-major axis is 10 ± 5 arcminutes for RMK 6.

RMK 1 (WDS 00524-6930). The probability of this pair being a binary system is ~ 49%. This system is unlikely to be binary, and further accurate observations are warranted. Figures 1 – 5 in the Appendix.

Table 1: Orbital Elements. All orbital elements have been rounded to their significant figures on the basis of their uncertainties. Residuals rounded to the nearest 10th arcsecond squared.

RMK	P yrs +/-	a " +/-	i ° +/-	Ω ° +/-	T yr +/-	e +/-	ω ° +/-	Orbital Residual "² +/-	Linear Residual "²
1	580000	170	66.4	14.1	6100	0.74	105	14.5	14.2
	40000	11	0.5	0.9	800	0.02	4	0.00	
3	26000	14	105	55	4900	0.8	210	8.8	8.7
	9000	3	2	13	900	0.3	40	0.01	
4	2400	8.0	70	54.9	1900	0.22	200	7.2	13.0
	400	1.1	2	0.7	110	0.05	30	0.01	
6	1000000	600	85	146	10000	0.9	340	23.7	23.7
	700000	300	1	2	4000	0.3	120	0.03	
8	30000	21	73	70.4	1950	0.8	350	1.2	1.34
	9000	7	3	0.7	150	0.3	30	0.00	

RMK 3 (WDS 04177-6315). Probability of this pair being a binary system is ~ 49%. This system is unlikely to be binary, and further observations are warranted. Figures 6 - 10 in the Appendix.

RMK 4 (WDS 04242-5704). Probability of this pair being a binary system is ~ 68%. This system is likely to be binary, and confirmation observations are needed. Figures 11 – 15 in the Appendix.

RMK 6 (WDS 07204-5219) Probability of this pair being a binary system is ~ 49%. This system is unlikely to be binary, and further observations are warranted. Figures 16 – 20 in the Appendix.

RMK 8 (WDS 08153-6255) Probability of this pair being a binary system is ~ 53%. This system is likely to be binary, and further confirmation observations are needed. Figures 21 - 25 in the Appendix.

5.1 Grading of These Orbits.

The Sixth Catalog of Orbits of Visual Binary Stars†, http://ad.usno.navy.mil/wds/orb6/orb6text.html#grading, maintained by the USNO, grades each orbit; Grade 1 being for a definitive orbit and Grade 5 being for an indeterminate orbit. The elements of Grade 5 orbits "may not even be approximately correct". Grade 5 orbits usually have short arcs with little curvature. We classify our orbits of the five RMK pairs (RMK 1, 3, 4, 6 and 8) as Grade 5 orbits, and claim validity only for the orbits of RMK 4 and 8.

6. Conclusion

Our objective method of quantifying the binary status of very wide slow moving binaries suggests that most of the Rümker doubles are unbound optical doubles. RMK 1, 3, and 6 are also likely to be optical doubles but further observation is warranted as the probability of them being a binary pair is about 50%. However, RMK 4, and to a lesser extent RMK 8, are likely to be binaries as this paper has detected an elliptical trend in the astrometric observations which leads to a probability of a bound pair of 68% and 53% respectively. As above, we classify the orbits of RMK 1, 3, 4, and 6 as Grade 5 orbits and claim validity only for the orbits of RMK 4 and 8. Given the importance of binarity in stellar formation models and possibly in the detection of dark matter, this outcome fully justifies the value of finding orbits for very short arc doubles.

Acknowledgements

The following were used in this research:

- The HIPPARCOS Catalogue (The Hipparcos and Tycho Catalogues (ESA 1997)) from VizieR, http://vizier.u-strasbg.fr/viz-bin/VizieR-3?-source=I/239/h_dm_com
- The GAIA Catalogue (Gaia DR1 (Gaia Collaboration, 2016)) from VizieR, http://vizier.u-strasbg.fr/viz-bin/VizieR-3?-source=I/337/gaia
- The *Washington Double Star Catalog* maintained by the USNO.

Spectral Types were obtained from Paper I, and the corresponding masses were obtained from Landon Curt Noll's website, http://www.isthe.com/chongo/tech/astro/HR-temp-mass-table-byhrclass.html .

References

Catović, Z., & Olević, D., 1995, "Visual Binary Orbit Determination. One Possible Approach", *Bulletin Astronomique de Belgrade*, **195**, 65–70. Retrieved from http://adsabs.harvard.edu/abs/1995BABel.152...65C.

Catović, Z., Olević, D., & Hartkopf, W. I., 1992, "Visual Binary Orbit Calculation with Help of a PC: One Possible Approach", *IAU Colloq. 135: Complementary Approaches to Double and Multiple Star Research*, H. A. McAlister, ed., **32**, 217–219. Retrieved from http://adsabs.harvard.edu/abs/1992ASPC...32..217C.

Chanamé, J., & Gould, A., 2004, "Disk and Halo Wide Binaries from the Revised Luyten Catalog: Probes of Star Formation and MACHO Dark Matter", *The Astrophysical Journal*, **601**, 289–310. Retrieved from http://adsabs.harvard.edu/abs/2004ApJ...601..289C.

Docobo, J. A., 1985, "On the analytic calculation of visual double star orbits", *Celestial Mechanics*, **36**, 143–153. Retrieved from http://adsabs.harvard.edu/abs/1985CeMec..36..143D.

Docobo, J. A., & Hestroffer, D., 2012, "The use of Docobo's analytic method for calculating visual double star orbits", *Orbital Couples: Pas de Deux in the Solar System and the Milky Way*, F. Arenou, ed., Retrieved from http://adsabs.harvard.edu/abs/2012ocpd.conf..119D.

Guinan, E. F., Harmanec, P., & Hartkopf, W. I., 2007, "Introduction & Overview to Symposium 240: Binary Stars as Critical Tools and Tests in Contemporary Astrophysics", *IAU Symposium 240: Binary Stars as Critical Tools and Tests in Contemporary Astrophysics*, W. I. Hartkopf, E. F. Guinan, and P. Harmanec, eds., **240**, 5–16, Cambridge, UK, Cambridge University Press. Retrieved from http://adsabs.harvard.edu/abs/2007IAUS..240....5G.

† http://ad.usno.navy.mil/wds/orb6/orb6text.html#grading

Letchford, R. R., White, G. L., & Ernest, A. D., 2017, "The Southern Double Stars of Carl Rümker I: History, Identification, Accuracy", *JDSO*, **13**(2), 220–232, Retrieved from http://www.jdso.org/volume13/number2/Letchford_220-232.pdf.

Letchford, R. R., White, G. L., & Ernest, A. D., 2018, "The Southern Double Stars of Carl Rümker II: Their Relative Rectilinear Motion", *JDSO*, **14**(2), 208–222. Retrieved from http://www.jdso.org/volume14/number2/Letchford_208_222.pdf.

Longhitano, M., Binggeli, B., & Zejda, M., 2010, "The Widest Binary Stars: A Statistical Approach", *ASP Conference Proceedings 435: Binaries - Key to Comprehension of the Universe,* A. Prša and M. Zejda, eds., **435**, 67–70. Retrieved from http://adsabs.harvard.edu/abs/2010ASPC..435...67L.

Németh, P., Ziegerer, E., Irrgang, A., Geier, S., Fürst, F., Kupfer, T., & Heber, U., 2016, "An extremely fast halo hot subdwarf star in a wide binary system, *The Astrophysical Journal Letters*, **821**(L13), 1–7. Retrieved from http://adsabs.harvard.edu/abs/2016ApJ...821L..13N.

Olević, D., & Cvetković, Z., 2004, "Orbits of 10 interferometric binary systems calculated by using the improved Koval'skij method", *Astronomy and Astrophysics*, **415**, 259–264. Retrieved from http://adsabs.harvard.edu/abs/2004A&A...415..259O.

Olević, D., & Cvetković, Z., 2005, "Improved Koval'skij method and its new possibilities", *Publications of the Astronomical Society "Rudjer Boskovic,"* **5**, 237–240. Retrieved from http://adsabs.harvard.edu/abs/2005PASRB...5..237O.

van den Bos, W. H., 1962, "Is This Orbit Really Necessary?", *Publications of the Astronomical Society of the Pacific*, **74**(439), 297–301. Retrieved from http://adsabs.harvard.edu/abs/1962PASP...74..297V.

Worley, C. E., 1990, "Is this Orbit Really Necessary? (II)", *Errors, Bias and Uncertainties in Astronomy* (p. 419), Cambridge, UK, Cambridge University Press. Retrieved from http://adsabs.harvard.edu/abs/1990ebua.conf..419W.

Appendix

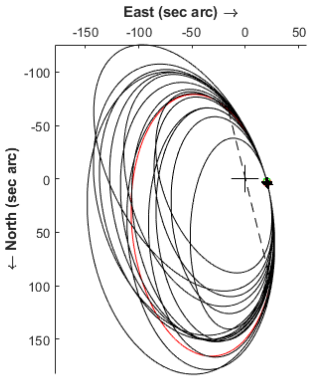

Figure 1: RMK 1 family of orbits. The best orbit, whose elements are in Table 1, is in red.

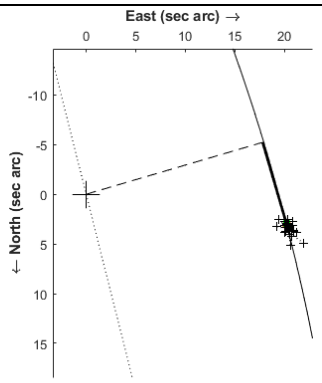

Figure 2: RMK 1 enlargement showing rectilinear line (thick line) and section of orbit (thin line).

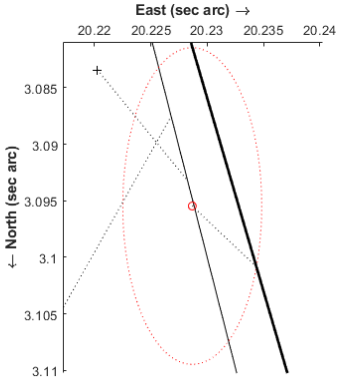

Figure 3: RMK 1 enlargement showing rectilinear line (thick line) and section of orbit (thin line) passing through the uncertainty space of the HIP position.

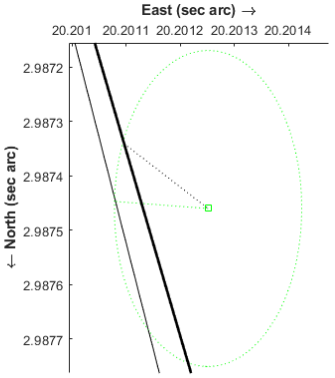

Figure 4: RMK 1 enlargement showing rectilinear line (thick line) and section of orbit (thin line) passing through the uncertainty space of the GAIA position.

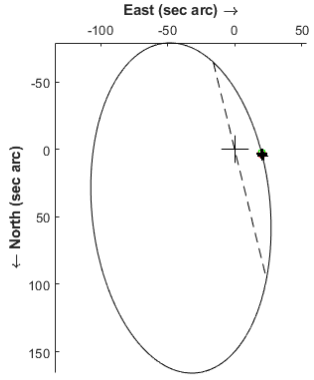

Figure 5: RMK 1 best obtained possible orbit. Orbital Elements in Table 1. Direction of motion is prograde (anti-clockwise).

The Southern Double Stars of Carl Rümker III: Quantified Probability of Boundedness ...

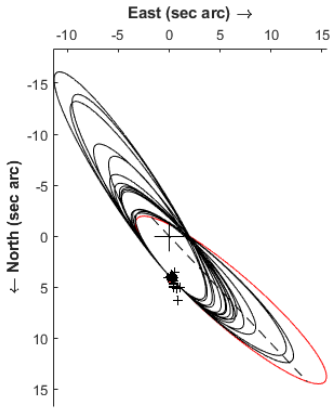

Figure 6. RMK 3 family of orbits. The best orbit, whose elements are in Table 1, is in red.

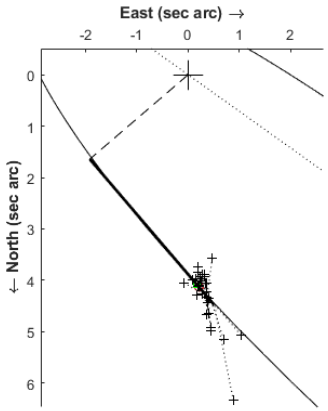

Figure 7. RMK 3 enlargement showing rectilinear line (thick line) and section of orbit (thin line).

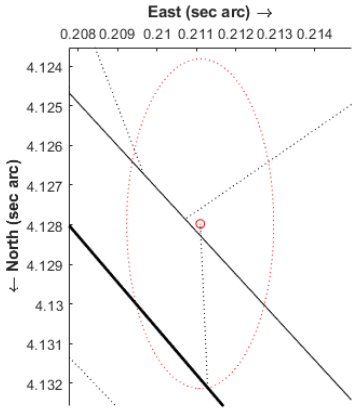

Figure 8. RMK 3 enlargement showing rectilinear line (thick line) and section of orbit (thin line) passing through the uncertainty space of the HIP position.

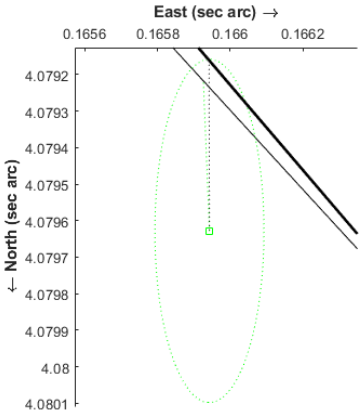

Figure 9. RMK 3 enlargement showing rectilinear line (thick line) and section of orbit (thin line) passing through the uncertainty space of the GAIA position.

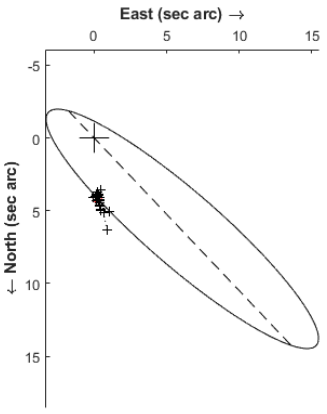

Figure 10. RMK 3 best obtained possible orbit. Orbital Elements in Table 1. Direction of motion is retrograde (clockwise).

The Southern Double Stars of Carl Rümker III: Quantified Probability of Boundedness ...

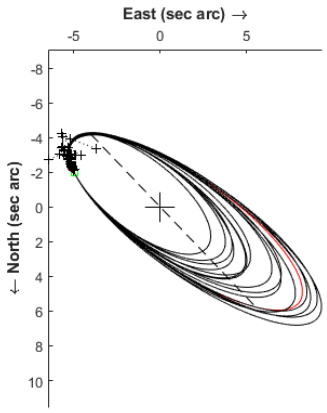

Figure 11. RMK 4 family of orbits. The best orbit, whose elements are in Table 1, is in red.

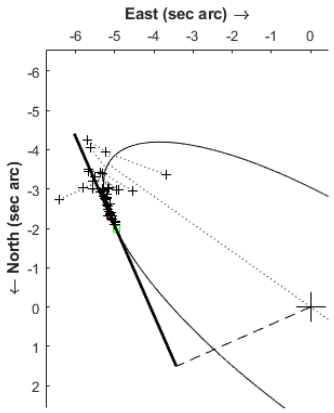

Figure 12. RMK 4 enlargement showing rectilinear line (thick line) and section of orbit (thin line).

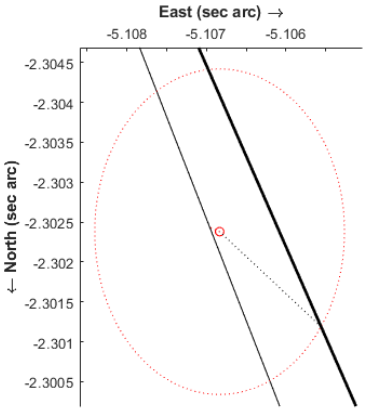

Figure 13. RMK 4 enlargement showing rectilinear line (thick line) and section of orbit (thin line) passing through the uncertainty space of the HIP position.

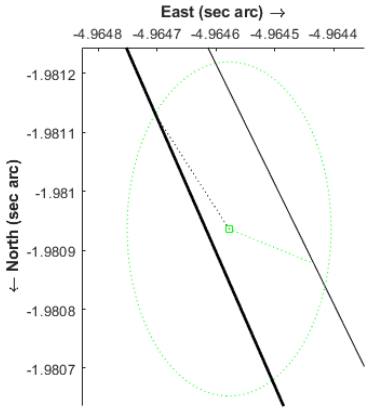

Figure 14. RMK 4 enlargement showing rectilinear line (thick line) and section of orbit (thin line) passing through the uncertainty space of the GAIA position.

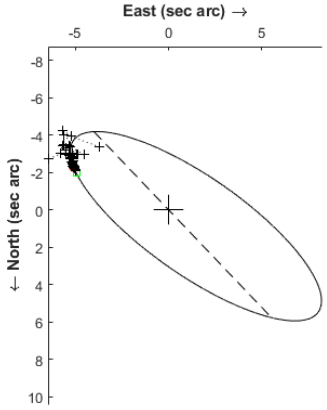

Figure 15. RMK 4 best obtained possible orbit. Orbital Elements in Table 1. Direction of motion is prograde (anticlockwise).

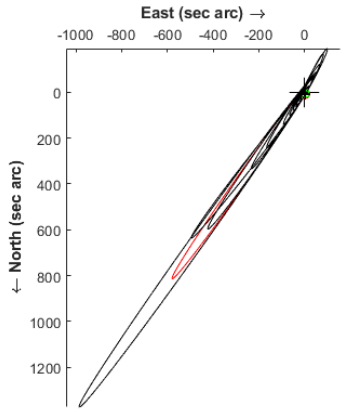

Figure 16. RMK 6 family of orbits. The best orbit, whose elements are in Table 1, is in red.

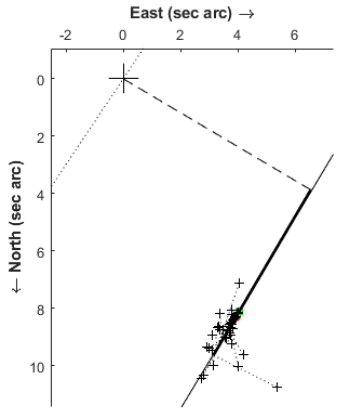

Figure 17. RMK 6 enlargement showing rectilinear line (thick line) and section of orbit (thin line).

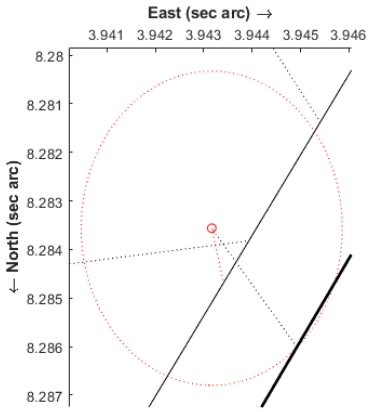

Figure 18. RMK 6 enlargement showing rectilinear line (thick line) and section of orbit (thin line) passing through the uncertainty space of the HIP position.

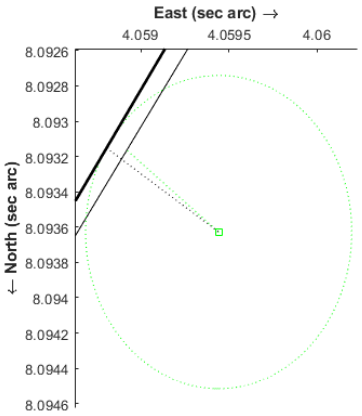

Figure 19. RMK 6 enlargement showing rectilinear line (thick line) and section of orbit (thin line) passing through the uncertainty space of the GAIA position.

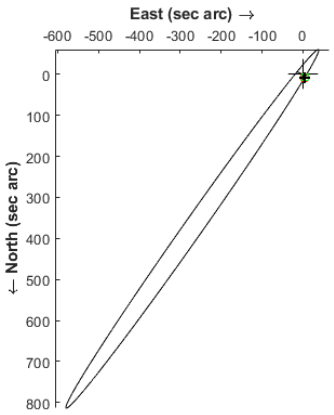

Figure 20. RMK 6 best obtained possible orbit. Orbital Elements in Table 1. Direction of motion is retrograde (clockwise).

The Southern Double Stars of Carl Rümker III: Quantified Probability of Boundedness ...

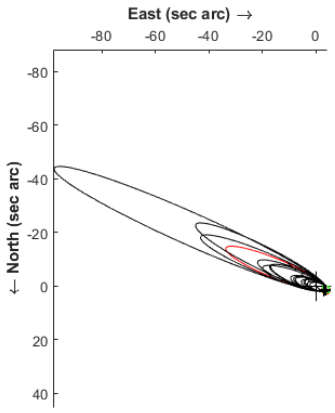

Figure 21. RMK 8 family of orbits. The best orbit, whose elements are in Table 1, is in red.

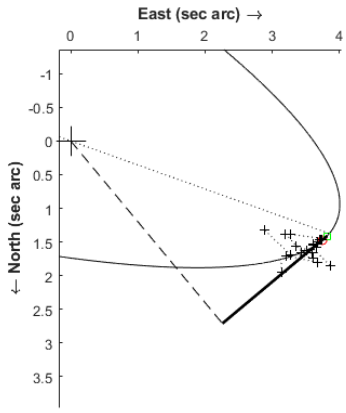

Figure 22. RMK 8 enlargement showing rectilinear line (thick line) and section of orbit (thin line).

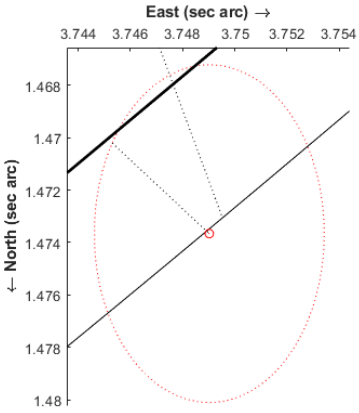

Figure 23. RMK 8 enlargement showing rectilinear line (thick line) and section of orbit (thin line) passing through the uncertainty space of the HIP position.

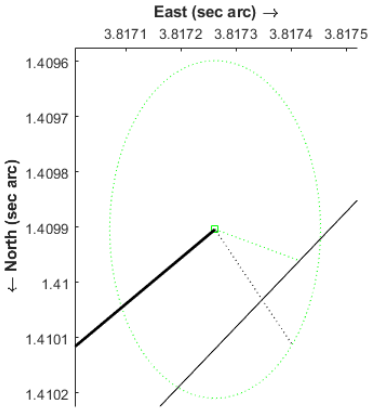

Figure 24. RMK 8 enlargement showing rectilinear line (thick line) and section of orbit (thin line) passing through the uncertainty space of the GAIA position.

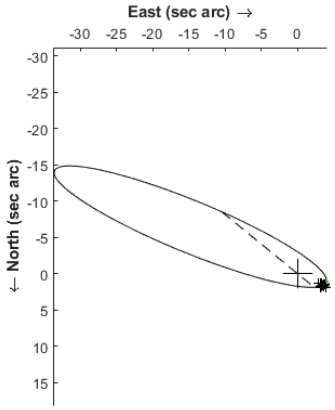

Figure 25. RMK 8 best obtained possible orbit. Orbital Elements in Table 1. Direction of motion is prograde (anticlockwise).

Journal of Double Star Observations

October 1, 2018
Volume 14, Number 4

The Journal of Double Star Observations (ISSN 2572-4436) is an electronic journal published quarterly. Copies can be freely downloaded from http://www.jdso.org.

Questions, comments, or submissions may be directed to rclark@southalabama.edu or to rmollise@bellsouth.net

The *Journal of Double Star Observations* (*JDSO*) publishes articles on any and all aspects of astronomy involving double and binary stars. The *JDSO* is especially interested in observations made by amateur astronomers. Submitted articles announcing measurements, discoveries, or conclusions about double or binary stars may undergo a peer review. This means that a paper submitted by an amateur astronomer will be reviewed by other amateur astronomers doing similar work.

Submitted manuscripts must be original, unpublished material and written in English. They should contain an abstract and a short description or biography (2 or 3 sentences) of the author(s). For more information about format of submitted articles, please see our web site at http://www.jdso.org

Submissions should be made electronically via e-mail to rclark@southalabama.edu or to rmolise@bellsouth.net. Articles should be attached to the email in Microsoft Word, Word Perfect, Open Office, or text format. All images should be in jpg or fits format.